Experimental and numerical investigation of the thermal decomposition of materials at three scales: application to polyether polyurethane foam used in upholstered furniture

Lucas Bustamante Valencia

THÈSE

pour l'obtention du grade de

DOCTEUR DE L'ÉCOLE NATIONALE SUPÉRIEURE DE MÉCANIQUE ET D'AÉROTECHNIQUE
(Diplôme National – Arrêté du 7 août 2006)

École Doctorale : Sciences pour l'Ingénieur et Aéronautique

Secteur de recherche : Energétique, Thermique, Combustion

Option : Energétique

Présentée par :

Lucas Bustamante Valencia

****

Étude expérimentale et numérique de la décomposition thermique des matériaux à trois échelles : Application à une mousse polyéther polyuréthane utilisée dans les meubles rembourrés

Experimental and numerical investigation of the thermal decomposition of materials at three scales: application to polyether polyurethane foam used in upholstered furniture

****

Directeur de thèse : Patrick ROUSSEAUX

Co-Directeur : Thomas ROGAUME

****

Soutenue le 20 novembre 2009
devant la Commission d'Examen

****

- Jury -

M. P. BOULET	Professeur, LEMTA Université de Nancy	Président
M. B. PORTERIE	Professeur, IUSTI Université de Marseille	Rapporteur
M. J.L. TORERO	Professeur, Université d'Édimbourg, Ecosse	Rapporteur
M. P. ROUSSEAUX	Professeur, LCD Université de Poitiers	Examinateur
Mme. C. CHIVAS-JOLY	Ingénieur de recherche, LNE de Trappes	Examinateur
M. E. GUILLAUME	Ingénieur de recherche, LNE de Trappes	Examinateur
M. G. REIN	Maître de Conf. Université d'Edimbourg, Ecosse	Examinateur
M. T. ROGAUME	Maître de Conférences, LCD Université de Poitiers	Examinateur

To Carine Cordier

Yes, this work is also yours…

To Luz Elena Valencia

Abstract

The fire behaviour of polyether polyurethane foam has been studied at three scales: matter scale, small scale and product scale. A method to determine the thermal decomposition mechanism of materials was defined at the matter scale. This method is based on the analysis of the mass-loss rate (solid phase) and gas release (gas phase) obtained in thermogravimetric analysis coupled to FTIR gas analysis. Using a model and genetic algorithms, the kinetic parameters of the decomposition process were calculated, which allowed an accurate prediction of the mass-loss rate.

Measurements of heat release rate and gas release were carried out in cone calorimeter coupled to gas analysers (small scale). This data as well as the results from the model were used as input data for the numerical simulation of fire behaviour. This study highlighted that some improvements need to be carried out to the simulation codes.

Measurements of heat release rate and mass-loss rate were also performed during the fire of a simplified piece of upholstered furniture (product scale). It was pointed out that the decomposition mechanism of the foam remains unchanged independently of the scale analysed.

Résumé

L'amélioration de la sécurité incendie au sein de l'habitat est un des principaux objectifs de la recherche actuelle. En effet, chaque année, un grand nombre de feux sont déclarés, générant la perte de nombreuses vies humaines, de fortes pertes financières, l'endommagement des structures et la pollution de l'environnement.

Face à cette problématique, on remarque qu'un grand nombre de pays d'Europe possèdent une législation très pauvre vis-à-vis de la protection incendie dans l'habitat. Historiquement, les bâtiments ont été dessinés suivant des obligations prescriptives. La tendance de l'ingénierie de la sécurité incendie (Fire Safety Engineering, FSE selon le sigle Anglais) a changé amplement pendant la dernière décennie : des groupes de recherche dans le domaine de l'incendie ont mis au point les principes du design fondé sur la performance (Performance Building Design, PBD en Anglais). Le PBD a permis une approche de la sécurité incendie fondée sur la prédiction du comportement d'un incendie dans des scénarios donnés, en utilisant des outils numériques d'ingénierie. L'approche PBD de FSE est une méthodologie qui a été initialement développée pour les établissements recevant du public, toutefois peu à peu cette approche commence à être utilisée dans tout type d'habitat.

La prédiction du comportement d'un incendie nécessite le calcul du débit calorifique (Heat Release Rate, HRR en Anglais) qui est la grandeur physique utilisée pour la mesure de la puissance d'un feu. En ingénierie, le HRR est indispensable à l'estimation de la sévérité du sinistre et des possibles endommagements causés dans un scénario donné. Sa détermination dépend des combustibles présents lors de l'incendie ainsi que de l'environnement du sinistre. La prédiction du HRR est réalisée à l'aide des codes de simulation numérique de l'incendie. Ceux-ci sont un assemblage de plusieurs sous modèles dont chacun calcule un ensemble des phénomènes présents dans la combustion p. ex. la pyrolyse, le rayonnement, la turbulence, etc.

La capacité à prédire correctement le HRR est limitée par les calculs très simplifiés du processus de décomposition thermique des solides. La décomposition est notamment dépendante des processus diffusifs et chimiques mis en jeu dans la zone comprise entre le solide et la flamme, lesquels ne sont pas modélisés de façon rigoureuse. Par le passé, plusieurs études expérimentales ont permis de mesurer le HRR d'un certain nombre de produits, cependant, ils ne contribuent pas à la compréhension de la physique du processus de décomposition de la matrice solide, donnée pourtant essentielle car source des espèces volatiles et du débit massique du combustible. En effet, un grand nombre de simulations trouvées dans la littérature font une approche empirique de la production de fuel ou considèrent une seule étape de décomposition.

C'est dans ce contexte que prend place la présente étude qui vise à caractériser la cinétique de décomposition de combustibles solides et de formation des espèces volatiles : les changements survenus dans la phase solide sont pris en compte ensemble avec ceux de la phase gazeuse (dégagement d'espèces). La détermination du mécanisme de décomposition est une tâche fondamentale de l'analyse thermique. Le mécanisme doit considérer la succession des transformations de la matière pendant la gazéification des solides. Cette succession inclus les échantillons vierges ainsi que ceux qui ont déjà souffert des attaques thermiques (sous produits des étapes de décomposition). Le mécanisme de décomposition constitue une des principales données d'entrée de la grande majorité de modèles de décomposition thermique.

Cette recherche tient compte de la décomposition thermique d'une mousse polyéther polyuréthane (PPUF) à trois échelles différentes. Chaque échelle caractérise le comportement au feu d'une masse différente de mousse et est concentrée sur l'étude de phénomènes particuliers :

- L'échelle matière permet l'analyse du comportement d'échantillons avec des masses proches d'un milligramme. À l'échelle matière, les effets de transfert de chaleur et des espèces sont minimisés et l'effet de l'augmentation de la température du solide peut être étudié précisément. L'échantillon est considéré comme une particule de masse et de dimension négligeables, de sorte que sa température soit homogène.

- La petite échelle permet l'analyse des échantillons avec des masses proches de dix grammes. À l'échelle matière des gradients de transfert de chaleur et d'espèces existent. L'échantillon est irradié seulement par une des surfaces, produisant ainsi

le déplacement du front de décomposition. La combustion de matériaux polymériques est complexe et concerne souvent des processus simultanés tels que la pyrolyse, la décomposition oxydative et le processus de combustion avec présence de flamme.

- L'échelle produit concerne des échantillons avec des masses proches d'un kilogramme. À cette échelle, la géométrie et le positionnement d'un produit ont un rôle fondamental dans la croissance du feu. La ventilation (la disponibilité d'oxygène et la turbulence) affecte également le processus de combustion. L'échelle produit montre le comportement au feu d'une mousse dans des conditions d'utilisation proches de celles de la réalité.

Les résultats obtenus dans cette recherche vérifient que le mécanisme de décomposition reste inchangé indépendamment de l'échelle. Dans la littérature, ces trois échelles n'ont jamais été considérées ensemble. Généralement, chaque échelle est considérée indépendamment et les chercheurs restent concentrés sur les phénomènes observés à l'échelle étudiée. De plus, les résultats de l'échelle matière sont souvent extrapolés à l'échelle produit. Toutefois, les phénomènes supplémentaires qui apparaissent entre une échelle et l'autre ne sont pas pris en compte, engendrant une grande incertitude dans la prédiction des résultats.

Cette recherche propose une contribution vis-à-vis de l'intégration verticale des résultats obtenus dans les trois échelles. L'intégration verticale signifie explorer la possibilité d'identifier quelles propriétés de la matière doivent être mesurées et fournies en tant que données d'entrée des codes de simulation incendie afin de pouvoir prédire la décomposition thermique des solides. Ces travaux constituent un pas dans une vision globale de la science des matériaux qui permettrait une prédiction très juste du comportement au feu des solides à diverses échelles tout en utilisant principalement des mesures menées à l'échelle matière et la petite échelle.

La cinétique de la décomposition a été étudié à la petite échelle grâce à des analyses thermogravimétriques (TGA). Cette technique a permis de mettre en évidence le nombre d'étapes, les espèces qui entrent en réaction et de détailler le mécanisme de réaction. En outre, des algorithmes génétiques ont été utilisés pour calculer les paramètres cinétiques optimum qui permettent de prédire le changement de la masse d'un échantillon en fonction de la température. Selon la démarche à échelle croissante décrite ci-dessus, les propriétés thermiques ainsi que les paramètres cinétiques de la

décomposition du PPUF ont été utilisés comme données d'entrée dans un code de simulation incendie. Les simulations ont été réalisées avec le code de calcul le plus amplement utilisé dans le monde, Fire Dynamics Simulator (FDS V 5.3).

Les simulations tentent de prédire le comportement du PPUF en cône calorimètre (petite échelle). Un faible calage entre les courbes de changement de la masse expérimentales et numériques a été observé. Une grande incertitude vis-à-vis de la façon d'introduire les données d'entrée a été identifiée ainsi que de leur interprétation. Des possibles voies d'amélioration des modèles de pyrolyse ont été proposées.

Acknowledgement

Contents

List of Figures

List of Tables

Nomenclature

Variables

A	Pre-exponential factor	[s^{-1}]
$Ab(\lambda)$	Absorbance in function of wavenumber	[-]
A_r	Area of the solid sample in CC	[m^2]
a_i	Slope of the straight line at irradiance level i	[-]
$a(\lambda)$	Molar absorptivity in function of wavenumber	[l·mol^{-1}·m^{-1}]
A_m	Amplitude of the modulation of a sinusoidal wave	[°C]
b_i	Y-intercept of the straight line at irradiance level i	[-]
c	Concentration of absorbing species	[mol·l^{-1}]
C	Orifice plate calibration constant	[kg$^{1/2}$·m$^{1/2}$·K$^{1/2}$]
c_p	Mass thermal capacity at constant pressure	[kJ·kg^{-1}·K^{-1}]
c_s	Solid material specific heat	[kJ·kg^{-1}·K^{-1}]
d	Thickness	[m]
E	Apparent activation energy	[kJ·mol^{-1}]
E_{O_2}	Heat of combustion per unit mass of oxygen consumed (13.1 in this work)	[MJ·kgO$_2$$^{-1}$]
EHC	Effective heat of combustion	[kJ·kg^{-1}]
h_c	Convective heat transfer coefficient	[W·m^{-2}·K^{-1}]
HRR	Heat release rate per unit area	[kW·m^{-2}]
IL	Irradiance level	[kW·m^{-2}]
k_s	Thermal conductivity	[W·m^{-1}·K^{-1}]
K_i	Solid mass fraction of the reaction i	[g·g^{-1}]
l	Path length of cell gas	[m]
m	Mass	[kg]
$\dot{m}_b$	Mass-flow rate of species b	[g·s^{-1}]
$\dot{m}_b''$	Mass flux of species b	[g·s^{-1}·m^{-2}]
$\dot{m}_e$	Mass flow rate at cone calorimeter exhaust duct	[kg·s^{-1}]
MLR	Mass Loss Rate	[g·s^{-1}]
MW_b	Molar mass of species b	[g·mol^{-1}]
n	Reaction order	[-]
P	Pressure	[atm]

P_{O_2}	Partial pressure of the oxygen	[Pa]
Q''_e	Incident irradiance level or heat flux by unit area	[kW·m^{-2}]
$Q_{f(r+c)}$	Incident heat from the flame (radiation and convection)	[kW·m^{-2}]
Q_{rr}	Reradiation heat losses	[kW·m^{-2}]
R	Universal constant of gases equal to 0.082	[l·atm·mol^{-1}·K^{-1}]
R_i^2	Least-square fitness factor	[-]
S	Shape index (Kissinger method)	[-]
SCP	Superior Calorific Power	[kJ·kg^{-1}]
$SMLR$	Specific mass-loss rate (per unit area)	[g·s^{-1}·m^{-2}]
T	Temperature	[°C] or [K]
T_e	Gas temperature at flow meter	[K]
$\dot{V}$	Volumetric flow in measurement apparatus	[l·s^{-1}]
$Vmol_b$	Volume of one mole of species b	[l·mol^{-1}]
W	Maximum weight in isothermal TGA tests (Norm.)	[-]
x	Distance	[m]
x_b^0	Initial concentration of species b	[ppm]
x_b	Volumetric concentration of species b	[ppm]
Y_b	Yield of the gaseous species b	[g·g^{-1}]
y_b	Mass fraction of species b	[g·g^{-1}]
Δp	Pressure difference across the orifice plate	[Pa]
ΔQ	Sensible heat	[kJ·kg^{-1}·K^{-1}]
ΔH	Enthalphy of the reaction	[kJ·kg^{-1}]

Greek symbols

α	Degree of conversion	[-]
β	Heating rate	[°C·min^{-1}]
Φ	Oxygen depletion factor	[-]
δ	Reaction order for oxygen mass fraction	[-]
λ	Wavelength	[m^{-1}]
ϕ	Fitness factor between curves	[-]
ρ	Density	[kg·m^{-3}]
υ_i	Stoichiometric coefficient of a solid or liquid product of reaction i	[-]
ω_i	Arrhenius reaction rate of reaction i	[s^{-1}]
ψ	Scale factor	[-]

Subscripts

b	Generic gaseous chemical compound (Yield)
blank	Blank (DSC)
cal	Calibration (Sample)
f	Final (mass)
g	Gas
i	Reaction index or irradiance level
m	Reference temperature of DTA deflection (Kissinger method)
mod	Modulation of temperature (Mamleev method)
qlt	Qualitative (FTIR)
qnt	Quantitative (FTIR)
s	Limit of conversion (isothermal TGA tests) or surface
sp	Sample
t	At a time t
us	Unburnt solid
v	Apparent solution in the IKP method
0	Initial (mass)

Abbreviations

CC	Cone Calorimeter
CFD	Computational Fluid Dynamics
DSC	Power Compensation Differential Scanning Calorimetry
DAT	Diamino Toluene
DTG	Differential Thermogravimetry
EVA	Ethylene-vinil acetate
FID	Flame Ionisation Detector
FTIR	Fourier Transform Infrared Spectroscopy Analysis
FTIR-ATR	FTIR - Attenuated Total Reflectance
FSE	Fire Safety Engineering
GC/MS	Gas Chromatography/Mass Spectrometry
GPC	Gel Permeation Chromatography
HPLC	High Performance Liquid Chromatography
IKP	Invariant Kinetic Parameters method
LC/MS	Liquid Chromatography/Mass Spectrometry
LNE	Laboratoire national métrologie et d'éssais, France
LP-FTIR	Laser Pyrolysis-FTIR
MDI	Diphenylmethane p,p'-diisocyanate
MALDI-MS	Matrix Assisted Laser Desorption/Ionisation Mass Spectrometry
NIST	National Institute of Standards and Technology – USA
NMR	Nuclear Magnetic Resonance
ND-IR	Non Dispersive Infrared Analysis

ODE	Ordinary Differential Equations
PAH	Polycyclic Aromatic Hydrocarbon
PBD	Performance-Based Design of Buildings
PE	Polyethylene
PMMA	Polymethylmethacrylate
PPUF	Polyether Polyurethane Foam
PU	Polyurethane
Py-GC/MS	Pyrolysis Gas Chromatography/Mass Spectrometry
SCA	Service central d'analyse – CNRS, France
SEM	Scanning Electron Microscopy
SFPE	Society of Fire Protection Engineers – USA
SwRI	Southwest Research Institute (SwRI) – USA
TDI	Toluene diisocyanate
TF	Tubular furnace
TGA	Thermogravimetric Analysis
THC	Total Hydrocarbons
WPI	Worcester Polytechnic Institute – USA
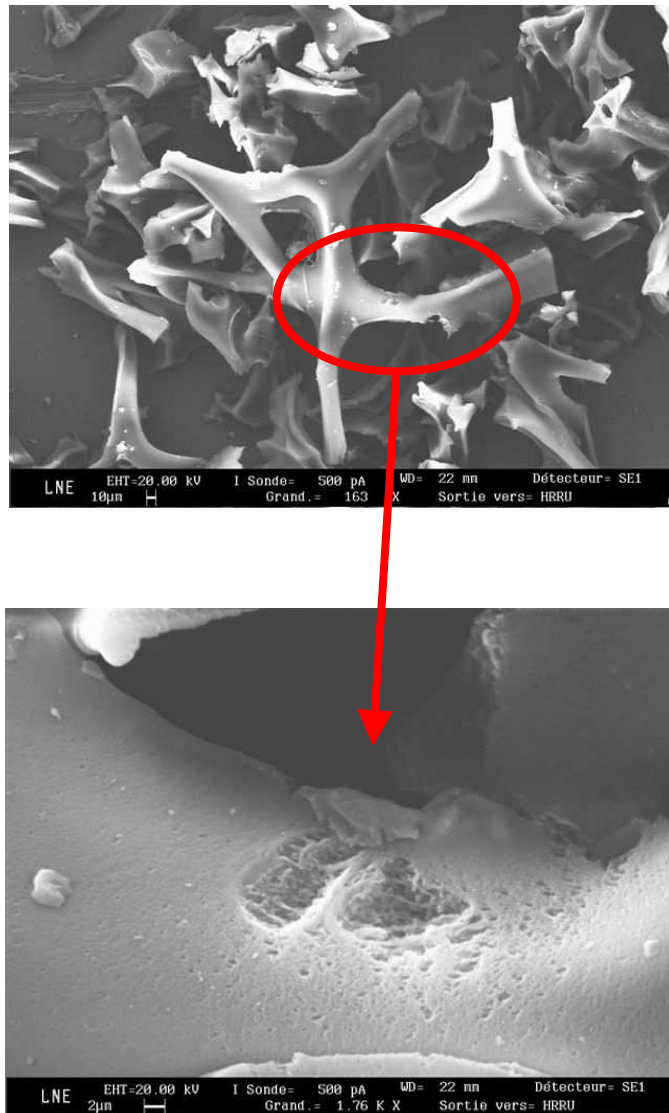
Example of the surface defaults caused in the main branches of polyether polyurethane foam by the increase of temperature up to 500°C und er air atmosphere.

1 General introduction

The improvement of fire safety in dwellings is a main concern for research teams around the world. According to data reported to DG Sanco by 14 Member States of the European Union and Norway from 2005 to 2007, accidental ignition caused by cigarettes in dwelling houses is at the origin of 11 000 fires every year, with 520 deaths, 1 600 injuries and 14 million € in material damage, for a population of about 160 million people [1][2]. A great number of fires are also produced every year by other multiple causes than cigarette. They are responsible for the loss of human lives, damages to structures and pollution to the environment. According to the Fire Statistics Report 2006 [3], in the UK in 2006, the fire services attended 862 100 fires or false alarms. There were 491 deaths caused by fire. The distribution of the deceases causes are: 40% intoxication by smoke inhalation, 21% by smoke inhalation and burning and 23% by burnings.

Many countries in Europe have a very poor legislation on fire protection in dwellings. Historically, buildings have been designed following prescriptive guidelines of handbooks. The trend in Fire Safety Engineering (FSE) has been changing during the last decade: fire research groups have developed the principles of the building Performance-Based Design (PBD) allowing new options to the prescriptive approach. The PBD of FSE is a methodology that has been initially developed for buildings destinated to the affluence of public. However, this approach has begin to be used for appartament buildings.

The PBD is based on the very near prediction of fire growth in various scenarios, which means the understanding of a great number of phenomena such as: the flame height, the heat transfer from the fire source to the structure, the fire propagation to the furniture, the fire behaviour of materials, the flashover and explosion risk, the displacement of the smoke stream, the rate of production of toxic gases, the evacuation of inhabitants, the improvement of the effectiveness of fire alarms, the fire fighters intervention, etc. In this complicated analysis process, the fire simulation has

become an essential tool, it allows improving the understanding of the key phenomena that contribute to the reduction of the hazards.

The heat release rate (HRR) is the magnitude used to measure the intensity of fire. In the engineering field, the HRR is required in order to estimate the possible damages caused by fire in a given scenario. The release of heat is only possible if the four components of the "fire tetrahedron" are present at the same time in a given place: gas combustible, reaction kinetics, oxygen, and a heat source. The analysis of gas fuel production and transport phenomena towards the flame has a primary role in the combustion process. It represents the source term in the global energy balance of the oxidization reaction. The source term is the potential chemical energy that can be converted into heat.

Many experimental studies are centered on the measurement of HRR, but they do not help improving the knowledge of the physics of the decomposition process. An accurate predition of HRR requires a huge understanding of the species production, the release of toxic gases and the chemistry of the process. This study deals with the chemistry of the decomposition process: the changes of the solid phase are analysed together with the ones of the solid phase (release of gas species).

In a very simplified manner, the combustion and the rate of solid decomposition of non-charring materials constitute an auto-catalytic process: the heat produced by the flame increases the irradiation level towards the solid, and the increase of irradiance level increases the rate of thermal decomposition of the solid. This loop simultaneously increases the reaction rate and the intensity of the flame allowing the fire growth. It is repeated until the complete depletion of the solid fuel. The fire growth is also affected by the external heat losses and the heat losses inside the solid matrix. This research covers all the aspects that affect the decomposition rate.

The production of gas fuel molecules is caused by the thermal decomposition of the solid. Thermal decomposition is "a process of extensive chemical species change caused by heat" [4]. Once it has occurred, the raw material cannot be obtained any more, the structure of matter has been definitively damaged. The major concern about thermal decomposition and fire safety engineering is the release of gas species and their successive combustion. However, effects such as dripping, leak and flow have also been studied because they represent a hazard of displacement of the flaming front through zones that are not involved in the initial fire.

Thermal decomposition was studied at the end of the 19th century by chemists during works on heterogeneous reactions in applications other than fire. The interest of scientists and fire researchers in the problem of how a solid becomes a potentially combustible gas has greatly increased in the last 20 years. This interest has been particularly motivated by the need of quantification of the source term of numerical simulations and by the increase of calculation capacities. The accurate prediction of the source term can only be attained by the very precise knowledge of the physics and the chemistry of the decomposition process. It other words, the pyrolysis products are combustible compounds with high chemical energy that are converted into heat in the flame region. Thus, the prediction of the fire growth requires the quantification of the dynamics of the solid fuel.

Since the first works on thermal decomposition, the main parameter used in order to characterise the process is the change of sample mass with temperature or time. These researches allowed the development of models and the calculation of reaction parameters. Unfortunately, the single data on mass change does not allow unambiguous determination of the decomposition mechanism.

Other researchers have analysed the decomposition mechanism according to the species identified in the gas stream released by the sample pyrolysis or combustion. A wide range of sophisticated analytical methods has been used to analyse the effluents. However, most of these laboratory results are useless in the field of fire safety, since the vast majority of the species identified are impossible to detect by analytical techniques at larger scales. Very few works have considered together the change of mass and gas release kinetics in function of time and temperature. The simultaneous analysis of data from solid and gas phases provide valuable information on the decomposition mechanism of solids.

The accurate determination of the decomposition mechanism is a primary task in thermal analysis. This mechanism accounts for the successive transformations of the matter that takes place during the gasification of solids. This succession includes virgin and thermally attacked samples. The decomposition mechanism is one of the main input data in a vast majority of thermal decomposition models.

This research analyses the decomposition mechanism of Polyether Polyurethane Foam (PPUF) at three different scales. Each scale characterises the fire behaviour of a given mass of foam and is centred in particular phenomena:

- The matter scale analyses the behavior of samples with masses near to one milligram. At the matter scale, the effects of heat and species transfer are minimized and the effect of the increase of temperature of the solid can be studied accurately. The sample is considered as a particle with negligible mass and dimensions. It is also accepted that the particle has an homogeneous temperature.

- The small scale analyses samples with masses around ten grams. At the matter scale, important gradients of heat and species exist. The sample is irradiated only by one of the surfaces producing the displacement of the decomposition front. The combustion of polymeric materials is complex and often involves simultaneous pyrolysis, oxidative degradation and flaming combustion processes [5].

- The product scale considers samples with masses around one kilogram. At this scale, the geometry and the positioning of the product have a prime role in the fire growth. The ventilation (oxygen availability and turbulence phenomena) affects the combustion process as well. The real product analysis shows the fire behaviour of the foam in real conditions of use.

Figure 1-1 presents the methodology of the multi-scale study performed in this thesis. The knowledge acquired at the small scale is used to understand the behaviour at the largest scale.
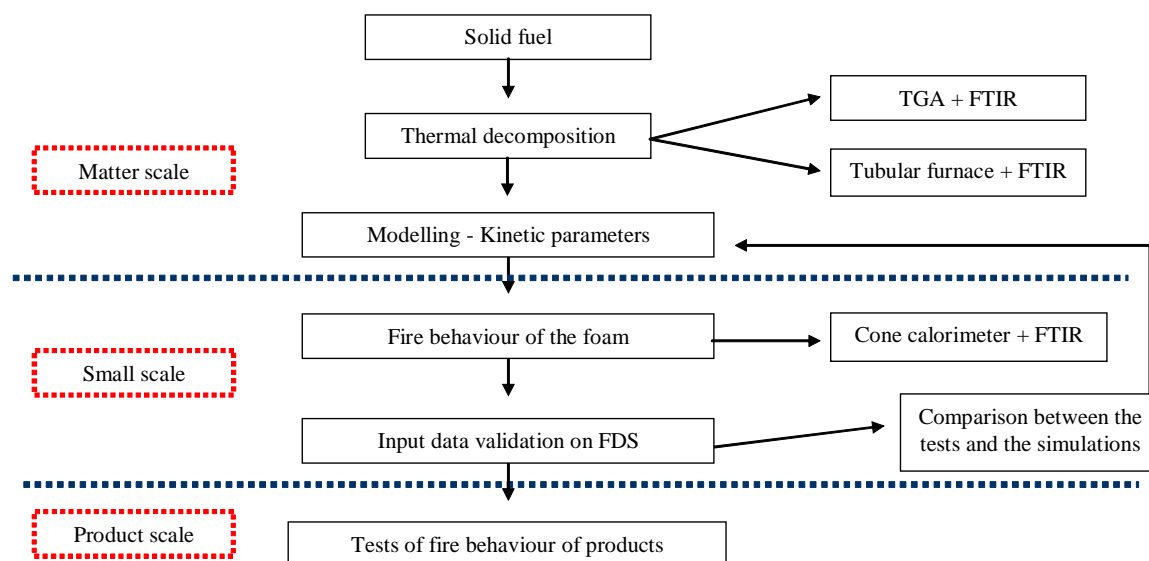
Figure 1-1 Methodology of the multi-scale investigation of the fire behaviour of polyether polyurethane foam presented in this dissertation.

The results obtained in this research verify that the decomposition mechanism remains unchanged independently of the scale. However, the number of peaks of the mass-loss rate curve (stages of decomposition) that can be identified at the matter scale is different from the number of stages that can be observed in the small and product scale. In literature, these three scales have never been considered together. Generally, each scale is considered independently and the researches remain centered on the phenomenon observed at the considered scale. The results from the matter scale are often extrapolated to the real product scale without further consideration about the phenomena controlling the process at each independent scale; a great uncertainty is introduced in the prediction results.

This research proposes a contribution to the vertical integration of the results obtained at the three scales. Vertical integration means exploring the possibility to identify which matter properties must be measured and provided as input data to fire simulation codes in order to accurately reproduce the thermal decomposition of solids. This work is a step in the vision of the science of materials that would enable a reliable prediction of the fire behaviour at the large scale based mainly in measurement carried out at the matter and small scales.

The total production of polyurethane in Western Europe was about 3.7 million tons in 2007 and will represent 4.1 millions tons in 2012. In 2007, the distribution of the applications of polyurethane was: 29% rigid foam, 37% flexible foam, 12% elastomers

and 12% coatings. From the proportion of flexible foams, 1.5 million tons represented slab stock and 0.5 million tons corresponded to molded foams [6][7]. PU refuses represent around 6% of the total plastic waste produced in Western Europe [8].

Flexible PU foams are mainly found in upholstered furniture [9], bedding and carpet underlay for home or office; semi flexible PU foams are used in motor vehicles; rigid PU foams mainly in buildings and insulated appliances such as refrigerator cabinets, deep freeze panels, tank and pipe insulation, sandwich panels, acoustical insulation, etc [10][11].

The main application of flexible non-flame-retarded PPUF, such as the one used in this research, is in upholstered furniture for dwelling houses, offices and seats for vehicles [4]. This type of foam is commonly used in France, Italy, Spain, Portugal and several countries in Latin America among others [12] in which legislation does not require yet flame-retarded furniture materials.

Polyurethanes are largely produced worldwide, are involved in numerous fires [5], have a high flammability and their effluents have very high toxicity (such as NH_3, NO, H_2CO, CO, CO_2, etc), so, polyurethane is a major concern in fire safety.

This thesis is divided into six chapters. Chapter 2 deals with matter scale tests. The first section of the chapter presents the state of the art of the techniques used to analyse the decomposition of a solid, including analytical techniques for solids and gases. The second section presents the results obtained in this research that allowed measuring the thermal properties and highlighting the decomposition mechanism of the foam.

Chapter 3 deals with matter scale modelling. The first section of this chapter presents a literature review of the methods used to model the thermal decomposition of solids and to calculate the kinetic constants. It includes the development of the model used in this research. The improvement carried out to the model allows calculating the kinetic parameters that enables the prediction of the mass-loss rate as well as the gas release in function of the temperature. The last section of the chapter is centered on the analysis of the code stability and sensitivity.

Chapter 4 has four main parts. The first part presents the experimental facility used to determine the fire behaviour of PPUF: cone calorimeter coupled with gas analysers.

The second part presents the experimental results of mass-loss rate and gas release. The change in mass and gas release is used to analyse the decomposition mechanism and to calculate the yield of the main species released. This analysis allows verifying that the decomposition mechanism remains unchanged in comparison to the results obtained at the small scale. The third part presents the numerical simulation of the cone calorimeter experiments. The input data for the fire simulation are those obtained at the matter scale (Chapters 2 and 3). The fourth part presents the experimental results obtained at the real product scale: heat release rate, mass-loss rate and yield of gas release of a simplified seat.

In Chapter 5 are discussed particular aspects of the experiments and calculations carried out. This discussion is the key to understand the fitting between the experiments and the simulations.

Chapter 6 are the general conclusion and future works.

2 Matter scale experiments

2.1 Introduction

The analyses carried out at the matter scale comprise masses between 1 mg and 110 mg of PPUF. These correspond respectively to the masses used in thermogravimetric analysis (TGA) and in tubular furnace (TF). These are the smallest masses considered in this research. The samples used in the analysis at the matter scale are called particles along the chapter. A particle denotes a small amount of mass and consequently a very small geometric dimension. In comparison to the volume and masses of foam used in real applications such upholstered furniture, the samples are negligible. The alveolar nature of the foam also contributes to this assumption while the effective area of heat and gas exchange is big compared to the size of the sample, thus the effect of gradients of temperature and especies concentration can be neglected. Moreover, this approach can be chosen because PPUF has an isotropic structure: The main branches are distributed randomly in the three dimensions but are short compared to the sample size. The interest of analysing such small masses is to reduce as much as possible uncertainties due to [13]:

- Thermal gradient between surface and centre of the particle

- Solid phase diffusion effects

- Aerodynamics of gaseous phase around the particle

- Heat transfer with environment

- Oxygen diffusion from the surface toward the centre of the particle

- Etc.

These simplifications allow to hypothesising that the behaviour observed in measurement instruments is caused mainly by the mechanism of decomposition and is very little influenced by external noise. Thus, the temperature and especies concentration particularly O_2 can be considered homogeneous all around the particle.

The aim of this chapter is to present the experimental devices and the results obtained at the matter scale. This experimental data is fundamental to understand the chemical and physical processes that take place during the thermal attack of the foam. The succession of stages of chemical and physical changes constitutes the decomposition mechanism of matter. According to the experiment carried out, the velocity at which the reactions take place can change. The velocity of reaction is called in this document "kinetics of reaction".

As shown along this chapter, the contribution of this work consists in considering experimentally the effect of the increase of temperature in the transformations induced in solid and gas phases. These transformations are studied at various heating rates and atmospheres. Considering various experimental conditions allows verifying if the decomposition mechanism is affected by the environmental conditions.

The data reported in this chapter represent input data to the model developed in chapter 3. The understanding of the decomposition mechanism obtained at the smallest scale showed to be of great interest to understand the experimental results obtained in cone calorimeter (see section 4.3). This data also represent the input data to the computational fluid dynamics simulations (CFD) presented in section 4.4. Information from the matter scale is also useful while analysing the behaviour of the foam in larger scale fire. This was verified by the test of a simplified seat presented in section 4.5.

The need of studying the decomposition of PPUF is to improve our hability to predict the transformation of the virgin solid into flammable and toxic gases. The detail of the chemistry and the physics of the process need to be taken into account.

2.2 State of the art in matter scale measurements

The present research deals with the thermal decomposition of solids. The phenomena occurring during thermal decomposition are of primary interest in fire safety engineering since the rate of thermal decomposition controls fire growth, spread velocity, release of toxic gases, dripping, production of liquid by-products, fire propagation, etc. As presented in the introduction, thermal decomposition concerns the changes in the chemical structure caused by heat. This research also deals with the thermal degradation of foam. Thermal degradation and thermal decomposition are different concepts, although these two terms are often considered as synonyms in literature (*e.g.* Ref. [14][15][16][17][18][19]). Thermal degradation is "a process whereby the action of heat or elevated temperature on a material, product, or assembly causes a loss of physical, mechanical, or electrical properties" [4]. The thermal degradation is mostly related to materials' applications. The thermal degradation is taken into account in this research because thermal properties are measured in function of temperature. Changes in thermal properties with temperature highly influences the heat transfer into the particle and the heat and mass transfer towards environment.

The thermal decomposition mechanism of solids has been typically studied using only the curve of mass-loss rate. The curves of mass-loss rate are obtained by registering the mass of a small sample in function of temperature. Nevertheless, the information that can be obtained is very limited. Multiple hypothetical kinetic mechanisms can fit very well the shape of the mass-loss rate *vs* temperature. It does not allow the assessment of a single kinetic mechanism. The analysis of gas effluents provides valuable information because:

a) It provides further information about the bulk chemical reactions taking place in the solid.

b) It allows the correlation of the mass change stages to the corresponding chemical reactions.

c) It allows the assessment of one kinetic mechanism. This mechanism can be considered as chemically correct because it takes into account the chemistry of the process.

d) It allows understanding the change of toxic compounds released with time or temperature as well as the calculation of yields [18]. Yields constitute the basis of comparison when interpolating results of gas species from bench-scale to full-scale tests [20].

The state of the art in matter scale measurements is focused on listing the mechanisms of polyurethane (PU) decomposition found in literature and the experimental methods that the authors used at this typical scale. Because of the widespread range of polyurethane formulations and applications, data from authors concern various products such as flexible foam, rigid foam and solid polyurethane. Nevertheless, in most cases, the decomposition mechanism remains unchanged.

2.2.1 Characteristics of polyurethane molecule

The urethane molecules have been discovered at the end of the 19th century. But it was Otto Bayer in 1937 [9] who discovered the polyaddition procedure that allowed the production of polyurethanes. His findings gave the structure and properties that made PU the very useful plastic used nowadays. The main reaction is the conversion of polyisocyanates with polyhydroxyl combinations to produce a covalent bond of polyurethane [21]. Polyaddition reaction is presented in Eq. (2-1) [22]:

$$n \underbrace{OCN\text{-}R\text{-}NCO}_{Polyisocyanate} + n \underbrace{HO\text{-}R'\text{-}HO}_{Polyol} \longrightarrow \underbrace{(R\text{-}NHCOO\text{-}R'\text{-}NHCOO)}_{Polyurethane}{}_n \qquad (2\text{-}1)$$
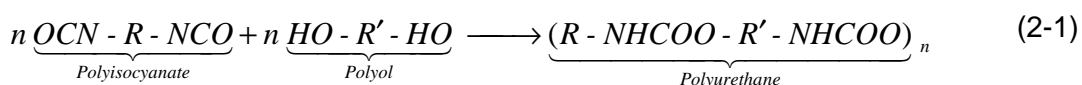
Where, R' is typically a polyester or a polyether chain. Additionally water or amines may be added as chain extenders [23].

Polyethers and polyesters are used as the preferable polyhydroxyl compound (alcohols that usually are not toxics). They constitute the "base resin" [8]. Depending on the functionality of polyol (molar weight, reactivity, viscosity, etc) different PU can be obtained. The change of the formulation allows controlling the characteristics of the

product according to the design requirements [10][18][24]. However, it influences as well the kinetic of thermal decomposition [25] and indirectly the fire behaviour.

Polyisocianates present highly polarised double bonds $R\text{-}N=C=O$ that react with hydrogenated compounds (alcohols); it constitutes the "catalyst" to reaction. The tolylene-diisocyanate (TDI) and diphenylmethane p,p'-diisocyanate (MDI) are the most commonly used compounds within the group of isocyanates. TDI is mainly used in flexible foam production and MDI in rigid polyurethane production [8][9][26][27]. Contrary to polyols, isocyanates require highly secured manipulations techniques because they are highly toxic [18], volatile and extremely reactive with water.

Formulations of common PU referenced in literature contains a wide range of isocyanate mass fraction from 8% up to 35% for TDI based PU and from 12% to 22% when based on MDI [22]. Selection of reactants allow controlling properties such as density, resistance to compression strain comfort, resistance to fatigue, resistance to linear traction, thermal resistance, thermal conductivity, reaction to fire, chemical inertia, etc [8]. Molecular weight of polymers is one of the principal characteristics that dictates the final properties. Additives, impurities and other compounds added to the matrix may largely modify the polymer chain structures and with it, the properties [28].

2.2.2 Generalities about the thermal decomposition of polyurethane

Polymers can be classified in a huge variety of forms depending on particular properties. All these possible classifications are the matter of interest here, and are therefore not detailed. For fire engineering applications, PU is considered as a thermoset plastic. When heated abroad a certain temperature, long chains of polymer are broken down into small molecules that are volatilized [4]; this process occurs without any change of state (melting or vaporisation). The breakdown mechanisms are typically divided into two groups: pyrolysis and oxidative decomposition. Pyrolysis is the irreversible chemical scission without oxygen availability. Oxidative decomposition is the scission occurring in the presence of oxygen from air [27][29].

Notling was the first to report the thermolysis of urethanes bounds in 1888 [30]. His works had to do with the destruction of the urethane molecule, since the polyurethane

had not already been discovered. Later, between 1929 and 1961, a number of papers were published which generally agreed that the initial thermal urethane breakdown occurs by combination of three independent mechanisms [18][21][30][31][32]:

1) dissociation to isocyanate and polyol

$$R - N(H) - C(=O) - O - R' \longrightarrow R - N = C = O \ + \ OH - R'$$
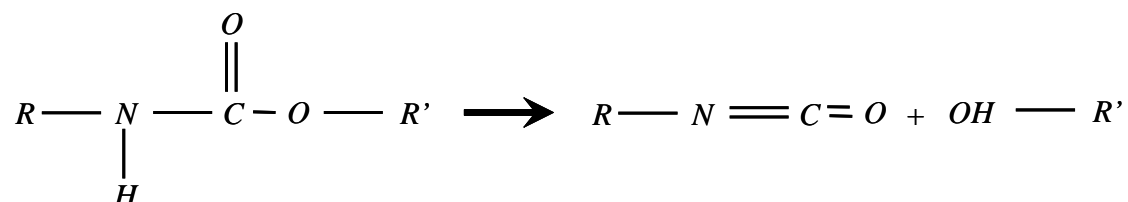
2) dissociation to primary amine, olefin and carbon dioxide

$$R - N(H) - C(=O) - O - CH_2 - CH_2 - R' \longrightarrow R - NH_2 + CO_2 + CH_2 = CH - R'$$
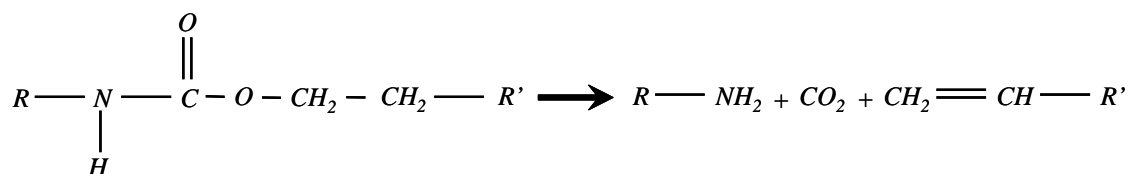
3) elimination of carbon dioxide, leading to formation of a secondary amine

$$R - N(H) - C(=O) - O - R' \longrightarrow R - N(H) - R' + CO_2$$
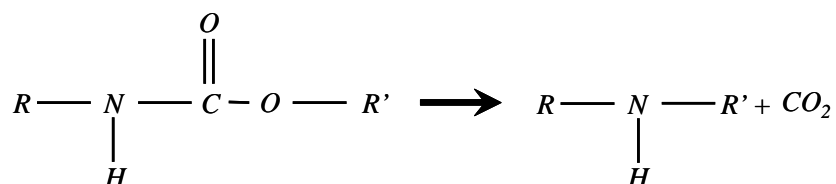
However, the description of large-scale material decomposition according to these reactions is not practical. During a fire, all of these reactions take place at the same time. Moreover, lack of knowledge makes this theoretical approach useless [33]. Thus, the analysis of the global kinetics of reactions is carried out using semi-mechanistic methods [9]. The semi-mechanistic methods are centred on the prediction of the bulk transformations suffered by the particle, but they do not allow gaining information about the phenomenon taking place at the main branches. Arrhenius equations are usually used to express the reaction rates in such methods.

The characterisation of gas products have been largely performed by conventional chemistry analytical techniques such as bubbling combined to High Performance Liquid Chromatography (HPLC) or Gas Chromatography/Mass Spectrometry (GC/MS). More

sophisticated systems such as Pyrolysis Gas Chromatography/Mass Spectrometry (Py-GC/MS) have also been used, in which pyrolysis is performed directly into the gas measurement apparatus. Various authors have combined these techniques in order to carry out analyses concerning particular groups of compounds. Some findings that clarify thermal processes are presented here after.

In 1976, Fabris [34] stated that urethanes containing primary and secondary alcohols start to decompose very slowly at temperatures between 150 °C and 200 °C. The decomposition proceeds at a measurable rate between 200 °C and 250 °C. In the temperature range of 200 °C and 300 °C, there is a rapid and complete loss of TDI [35] or MDI units [21], remaining a polyol residue. The characteristic yellow smoke formed during the process was not analysed. Rogers *et al.* [23] detailed more the chemistry of the process in 1981. They showed that the urethane is the most thermo-labile bond of PU (*i.e.* lower bounding energy [36]). The break up of the urethane urea blocks lead to the collapse of the cellular structure. At higher temperatures, the more stable polyol segments are fragmented. The yellow smoke released at temperatures between 200 °C to 300 °C is a TDI propylene oxide polymer. However, some TDI is retained during carbodiimide formation at the semi-liquid phase [23].

According to Saunders *et al.* [37] (1961), PU decomposition to amines and olefins is favoured when the corresponding alcohol is easily dehydrated (*e.g.* tertiary alcohols). Bilbao *et al.* [11] verified that PU decomposition gives rise to its original compounds (diisocyanates and polyols). Because of the breakage of the polymeric chain, amines, olefins and carbon dioxide are created. When the temperature reaches 300 °C, the PU decomposition is completed; polyol is decomposed at around 290 °C. The diisocyanate created during the first stage of decomposition may form carbodiimide that decomposes and vaporises at around 320 °C.

2.2.3 Determination of the polyurethane decomposition mechanism based on the analysis of the gas effluents.

Ohtani *et al.* [22] studied nine PU based on TDI, MDI and hexamethylene diisocyanate. Analytical technique was Py-GC/MS using a thermally stable fused-silica capillary column. Pyrolysis temperature was set to 600 °C. The gas carrier was nitrogen. Up to 41 organic pyrolysis products were identified, corresponding to the volatilisation of PU

raw products and repolymerisation compounds. Because of the absence of oxygen in the gas stream, combustion gases such CO and CO_2 were not observed.

Under current experimental conditions, urethane linkage in the polymer chain predominantly cleaves through a reaction that produces isocyanate terminal groups and hydroxyl terminal groups. Increasing carrier gas flow from 50 ml·min^{-1} to 200 ml·min^{-1}, the authors evidenced that the liberated isocyanate (MDI) undergoes secondary reaction in gas phase (in the hot zone). This is characterized by an incomplete diisocyanate recovery comparing pyrogram to chromatogram mass measurements. Authors also stated that fragments from the polyol moiety decompose to produce less volatile products. Polyol segments degrade as presented in Eq. (2-2) [22].

$$HOROCOR' \sim \longrightarrow THF, HO \ or \ VC + HOCOR' \sim \qquad (2\text{-}2)$$

$$R' = (CH_2)_4, (CH_2)_6 \ or \ (CH_2)_2 O(CH_2)_2$$
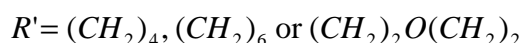
Where, THF is tetrahydrofuran and VC is vinil-cellosolve. Hydrolysis, followed by various chromatographic separations and/or spectroscopic determinations, has been used for elucidation of the chemical components of PU. However, these methods not only involve time-consuming procedures but also provide limited structural information on the polymers [22].

Hileman *et al.* [5] in 1975 carried out an interesting study of the decomposition of flexible PU using a pyrolyser and setting the temperature between 300 ℃ and 1000 ℃ in helium or argon atmosphere. The pyrolysates were analysed using a gas chromatograph set out with two detectors: thermal conductivity detector and flame ionisation detector. About 30 different gases were identified. They observed, by analysing independently PU and the raw chemicals, that the pyrolysis products of urethane can be obtained by combining the pyrolysis products of the individual constituents. Thus, lightweight hydrocarbons (CH_4, C_2H_6, etc.) result from the decomposition of TDI, polyol and urethane. In contrast, CO_2 appears to come mainly from the decomposition of TDI and urethane, since little or no CO_2 is detected from the pyrolysis of the polyol. Oxygen containing compounds such as aldehydes and ketones results from the decomposition of polyol and urethane. Nitrogen containing compounds

result from the decomposition of urethane and TDI. This analysis was carried out in a qualitative manner, no transformation yields of the different products were reported.

The authors also analysed a crystallised portion of the residue during pyrolysis process. A higher nitrogen content was found compared to virgin PU. The high nitrogen content of residue points out that the nitrogen is being concentrated in the residue during the pyrolysis process. The yellow crystals were also pyrolysed, residues were comparable to the original urethane. This suggests that the yellow crystals were small molecular weight pieces of the original foam. In their paper [5], the authors do not discuss how it is possible that the solid phase of yellow crystals contains more nitrogen, but that their gaseous residues are comparable to the original urethane ones.

Voorhees *et al.* [30] in 1978 developed a methodology for in-depth product analysis by GC/MS to study the thermal decomposition of the polyol portion after breakdown of the PU bounds. Chemical analyses allowed identification of up to 50 chemical compounds released during pyrolysis. They observed that as the pyrolysis temperature increased, the percentage of char residue was reduced while the percentage of volatiles increased significantly. The authors proposed a complete decomposition mechanism for PU. They highlighted that a major fraction of the polyol decomposes by a systematic sequence of reaction rather than by random fracture.

Ravey *et al.* [38] and Ketata *et al.* [18] studied the pyrolysis of a commercial PU foam based on polyether. In the first decomposition stage, the foam collapses to a liquid losing one third of its weight as volatile decomposition products. The composition of the products depends on the condition of the pyrolysis and the nature of the substituents on the nitrogen and oxygen atoms. If the volatiles were rapidly removed from the system, they would contain TDI. However, under defined conditions, the TDI would be replaced by diamino toluene (DAT). They showed that during pyrolysis, the urea groups in the foam dissociate into TDI and DAT. These products would recombine in the vapour phase to form an aerosol of polyurea. This aerosol is the yellow smoke reported in the literature, and therefore it is not a condensate or polymer of TDI as was proposed by other authors (*e.g.* Rogers *et al.* [23]).

Many references claim that TDI is a major decomposition product of PU, nevertheless quantification of this chemical component showed that only a low fraction was recovered. Pyrolysis residues are very similar to source TDI and polyol, however not

identical. In addition, the released TDI undergoes a secondary reaction in the pyrolysis zone.

Ravey's research was carried out using a large panoply of instruments such as TGA, capillary tube pyrolysis, in-line pyrolysis-GC, glass tube pyrolysis, GC/MS, etc. The key of their experiments consists in maintaining a constant temperature of 340 ℃ while varying the total time of pyrolysis. There has been a vast debate on the kinetics of the transformation of nitrogen. Above a weight loss of 35% of the virgin PU sample, a maximum nitrogen loss is reached of about 96% during TDI gasification. However, the few reported attempts to recover the released TDI, results under nitrogen recoveries of 2% and less. The authors analysed the residues of PU pyrolysis which are composed of solid and semi-liquid portions: TGA tests combined with elementary analysis showed that the solid black portion contains a higher proportion of nitrogen than the virgin PU molecule. On the other hand, the semi-liquid is soluble in alcohol while the solid is not. This research highlighted the difficulty to recover the nitrogen contained in the solid matrix as well as to prove the process of nitrogen transformation during the solid decomposition.

Rotival *et al.* [39] studied thermal decomposition of a polyurethane adhesive by TGA at a Heating Rate (β) of 5 ℃·min^{-1} under air. Gases released in the two decomposition steps were collected by bubbling and solutions were analysed by HPLC. Authors find that the yield of formed carbon dioxide is higher in the second decomposition step than in the first one. Therefore, in the second zone, less carbon monoxide is released. This is in opposition to the observations of Hileman *et al.* [5]. The measured nitrogen compounds were HCN and isocyanate; nitrogen balance shows that only 1% of total nitrogen contained in sample was found in gaseous products.

Yang *et al.* [21] used DSC and Gel Permeation Chromatography (GPC) to study the thermal decomposition of monodisperse urethane based on MDI/butanediol. They found that polymerization as well as depolymerization occurs through the recombination of the dissociated segments, so that an original monodisperse sample is converted to one with a broad molecular weight distribution. They used an interesting technique to study the decomposition of PU in solid phase with FTIR: A thin polymer film was cast in a NaCl plate. The plate was placed in a temperature-controlled cell from room temperature up to 260 ℃. FTIR beam shots were carried out at 10 ℃ intervals; traces of free isocyanate become detectable as temperature increases.

46

Zhang *et al.* [31] studied two PU, the first one based on isophorone diisocyanate of stoichiometric formula $C_1H_{1.67}O_{0.34}N_{0.08}$ and the second one base on Toluene diisocyanate (TDI). Around 20 different gases were identified with Pyrolysis Gas Chromatography/Mass Spectrometry (Py-GC/MS) at ten different pyrolysis temperatures ranging from 250 °C to 700 °C in helium atmosphere. In this analytical technique, thermal decomposition was carried out inside the mass spectrometer during 6 s. For both PU, the authors classified chemical compounds in three groups, each one released by a particular reaction: 1) solvents and additives; 2) primary scission of the urethane linkages and the ester bonds; 3) thermal degradation of polyether-polyol, followed by dehydration, hydrogen transfer and ester exchange reactions. This classification means that the catalyst used during PU production may change the yield of gases. Authors found that pyrolysates distribution of PU depends strongly on the pyrolysis temperature. However, the mechanism of CO_2 production could not be clarified according to experimental results.

Gaboriaud *et al.* [40] studied the thermal decomposition of polyurethane based on MDI and propoxylated trimethylol propane. A sample was pyrolysed at 600 °C in a helium stream. Pyrolysis gases were analysed using a GC/MS with two detectors, flame ionisation and thermal conductivity. Their results pointed out that the first step of the decomposition process is the break-down into polyol and isocyanate. Polyol decomposed at relative low temperature producing various volatile species. The MDI vaporised and condensed at 200 °C, undergoing more or less extended polymerization. This kinetic mechanism is opposed to the one observed by other authors [5][21][30][41], in which polyol is more thermally stable and remains in the holder as semi-liquid residue.

Lattimer *et al.* [32] studied the gases and the solid residue from pyrolysis of a PU consisting of MDI, poly(butylenes adipate) and 1,4-butanediol. Pyrolysis was carried out under argon flow at temperatures ranging from 250 °C to 325 °C. Gases were analysed by GC. The solid residue in the pyrolysis tube was analysed by Matrix-Assisted Laser Desorption/Ionisation Mass Spectrometry (MALDI-MS). At lower temperatures (up to 250 °C), the products of pyrolysis were explained by two principal mechanisms: The first the is dissociation of the urethane linkage (by depolimerization) releasing isocyanate and hydroxyl end groups; the second is the ester exchange producing cyclic pyrolyzate oligomers. However, their results suggest that nitrogen-containing series have essentially disappeared at 300 °C. At temperatures above

300 °C, dehydration occurs to yield products with unsaturated end groups, although this mechanism has not been widely studied. The results of their work are in agreement with results from Rotival *et al.* [39].

These analytical pyrolytic techniques are readily applicable even to intractable polymers. However, it is often difficult for the former technique to discriminate whether the fragments of interest are formed through thermal decomposition or mass spectral fragmentation during the ionisation processes, except for the very soft ionisation methods [22].

This subsection presented multiple analytical techniques reported in literature to determine the composition of effluents produced during the decomposition of PU. Authors used the information of gas release to determine the reactions taking place in the solid phase and sense the decomposition mechanism of PU. However, the analysis of gases remains a tricky task and provides limited information on how heat affects the PU molecules and on the induced reactions.

As presented, the complete recovery of sample mass according to the mass measurement of gas effluents cannot be performed successfully. Because of the limitation of the gas analytical techniques, the study conducted in the present research was focused on the identification of the main gases. The main gases are the result of a combination of heterogeneous and homogeneous reactions. Thus, the composition of main gases can change with residence time and with reactions occurring with oxygen. Table 2-3 presents a summary of the main researches carried out to determine the decomposition mechanism of PU. These findings of many authors have been allowed by the analysis of the solid and gaseous residues by using multiple analytical facilities.

The next subsection describes the use of tubular furnace in FSE; further subsections describe the test protocol used to improve the accuracy of the gas measurements.

2.2.4 Use of tubular furnace in the determination of the decomposition mechanism of materials.

The Tubular Furnace (TF) is a primordial instrument used in this research. It is used to analyse the gas release and to calculate the yield of the main exhaust gases. This

subsection reports on the few researches found in which the tubular furnace was used to analyse the decomposition mechanism of materials. Unfortunately, the researches cited here-after did not take into account polyurethane only but various materials; they are not specific to the French tubular furnace but also the to Purser tubular furnace.

Esperanza *et al.* [42] analysed the pyrolysis of varnish waste based on polyurethane. They studied the influence of gas residence time into the reactor in their composition. The reactor used was a tube furnace in which the speed of the insertion of the sample may be set from 20 to 0.05 mm·s^{-1}. In total, 31 organic compounds were analysed by GC/MS under air atmosphere. The main evolved gases were CO, CO_2, ethylene, naphthalene and acetylene. They found that the amount of lighter hydrocarbons, CO, CO_2, benzene and Polycyclic Aromatic Hydrocarbon (PAH) increases proportionally to the degree of conversion of decomposition. The presence of PAHs in pyrolysis products means a severe fuel-rich pyrolytic condition. The concentration of other organic gases decreases as the residence time increases. Differential thermogravimetry (DTG) experiments present two decomposition stages for all the heating rates. The first series of peaks appears at temperatures between 340 ℃ and 380 ℃ and the second between 420 ℃ and 450 ℃. Ta ble 2-1 presents the mass balance established by the authors according to the species measured.

Table 2-1. Mass balance for three TGA experiments of PU waste pyrolysis products. Tests carried out from room temperature up to 700 °C. Three residence times were analysed (Source [42]).

Species	Residence time [s]		
	0.1	4	4.5
Gas fraction	37%	47%	60%
Tars and soot	31%	20%	15%
PAHs	6%	6%	6%
Water	-	-	-
Total	74%	71%	79%

As presented in Table 2-1, with increasing the residence time, the mass of tar and soot decreases while the portion of gaseous products increases. Thus, the residence time of the gases in the reactor is a capital parameter to control the pollutants emission. This siggest that the composition of the gases in a closed room in fire can drastically change with time.

Morimoto *et al.* (1976) in reference [9] measured the yield of chemical compounds listed in Table 2-2 during the combustion of polyurethane in tubular furnace at 700 ℃.

Stec *et al.* [43] presented the yields of gaseous products generated during isothermal tests in Purser Furnace apparatus (BS7990 and ISO TS 19700) together with FTIR. They studied the relationship between furnace temperatures (from 650 °C to 850 °C) and ventilation conditions (the type of fire) to the yield of toxic products. Four bulk polymers were studied: low-density polyethylene (PE), polystyrene, polyamide 6.6 and polyvinyl chloride. Yields of CO, HCN, THC and HCl have shown that they are highly dependent upon the fuel/oxygen ratio as well as the nature of the material. Yields have show not to be highly affected by furnace temperature. The authors did not compare data to the mechanisms of decomposition of each plastic and to the kinetics of gas release with time.

Blomqvist *et al.* [44] used the same furnace to determine the yields of fire-generated products from seven materials including expanded polymers, flame retarded materials, pelletized polymer materials and electrical cables. Experiments were performed under well-ventilated and vitiated combustion conditions, showing a good repeatability and stability. The yields measured for a mattress PU of composition $C_1 H_{1.53} O_{0.30} N_{0.09}$ are presented in Table 2-2. The yields of effluents showed to be highly dependent on the ventilation conditions. Focusing on nitrous compounds, they highlighted that NO was found only in well-ventilated condition and NH_3 only in vitiated condition, whereas HCN was found in both cases. Particles sizes were also measured with a low-pressure impactor. The maximum diameter of particles is larger under vitiated conditions; the larger particles are found in pyrolysis. The authors have not discussed the recombination of particles to form large-size particles in function of residence time.

Table 2-2 Yield of gaseous compounds produced by combustion of PU in tubular furnace at 700 °C (Source [9][44]).

Author Year Ref.	Material	Temp. [°C]	Atm.	Mass [mg·min⁻¹]	Gases released	Yield [$mg_b \cdot g_{sample}^{-1}$]	Gases measurement		Remarks
							Sampling	Analysis	
Marimoto 1976 [9]	Polyester PU - TDI	700	Air	N/D	CO_2	666.00		N/D	
					CO	173.00		N/D	Tubular furnace
					HCN	3.00		N/D	Air flow rate
					CH_4	21.00		N/D	1.6 l·min⁻¹
					C_2H_4	43.00		N/D	
					C_2H_2	14.00		N/D	
		700	Air	N/D	CO_2	625.00		N/D	
					CO	160.00		N/D	Tubular furnace
					HCN	1.00		N/D	Air flow rate
					CH_4	17.00		N/D	0.83 l·min⁻¹
					C_2H_4	37.00		N/D	
					C_2H_2	6.00		N/D	
Blomqvist 2007 [44]	Mattress PU	650	Air	25	CO_2	1800		FTIR	Purser tubular furnace.
					CO	50		FTIR	Well ventilated
					HCN	3		FTIR	($\Phi = 2$).
					NO	3 to 1[a]		FTIR	Air flow rate
					NH_3	N/P		FTIR	5 l·min⁻¹
					Isocyanates	1.5	Impigers	LC/MS	
		825	Air	25	CO_2	900		FTIR	Purser tubular furnace.
					CO	190		FTIR	Vitiated cond.
					HCN	8		FTIR	($\Phi < 0.75$).
					NO	N/P		FTIR	Air flow rate
					NH_3	0.8 to 2.5[a]		FTIR	1.9 l·min⁻¹
					Isocyanates	1.5	Impigers	LC/MS	

[a] No steady state is observed during the measurement time
N/D No data is available

As presented in Table 2-2, the proportions of measured CO and CO_2 depend on the temperature of combustion and on the amount of available oxygen [9]. Thus, the stoichiometric amounts of gases released are not allowed to predict the concentration of toxic compounds found in real combustion.

Purser tube furnace is a promising technique because it enables the simulation of various fire scenarios (equivalence ratio), but presents some disadvantages: a) The stoichiometric air-to-fuel ratio and the combustible part of the sample must be determined very precisely. This requires complementary testing, standards, includes uncertainty, etc; b) If a material burns faster than the sample feed rate (propagation at counter flow) combustion does not occur in steady-state; c) Steady-state combustion is one of the main hypotheses of purser furnace; d) Primary and secondary flow rates need to be adjusted for each material; e) The last part of the sample is introduced into the entrance of the tube furnace, where the temperature is low, resulting in around 16% of the total mass that may be unharmed by heat damages; f) The test run-time test is

very long (t~25 min); g) Further comparison with yields from full-scale fire tests are needed.

The French Tubular Furnace and Purser Tubular Furnace have been used to analyse the toxicity of the effluents generated during the decomposition of materials. The analysis of the toxicity of combustion gases, though not part of the aim of this work, is actually one of the numerous effects of fire on people [45]. The effects of fire on people are a very active research topics but also remain very controversial. Aspects such as irritation, evacuation, incapacitation, lethality, etc, are also part of the effects and must be considered when elaborating a safety strategy. In this field, a very precise knowledge of the effluents released during materials combustion is required. In this regard, nitrogenated compounds have a main role. However, further analyses are required, while the amount of nitrogenated compounds measured in materials containing nitrogen is lower than expected according to theoretical considerations [9]. Improving the balance of the nitrogen contained in the solid matrix and in the gas effluents is not part of the aim of the present research, but is of great importance because of the potential to save lives.

2.2.5 A few comments on the thermogravimetric technique

As has been shown, many authors have used Thermogravimetric Analysis (TGA) for analysing the mechanism of PU molecules breakdown. However, the elucidation of decomposition mechanisms generally involves identifying and quantifying the primary decomposition products [38]. The semi-liquid product has also been intensively studied with analytical chemistry techniques [18].

TGA experiments are carried out both under isothermal and dynamic temperature conditions. Isothermal experiments start at room temperature; a relatively low heating rate is imposed (*e.g.* 10 °C·min^{-1}) until the desired temperature is reached. The temperature is kept constant throughout the pyrolysis process and the experiment is considered finished when no further weight loss is observed.

Dynamic temperature experiments begin at the room temperature. The desired heating rate is imposed until the final temperature is reached. In general, the heating rate is

constant in over the whole temperature range. Bockhorn *et al.* [46] suggest that both isothermal and non-isothermal experiments should be combined in kinetic studies.

Thermal decomposition of molecules is one of the first steps in the combustion process of solid and liquids [42]. It provides fuel to fire in gaseous phase. The analysis of chemical compounds released by pyrolytic decomposition have multiple applications: Determination of the decomposition mechanisms of materials, calculation of fire loads, thermal recovery of wastes [26][47], reactors design [13], research of fossil energy resources [48], forensic sciences and toxicology [49], etc.

The thermal decomposition of polymers, particularly PU, is highly dependent on the following factors: type of polymer, heating rate, atmosphere, oxygen concentration, catalyst used in the production, fire retardants, and other parameters [42][44]. Oxygen has a critical influence in decomposition kinetics; an excess of oxidizer may accelerate the reaction, *i.e.* the minimum temperature of decomposition may become lower [4]. Some authors claim that in the solid phase of plastics, the thermo-oxidative reactions are negligible because of the low capacity of oxygen to diffuse itself into the polymer. The thermal decomposition controls the consumption of the material and combustion occurs at the surface. This is not the case in PPUF, due to their alveolar structure.

In the case of smoldering combustion, the PU semi-liquid decomposition by-product, "tar", can restrict the flow of air and consequently, inhibit the propagation of such a smolder wave. The power consumed by pyrolysing processes is much smaller than the power released in the reaction zone, for steady smolder. Thus, the decomposition reaction has only a small effect on the temperature profile [50].

2.2.6 Summary of the state of the art in matter scale measurements

This subsection presents a summary of the state of the art in matter scale measurements described in this section.

Table 2-3 Summary of the main researches found in literature related to the determinatikon of PU decomposition mechanism.

Author/Ref.	Year	Comment
Notling [30]	1888	Discovery of urethane bounds thermolysis.
Bayer [9]	1937	Discovery of polyaddition procedure used for PU production.
Woolley [35]	1972	All the isocyanate contained in the PU molecule is lost in the temperature range of 200 ℃ and 300 ℃.
Hileman [5]	1975	The pyrolysis products of PU can be obtained by combining the pyrolysis products of individual constituents. The crystallized pyrolysis product present higher nitrogen content than the virgin PU.
Voorhees [30]	1978	Summary of the urethane decomposition mechanism as independent molecular reactions. Polyol decomposes by a systematic sequence of reactions rather than by random fracture.
Rogers [23]	1981	The urethane bound has the lower bounding energy in PU. The yellow smoke released at temperatures between 200 ℃ to 300 ℃ is a TDI propylene oxide polymer.
Gaboriaud [40]	1981	Presented experimental results showing a decomposition mechanism in which the polyol is released in the first stage of decomposition. It is opposed to observed by other authors.
Yang [21]	1986	The depolymerization of PU occurs through the dissociation of molecules forming monodisperse samples with low molecular weight.
Ohtani [22]	1987	The pyrolysis products of PU can repolymerise in the gas stream. However, isocyanate undergoes secondary decomposition reaction in the gas stream. Incomplete recovery of diisocyanate is evidenced.
Allen [28]	1992	The molecular weight of reactants dictates the final properties.
Rotival [39]	1994	The decomposition of PU under air present two stages.
Bilbao [11]	1996	The yield of formed carbon dioxide is higher in the second decomposition step than in the first one. Therefore, in the second zone, less carbon monoxide is released.
Ravey [38]	1997	Affirm that PU decomposition gives rise to its original compounds. Polyol decomposed at around 290 ℃.
Esperanza [42]	1997	The yellow smoke released during PU pyrolysis is an aerosol of polyurea. It is not a condensate or polymer of TDI.
Lattimer [32]	1998	Showed that in tubular furnace the residence time has a prime role in the composition of the gases released.
Marotel [8]	2000	Presented a new mechanism for the nitrogen transformation. The nitrogen containing series have disappeared at 300 ℃.
Prager [27]	2006	Polyol is the base resin of PU. It gives the characteristics to the final product.
Blomqvist [44]	2007	Isocyanate is the catalyst of PU. The TDI and MDI isocyanates are used in the manufacture flexible and rigid foams respectively.
Stec [43]	2008	Verified that the release of higly toxic nitrogenated compounds is function of the ventilation

Author/Ref.	Year	Comment
Ezekoye [33]	2008	The theoretical approach of molecular reactions is not useful in fire applications because of the lack of understanding of the processes.
Zhang [31]	2009	The catalyst and additives used for the manufacture of PU may strongly change the yield of gases.

This section presented the state of the art in measurements carried out in order to determine the decomposition mechanism of polyurethane. As presented along the section, these analyses have been carried out for the gas and solid phases. Many chemistry analytical facilities such MALDI-MS, GC/MS, Py-GC/MS, GPC, TGA, TF and FTIR have been used to detect the chemical species released during PPUF decomposition under air and nitrogen atmospheres. The vast majority of authors agree that PPUF decomposition takes place in two phases: the first is the breakdown of urethane molecules releasing mainly isocyanate as yellow smoke; the second is the thermal decomposition of polyol and combustion in the gas phase. A part of the aim of this research is to verify these observations.

2.3 Characteristics of the Polyether Polyurethane Foam used in this research

The polyether polyurethane foam used in this research is a commercial foam of nominal density 22 kg·m^{-3}. Measurements of dimensions and mass showed that real density is 20.9 kg·m^{-3}. Density is an essential parameter in the fire behaviour of foams. However, because of the blowing-up process, it is very difficult to ensure homogeneous density all around the foam slab.

The foam is the "simplest" commercial foam available on the market, without fillers or fire retardants. This material has been used for years at the LNE as reference material for analysing the protection effect against fire of fabrics commonly used in the production of upholstered furniture. The tests are performed following the procedures of the standards NF D 60-013 [51] and BS 3379:1991 [52].

According to reactive purchaser, the PPUF is manufactured with polyoxyalkylene triol CAS No. 25791-96-2. and TDI, toluene Diisocyanate – Type 1 composed 80% from

2,4 Isomer – TDI and 20% 2,6 Isomer – TDI. The proportion by mass of reactants used was approximately 32% toluene diisocyanate and 68% polyol.

In order to carefully identify the foam, elementary analyses were carried out by the SCA laboratory using a combination of catharometry and Non Dispersive Infrared Analysis (ND-IR). This has a precision of ± 0.3 Wt% absolute and accounts for up to 98.8% of the total mass of the sample (the difference is ash). Analyses have been repeated three times. Table 2-4 presents the mean composition of the virgin foam used in this research as well as elementary analyses reported by various authors.

Table 2-4 Elementary analysis of the foam used in this research and reported by other authors. 'Coeff' is the stoichiometric coefficient of the molecule formula
(Source [5][30][26][31][42][44])

Source	Magnitude	Element						Remarks
		C	H	O	N	Others	Total	
This research	**Wt [%]**	**61.90**	**8.50**	**22.50**	**5.90**	**<0.2**	**98.80**	**Virgin foam**
	Coeff	**1.00**	**1.53**	**0.27**	**0.08**			
LNE Data base	**Wt [%]**	**57.80**	**5.86**	**25.64**	**10.70**		**100.00**	
	Coeff	**1.00**	**1.13**	**0.33**	**0.16**			
Hileman *et al.* [5]	Wt [%]	61.66	8.74	23.12	5.63	0.85	100.00	Foam
	Coeff	1.00	1.58	0.28	0.08			
Hileman *et al.* [5]	Wt [%]	47.95	5.47	38.06[a]	8.52		100.00	Crystals residue
	Coeff	1.00	1.27	0.60	0.15			
Font *et al.* [26]	Wt [%]	63.90	8.30	1.60			73.80	
	Coeff	1.00	1.44	0.02				
Voorhees *et al.* [30]	Wt [%]	64.00	6.50	22.40[a]	7.1		100.00	Foam
	Coeff	1.00	1.13	0.26	0.10			
Voorhees *et al.* [30]	Wt [%]	55.00	5.73	33.28[a]	5.99		100.00	Particulate
	Coeff	1.00	1.16	0.45	0.09			
Voorhees *et al.* [30]	Wt [%]	78.21	2.87	8.69[a]	10.23		100.00	Char
	Coeff	1.00	0.41	0.08	0.11			
Zhang *et al.* [31]	Wt [%]	59.10	8.90	26.70[a]	5.3		100.00	
	Coeff	1.00	1.67	0.34	0.08			
Esperanza *et al.* [42]	Wt [%]	64.03	7.19	3.31		8.00	82.53	
	Coeff	1.00	1.25	0.04				
Blomqvist *et al.* [44]	Wt [%]	60.90	8.40	24.30[a]	6.4		100.00	
	Coeff	1.00	1.53	0.30	0.09			
Mean	Mean	61.31	6.95	20.87	7.31			
	St. Dev.	7.37	1.87	11.65	2.03			

[a] Data not reported by the authors, calculated as the difference in mass balance

As can be seen in Table 2-4, PU formulations are widespread. However, in most cases carbon and oxygen represent between 80% and 90% of the total sample mass. As presented in subsection 2.2.1, the composition affects the fire behaviour of materials and toxic gases releasing. Pal *et al.* [9] consider that the combustibility of materials may not be characterised only on the basis of the elementary composition. It is highly

influenced by the chemical structure and the molecular size. Furthermore, the flammability of organic compounds is affected by the types of component elements, their ratios, oxygen availability, temperature, etc.

2.4 Measurement of thermal properties

The previous subsections presented the experiments carried out in this research in order to determine the kinetic mechanism of the decomposition of PPUF. These measurements include the behaviour of the solid and the gas phases. A discussion was performed about the possibility of analysing together the data obtained at the solid and gas phases.

The following subsection presents the measurements of thermal properties of PPUF performed at the LNE. The measured thermal properties are: Enthalpy of reaction (ΔH) under air and nitrogen atmospheres, mass thermal capacity (c_p) and superior calorific power (SCP). These results, are very useful to characterize the thermal decomposition of PPUF and to determine the thermal decomposition mechanism that is presented in chapter 3. However, the main utility of these data, is that they constitute input data for the fire simulations presented in chapter 4.

2.4.1 Enthalpy of reaction

Measurements of reaction enthalpy were performed with a Power Compensation Differential Scanning Calorimeter (DSC) PerkinElmer DSC 7 according to method described in NF EN ISO 11357-1 standard [53]. DSC measurements are based on the determination of the difference of power that must be provided to a sample pan with respect to a reference pan in order to follow the temperature program. DSC measurements are carried out in non-isothermal condition with a constant heating rate. In this research the heating rate was set to 8 ℃·m in^{-1}. The range of temperatures was between room temperature and 500 ℃.

PPUF masses used for DSC measurements were around 7 mg. Air or nitrogen volume flow rates were 50 ml·min^{-1}. Sample and reference pans were manufactured in aluminium and had a volume of 10 μl. The pans were covered with a reforming tool in order to improve homogeneity of the heat flux toward the sample.

When carried out under nitrogen atmosphere, the DSC test provides information on the endothermic energy required to break down the molecules while the material is heated up. When performed under air atmosphere, they provide information on the heat release rate by heterogeneous reactions. DSC results are expressed as heat flux endo up [mW]. When the measurement curve is downwards from baseline, the sample is releasing energy (exothermic reactions). In PPUF, exothermic reactions only occur under air atmosphere. When DSC curve is upwards from baseline, the reaction is endothermic and the molecules are dissipating energy in the breakdown process.

TGA data provide invaluable information for DSC curves interpretation. They allow distinguishing between irreversible or slow-reversible phase transitions (*e.g.* vitreous transition, crystalline structure transformations) and decompositions [41]. Figure 2-1, presents the experimental results from DSC together with TGA obtained under air and nitrogen atmospheres at a heating rate of 8 °C·min^{-1}.

One major limitation in the comparison of DSC data with TF or TGA results is that the experimental conditions are highly different in each test: The main heat transfer mechanism between DSC pan and sample is conduction. The heat transfer occurs mainly by the bottom of the pan. In TGA and TF, the heat transfer occurs mainly by radiation, particularly at higher set temperatures. The sample is located in the center of the isothermal zone. Thus, it can be considered that the particle is homogeneously irradiated on all surfaces and the side effects can be neglected.

It was observed that in TGA and DSC tests where PPUF was heated up to 500 °C, the remaining residues had dissimilar visual characteristics. Analytical tests were performed in order to figure out differences in their structures. None could be found, however.
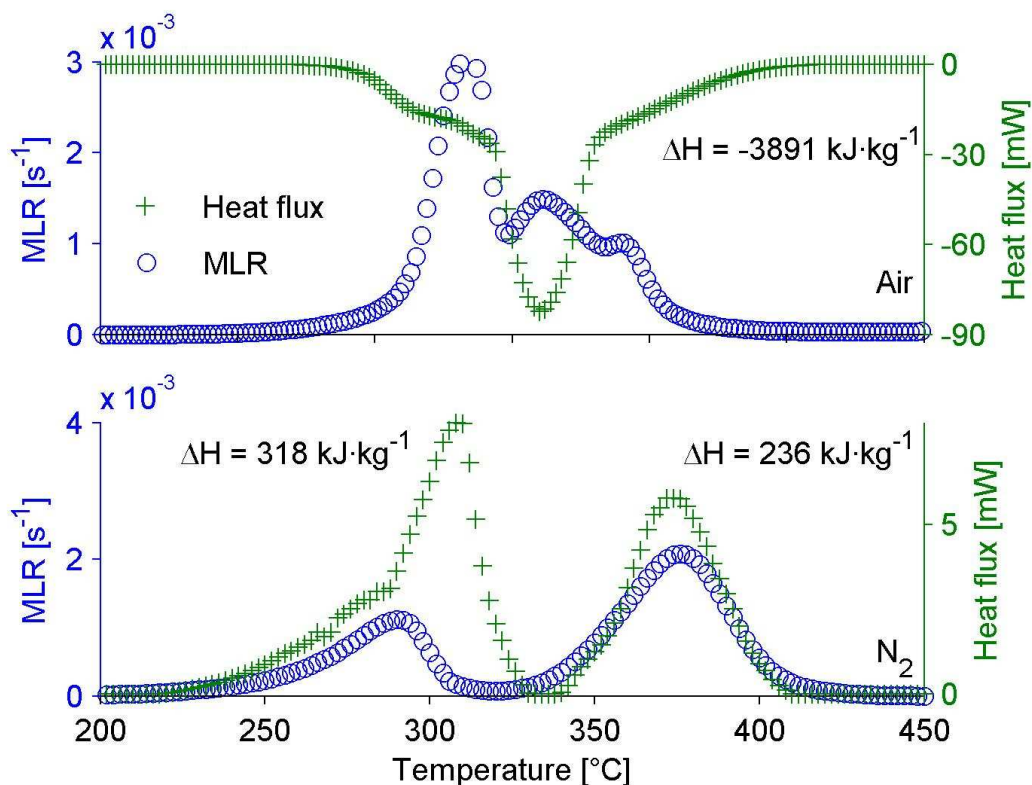
Figure 2-1. DSC and TGA results under air and nitrogen atmospheres. Upper curves are under air atmosphere. Bottom curves are under nitrogen atmosphere. TGA curves are presented in blue circles, referenced at the left hand side y-axis. DSC curves are presented in green pluses reported at the right hand side y-axis. Heating rate was 8 °C·min^{-1}. Positive enthalpy means endothermic reaction. Enthalpy is negative in exothermic reactions.

DSC is essentially a test designed to measure enthalpy in non-decomposing materials such as metals or ceramics. Using DSC with plastics during thermal decomposition could perhaps be interpreted as "out of the limits of the instrument". The feature of interest in DSC curves is the deviation of the signal from the baseline. Nevertheless, the baseline is not always easy to establish. In this research, a sloping baseline was found, which required particular treatments to make data interpretation possible [54]. A sloped baseline means that after thermal events, the response of the instrument does not return to the original baseline level. The baseline tends to have a higher slope after a decomposition event. This is due to:

- The fact that the thermal properties of the residue (by-product) left by one reaction are different from those of the reactive (*e.g.* virgin material) . This behaviour remains the same in successive reactions. For example, the baseline slope after

the second reaction under nitrogen (see bottom plot of Figure 2-1) was higher than the slope after the first reaction.

- The mass of the sample changes during each reaction. However, in the current test, the calculation of the power supplied to the sample is referenced to the initial mass and not to the actual mass. Unfortunately, DSC facility does not allow measuring the mass in real time. Thus, the actual amount of energy required per unit of mass to decompose the solid is difficult to establish.

Because of the problem of baseline, under nitrogen tests, a sigmoid baseline was used. This curved baseline allowed calculating the first peak of heat flow endo up. It was observed that a straight baseline did not allow to calculating the heat exchange caused by the first reaction. The standard NF EN ISO 11357-1 [53] describes an onset temperature method to define a DSC baseline. This method turned out not to be adequate to be applied to the data of this research.

DSC results under air showed to be dependent on ventilation in the sample holder. The first series of tests were performed using a cover. The tests were repeated later, using hand-perforated covers. The results were highly different. Nevertheless, in the case of materials that may burn, this technique is not designed to separate the effect of the heterogeneous reactions in the solid phase and the possible effects of the homogeneous reactions in the gas phase.

As shown in Figure 2-1, TGA and DSC peaks under air and nitrogen do not fit very well. This is a topic requiring further research. In particular, the deviation of enthalpy measurement caused by the heat release rate of PPUF heterogeneous reactions under oxidizing atmosphere (if any) must be quantified. This could also give an idea of the proportions of heat produced at the solid phase and at the gaseous phase. Nevertheless, there are no further methods available to measure the enthalpy of reaction, so espite of this cause of uncertainty, one enthalpy datum is calculated under air and two data under nitrogen [54]. The enthalpy of reaction data is used in fire simulation (Chapter 4).

2.4.2 Mass thermal capacity

Mass thermal capacity at constant pressure is also measured by the principle of differential calorimetry. The instrument used is a Setaram DSC III. Measurements are conducted according to the standard ISO 11357-4:2005 [55]. Mass thermal capacity of sample, $c_{p,sp}$, is calculated in function of thermal capacity of calibration sample, $c_{p,cal}$, initial sample mass, m_{sp}, mass of calibration sample, m_{cal}, their respective heats ΔQ_{sp} and ΔQ_{cal} and heat at blank ΔQ_{blank}. It is mathematically expressed in Eq. (2-3).

$$c_{p,sp} = c_{p,cal} \cdot \frac{m_{cal}}{m_{sp}} \cdot \frac{\Delta Q_{sp} - \Delta Q_{blank}}{\Delta Q_{cal} - \Delta Q_{blank}}$$

(2-3)

Because of PPUF thermal decomposition processes, thermal capacity of the foam is only defined at low temperature, up to T~200 °C. As shown in TGA curves, above this temperature, the solid structure begins to decompose and gas is released. At higher temperatures, it is uncertain what is in reality being measured. c_p measurement is performed withunder airtight settled holders in which pressure can increase due to PPUF gasification. Increase of pressure is a cause of uncertainty as well. Figure 2-2, shows the thermal capacity results of virgin PPUF and char. The char considered here is the residue obtained in cone calorimeter during tests carried out in non-flaming condition at an irradiance level of 30 kW·m^{-2} (see chapter 4).
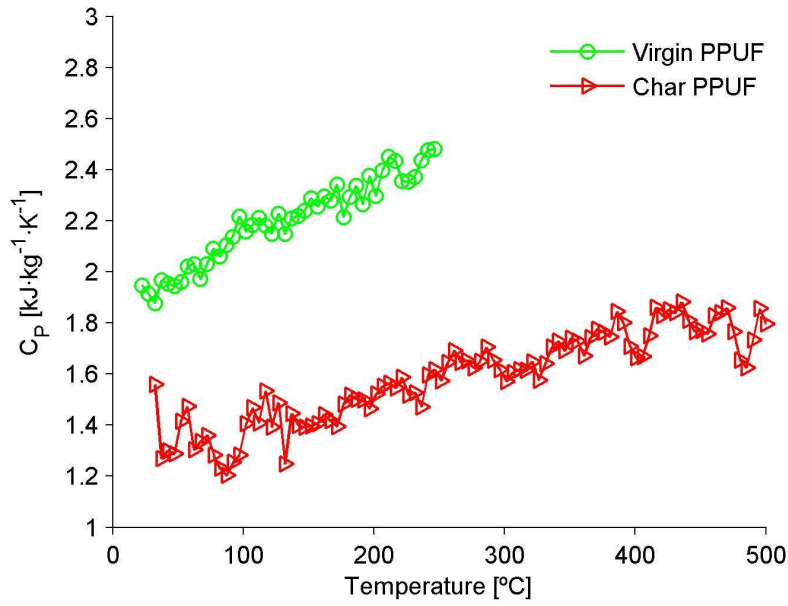
Figure 2-2. Thermal capacity data of virgin PPUF and char. Char data have been obtained without settled holder.

c_p measurement of virgin PPUF has been performed once, while c_p measurement of char has been performed four times: twice with settled holders and twice with open holders. As shown in Figure 2-2, c_p of virgin foam at environment temperature is 2 kJ·kg^{-1}·K^{-1} and increases linearly up to 2.4 kJ·kg^{-1}·K^{-1} at T~200 °C. c_p of char at environment temperature is around 1.4 kJ·kg^{-1}·K^{-1} and increases to 1.8 kJ·kg^{-1}·K^{-1} at 500 °C. When c_p measurements are performed with settled holder, an important noise is registered from T~50 °C to T~150 °C. The noise i s manifested as a peak with a maximum thermal capacity of 7.2 kJ·kg^{-1}·K^{-1} (This curve is not presented). Char samples were dried prior to the test in an oven at 250 °C for 15 min, so as to discard any potential influence of moisture. This peak is not observed in the tests with opened holders.

2.4.3 Thermal conductivity

The thermal conductivity of virgin PPUF as a function of temperature is measured. The measurement was conducted from the room temperature up to 190 °C. It was found that after 190 °C, the structure of the solid is hi ghly degraded and the dimensions of the

foam change, leading to the lose of the contact between the sample and the measurement plates.

The facility that enables the measurement of conductivity in function of temperature is not yet a standard method. It has been designed and built in at the LNE. The method is called guarded hot plate for thermal conductivity measurement at high temperature [56], which can perform conductivity measurements up to 250 ℃. The cross-section view of the LNE's high temperature guarded hot plate is presented in Figure 2-3.
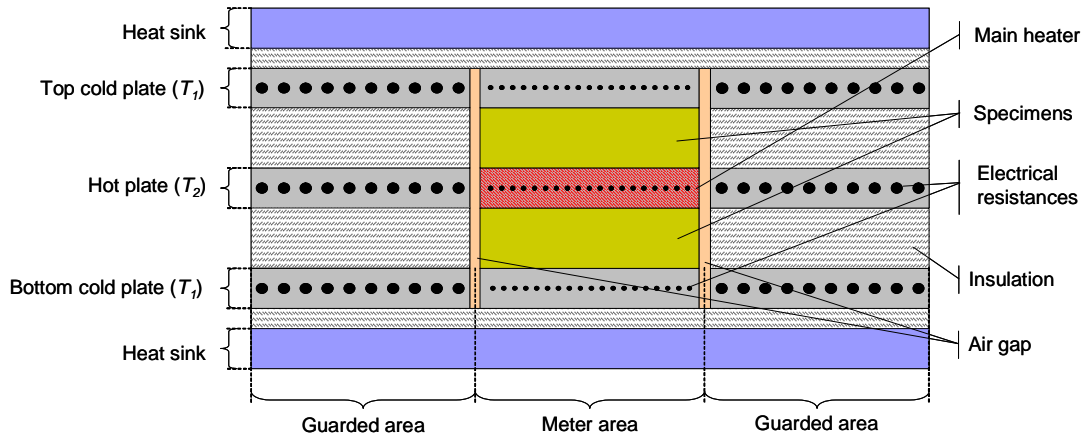
Figure 2-3 Cross-section view of the LNE's high temperature guarded hot plate. This facility enabled the conductivity measurement of PPUF from room temperature up to 250 ℃ (Source [56])

Basically, the measurement of conductivity (k_s) with the high temperature guarded hot plate facility consists in determining the power required at the hot plate (centre at temperature T_2) to attain reach a difference of in temperature equal to 10 ℃ with the cold plates (boundaries at temperature T_1) for samples of thickness d. The calculation of conductivity is carried out using Eq. (2-4). In order to avoid diffusion and boundary condition problems, two samples are used at the same time.

$$Q_e'' = \frac{k_s \cdot (T_2 - T_1)}{d}$$
(2-4)

Figure 2-4 presents the results of conductivity carried out in virgin PPUF.
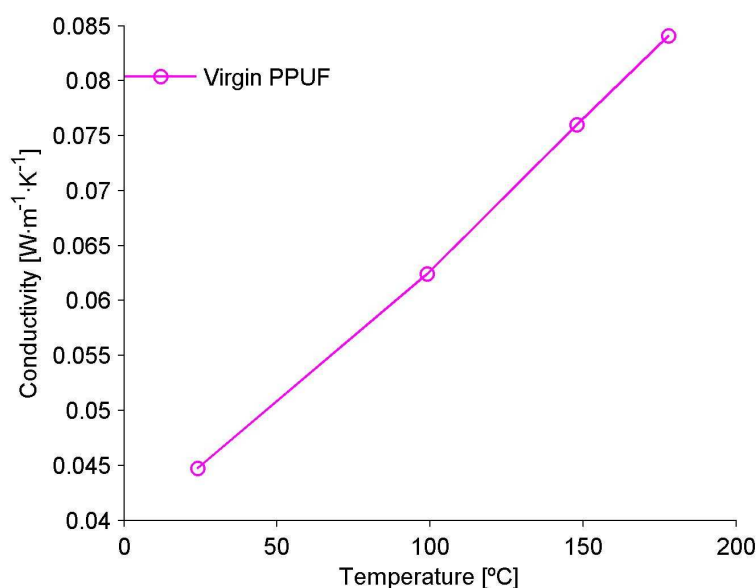
Figure 2-4 Conductivity of virgin PPUF from room temperature up to 190 °C. Measurement carried out with high temperature guarded hot plate.

As shown in Figure 2-4, the conductivity of the foam increases from 0.045 $W \cdot m^{-1} \cdot K^{-1}$ at room temperature up to 0.085$W \cdot m^{-1} \cdot K^{-1}$ at 190 °C.

2.4.4 Superior calorific power

Superior Calorific Power (SCP) is measured with a bomb calorimeter Parr 1266. The measurement procedure used is described in the standards NF EN ISO 1716:2002 [57] and NF ISO 1928:2004 [58]. Test masses are 215 ± 5 mg. No benzoic acid is used because PPUF is combustible. Tests are repeated three times, the mean SCP is $29\,832 \pm 221$ $kJ \cdot kg^{-1}$. As shown in the next section this measurement allows calculation of combustion efficiency. The Inferior Calorific Power and Thornton factor can also be calculated with this data.

2.5 Experimental measurement of the solid and gas phases

This section describes the experimental measurements carried out in order to determine experimentally the decomposition mechanism of PPUF. The measurement techniques that are described here are thermogravimetric analysis, tubular furnace and Fourier transform infrared spectroscopy analysis.

A discussion is performed in order to validate the comparison of the results obtained with TGA coupled to FTIR, and those of TF coupled to FTIR. The TGA coupled to FTIR is mainly used to characterise the behaviour of the solid phase across mass loss measurement, while TF coupled to FTIR data is used mainly to characterise the behaviour of the gas phase. Quantitative data from gas phase was collected at the LNE. It allowed the calculation of the yield of release of the main gas species.

A particular attention is given to TGA results since it is the most conventional measurement technique to study the decomposition of materials. It provides information that allows to inferring the decomposition mechanisms. However, it turned out to be insufficient to select an unambiguous decomposition mechanism. In this research, TGA data is combined with information from gas analysis instruments. The coupling of data from both phases allows determining a decomposition mechanism in agreement with the chemistry of the processes [59]. The changes in solid phase simultaneously with gaseous phase as a function of time (or temperature), has been poorly analysed in the past [52][60]. Data from both phases together with a mathematical model are used to calculate the kinetic parameters of the decomposition reaction.

2.5.1 Fourier Transform Infrared Spectroscopy gas analysis (FTIR)

The Fourier Transform Infrared Spectroscopy gas analysis is the only measurement technique used at all the scales considered in this research. FTIR is a powerful technique that is currently used for a wide range of industrial and research applications

such as: classification and authenticity verification of lactic products [61], polymer additive decomposition [62], nitrogen transformation in catalytic reactions [63], alloy oxidization processes [64], analysis of pharmaceutical products ageing and stability [65], etc.

The chemical bounds of a sample can absorb the energy from an IR source in the near and mid-infrared wavelengths (5 000 cm^{-1} to 200 cm^{-1}). The absorption of radiative energy is caused by the interaction of light beams and chemical bonds, the atoms vibrate one with another at a given frequency. If atoms are of different nature, an induced electrical dipole vibrates at the same frequency of mechanical vibrations. When a non-symmetric bond is irradiated by a monochromatic light source with the same frequency of bond vibration, an interaction with the electric dipole is produced. The energy absorbed correspond to vibration frequency

FTIR is a simple light IR beam apparatus in which an interferometer (Michelson type) is located between an IR radiation source and sample [66]. An Interferometer allows the modulation of infrared frequencies. The displacement of a mobile mirror scans the entire range of IR frequencies enabling the measurement of sample transmittance. The position of the mirror needs to be measured as well because it allows determining the frequency of the spectral response; it is measured using a helium neon laser beam. In other words, two measurements are performed at the same time using two sensors: the position of the mirror (the frequency) and the intensity of the IR beam (the transmittance). The signal obtained is an interferogram that is converted in IR spectrum by using a mathematical function called Fourier Transform. FTIR provides absorbance in function of wavenumber, $Ab(\lambda)$, calculated as a logarithm of ratio between source intensity, $I_0(\lambda)$ and intensity measurement of the beam passing through the sample, $I(\lambda)$. It is mathematically expressed in Eq. (2-5) [67].

$$Ab(\lambda) = \log\left(\frac{I_0(\lambda)}{I(\lambda)}\right) \tag{2-5}$$

The group of frequencies absorbed by a molecule constitutes its "digital identification"; which is related to geometry, chemical bonding and functional groups. It is possible to carry out a qualitative identification of a gas mixture by analysing the absorbance response in a wide range of wavenumbers. In this research, qualitative

characterisations of species are noted FTIR$_{qlt}$. Figure 2-5 shows the spectral response (absorbance) of various gases commonly found during the combustion of PPUF.
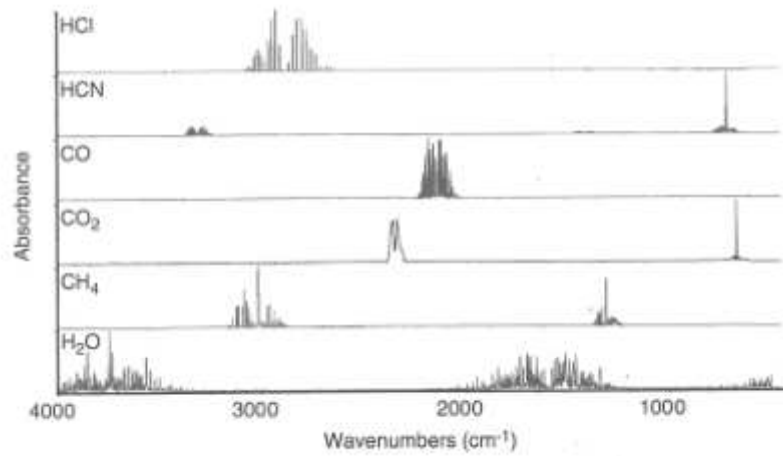
Figure 2-5. Exemple of the absorbance spectra measured in FTIR for various common combustion gases of PPUF (Source [43])

The characteristic of spectral response in precise regions is used to calibrate FTIR (quantitative measurement). For calibration, the absorbance is expressed in function of molar absorptivity, $a(\lambda)$, path length of cell gas, l and concentration, c. This is mathematically presented in Eq. (2-6). Reference gas mixtures are used to perform quantification of the chemical species present in a sample. Nevertheless, the complex spectral features of many multi-component data sets often make it difficult or even impossible to develop reliable IR quantitative methods.

$$Ab(\lambda) = a(\lambda) \cdot l \cdot c \qquad (2\text{-}6)$$

The analysis of multi-component spectra is done in two steps. First, a method is constructed, based on the spectra obtained with known concentrations of the gases of interest. It is usually called the calibration or training step. Second, the method is validated and used to predict the unknown concentrations of the gases in the spectra contained in an independent data set.

One calibration point is the peak height at one or more wavenumbers according to a known concentration of a gas (see Eq. (2-6) and Figure 2-5). The calibration of a gas consists in establishing the relation between the intensities in the wavenumber region and the gas concentrations (curve of calibration). Gases dilution or mixing of certified

standard gases enable to obtain a batch of spectra of several concentrations. It represent a major task of the operator during facility calibration.

The curve of calibration needs to be modelled using conventional methods such as least squares or partial least squares. Prediction of unknown concentrations is performed using the model established for each species. A variety of methods, univariate and multivariate, linear and non-linear, exist to perform the quantification of gas components in real smoke gas spectra (for more details about FTIR calibration see reference [68]). The column "Calibration points" of Table 2-5 show the total number of concentrations acquired over the whole range of quantification of the listed gases; they link up the concentrations of the calibration gases with the spectral absorbances.

Table 2-5. List of calibrated products in the FTIR of LNE. Lower and higher quantification limits are also presented.

Calibrated gas		Quantification limits [ppm]		Calibration	Reference gas cylinder	
Component	Symbol	Low	High	points	Conc [ppm]	(2σ) [%]
Carbon monoxide	CO	2.5	8802	50[a]	10006[bc]	0.3
Carbon dioxide	CO_2	260.4	50140	56[a]	50140[bc]	0.7
Water[e]	H_2O	21.1	22560	13	-	-
Nitrogen monoxide	NO	4.9	494	22	494[bd]	0.8
Nitrogen dioxide	NO_2	1.0	499	5	499[bc]	0.6
Nitrous oxide	N_2O	8.5	1005	31	1005[c]	2
Hidrogen cyanide	HCN	5.0	1020	55	4840[c]	3
Hidrogen chloride	HCl	2.1	5000	24	5000[c]	5
Hidrogen bromide	HBr	2.0	998	1	998[c]	2
Methane	CH_4	0.3	4990	37	4990[c]	2
Acetylene	C_2H_2	2.1	994	35	994[c]	2
Ethylene	C_2H_4	2.7	995	34	995[c]	2
Formaldehyde	H_2CO	21.7	131	10	198[c]	2
Sulfur dioxide	SO_2	1.0	852	26	1001[bc]	0.2
Ammonia	NH_3	1.0	1085	17	1085[c]	3

[a] Two ranges of measurement
[b] Cofrac calibration certification
[c] Certification of concentration by weight
[d] Analysis by chimiluminescence spectrometry
[e] The calibration of water is performed by the combustion of methane

The last three columns at the right hand side of Table 2-4 show very important data for the calibration process: the number of calibration points, the concentration of the reference cylinder and the relative uncertainty of the concentration expressed in percentage. CO, CO_2, NO, NO_2 and SO_2, are reference gas cylinders with the quality label "Cofrac" which guarantees a high standard production process process allowing a very low concentration uncertainty.

The calibration concentrations are experimentally generated using the certified cylinders and a diluter that mixes very precise amounts of the calibration gas with high purity nitrogen ($2\sigma = 0.3\%$). The dilutors are also calibrated guaranteeing a mass flow deviation lower than $\pm 0.7\%$. A schematic layout of the dilution facility is shown in Figure 2-6: Pressure regulators reduce the pressure of the gases contained in the cylinders; the mass flows are then regulated to obtain the desired concentration and the mix of gases is finally transported to the FTIR.
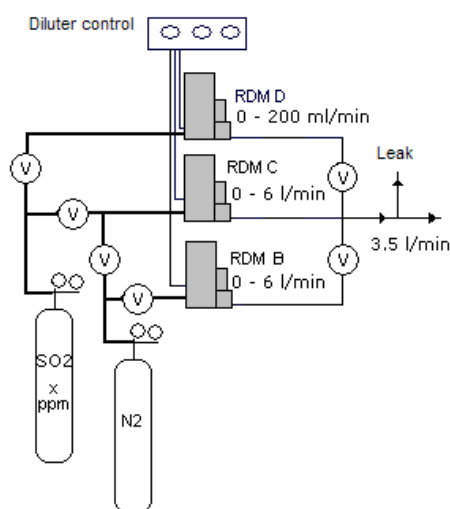
Figure 2-6 Scheme of the diluter used during the FTIR calibration. RDM B, RDM C RDM D are mass flowmeters. "V" are gas valves (Source [69])

In Figure 2-6 the volume flow rate of the three flowmeters are specified. At room temperature and pressure, they behave as ideal gases, thus, the mass flow rate is determined accurately. The dilution facility allows a large range of gas mix with very high precision: The flow meters RDM B and RDM C are used for high concentrations and the flow meters RDM B and RDM D are used for low concentrations. A very detailed description of the dilution procedure and of the calculation of the uncertainty of the calibration curve is presented in Ref. [69]

After calibration, performing continuous absorbance analysis vs time allows FTIR to make a large number of spectrum with relatively higy frequency. Thus, the change of concentration with time of a sample stream can be determined. In fire applications, FTIR would be able to measure, in real time, the composition of products streams generated by flames of different natures [68]. In this research, when quantification is possible, notation is FTIR$_{qnt}$.

In comparison to conventional analytical methods, FTIR offers a main advantage in terms of flexibility of information analysis: Data acquisition and interpretation are separated processes. Spectra obtained from a particular sample can be compared later with data from an additional library of spectral response in order to identify and quantify new gases that were not observed with current libraries. This reduces the need to repeat tests in order to identify particular gases.

Figure 2-7, presents a schematic layout of the FTIR facility used in this research. The entire transport line (from the sampling point until the gas cell) is heated up to 180 °C. It allows the transport of combustion products while avoiding water vapour condensation and water-soluble compounds trapping. Sampling line is 5 m length giving FTIR facility more flexibility to be used together with test apparatuses. The FTIR facility is in accordance with the guidelines of the standard ISO 19702:2006 [70].
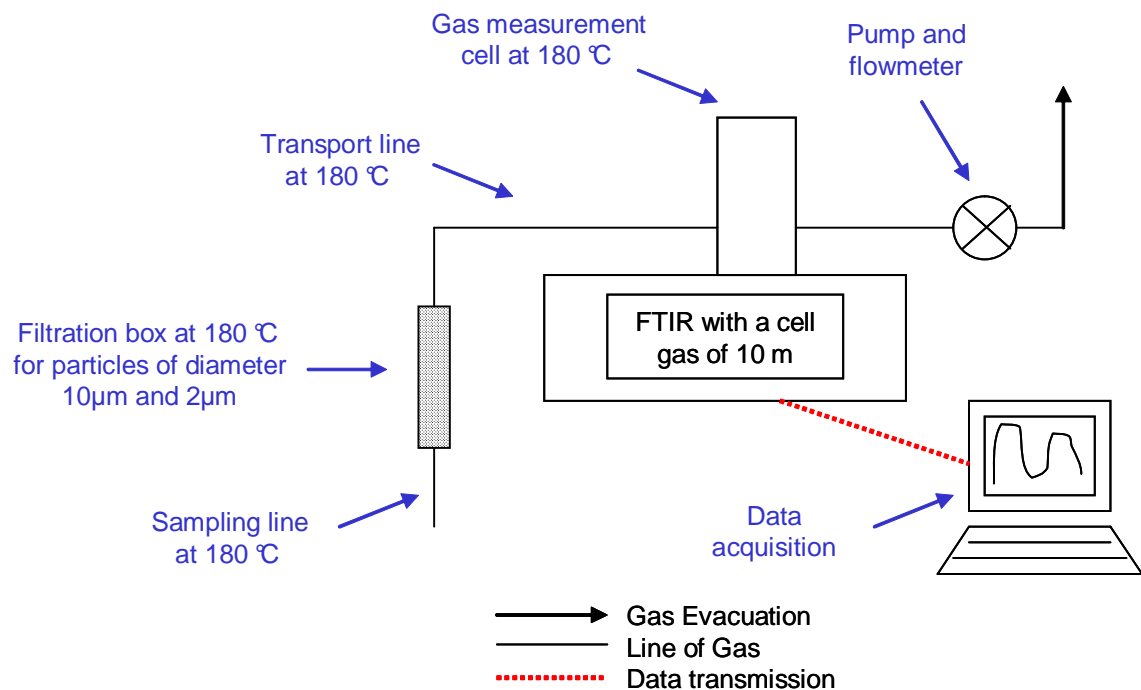
Figure 2-7. FTIR facility layout

The sampling line is connected to a filtration box where two stainless steel filters are used to retain soot particles and heavy products. The first filter retains particles of diameter greater than 10 µm and the second one particles of diameter greater than 2 µm. The two filters are regularly pyrolysed at 600 °C to eliminate all the particles laid

70

down in the filtration grid. After filtration, gases are transported to the gas measurement cell. It has an optical length of 10 m and a volume of 2 l.

The spectrometer for gas analysis is a FTIR Thermo-Nicolet Magna IR 550 Series II equipped with MCT-A detector. The data acquisition resolution can be set between 0.5 and 4 cm^{-1}. In this research, the resolution was set to 0.5 cm^{-1} in order to improve the sensitivity and the capacity to identify qualitatively minor species. The pressure of the gas cell is regulated in real time. Previous studies carried out at the LNE (not published yet), have shown that pressure is one of the main experimental parameters to control in order to ensure the accuracy of FTIR measurement. Pressure is regulated at 86.7 ± 0.7 kPa (650 ± 5 torr) and gas flow rate is set at 6.5 l·min^{-1}. Finally, the gases are cooled, dried and filtered before being extracted and eliminated with a membrane pump.

The sampling gas flow is not dried before passing through FTIR cell measurement. This enables quantification of H_2O (vapour). H_2O is not a toxic gas, but is very useful to establish the mass balance of combustion effluents and to analyse the kinetics of decomposition of PPUF. The FTIR Analyser is calibrated to quantify around 15 gaseous combustion products at the same time; this analysis technique (including sampling and filtering device) has been validated during the SAFIR project [71] in the year 2000. This project constituted the basis for toxicity analysis carried out following the guidelines of the standard ISO 19702:2006 [70].

Table 2-5 presents the current calibrated gases in the FTIR used in this research. The lower and higher quantification limits are presented as well. The lower and higher FTIR limits presented in Table 2-5, allow the analysis of the gas effluents from the vast majority of the materials tested.

Quantification of particular gases is the basis for calculation of the yield of gaseous products. Yield of production of a particular gaseous species b in function of time, Y_b, is calculated as the ratio between mass-flow rate of gas b and Mass-Loss Rate (MLR) of sample (see Eq. (2-7)). The mass-flow rate of a species, expressed in Eq. (2-8), is given by the following: The product of the species concentration, the volume flow rate in the exhaust line times, the molar mass divided by the volume of one mole of the species. Eq. (2-9) is used to calculate the volume of one mole of species b. The main hypothesis of Eq. (2-9) is that exhaust gases behave as perfect gases.

$$Y_b = \frac{\dot{m}_b}{MLR} \qquad (2\text{-}7)$$

$$\dot{m}_b = x_b \cdot \dot{V} \cdot \frac{MW_b}{Vmol_b} \qquad (2\text{-}8)$$

$$Vmol_b = \frac{R \cdot T}{P} \qquad (2\text{-}9)$$

Calculation of yield in function of time is desirable because it provides important information on the interaction of the transformations carried out in solid and gaseous phases (decomposition mechanism) and about the change of toxicity of gases according to the advancing of decomposition. Unfortunately, some tests, such as TF, do not allow real-time mass measurement. In this case, the yield cannot be expressed in function of time. Thus, a single global data is calculated. This single data is the global yield of species b. It is calculated as the ratio between total mass released of gas b and total burnt mass.

2.5.2 Thermogravimetric analysis (TGA)

Thermogravimetric analysis is the measurement of sample mass with the increase in temperature [41]. It is essentially used to determine the properties of materials in fields such as pharmaceutics, mineralogy, chemical industries, fire retardancy, etc. The key of the TGA technique is the very high resolution of the mass measurement even with sample temperatures up to 1600 °C. Recent developme nts of TGA instruments allow simultaneous DSC measurements by an assembly of thermocouples located into the sample ceramic support. The DSC measurement is performed comparing heat fluxes in sample and reference pans [72].

A schematic representation of TGA apparatus is presented in Figure 2-8. Essentially, TGA is a cylindrical electric heated furnace disposed horizontally. The furnace can be displaced so as to allow positioning the samples into the high-precision weighing device (position open). The high precision weighing device is stationary and thermally conditioned. TGA facility supports the sample and reference holders at the end of a horizontal beam built with a low conductivity material. In thermogravimetric analysis an

infinite quantity of heating protocols can be defined, but they can be classified into two configurations detailed here-after:

- Isothermal condition: The temperature remains stable during the tests. The main parameter of this condition is the reaction time. Isothermal tests are used to analyse in detail the processes of phase change (fusion or evaporation), virtuous transitions of plastics, inner structure change of metals, etc.

- Non-isothermal or dynamic temperature condition: The temperature changes with time, following in general a linear heating rate. Heating rate and atmospheres are the main parameters to be controlled in this configuration. The kinetics of decomposition have shown to be affected by these two parameters. These tests provide information on the temperatures at which the phases of the materials change, and help to define the number of stages of polymers decomposition.

It is known that high amounts of sample in TGA tests would involve a significant gap between actual sample temperature and temperature registered by the thermogravimetric system. A main parameter in thermogravimetry experiments is a very reliable knowledge of the actual temperature of furnace and sample [73].
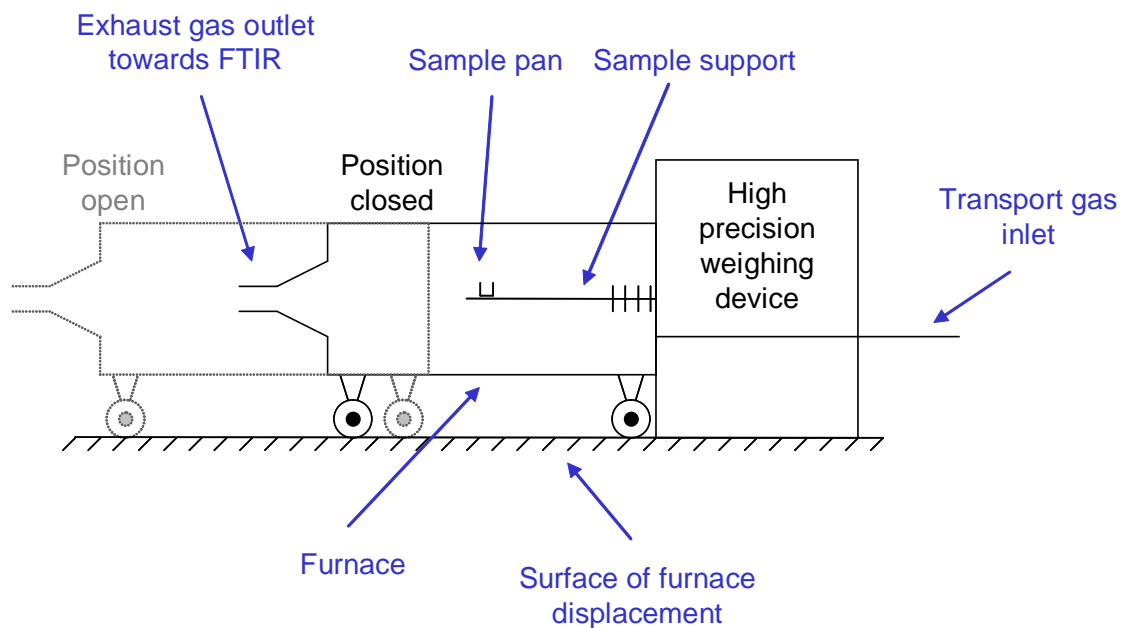
Figure 2-8. Scheme of the horizontal TGA facility used in this research.

The TGA tests used in this research were gently performed by Mettler Toledo using a Mettler Toledo TGA/DSC 1 Star System with a precision in temperature of ± 0.5 K and in mass of ± 1 µg. The decomposition atmosphere is provided by a gas flow of 20 ml·min^{-1} of air or nitrogen. Figure 2-9, presents the curves of mass and MLR obtained by Mettler Toledo with PPUF. In Figure 2-9, curves are not grouped by atmosphere as generally presented in literature, but are instead grouped by type of curve (mass or MLR curves). This is interesting to easily evidence the influence of oxygen on the decomposition mechanism.
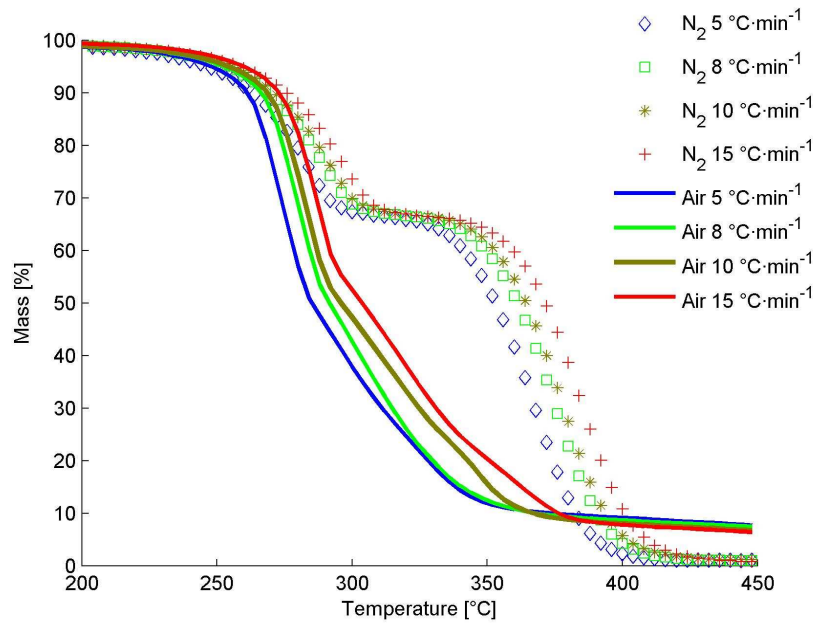
a)
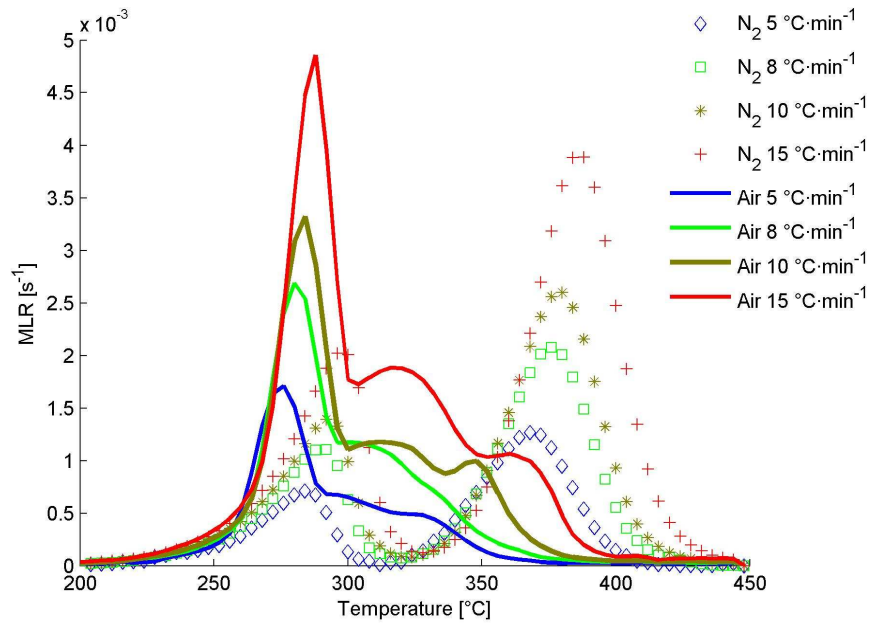
b)

Figure 2-9. Results of TGA tests carried out under air and nitrogen at four heating rates: 5, 8, 10 and 15 °C·min $^{-1}$. a) Mass change *vs* temperature; b) MLR *vs* temperature.

Phenomena of sample drying occurring between T~95 °C and T~105 °C are highly dependent on sample conditioning. In real fire conditions, the humidity has a very importante role in the fire spread velocity and intensity of the fire. In this research, the influence of humidity is avoided by adopting the next heating up protocol: From room

temperature up to 120 °C, a low heating rate is imp osed *i.e.* 5 °C·min $^{-1}$. Temperature remains at 120 °C for 30 min or until mass stabiliz ation. Finally, the heating rate of the test is imposed until a final temperature set to 450 °C. As shown in Figure 2-9, under air and nitrogen atmospheres, PPUF thermal decomposition begins at 200 °C; the slope of MLR curve changes rapidly. Nevertheless, deep different kinetics are observed after T~250 °C under air and nitrogen atmo sphere. This difference is created by the influence of oxygen in the decomposition mechanism. Shifts through high temperatures with increasing β have been largely reported in literature [26].

Under nitrogen, two stages of decomposition are identified, while under air three decomposition stages are identified at all the heating rates studied. The temperatures of MLR peaks for two atmospheres and four heating rates are summarized in Table 2-6.

Table 2-6. Temperatures corresponding to peaks of MLR observed in TGA experiments. Air and nitrogen atmospheres at four heating rates 5, 8, 10 and 15 °C·min $^{-1}$.

Atmosphere	Heating rate [°C·min $^{-1}$]	Temperature [°C]		
		First peak	Second peak	Third peak
Nitrogen	5	285	269[b]	-
Nitrogen	8	290	376[b]	-
Nitrogen	10	292	379[b]	-
Nitrogen	15	298	386[b]	-
Air	5	276[a]	294	326
Air	8	281[a]	299	332
Air	10	284[a]	312	347
Air	15	287[a]	316	360

[a] Main reaction rate under air atmosphere

[b] Main reaction rate under nitrogen

As shown in Figure 2-9 and Table 2-6, oxygen from air accelerates the breakdown of molecules at relatively lower temperatures; this explains the differences in shapes observed with the two atmospheres in all the heating rates. The second and third peaks are caused by the subsequent by-products of pyrolysis or oxidization. It is important to highlight that the most intense peaks of MLR under air atmosphere correspond to the first decomposition reactions. The main MLR peaks under air are found at T~284 °C. Under nitrogen, the main MLR pea ks are the second peaks. The second peaks under nitrogen take place at T~379 °C. This is a sign that the oxygen interacts directly with the solid phase of PPUF.

A higher amount of solid residue remains in sample holder at the end of the test under air atmosphere than under nitrogen atmosphere for a given β. It evidences heterogeneous chemical reactions where oxygen from air is trapped by PPUF by-products to form a solid residue. This residue can pyrolyse and oxidize at temperatures around 500 ℃. The oxidization of the residue is not considered in this research because of the low amount that remained after combustion of the PPUF.

In large-scale tests, the radiative heat flux from flame towards the sample modifies the thermal balance of the solid. The thermal balance of the solid also changes the decomposition kinetics of the element; the decomposition kinetics along with ventilation control the pollutant emissions. The radiation of flame is of main interest in fire research. The problem of flame radiation towards the solid was analysed by Rhodes *et al.* in 1996 [74]. Their study was performed in cone calorimeter using PMMA as analysis material. In order to analyse if this is also the case with TGA, the MLR is compared to the actual heating rate. Figure 2-10, presents the comparison of MLR and actual heating rate at a set β of 10 ℃·min^{-1}.
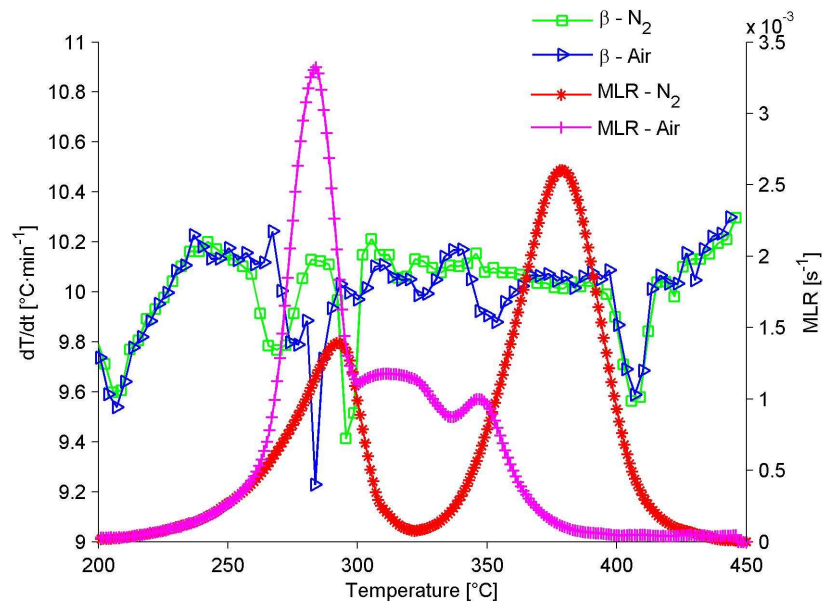
Figure 2-10. Plot of actual heating rate calculated at each second together with MLR under air and nitrogen atmospheres at set heating rate of 10℃·min^{-1}.

In Figure 2-10, the calculation of actual heating rate was performed every second for the two atmospheres. If heat release rate produced by the particle would have an influence in heating rate of the furnace, vibration in the temperature program would be observed. This vibration would be evidenced by local noise in the actual heating rate curve. Moreover, the noise in the heating rate curve would appear in regions were the shape of MLR changes strongly (producing endothermic or exothermic reactions). A change in the slope of MLR leads to a high production of combustible gases.

Nevertheless, as can be seen in Figure 2-10, the temperature controller fits very well with set temperatures. Some deviations can be observed in the region from 250 ℃ to 300 ℃ and from 390 ℃ to 420 ℃. These deviations, however, are of low duration and they are not observed systematically in the regions where the mass changes strongly. In conclusion, the mass-loss rate measured in TGA is not influenced by the kinetics of degradation nor by the heat release rate of the particle. This also means that the heat released in the gas phase does not control the dynamics of the decomposition process such observed in larger scale tests (*e.g.* cone calorimeter, etc). In large-scale tests, the kinetics of decomposition are controlled by factors such as the temperature and ventilation at the decomposition front.

TGA provide valuable information about changes of total mass remaining in the sample holder. However, the identification of the phenomenon causing these mass changes remains a tricky task. It must be identified with complementary experimental analysis, data from literature or theoretical approaches. In this research, the nature of solid phase transformations is identified by the analysis of the released gas products. The main hypothesis in this methodology is that in TGA, each reaction of the solid releases particular gaseous compounds in a precise temperature range. In order to validate this assumption, two series of tests have been performed:

- TGA + FTIR test: As TGA apparatus is available in any of the groups co-operating in this research, these tests were performed by the SCA laboratory. Unfortunately, gas identification are only qualitative ($FTIR_{qlt}$). No calibrations have been performed to allow quantification.

- Tubular Furnace + FTIR test: These test have been performed in LNE. FTIR analyser calibration allows gases quantification ($FTIR_{qnt}$). Nevertheless, TF does not allow real-time mass measurement. While using TF, calculation of the change

of gas yield with increasing temperature is not allowed. Thus, a single global yield is found.

TGA + FTIR$_{qnt}$ were not performed because of the technical difficulties and the very high fares to have these tests performed by a third-party organization.

The next subsection describes the tests performed in tubular furnace together with FTIR in order to identify the kinetics of gas release.

2.5.3 Tubular furnace

Tubular furnace was developed at the end of the 1970's by different research groups, including the LNE. It was first used to analyse the chemical compounds released by cables on fire. In the early 1980's this facility was adopted by train design and operation companies to analyse toxicity of materials used for the manufacture of trains [75]. TF facility was largely used in research projects such as Firestarr (finished in 2001) [76], in which were largely studied the fire risks in European trains.

The TF is constituted of a quartz tube located in the centre of a cylindrical furnace disposed horizontally (see Figure 2-11). The inner TF temperature changes with transversal distance from side wall. Sample must be carefully placed at the isothermal zone located in the centre of the furnace. Contrary to Purser Furnace apparatus (BS7990 and ISO TS 19700) [43], in TF, sample boat is introduced manually using a stainless still rod. A gas flow passes through the quartz tube (vector gas) transporting the products released by the sample directly to the FTIR. A bypass allows atmospheric air to enter to the gas line in order to dilute the highly concentrated gas products released in TF and ensures atmospheric pressure in the transport line.

The tubular furnace used in this research is 600 ± 10 mm long. The combustion tube has an inner diameter of 40 ± 10 mm and a nominal length of 1000 ± 10 mm as specified in reference [77]. The temperature programmer is a XS30 Perkly Herrmann Moritz. The TF is installed under a hood in order to ensure the safety of the operators in case of leak a of combustion gases.
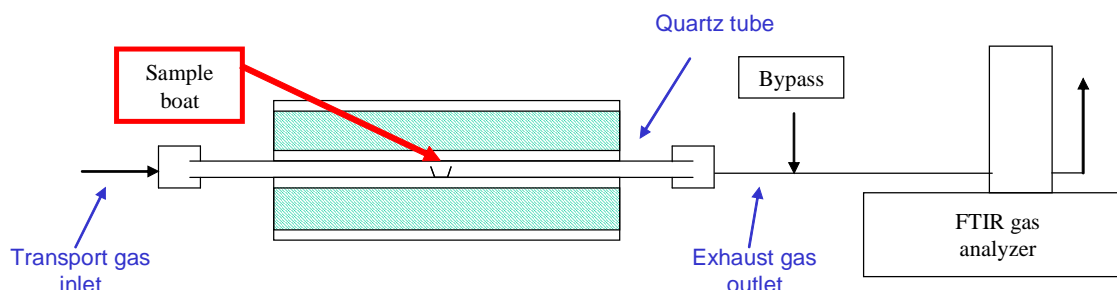
Figure 2-11. Scheme of tubular furnace facility coupled to FTIR gas Analyser for analysis of exhaust gas release produced during combustion of PPUF

According to the standards NATO AFAP 3 [77], NF X 70-100-2 [78] and ISO 16312-2:2006 [79], samples used in TF must have a mass of 1 g. However, because of low PPUF density, the mass of samples was 110 ± 20 mg (see Figure 2-12). Greater masses than those actually used would cause the samples to touch the walls of the TF, producing additional measurement uncertainties. TF+FTIR$_{qnt}$ experiments were performed with air and pure nitrogen at an inlet volume flow of 2 l·min^{-1}. The volume flow rate is set manually using a float flow meter (rotameter). The volume flow rate that enters by the bypass is 4.5 l·min^{-1}. It corresponds to the difference between FTIR flow rate (6.5 l·min^{-1}) and the TF vector gas flow rate (2 l·min^{-1}). All volume flow rate measurements are carried out at room temperature.

The masses of tubular furnace samples were chosen as the best compromise between the smallest sample mass and the best FTIR sensitivity. A small sample mass allows the agreement of the test with the two main hypotheses of tubular furnace: a thermally thin sample and laminar flow near to the sample. A greater mass increases the mass flow rate of evolved gases and the sensitivity to low yielded effluents. Figure 2-12 presents the samples used in tubular furnace measurements.

Figure 2-12 Tubular furnace sample. The mass is around 110 mg

In this research a dynamic temperature condition was imposed to TF. Unfortunately, because of the thermal inertia of the instrument, the maximum β is 10 °C·min^{-1}. The non-isothermal condition allows studying the influence of temperature in the dynamics of release of gaseous products.

In this research, the influence of the vector gas flow rate in the exhaust gas composition was not studied, during the dynamic temperature experiments it was set to 2 l·min^{-1}. Some experiments were performed in TF in isothermal condition. The temperature was set to 650 °C and the volume flow r ates of the vector gas were set to 2 l·min^{-1} and 4 l·min^{-1}. A clear influence of the ventilation was observed in the yield of CO_2, CH_4 and C_2H_2 but not for the other gases (see Table 2-5). The main difference between the isothermal and non-isothermal tests is that the reaction time in isothermal tests is of the order of 100 s, while in non-isothermal tests the reaction time is near to 30 min. Thus, the effect of vector gas flow rate (*i.e.* ventilation) cannot be compared.

2.5.4 Results of TGA + FTIR$_{qlt}$ and TF + FTIR$_{qnt}$

As already explained, TGA tests are necessary because they provide information centered on the decomposition mechanism of PPUF. FTIR$_{qlt}$ measurements were performed in this research because they served to write a "chemically correct" model of PPUF decomposition which is presented in Chapter 3. A "chemically correct" model

means that the stages of the decomposition mechanism are in agreement with the evidence of the release of gas effluents. This allows a model that includes the reactions taking place in the solid phase.

This subsection presents the results obtained during tests carried out in TGA + FTIR$_{qlt}$ and TF + FTIR$_{qnt}$. Before following the analysis, it is necessary to verify that the release of gas compounds during PPUF decomposition is the same in both experimental techniques. In other words, to check if the combustion models are equivalent. As explained, this approach is used because no TGA experiments coupled to quantitative FTIR have been performed during this research.

Figure 2-13, presents the curves of release of isocyanate, polyol and aldehyde compounds obtained in both experiments. As stated, these results were obtained in different laboratories (LNE and SCA) and with different instruments (TF and TGA). The convention for gases labelling is: TGA + FTIR$_{qlt}$ corresponds to experiments performed in SCA laboratory, where the FTIR measurement are purely qualitative, and TF + FTIR$_{qnt}$ correspond to tests performed at the LNE, where the FTIR measurements are quantitative. The experimental conditions for this comparison are: a heating rate of 10 °C·min^{-1} and nitrogen atmosphere.
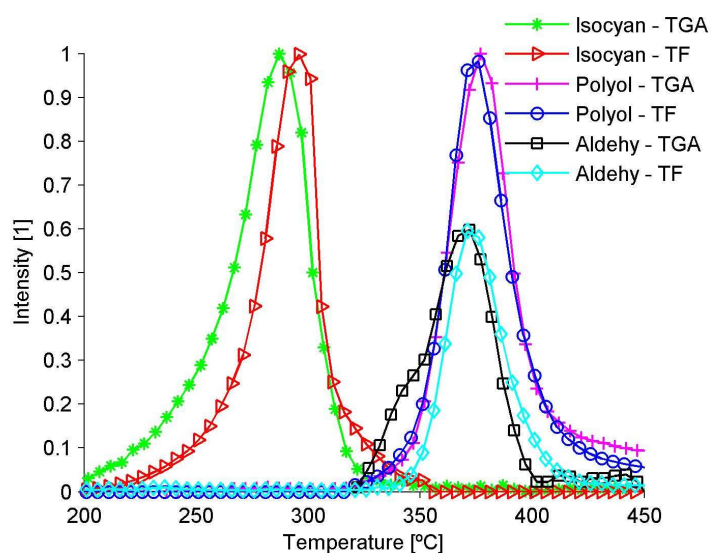
Figure 2-13. Releasing of isocyanate, polyol and aldehyde compounds in TGA + FTIR$_{qnt}$ and FT + FTIR$_{qlt}$ at β of 10 °C·min^{-1} under nitrogen atmosphere. Aldehyde compounds has been scaled by a factor of 0.6.

The aim of the comparison presented in Figure 2-13, is to see if the shapes of gas release are similar in both experiments. This comparison is merely qualitative, the

y-axis has no dimension. Intensities in the y-axis were normalized, and for ease of view the intensities of aldehyde compound were multiplied by a factor of 0.6. The intensities reported for FTIR$_{qlt}$ (SCA laboratory) were calculated quantifying the change of area of the spectral response of each gas. The quantification of the area of the spectral response is the principle of FTIR quantification (see subsection 2.5.1).

Figure 2-13, shows clearly that under nitrogen atmosphere at a β of 10 ℃·min^{-1}, the shapes of gases release in function of temperature are very close for polyol, isocyanate and aldehyde compounds. The small difference in shapes can be due to a difference in the spectral bands considered for gases identification in both laboratories.

A similar analysis to the one performed in Figure 2-13 is performed under air atmosphere in Figure 2-14. The interpretation turned out to be complicated because some shifts between curves were found. The comparison is performed by families of gases. Contrary to the case of nitrogen, under air atmosphere the curve of MLR (blue line with triangles) is taken as reference in all the plots.

It is highlighted that in Figure 2-13 and Figure 2-14, the compound labelled as 'polyol', corresponds to $-OH$ functions found in the gas effluents. These functions are created during the thermal decomposition of polyol that cannot be found in vaporised form. The molecules found in gas effluents have a structure that is near to the one of virgin polyol. To clarify, in this dissertation polyol represent a semi-liquid product of the decomposition of PPUF (particularly in Chapter 3) and a gas produced by the decomposition of the semi-liquid. The particular discussions concerning the solid or the gas phases would say to the reader which one is being considered.

Similarly to poluol, the gas labelled 'Isocyanate' corresponds to $-OCN$ functions which are residues from the decomposition of the isocyanate contained in the polyurethane molecules. Along this manuscript, 'isocianate' in the gas phase represent the family of effluents described.
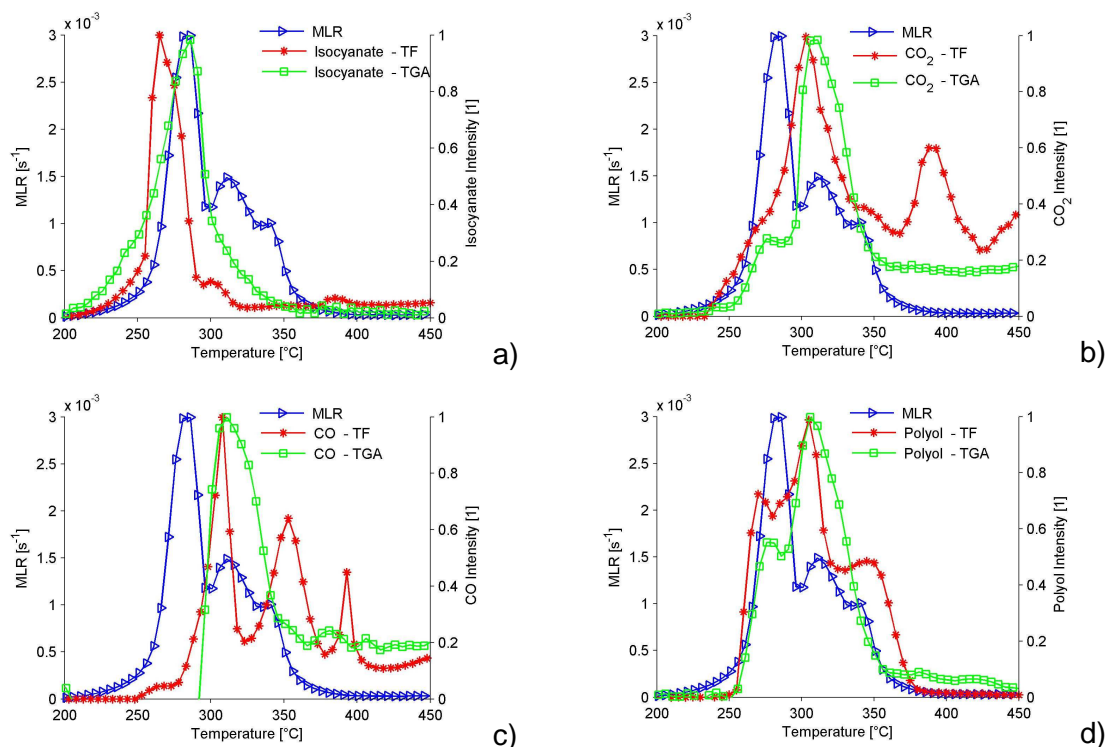
Figure 2-14. Releasing of a) isocyanate; b) CO_2; c) CO and d) polyol *vs* temperature in TGA + $FTIR_{qlt}$ and FT + $FTIR_{qnt}$ at β of 10 °C·min^{-1} under air atmosphere. The experimental curve of MLR is used as reference in all the plots.

Figure 2-14 a), presents the release of isocyanate. The curve obtained in TF is shifted around 25 °C toward the lower temperatures compared to MLR and TGA curves. This shift does not seem to be very physical because it does not correspond to an important change of mass. This can be caused by interference of water bands produced during combustion or to the earlier break-down of PPUF molecules in TF due to the sample surface.

$$n \underbrace{OCN\text{-}R\text{-}NCO}_{Polyisocyanate} + n \underbrace{HO\text{-}R'\text{-}HO}_{Polyol} \longrightarrow \underbrace{(R\text{-}NHCOO\text{-}R'\text{-}NHCOO)}_{Polyurethane}{}_n \qquad \text{Recall of Eq. (2-1)}$$
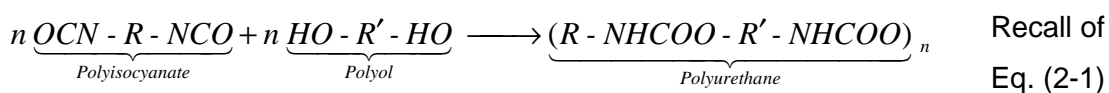
The structure of the polyurethane molecule is recalled in order to facilitate the comprehension of the following analysis. Figure 2-14 b), presents the release of CO_2. In both experimental techniques the peak of CO_2 release takes place at a temperature corresponding to the second peak of MLR, *i.e.* T~312 °C. At the temperature of the first peak of MLR, at T~284 °C, the curves of TF and TGA present important inflection points. The shape of LNE's curve (TF) is smoother than SCA's (TGA). This is a typical

behaviour caused by the difference in volume of gas cell measurements: LNE cell measurement is 2 l while SCA cell measurement is 0.17 l volume for similar flow rates. The peak of CO_2 release observed in the TF measurement at T~390 ℃ does not appear in TGA's curve. This peak can be produced by the post-combustion of soot or solid particles laid in the quartz tube.

Figure 2-14 c), presents the release of CO. The peak of CO release is found at T~310 ℃; this is also the temperature of the secon d peak of MLR. The second and third peaks of CO production are detected in TF tests at T~360 ℃ and T~390 ℃ respectively. These temperatures correspond to changes in slope of CO curve found by TGA.

Figure 2-14 d), presents the comparison of release of polyol. TF curve presents three peaks while TGA presents two. The first peaks are found at T~284 ℃ and the second at T~312 ℃. However, the third peak found in TF is not found on the TGA curve.

In conclusion, a quite satisfying correspondence is found between gases detected by SCA and LNE in comparison to the MLR curve. This has two meanings: first that gases release in TGA and TF during PPUF decomposition are the same, and second, that the shapes of gas release in function of temperature are quite similar in both cases. This allows the comparison of the results. The aim of this comparison is to be able to analyse together the results obtained in TF for the gas phase and the results of TGA for the solid phase. Thus, the coupling of measurements of solid and gaseous phases of PPUF decomposition can be carried out.

2.6 Analysis of the solid phase - Verification of the decomposition mechanism of PPUF

In the previous subsections, the experimental results that allowed coupling the behaviour of the solid and gas phases have been presented. This information as well as the measurements of thermal properties represents input data for the numerical studies presented in the following chapters. Nevertheless, direct analysis in the solid phase are required in order to study the heterogeneous chemical reactions that occur,

particularly those with oxygen. This section presents the works carried out in order to extract information directly from the solid phase. This information is of prime importance to understand the physics of the reaction.

During this research, important means were employed to try to identify which changes are induced by heat in the main structure of foam (condensed phase). The transformations induced by heat in the solid structure, force all "chemical components" of virgin matter to react. However, each component reacts at a different time during the thermo-oxidative process. This produces the different PPUF combustion stages that were presented in section 2.4.

The aims of analysing the chemical transformations of the solid phase are:

- To identify how they influence the combustion process,

- To identify the reactants and products of each reaction stage (in the solid phase),

- To identify how each reaction in the solid phase can influence the production of pollutant gases,

- To establish the mass balance in the solid and gas phases.

Data from the solid and gas phases are primordial to determine the decomposition mechanism of PPUF. Coupled information from both phases allows giving a chemical meaning to the reaction mechanism proposed in chapter 3.

Extracting useful information in the solid phase turned out to be a tricky task. More specifically, it was very difficult to get quantitative information because the analytical methods do not seem fit for the problem addressed in this research (microanalysis X, FTIR in condensed phase, ATR, elementary analysis, etc). Thermal attack and fire cause modifications in the structure that are not well known. In addition, the classical techniques of analysis used for verification in industrial processes cannot be accurately used here because of strong difference between the samples required for the instruments and the actual samples found in fire applications.

Conventional spectroscopic methods such as IR and Nuclear Magnetic Resonance (NMR) have been widely used for the characterisation of PU, but their applications are often limited and complete analysis is hard to perform [22]. Indeed these methods are

based on the study of the spectral response of molecules when irradiated in a given range of frequency. Still, the interpretation of the spectral response is difficult because: a) A huge number of libraries of spectral response are required in order to compare the current response with data from the library; b) Multiple molecules can have very close spectral responses, which makes it difficult to distinguish the actual molecules of the solid.

In this research, two types of analysis of the solid phase have been carried out: a visual characterisation and measurements using various analytical techniques. The techniques and findings are detailed here after.

2.6.1 Visual characterisation of the solid phase

The visual characterisation was performed at various scales by binocular images and Scanning Electron Microscopy (SEM). Binocular images were taken from structure of virgin foam and the residues remaining after heating up to 500 °C. The binocular instrument used was a Leica M3Z with maximum zoom of 260X. Scales of the binocular images were between 500 μm to 1 mm. The images were of great usefulness because they suggested that imagery at smaller scale would give more information on the PPUF decomposition phenomena.

Scanning Electron Microscopy (SEM) pictures were taken of four types of PPUF residues: samples after DSC measurement under air and nitrogen atmospheres and samples obtained directly from cone calorimeter under air and nitrogen. The SEM instrument used was a LEO 440, S440 3802 series. SEM images can be taken only in power conductive materials. A gold electroless deposition of about 1.5 nm to 3 nm was laid on the surface of virgin and PPUF residues in order to enable image acquisition. PPUF is not a electrical conductor material, thus it can be hypothesised that this surface treatment does not change the sample properties.

Figure 2-15, presents binocular and SEM pictures of virgin foam. Pictures are presented in a two columns table. The larger scale image is on the left presenting the global morphology of the sample (observed used optical instruments), and the smallest scale is shown on the right presenting the inner structure (SEM photographies). This distribution of pictures lets to the reader know what the SEM picture is showing.
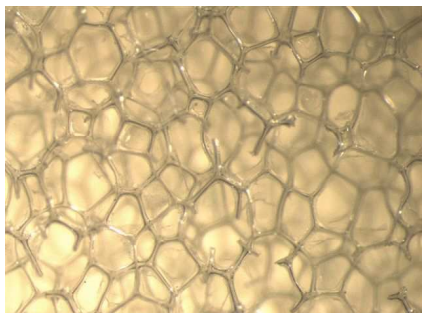
Global morphology of the sample	Focusing on the inner structure
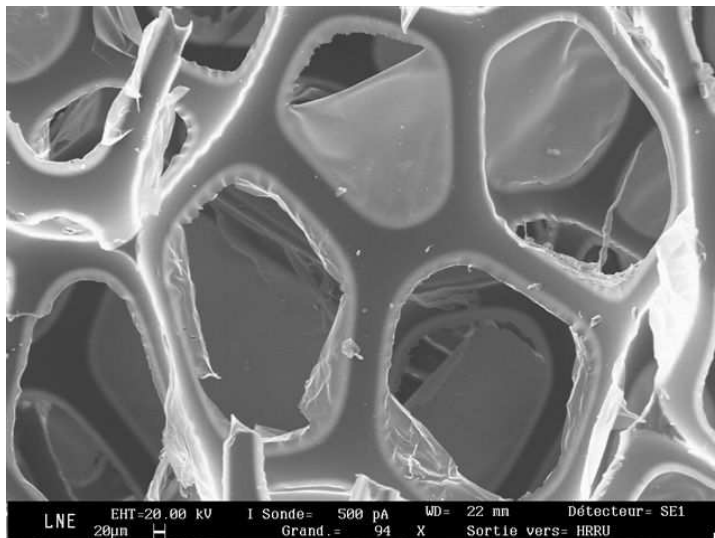
Figure 2-15. Binocular and SEM pictures of virgin PPUF

The virgin structure of the foam is very regular and presents very thin PU "films" between main branches remaining from the expansion process. When heated up, PPUF decomposition produce surface irregularities in the main branches. Examples of these surface defaults are shown in Figure 2-16 presenting the binocular and SEM pictures of DSC residues obtained when PPUF samples were heated up to 500 °C under air and nitrogen atmospheres.
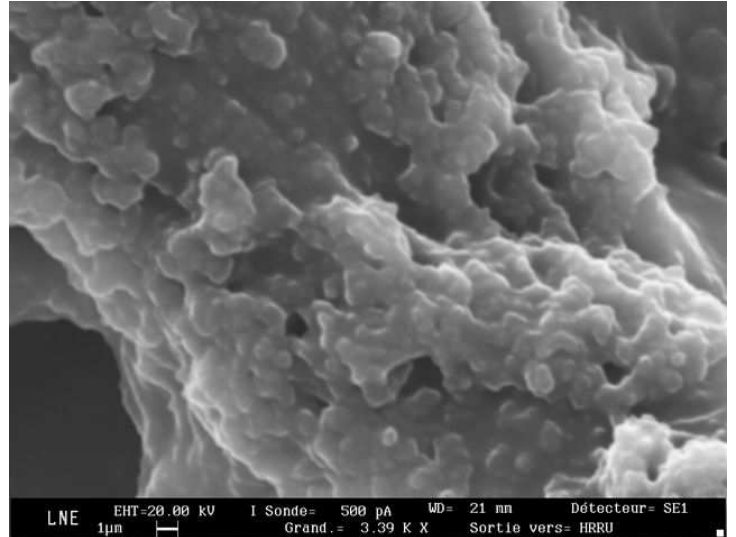
	Global morphology of the sample	Focusing on the inner structure
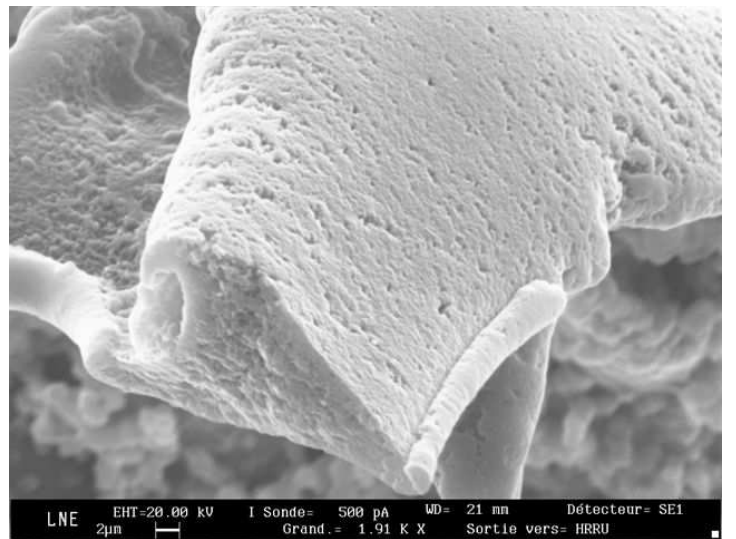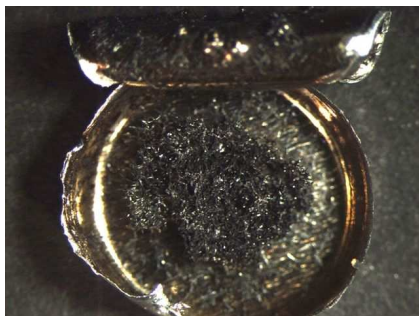
Figure 2-16. Binocular and SEM pictures of DSC residues. PPUF samples were heated up to 500 °C under nitrogen (top) and air (bottom) atmospheres.

As shown in Figure 2-16, SEM pictures reveal that the thermal attack directly affects every main branch of the solid structure. However, the marks produced by heat are not homogeneous on all residue surfaces. Because of the diversity of effects, multiple types of signs can be found in a single sample and conducting a complete characterisation based in these observations is not possible.

As shown in Figure 2-16, a strong difference is found in samples decomposed under nitrogen (Top) and air (Bottom) atmospheres. Under nitrogen, the smooth main branches are transformed into solid structures full of blisters and "scraps". The blisters and "scraps" are groups of the more thermally stable molecules present in the structure of the virgin foam. Blisters and "scraps" are linked by a solidified substance. This one is the residue of the less thermally stable molecules of the virgin PPUF that have been transformed into a semi-liquid during the heating-up process. According to the PU decomposition mechanism described in literature and confirmed in this research, the solid observed in the picture is a mix between the residue of isocyanate (Blisters and "scraps") and the residue of polyol (matter between the blisters and "scraps").

The deposit generated under air (Bottom of the Figure 2-16) is smoother than the one observed under nitrogen. The main branches present marks of thermal attack that can be described as micro-holes and craters. These defaults are caused by the increase of pressure in the main branch and a successive fracture of the skin. The fracture of the skin liberates a sac of combustible gas that reacts with oxygen in the gas phase. According to the decomposition mechanism and the measurements of gas release, it can be stated that oxygen triggers the reaction of both components of the molecule at the same time (polyol and isocyanate). However, while isocyanate is the less thermally stable, it is released at a lower temperature.

Nevertheless, the marks produced during the thermal decomposition are not uniformly distributed. This is certainly evidence that the oxygen diffusion is not homogeneous through the surface of the sample. The higher reactivity of oxygen with both components of PPUF virgin foam (polyol and isocyanate), promote reactions on the surface of the branches rather than in the centre of them.

Figure 2-17 presents photographs and SEM pictures of cone calorimeter residues. At the top, it is shown the residue obtained under nitrogen. At the bottom, the residue under air (non-flaming condition). The residues presented under both atmospheres were obtained exposing the PPUF samples to an irradiance level of 30 kW$\cdot$m^{-2} for

about 10 min. These figures can be compared with the SEM pictures obtained by Branca *et al.* [10] presented on Appendix A

Global morphology of the sample	Focusing on the inner structure
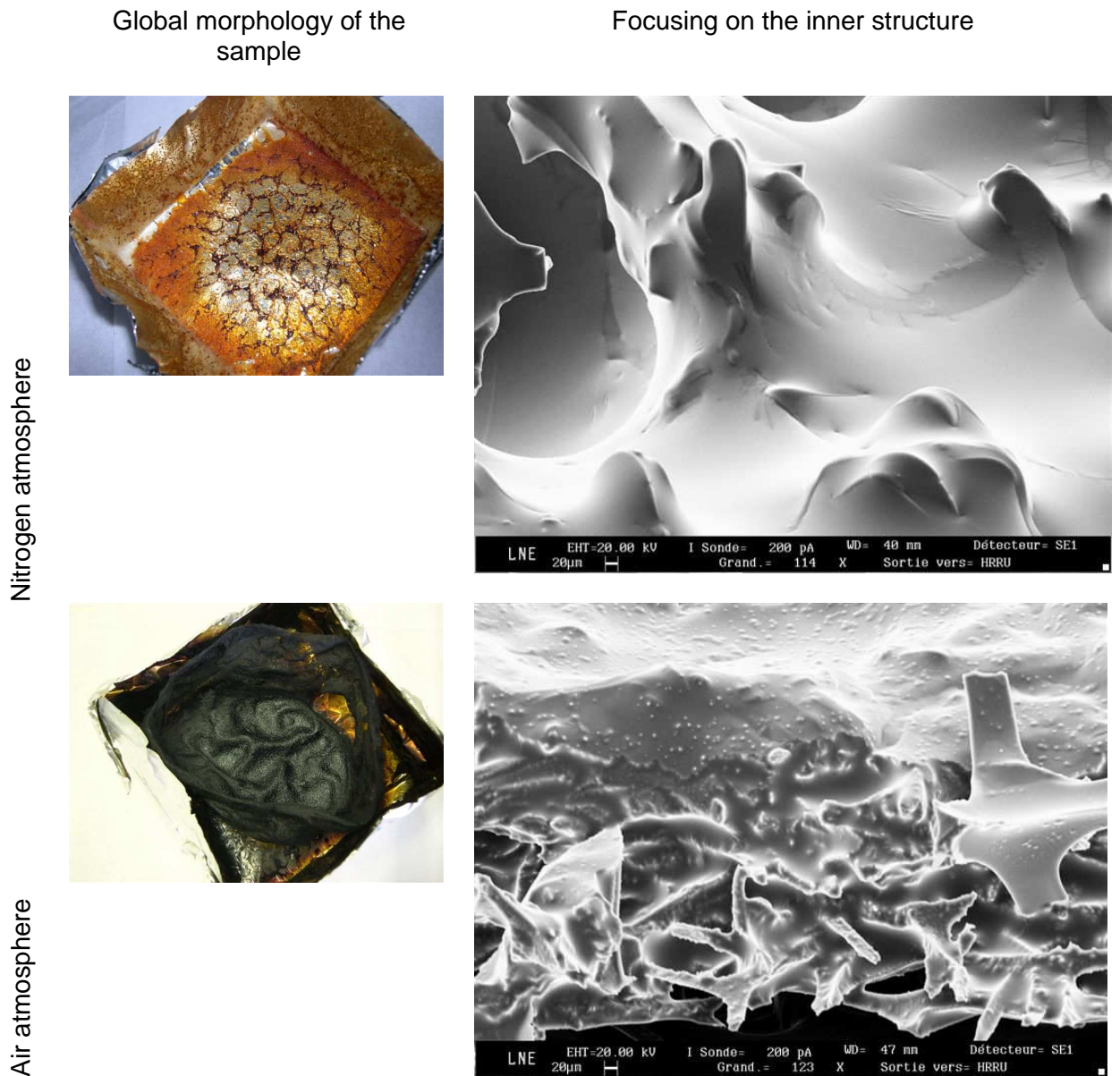
Figure 2-17. Pictures and SEM images of cone calorimeter residues. PPUF samples were exposed to irradiance level of 30 kW·m^{-2} under nitrogen (top) and air (bottom) atmospheres.

As shown in Figure 2-17, the characteristics of the surfaces are highly different in function of the atmosphere. Under nitrogen, solidification of a semi-liquid product is evidenced by folds indicating that the surface has been submitted to strain, as can be observed when a fabric is stretched. Under air, a very thin layer at the top of the sample can be observed. The thin layer is the decomposition front that shifts from the top towards the bottom of the sample during decomposition. Under this layer, thermally

attacked branches are found. The decomposition front constitutes a thermal barrier that reduces the damage rate caused by heat in the structure of the branches. These observations are in agreement with those made on DSC residues, which suggests that the decomposition mechanism remains constant independently of the test.

Under both atmospheres, the displacement shift of the decomposition front is always parallel to the top of the sample, denoting a homogeneous irradiance level from CC in the radial direction of the cone.

Comparison of SEM photographs of Figure 2-16 and Figure 2-17 shows that the remaining branches in cone calorimeter (under both atmospheres) present smoother surfaces than the remaining residues of DSC tests. It allows concluding that the mode of heat transfer affects the kinetic of solid decomposition. Nevertheless, the decomposition mechanism remains constant: The first decomposition stage is the breakdown of PPUF molecules that allows release of isocyanate and the second is the decomposition and further reaction of polyol.

In cone calorimeter, the semi-liquid polyol is formed in the decomposition front. It is present almost homogeneously in the surface exposed to the irradiance level from the heater. This semi-liquid produces the smooth surface observed in both atmospheres in Figure 2-17. At the matter scale (DSC), the liquid polyol is formed and decomposed directly in the surface of the main branches, and it does not spread from one branch to the next one. So, as the polyol cannot spread between the branches, a smooth surface is not generated. The surface defaults are produced by the physical and chemical transformation occurred into the branch.

2.6.2 Characterisation of the molecular structure of the solid

Various analytical techniques were used in order to identify the transformations of the solid phase. These analyses provided information about the nature of the molecular structure of the virgin foam. Unfortunately, they provided few information about the transformation induced by heat in the solid matrix. We consider it is of main interest to reference these tests even if the result were not very useful the determination of the effects of thermal attack in the solid phase. The techniques used were:

- Fourier Transform Infrared – Attenuated Total Reflectance (FTIR-ATR): is a qualitative test based on the analysis of the spectral response caused when a IR bean is transmitted through a diamond (monoreflexion) that is in contact with the solid samples. Spectra of ten samples that suffered various processes of thermal decomposition were acquired and compared between them. This analysis allowed identifying that the virgin foam under analysis is actually a Polyether Polyurethane Foam and not a polyurethane foam as we originally thought. However, the spectra acquired with FTIR-ATR technique did not reveal differences in the main structures of various PPUF residues.

- Microanalysis X: is a technique for elements identification (C, O, N, Si, Al, Sn, Ca and H) that works in association with a SEM facility. It was performed using an instrument PGT 3537 series. This technique is based on analysis of X-rays reflected by the sample when irradiated with a X-ray source. These analyses did not provide useful information about residues composition. It is important to highlight that the results from virgin foam did not match with data obtained by the elements analysis.

- FTIR in liquid phase: is the analysis by FTIR of a liquid rather than a gas. This technique has been used to study the semi-liquid PPUF decomposition by-product. The semi-liquid residue has been spread in a NaCl disc placed in a FTIR holder. The NaCl disc is transparent to IR beam. Spectra analysis did not provide further information about the nature of the liquid. The spectral response is very close to virgin polyether polyurethane foam.

2.7 Conclusion

This chapter has presented the state of the art in the analytical techniques used by many authors to determine the decomposition mechanism of polyurethane. The determination of the decomposition mechanism has been performed using a huge panoplie of methods centred on the analysis of gas release or in the change of mass in function of time or temperature. Some authors have analysed the decomposition mechanism at the molecular scale, but, the lack of knowledge of the phenomena

occurring at this scale makes this approach useless for fire safety engineering applications.

The experimental results obtained at the matter scale have been presented. The matter scale takes into account samples from 1 mg up to 110 mg, which are the smallest samples considered in this research. The equipment for measurements at the matter scale have been designed in order to reduce the influence of environmental conditions, and to focus on the analysis of some particular phenomena. The main assumption is that they do not deal with the diffusive effect and the mass and heat transfer phenomena from the centre of the particle towards the boundaries. This is a powerful hypothesis that allows considering that the experimental results are not affected by external noise. Nevertheless the very low density and the alveolar structure of the foam can probably be a cause of noise in the results while the effective area of heat and species exchange is unknown. However, up to date there is no mean to verify and quantify these effects. Despite of this, It was accurately determined the decomposition mechanism of PPUF under air and nitrogen atmospheres.

The experimental facilities used were TGA+FTIR$_{qlt}$ and TF+FTIR$_{qnt}$, which provided information on the change of the solid mass and gas release. Each event of mass change of the condensed phase has been correlated to particular gases release. It allowed verifying the decomposition mechanism, based on information from the solid and the gas phases with increasing temperature. This information, as well as the measurements of thermal properties represent the main input data for the numerical studies presented in the following chapters.

The transformations of the solid phase have also been analysed by imagery and chemical analyses. Binocular and SEM pictures were performed in order to examine the transformations suffered by the solid phase and the influence of oxygen during the decomposition process. The visual observation confirmed the mechanism found while analysing the change of mass and gas release. It was also found that the oxygen and the mode of heat transfer influence the kinetics of decomposition but that the mechanism of decomposition remains unchanged: Two decomposition stages are observed, the first decomposition stage is the breakdown of PPUF molecules that allows release of isocyanate and the second is the pyrolysis and further oxydation of polyol.

3 Matter scale model

3.1 Introduction

The experimental results obtained at the matter scale were presented in chapter 2. They provided valuable information on the behaviour of PPUF with the change of temperature. These results allowed determining the decomposition mechanism of PPUF based on the observations of solid as well as the gas phases.

The prediction of thermal decomposition is a main concern in FSE because it allows calculating the source term of fire. The source term is the quantification of the chemical energy that can be converted into heat by the flame. The prediction of thermal decomposition also allows calculation of pollutants release and fire spread, which are primary hazards of fire. The main limitations for the improvement of the predictions of fire behaviour of materials is the diversity of physical chemical phenomena that must be taken into account. Moreover, during the fire spread the heat and species transport occurs in transient state. The accurate prediction of the decomposition kinetics of solids must take into account parameters such as: temperature, heating rate, thermal history [80], oxygen concentrarion, porosity, nature of the solid fuel, etc.

The decomposition mechanism is the succession of stages that take place during the thermo-chemical decomposition of matter. This allows writing the mass balance and the comparison of experimental and calculated results, which is the basis of the method used to "calibrate" the model and to find the kinetic parameters of the reaction. So, the decomposition mechanism is the main input data for the model of PPUF thermal decomposition.

All the models referenced to matter scale found in literature are based on the hypothesis that samples behave as particles and no gradients between the centre and the boundary are found. Many authors have proposed methods to calculate the kinetic parameters of matter decomposition. Each model of thermal decomposition allows the calculation of a group of kinetic parameters, usually those of Arrhenius equations: Activation energy, pre-factor and reaction order. Nevertheless, up to now, all the methods used to determine the decomposition mechanism and to calculate the kinetic parameters are based on the single information of the condensed phase (TGA experiments).

The models from literature do not take into account information from the gas phase. As presented in chapter 2, the kinetic of gas release provide information on the reactions taking place in the solid phase. Analysing together information of the solid phase and gas phases allowed verifying that the decomposition mechanism is in agreement with the chemistry of the process. A decomposition mechanism that takes into account both information from the solid and gas phases, can be considered as "chemically correct" which is necessary for further improvements of the model.

The aim of this chapter is to improve a model of thermal decomposition of PPUF in order to be able to predict both the change of total mass and the kinetics of gases release in function of time or temperature. This allows calculating the kinetic parameters of a chemically correct process. Moreover, the groups of parameters found allow an accurate prediction of the decomposition process of PPUF under various experimental conditions, notably concerning the heating rates and atmospheres.

The kinetic parameters calculated by the current model are used into the pyrolysis models of Computational Fluid Dynamics (CFD) in order to simulate large-scale fire tests. Calculation of the decomposition rates constitutes a crucial challenge for the development of fire codes in order to make reliable predictions of HRR and pollutants formation.

This chapter is divided into six sections. Section one is the introduction. Section two is the state of the art in matter scale models with notably:

- A literature review of the methods defined by other authors to analyse mathematically the decomposition of PU and to calculate the kinetic parameters.

- The methods of thermal analysis applicable to PU, but used for various types of organic materials commonly found in buildings: wood, plastics, waste, biomass, etc.

Section three presents the improvements carried out to the model in order to take into account the gas phase. Section four deals with the analysis of stability of the model's code. Section five is the analysis of sensitivity. Section six presents the conclusions of the chapter.

3.2 State of the art in matter scale modelling

A better description of the source term is a current need for the evolution of FSE. The study and modelling of thermal decomposition of the materials involved in real fire is a crucial issue to accurately predict the source term. However, It is usually not well predicted or neglected in the fire simulation codes that are found on the market. A very precise prediction of fire behaviour is needed in the performance-based design of structures, which is the current trend in fire protection building design [80][81].

3.2.1 Background

The basic kinetic concepts used in thermal decomposition have been stated at the end of the nineteenth century by van't Hoff (1884), Arrhenius (1889), Wilhelmy (1891), Guldberg (1899) and Lewis (1905) during studies of single-step heterogeneous reactions. The rates of multi-step reactions were experimentally studied in the beginning of the twentieth century [82]. The modelling methods for multi-step thermal decomposition as known (used) nowadays have been developed in the end of the 1950's [83]. Since then, different methods have been proposed; the most widely used methods are described in the next subsections.

The models of thermal decomposition of solids is a compromise between simplifications of physical phenomena and the ability to take into accound as many details as possible. This compromise allows reproducing the reality in an acceptable manner dealing with mathematical and physical problems that can be resolved in a reasonable calculation time. Models are limited by: the knowledge of the physics [84],

calculation time [85], availability of measurements of material properties (data from literature), accuracy of these measurements [86], experimental perturbations, chemical knowledge of the process [87], criteria about what is acceptable and what is not, etc.

The problem of the validity of decomposition models at different scales appears very often: Very few models consider the transformations at the molecular level [33]. The analysis at the molecular level is crucial to understand the physics of the decomposition. Yet, the reactions at the scale of molecular chains such as initiation, branched chain, propagation and termination do not follow Arrhenius' law behaviour [9]. The models are stated at scales at which the mass is of a few milligrams, for which the reaction rates of the overall processes can be described using Arrhenius' equations.

Nevertheless, the most useful applications of decomposition models are in FSE, where the masses burning are of a few kilograms. The description of thermal decomposition required in FSE (behaviour in the solid phase) must reproduce the pattern observed at sizes near to the one of the product that is burning; this is not the case of the information found in literature. All the kinetic schemes of thermal decomposition considered in this work allow the prediction of solid transformations of masses of a few milligrams. Although, at the real scale, gradients of temperature and oxygen mass fraction as well as the interaction between the flame and the solid modify the decomposition kinetics. These effects are not considered at the matter scale because the dimensions of the sample are negligible: the sample is considered as a particle.

As stated, for years the main application of the modelling of thermal decomposition has been the FSE. But, the knowledge of decomposition mechanisms also has other applications such as: lost foam casting [88], smoldering combustion [89], remediation of polluted soils [15], pyrolysis and combustion of toxic and dangerous wastes [42][90], processes optimization [91][92], energetic recovery of biomass [93][94], etc.

Experimentally, TGA is the most widely used technique for estimating the kinetic mechanism and the corresponding kinetic parameters of thermal decomposition. Nevertheless, thermal analysis carried out based on TGA experiments may present some difficulties such as: scatter on kinetic parameters calculated with various methods, scatter on TGA curves with various heating rates or atmospheres, various kinetic behaviors of a single material, different kinetic parameters found from different manufacturers, possible influence of the transport phenomena into the material (generally neglected), etc [13][15].

Prior to the calculation of the kinetic parameters, the kinetic mechanism of decomposition must be found. It is one of the main tasks in FSE research. It requires the analysis of data from TGA and other experimental techniques.

In order to settle these difficulties, TGA data must be analysed together with qualitative and quantitative results from other experimental facilities. It allows the division of the bulk decomposition process into successive sub-processes activated when the matter temperature is increased. The division into sub-processes allows a particular characterisation and independent analysis of the species created and decomposed in each phase. Particularly, it allows an interpretation of the peaks observed in TGA mass-loss rate curve.

The next subsections present a detailed literature review of the methods existing for calculating the kinetic parameters of the thermal decomposition of solids. However, it has been found that the methods for determining the decomposition mechanism have not been as widely discussed, the one used in this research is discussed in subsections 2.5.4 and 3.3.1.

3.2.2 The model-fitting (modelistic) method

3.2.2.1 Principle of the model-fitting method

The model-fitting (modelistic) method consists in selecting from a list of models the one that best fits TGA non-isothermal experimental curves. In this method, the Arrhenius equations are referenced to remaining mass in sample holder. Thus, the model-fitting method is expressed in terms of the degree of conversion, α, which is equal to 0 at the beginning of the test and to 1 when all the mass has been decomposed. The degree of conversion is an overall property of the transformation kinetics, defined in Eq. (3-1).

$$\alpha = \frac{m_0 - m_t}{m_0 - m_f}$$

(3-1)

Where, m_0 is the mass of the sample at the beginning of the process, m_t is the mass of the sample at an arbitrary time t. m_f is the mass of the sample at the end of the process. The solid-state rate of reaction is assumed to be described by the product of two separate functions: $k(T)$, the rate constant and $f(\alpha)$, differential conversion function. The rate constant is the Arrhenius equation, while the conversion function is the reaction model. The reaction rate is defined mathematically in Eq. (3-2). The main hypothesis for allowing the use of Eq. (3-2) is that reactions are autocatalytic, in other words, they do not require a complementary chemical product to initiate the reaction. Thus, $f(\alpha)$ is only function of the degree of conversion and $k(T)$ is only function of temperature [95].

$$\frac{d\alpha}{dt} = k(T)f(\alpha) = A\exp\left(-\frac{E}{RT}\right)f(\alpha) \tag{3-2}$$

The Arrhenius equation is expressed in function of: A, pre-exponential factor. E, apparent activation energy. R, universal gas constant. T, absolute temperature. For non-isothermal conditions, authors prefer to write Eq. (3-2) as a function of heating rate, β. In this case, the derivative of the degree of conversion is expressed with respect to temperature, see Eq (3-3).

$$\beta\frac{d\alpha}{dT} = A\exp\left(-\frac{E}{RT}\right)f(\alpha) \tag{3-3}$$

$$\therefore \beta = \frac{dT}{dt}$$

In Eq. (3-2) and (3-3), the reaction model, $f(\alpha)$, represents a certain solid-state mechanism that gives rise to the characteristic change of the degree of conversion with time (α vs t). Experimental data can be compared against a set of model plots in order to choose the one that accurately reproduces experiments. This enables the data to be interpreted in terms of the mechanism represented by the chosen reaction model [82][96].

The Arrhenius law of Eq. (3-3) relates the rate constant of a single-step reaction to temperature. It is generally assumed that E and A remain constant. However, it has been shown that in solid-state reaction kinetics, the parameters may vary with the

degree of conversion. In solid state, a variation in apparent activation energy could be observed due to a complex decomposition mechanism [82].

The reaction models, $f(\alpha)$, are in general listed in the integral form, $g(\alpha)$, of Eq. (3-3), which is presented in Eq. (3-4) [97].

$$g(\alpha) = \int_0^\alpha [f(\alpha)]^{-1} d\alpha \qquad (3\text{-}4)$$

The models the most commonly used are listed in Table 3-1.

Table 3-1. Set of reaction rate models applied to describe the reaction kinetics in heterogeneous solid state systems (*e.g.* polymers). (Source [23][41][82][98][99]).

No.	Symbol	Reaction model source	$f(\alpha)$	$g(\alpha)$
1	P1	Power law [23][41][82][99]	$4\alpha^{3/4}$	$\alpha^{1/4}$
2	P2	Power law [23][41][82][99]	$3\alpha^{2/3}$	$\alpha^{1/3}$
3	P3	Power law [23][41][82][99]	$2\alpha^{1/2}$	$\alpha^{1/2}$
4	P4	Power law [23][41][82][99]	$\frac{2}{3}\alpha^{-1/2}$	$\alpha^{2/3}$
5	R2	Phase boundary controlled reaction (contracting cylinder, *i.e.* bidimensional shape) [23][41][82][98][99]	$2(1-\alpha)^{1/2}$	$1-(1-\alpha)^{1/2}$
6	R3	Phase boundary controlled reaction (contracting sphere, *i.e.* tridimensional shape) [23][41][82][98][99]	$3(1-\alpha)^{2/3}$	$1-(1-\alpha)^{1/3}$
7	F1	First-order (Marpel)/ Random nucleation [23][41][82][98][99]	$1-\alpha$	$-Ln(1-\alpha)$
8	F2	Second-order reaction [41]	$1/(1-\alpha)$	$(1-\alpha)^2$
9	F3	Third-order reaction [41]	$\left[1/(1-\alpha)\right]^2$	$(1-\alpha)^3$
10	E1	Exponential law [41][98]	α	$Ln(\alpha)$
11	A2	Avrami-Erofe'ev(m=2) [23][41][82][98][99]	$2(1-\alpha)\left[-Ln(1-\alpha)\right]^{1/2}$	$\left[-Ln(1-\alpha)\right]^{1/2}$
12	A3	Avrami-Erofe'ev(m=3) [23][41][82][98][99]	$3(1-\alpha)\left[-Ln(1-\alpha)\right]^{2/3}$	$\left[-Ln(1-\alpha)\right]^{1/3}$
13	A4	Avrami-Erofe'ev(m=4) [23][41][82][99]	$4(1-\alpha)\left[-Ln(1-\alpha)\right]^{3/4}$	$\left[-Ln(1-\alpha)\right]^{1/4}$
14	A5	Avrami-Erofe'ev(m=3/2) [23]	$\frac{3}{2}(1-\alpha)\left[-Ln(1-\alpha)\right]^{2/3}$	$\left[-Ln(1-\alpha)\right]^{2/3}$
15	B1	Proust-Tompkins [41]	$\alpha(1-\alpha)$	$Ln(\alpha/(1-\alpha))$
16	D1	One-dimensional diffusion [23][41][82][98][99]	$\frac{1}{2}\alpha^{-1}$	α^2

No.	Symbol	Reaction model source	$f(\alpha)$	$g(\alpha)$
17	D2	Two-dimensional diffusion (bidimensional particle shape) Valensi Equation [23][41][98]	$\left[-Ln(1-\alpha)\right]^{-1}$	$(1-\alpha)Ln(1-\alpha)+\alpha$
18	D3	Three-dimensional diffusion (bidimensional particle shape) Jander Equation [23][41][82][98][99]	$\dfrac{3}{2}(1-\alpha)^{2/3}\left[1-(1-\alpha)^{1/3}\right]^{-1}$	$\left[1-(1-\alpha)^{1/3}\right]^{2}$
19	D4	Three-dimensional diffusion (bidimensional particle shape) Ginstling-Brounshtein Equation [23][41][98]	$\dfrac{3}{2}\left[(1-\alpha)^{1/3}-1\right]^{-1}$	$\left[\left(1-\dfrac{2\alpha}{3}\right)-(1-\alpha)^{2/3}\right]$

The model-fitting method involves the comparison of various calculated α vs T curves with non-isothermal experimental ones. Simultaneously, the calculation of E and A is carried out by resolving the model. The main disadvantage of this method is that usually, different reaction models may lead to indistinguishable fits of experimental data, whereas the numerical values of the corresponding Arrhenius parameters crucially differ. The various acceptable Arrhenius parameters have been shown to be correlated through the relation of compensation effects. The opposite situation may also be found: the experimental data do not closely follow any of the model plots. In both cases, the model cannot practically lead to unambiguous mechanistic interpretation.

Eq. (3-4) is also usually presented in the form of Eq. (3-5).

$$g(\alpha)=\frac{A}{\beta}\int_{T_0}^{T}\exp\left(-\frac{E}{RT}\right)dT=\frac{AE}{\beta R}\int_{x}^{\infty}\frac{\exp(-x)}{x^2}dx=\frac{AE}{\beta R}p(x) \tag{3-5}$$

Where, $x=\dfrac{E}{RT}$

The term $p(x)$ is the temperature integral that does not have analytical solution. Many of the problems connected with the application of the reaction rate containing the $p(x)$

term result from the inability to accurately approximate the temperature integral by a simple closed-form. $p(x)$ is suitable for use in graphical form to determine the Arrhenius parameters [95]. According to Flynn [95], at least several hundred papers can be found in literature about the temperature integral. Most of them have been devoted to its evaluation by series, to numerical solutions and various approximations. Many authors presented tables of $p(x)$ for wide ranges of values of x. The aim of the present research is not to discuss the approximations and accuracy of the temperature integral term.

3.2.2.2 Application of the model-fitting method to polyurethane

Rogers *et al.* [23] in 1981, studied the kinetics of the decomposition of a flexible polyurethane foam composed of tolylene diisocyanate (TDI, 80% of 2,4 isomers and 20% of 2,6 isomers). They used TGA experiments under nitrogen atmosphere. Two steps of decomposition were observed. These steps corresponded to the mechanism stated in the chapter on matter scale experiments: The first stage, is the collapse of the cellular structure of the foam to form a tarry viscous liquid. The second stage, is the decomposition of the intermediate product.

They apply the model-fitting method using reaction rate models of Table 3-1. Selection of the best reaction laws was not a simple task. They use the Gorbachev equation presented in Eq. (3-6) to find a solution of the reaction rate law.

$$g(\alpha) = \frac{A}{\beta} \int \exp\left(-\frac{E}{RT}\right) dT \approx \frac{ART^2}{\beta(E+2RT)} \exp\left(-\frac{E}{RT}\right) \tag{3-6}$$

The authors validated this approach with an integral Runge-Kutta algorithm of the random nucleation model (model No. 7 in Table 3-1). They found good accuracy between the algorithm and the theoretical approach. This allowed the authors to calculate the kinetic parameters at a heating rate of 5 °C·min^{-1}. The non-uniqueness of the kinetic parameters did not permit the authors to accurately define a decomposition mechanism. In order to clarify the mechanism, authors compared results from model

No. 7 with results obtained supposing simple competitive, independent and consecutive reactions models No. 13 and 16 from Table 3-1.

Branca *el al.* [10] analysed the thermogravimetric curves obtained in isothermal and non-isothermal tests. The material analysed was a rigid polyurethane foam of density 38 kg·m^{-3}. Authors stated that the polyurethane foam conversion in isothermal tests is higher under air than under nitrogen at a given time. This is produced by the highest reactivity in presence of environment oxygen causing breakage of the polymeric chains. In our works no isothermal tests were performed, nevertheless, this behaviour can be derived from dynamic tests, setting a low pyrolysis temperature.

MLR curves obtained in TGA non-isothermal tests (5, 10, 15 and 20 °C·min^{-1}.) presented three peaks under both atmospheres, air and nitrogen. Authors found that at low heating rate (3 °C·min^{-1}), the first pick remained at the same temperature independently of the atmosphere. The second and third peaks of MLR under air were delayed respectively of 30 °C and 55 °C through the lower temperatures with respect to nitrogen tests. Based on those results, the authors concluded that the "oxygen exerts a small influence on the decomposition rate of polyurethane to diisocyanate and polyols […]". As shown in last section, in our research MLR curves under nitrogen present only two peaks and oxygen has a very strong influence on PPUF decomposition kinetics.

The three reactions mechanism proposed by Branca *el al.* [10] is (3-7):

$$Foam \rightarrow \upsilon_1 \cdot Char_1 + (1 - \upsilon_1) \cdot Volatile_1 \qquad (3\text{-}7)$$

$$\upsilon_1 \cdot Char_1 \rightarrow \upsilon_2 \cdot Char_2 + (\alpha - \upsilon_2) \cdot Volatile_2$$

$$\upsilon_2 \cdot Char_2 \rightarrow \upsilon_2 \cdot Volatile_3$$
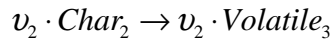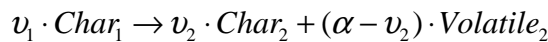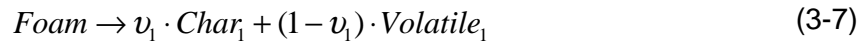
Where, υ_1 and υ_2 .are stoichiometric coefficients. The reaction rates were calculated with Eq. (3-8) and MLR were considered to be linear functions of the solid mass fractions, K_i (see Eq. (3-9)).

$$\omega_i = A_i \exp\left(-\frac{E_i}{RT}\right) \qquad (3\text{-}8)$$

$$MLR_i = -\omega_i K_i \qquad (3\text{-}9)$$

Authors found that the agreement between the measurements and predictions, was good when the stoichiometric parameters were allowed to vary with the heating rate. The stoichiometric coefficients found were: $\upsilon_1 = 0.94 \pm 0.02 \; g \cdot g_{sample}^{-1}$ and $\upsilon_2 = 0.47 \pm 0.02 \; g \cdot g_{sample}^{-1}$.

Lefebvre *et al.* [100] modelled the decomposition of rigid polyurethane foam under nitrogen atmosphere as a three-stage process using the Invariant Kinetic Parameters (IKP) method. This one uses the Arrhenius law presented in Eq. (3-3) and is based on the Coast and Redfern principle. According to this principle, fourteen (Table 3-1) "apparent" activation energies, E_v and pre-exponential factors, A_v are calculated. The same number of MLR curves is modelled with each group of parameters.

For each function $f_v(\alpha)$ (Eq. (3-3)), at a heating rate β_v, the $\log A_v$ is plotted as a function of the E_v. If a compensation effect is observed, then, a linear relation may be established for each heating rate. The linear relation is defined in function of rate constant k_v (see Eq. (3-10)).

$$\log A_v = B_v + I_v E_v \qquad (3\text{-}10)$$
$$B_v = \log(k_v)$$
$$I_v = (2.3RT_v)^{-1}$$

The slopes and the intercepts of the straight lines allow calculating B_v and I_v. T_v and k_v are parameters characteristic of the experimental conditions. Finally, $\log(k_v)$ *vs* $1/T_v$ is plotted. A straight line is expected in Eq. (3-11).

$$\log(k_v) = \log(A_{inv}) - \frac{E_{inv}}{2.3RT_v} \qquad (3\text{-}11)$$

The invariant A_{inv} and E_{inv} are calculated respectively with the slope and the y-intercept of Eq. (3-11). The IKP method, calculates a single kinetic function or a combination of kinetic functions occurring at each stage of the decomposition. The authors highlighted that the activation energies increase with the stage of

decomposition. Moreover, the calculation of the kinetic parameters is only carried out taking into account the degree of conversion between 0.1 and 0.5 at each stage. The main disadvantage of this method is that if no compensation effect is identified, it is impossible to calculate the invariant kinetic parameters. The compensation effect has not been precisely characterized yet (some more comments on the compensation effect are given in subsection 3.2.5).

Esperanza *et al.* [42] modelled the thermal decomposition of polyurethane refuses. Because of the heterogeneity of raw materials, they considered a sample as constituted of three different fractions of refuse, M_i. The fractions follow competitive parallel decomposition. Each fraction follows a reaction with different kinetic parameters. R_i and V_i are respectively the solid residues and the volatiles generated during the reactions, see Eq. (3-12).

$$M_i \rightarrow a_i R_i + b_i V_i \, , \ i = 1, 2, 3 \qquad (3\text{-}12)$$

Where, a_i and b_i are respectively the yields of solid and volatiles released per unit of burnt mass. Eq. (3-13) expresses the MLR as a function of: W_i, the remaining mass at a time t. $W_{\infty i}$, the final fraction of solid residue; k_i is the Arrhenius rate constant of the process, and n_i is the reaction order.

$$\frac{dW_i}{dt} = -k_i \left(W_i - W_{\infty i} \right)^{n_i} \, , \ i = 1, 2, 3 \qquad (3\text{-}13)$$

Authors numerically integrated Eq. (3-13) and optimized a total of seventeen parameters. Optimization was performed using the Objective Function (OF) presented in Eq. (3-14), which compares experimental and calculated data. The optimization method is not detailed in their paper.

$$OF = \left(\left(\frac{\Delta W}{\Delta t} \right)_{\exp} - \left(\frac{\Delta W}{\Delta t} \right)_{calc} \right)^2 \qquad (3\text{-}14)$$

Font *et al.* [26] used in 2001 the model proposed by Esperanza *et al.* [42] in 1997 to calculate the kinetic parameters of decompositions of PU-based additives. Authors, numerically integrated the differential equations (Eq. (3-13)) and used a "flexible

simplex method" to optimize the kinetic parameters. The objective function is the one presented in Eq. (3-14). Font *et al.* [26] stated as a conclusion of their work, that the reactions leading to the formation of volatiles have similar apparent activation energies to those leading to the formation of carbon residue. However, this represents a general hypothesis of the models of thermal decomposition, because a single reaction transforms a reactive into a solid residue and gases.

As shown, multiple methods relative to the model-fitting technique have been proposed by various authors. Nevertheless, the uncertainty mentioned above in the Arrhenius parameters obtained by model-fitting makes them virtually useless for practical purpose, *e.g.* predicting the reaction kinetics at an arbitrary temperature [82].

3.2.3 The free model method (Isoconversional)

3.2.3.1 Principle of the isoconversional method

Kissinger, in 1957 [83], described a method to determine the pre-exponential factor, the activation energy and the reaction order of thermal decomposition of magnesite, calcite, brucite, kaolite and halloysite. The type of reactions observed with these minerals are single-stage. In these reactions, the solid is transformed into residue and gas. The experimental approach was Differential Thermal Analysis (DTA). The reaction rate is presented in Eq. (3-15).

$$\frac{d\alpha}{dt} = A\exp\left(\frac{-E}{RT}\right)(1-\alpha)^n \qquad (3\text{-}15)$$

Kissinger's method is based on the analysis of the conditions needed to attain the maximum reaction rate. The postulate is: if a reaction proceeds at a rate varying with temperature (*i.e.* possesses an activation energy), the position of the peak varies with heating rate if the others experimental conditions are kept unchanged.

The activation energy E may be calculated by resolving Eq. (3-16), where, β is the heating rate and T_m is the sample temperature at which the peak DTA deflection occurs.

$$\frac{d\left(Ln\dfrac{\beta}{T_m^2}\right)}{d\left(\dfrac{1}{T}\right)} = -\frac{E}{R}$$

The calculation of the reaction order, n, is performed using a variable called the "shape index", S. The shape index is the absolute value of the ratio of the slopes of tangents at the inflection points of the curve of MLR *vs* temperature. It accounts for the asymmetry of the MLR (single peak curve). n is calculated according to Eq. (3-17).

$$n = 1.26 \cdot S^{\frac{1}{2}}$$

$$S = \left|\frac{a}{b}\right|$$

Where, a and b are the horizontal distances from the centre of the MLR peak to the tangents of the inflections points (asymmetry) as presented in Figure 3-1.
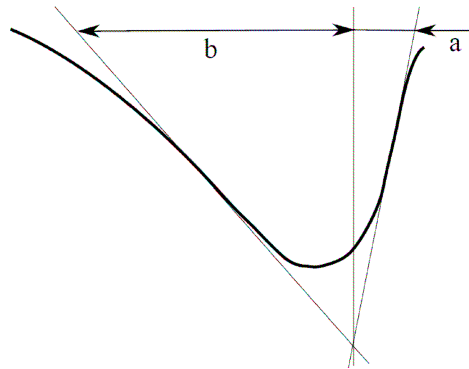
Figure 3-1 Definition of the asymmetry of MLR curves in the Kissinger's method.
Source (Kissinger [83]).

Kissinger [83], assumed that n remains constant during a TGA run. This is the main hypothesis for deduction of Eq (3-16). Thus, this method is valid only for single-stage reactions. The pre-exponential factor, can be calculated as shown in Eq. (3-18).

$$A = \frac{E\beta}{RT_m^2 n(1-\alpha)_m^{n-1} \cdot \exp\left(-\dfrac{E}{RT_m}\right)}$$

Friedman, in 1963 [19], studied the kinetics of thermal decomposition of a phenolic resin reinforced with laminated fiberglass composite. In this research, the kinetic parameters were calculated using a method based on the intercomparison of TGA experiments carried out at several different rates of temperature rise. The linear heating rates were between 0.8 °C·min^{-1} to 6 °C·min^{-1}. Tests were performed under nitrogen atmosphere up to a temperature of 900 °C. Finally, the residues were burnt under air at 1000 °C. This constitutes the basis for the development of the isoconversional method for non-isothermal conditions.

Friedman defined the mass change in terms of kinetic parameters in Eq. (3-19).

$$Ln\left[\left(-\frac{1}{m_0}\right)\left(\frac{dm}{dt}\right)\right] = Ln(A) + Ln\left(f\left(\frac{m}{m_0}\right)\right) - \frac{E}{RT} \qquad \text{(3-19)}$$

Where, m, is the mass of organic material. m_0, is the original weight of the reinforced plastic. $f\left(m/m_0\right)$, is a function of the weight of organic material. $f\left(m/m_0\right)$ is assumed to be constant for constant values of m/m_0. This is comparable to assuming that the process is independent from the temperature and is only dependent on the instantaneous weight of the organic material. Friedman selected twelve values of m/m_0 between 0.675 and 0.950 and plotted $Ln\left[\left(-\frac{1}{m_0}\right)\left(\frac{dm}{dt}\right)\right]$ vs $\frac{1}{T}$, finding straight lines.

$\left[-\frac{E}{R}\right]$ are the slopes of straight lines and $Ln\left(Af\left(\frac{m}{m_0}\right)\right)$ the intercepts to y-axis. From this analysis Friedman [19] pointed out a compensation effect between kinetic parameters: "[…] a positive error in A, which would make the reaction appear to go faster, is compensated for by a positive error in E [ΔE in the paper], which would tend to make the reaction appear to go slower." The author also defined the function of mass change in terms of the initial mass of sample, m_0, the final mass of char, m_f and kinetic order of the reaction, n; see Eq. (3-20).

$$f\left(\frac{m}{m_0}\right) = \left(\frac{m - m_f}{m_0}\right)^n$$

<div align="right">(3-20)</div>

The plot of $Ln\left(Af\left(\frac{m}{m_0}\right)\right)$ vs $Ln\left(\frac{m - m_f}{m_0}\right)$ is a straight line, in which n is the slope and $\ln(A)$ is the y-intercept. This method present a particularity: The fitting between the experimental and the theoretical curves is highly dependent on the value of m_0.

The isoconversional method is often called in literature the Friedman method. It allows the estimation of the Arrhenius parameters in a model-independent manner. This analysis is recommended in order to obtain a reliable kinetic description of the process studied. It provides a good compromise between the oversimplified but widely used single-step Arrhenius kinetic treatment and the prevalent occurrence of processes with multi-step and/or non-Arrhenius kinetics. The isoconversional methods usually produce E values that vary with α and T. This can be used to detect multiple-step kinetics [82].

The isoconversional integral method is based on an approximate form of the temperature integral that results from the rearrangement and integration of Eq. (3-5). However, as explained, the temperature integral, $p(x)$, has no analytical solution. Various authors proposed approximations of the integral temperature term in the isoconversional method. Some of these simplifications are presented in Table 3-2. This table presents the method, approximations, forms of integral temperatures and required plots.

Table 3-2. Approximations of the integral temperature in the isoconversional method (Source [99][101]).

No	Method, source	Approx.	Form of the integral temperature	Plot	
				X-axis	Y-axis
1	Kissinger-Akahira-Sunose [99]	Coats-Redfern	$Ln\left(\dfrac{\beta}{T_\alpha^2}\right) = Ln\left(\dfrac{A_\alpha R}{E_\alpha g(\alpha)}\right) - \dfrac{E_\alpha}{RT_\alpha}$	$Ln\left(\dfrac{\beta}{T_\alpha^2}\right)$	$\dfrac{1}{T_\alpha}$
2	Flynn-Wall-Ozawa [99]	Doyle	$Ln(\beta_i) = Ln\left(\dfrac{A_\alpha E_\alpha}{Rg(\alpha)}\right) - 5.331 - 1.052\dfrac{E_\alpha}{RT_\alpha}$ Where $Ln(p(x)) = -5.331 - 1.052x$	$Ln(\beta_i)$	$\dfrac{1}{T_\alpha}$
3	Vyazovkin [101]	Senum-Yang	$\phi = \left|\displaystyle\sum_{i=1}^{m}\sum_{j\neq i}^{m}\dfrac{I(E_\alpha,T_{\alpha,i})\beta_j}{I(E_\alpha,T_{\alpha,j})\beta_i}\right|$ Where $p(x) = \dfrac{\exp(-x)(x^3 + 12x^2 + 36x + 24)}{x(x^2 + 10x + 18)}$		

For $\alpha = const.$, the plots of Table 3-2, are obtained from thermal curves recorded at several heating rates. In the straight lines, the slopes allow evaluation of the apparent activation energies and y-intercepts allow calculation of the pre-exponential factors. These approximations imply that A and E are calculated for a known analytical form of the integral function of conversion $g(\alpha)$ (see Table 3-1) [101]. The approximations in Table 3-2 are allowed by very important simplifications of the temperature integral that can induce error in the parameters calculated [99].

In the Doyle approximation, if $x < 20$ errors are higher than 10%. Flynn in Ref. [82] suggested corrections in order to obtain accurate activation energy values. These corrections are not presented here.

The Vyazovkin method is called nonlinear isoconversional method, where m is the number of heating rates. $I(E_\alpha, T_{\alpha,i})$ is the exponential integral ($p(x)$) that results from the heating rate β_i. $I(E_\alpha, T_{\alpha,j})$ is the exponential integral from heating rate β_j. The apparent activation energy is the value that minimizes ϕ for given values of T_α and β [99].

3.2.3.2 Application of the isoconversional method to various materials

In literature, the application of the isoconversional method to PU has been very limited. Hereafter are presented some applications and improvements proposed by various authors in order to study the thermal decomposition of diverse materials. These methods could be used with PU.

Jankovic [101], in 2008, used the master plot method to determine kinetic parameters of potassium metabisulfite. The master plot method is based on the comparison of theoretical plots with experimental plots. Theoretical plots are obtained for a wide range of ideal kinetic models (Table 3-1). The comparison requires the previous transformation of the experimental data into the corresponding master plots. This leads to the selection of the appropriate conversion model for the solid state reaction investigated.

One of the most used master plots is at $\alpha = 0.5$, Eq. (3-21) presents the method to find the master plot at a conversion of 50%.

$$g(0.5) = \frac{AE}{\beta R} p(x_{0.5}) \qquad (3\text{-}21)$$

$$\frac{g(\alpha)}{g(0.5)} = \frac{p(x)}{p(x_{0.5})}$$

Where, $x_{0.5}$ is calculated using the temperature required to attain 50% of conversion degree. Plots of $g(\alpha)/g(0.5)$ *vs* α for various $g(\alpha)$ (Table 3-1) corresponds to the theoretical master plots. Both the conversion-temperature profile (α *vs* T) and the values of E should be known in advance in order to draw the experimental master plots of $p(x)/p(x_{0.5})$ *vs* α. The master plots method requires approximated formulas of the term $p(x)$. Eq. (3-21) indicates that for a given α, the experimental value of $p(x)/p(x_{0.5})$ and the theoretically calculated values of $g(\alpha)/g(0.5)$ are equivalent when an appropriate conversion model is used. Consequently, the integral "model-fitting" master-plot method can be used to determine reaction models for solid-state

reactions. The author also concluded that even combining the analytical methods, the kinetic data cannot be calculated unambiguously.

Mamleev *et al.* [102] proposed a model-free method called Modulated Thermogravimetric Analysis (MTGA). It is based on a TGA test in which the linear heating rate is perturbed by a sinusoidal wave with controlled amplitude and frequency. The modulated temperature $T_{mod}(t)$ at a time t, is calculated with Eq. (3-22).

$$T_{mod}(t) = T_0 + \beta t + A_m \sin(2\Pi \omega_m t) \tag{3-22}$$

Where, A_m is the amplitude of the modulation ($A_m = 5°C$) and ω_m is the number of oscillations per second [s^{-1}]. The aim of temperature modulation is to predict a hypothetical derivative of mass-loss that corresponds to the absence of the modulation (perturbation). The advantage of their method is that kinetic parameters can be calculated with a single experimental curve.

Authors illustrated the method with a hypothetical example of a two-stage decomposition similar to observed in PPUF under nitrogen atmosphere. The equations that governed the reactions are of the type:

$$\frac{d\alpha_1}{dt} = k_1(1-\alpha_1)^2 \exp\left(-\frac{E_1}{RT}\right) \tag{3-23}$$

$$\frac{d\alpha_2}{dt} = k_2(1-\alpha_2)\exp\left(-\frac{E_2}{RT}\right) \tag{3-24}$$

Note that the first reaction (Eq. (3-23)) is a second-order equation and the second reaction (Eq. (3-24)) is of the first order. In the MTGA method, the oscillation of the derivative is the main source of kinetic information. The perturbation function allowed the authors to conclude that the unmodulated MLR curve corresponds to the modulated one at the inflection points (maxima and minima) for the periodic component of temperature.

The method proposed by Mamleev *et al.* [102], becomes less accurate when increasing the heating rate. The accuracy is acceptable only if the heating rate is selected providing 10 to 15 periods of modulation for each stage of decomposition (*i.e.* the heating rate is less than 5 °C·min^{-1}). The calculation of the kinetic parameters A

and E for a given n is accurate only for a one-stage process and small periods of modulation. The calculation of kinetic parameters is based on the minimization of a deviation function between experimental and calculated curves [103].

Mamleev *et al.* [103], affirmed that the activation energy is an effective (apparent) value for a model. E may not be associated with a temperature range or degree of conversion. Otherwise, no physical sense may be attributed to it. In consequence, it cannot be used for predictions. This does not seem to be a very precise conclusion, because a reaction rate calculated with given kinetic parameters is measurable only in a particular range of temperature.

Mamleev *et al.* [16], presented a generalisation of the MTGA method. It allowed the analysis of TGA results for materials with more than one decomposition stage. A point of their procedure that needs to be highlighted is the requirement that each stage must be independent and well resolved. The presence of several stages not well resolved represents complications to the analysis [103]. The methodology was used for the analysis of rigid PU foam. Under air, the TGA curves presented three decomposition stages.

3.2.4 Combined model-fitting and model-free methods

This procedure is issued from a combination of the model-fitting and the model-free methods explained above. It was used by Cancellieri *et al.* in 2005 [104] to determine the kinetic parameters of the thermo-oxidative decomposition of organic materials (biomass). DSC and TGA data were obtained under air sweeping. The experiments allowed identifying two oxidative reactions at heating rates between 10 ℃·min^{-1} and 40 ℃·min^{-1}. This method requires the numerical and experimental individualization of each reaction peak. This allowed the measurement of the enthalpy variation of each exothermic reaction.

The numerical separation of the reaction peaks was carried out fitting the global curve with empirical equations. These equations have adjustable parameters for each peak of fuel release. The parameters of the empirical equations showed to be constant for all the species and heating rates.

A model-free method was used to determine the apparent activation energies of each insulated curve. Cancellieri *et al.* [104] used the Kissinger-Akahira-Sunose approximation described in Table 3-2 for degrees of conversion between 0.1 and 0.9. The enthalpy variations and the apparent activation energies calculated experimentally were injected in a model-fitting method. It allowed calculating the reaction order and pre-exponential factor of each oxidative reaction. Their model-fitting method is based on Eq. (3-2) and the $f(\alpha)$ was chosen from the options of the Table 3-1.

However, the interpretation of DSC curves showed not to be a simple task. Particularly, because of the position change of the DSC baseline. The abrupt changes in slope or position of the DSC baseline usually indicate second-order transitions (*i.e.* glass transition in polymers) [41] and strong change in the nature of the solid sample.

3.2.5 Models of the decomposition of solids based on TGA isothermal tests

The main disadvantage of the results obtained from TGA isothermal experiments is that they are strictly valid for the temperatures for which they have been obtained [96].

Ceamanos *et al.* [13], used a variation of Eq. (3-3) (reminded here after) to model the isothermal test of polyethylene, allowing the deduction of an expression for the change of the degree of conversion (see Eq. (3-25)).

$$\beta \frac{d\alpha}{dT} = A \exp\left(-\frac{E}{RT}\right) f(\alpha) \qquad \text{Reminder of Eq (3-3)}$$

$$\log\left(\frac{d\alpha}{dt}\right) = \log k_i + n \log(W_s - \alpha) \qquad (3\text{-}25)$$

Where, W_s, is the weight of the non-pyrolysable fraction at the set temperature. The reaction order, n, is the slope of the plot $\log(d\alpha/dt)$ *vs* $\log(A_s - X_s)$. n, is defined

between a range of conversion factor from 0.1 to 0.95. The kinetic constant, k_i, may be calculated from the slope of the plot $Ln(A_s - X_s)$ vs t.

In the same study, the authors plotted pre-exponential factors in function of the activation energies issued from the literature (for PE). They found a linear relation between the all data groups. Ceamanos *et al.* [13] explained the linearity by the compensation effect resulting from the combination of mathematical, physicochemical and experimental causes. The points (couples of A and E) have been obtained under different experimental conditions and with reaction orders.

Bilbao *et al.* [11], determined kinetic equations and the corresponding constants for the weight loss of TGA tests. The materials used were PPUF of densities between 20 kg·m^{-3} and 30 kg·m^{-3}. They performed isothermal and dynamic runs under air and nitrogen atmospheres. Under nitrogen, the experiments were carried out between 200 ℃ and 385 ℃. Under air the range was between 200 ℃ and 300 ℃.

They observed the same dynamics of mass change independently of the density. However, Kanakia in [23] stated that the increase in the molecular weight of polyol generates a decrease of the activation energy and the reaction order, and thus a variation in the dynamics of mass.

Bilbao *et al.* [11] referenced the works of Benbow and Cullis (1975) [105]. They wrote that "the presence of oxygen does not influence the decomposition rate of polyurethane to diisocyanate and polyols, although it affects the breakage of the polymeric chains". First, this is not a conclusion of the works of Benbow. Second, this is in contrast to experimental results found in this research (see Figure 2-9 b).

Criado *et al.* [98], studied in 1984 methods to calculate the activation energies based on a series of laws for the mass change. They conducted their study using hypothetical isothermal experiments. They assumed that discrete isothermal data allowed the discernment of the best kinetic model. The authors proposed the Arrhenius law dependent on time instead of temperature. The integral function of the degree of conversion is presented in Eq. (3-26).

$$g(\alpha) = A\exp\left(-\frac{E_i}{RT}\right)(t - t_0)$$

(3-26)

Where, t is the total time of the test. t_0, is the time elapsed until the setting temperature is reached (steady state temperature). The authors concluded that the proper value of the activation energy is obtained independently of the kinetic equation taken for the calculations. They also found linear relation between the different kinetic laws, taking randomly one law as reference. The linear relations are valid for reaction fractions between $0.05 < \alpha < 0.95$.

3.2.6 Deduction of a multi-reaction, multi-step model of thermal decomposition

The previous subsection presented some of the most common methods that allowed many authors calculating the kinetic parameters of thermal decomposition of various materials. Most of these models were performed to predict the thermal decomposition of solids with single-stage decomposition. However, most of them were developed for materials others than PPUF. The literature relative to the calculation of kinetic parameters of polyurethane decomposition is scarce [42].

The model presented in this subsection is the one improved and used in this research. It has been particularly proposed to analyse polyurethane foam decomposition. The use of this method was allowed thanks to the improvements of computers and the power of calculation: The solution of the mathematical equations is determined computationally and an optimization technique is used to calculate the kinetic parameters. More details about the solution of the mathematical equations with this method are given in section 3.3. In this subsection, the development of the method is presented.

The first reduced mechanism used in order to model the PF decomposition was proposed by Ohlemiller in 1985 [106]. Based on the works of Rogers *et al.* [23], Ohlemiller used the thermo-oxidative decomposition mechanism to study PF smouldering combustion. This mechanism of thermal decomposition has been largely used to describe the decomposition of polyurethane in fire conditions different from smouldering. The mechanism included three reactions (see Table 3-3).

Table 3-3. Kinetic mechanism for thermal and thermo-oxidative decomposition of PU foam. Proposed by Ohlemiller in 1985 (Source [23][106]).

No	Reaction	Transformation
1	$foam \rightarrow v_{c,p} char + v_{g,p} gas$	Foam pyrolysis
2	$foam + v_{O_2,o} O_2 \rightarrow v_{c,o} char + v_{g,o} gas$	Virgin foam oxidization
3	$char + v_{O_2,c} O_2 \rightarrow v_{a,c} Ash + v_{g,c} gas$	Char oxidization

This mechanism only considers one pyrolysis reaction. It is not able to reproduce the double peak behaviour of PF decomposition under inert atmosphere presented in Figure 2-9 and Figure 2-13.

The TGA experimental results of Chao *et al.* [92] performed in non-fire-retarded PU foam, showed two peaks under nitrogen and three peaks under air. Based on this works, Rein in his PhD research (2005) [107], proposed a five-reactions mechanism where each peak in the MLR curve corresponded to the MLR of one solid species. The calculated shape of MLR is produced by the addition of the individual shapes of the competing pyrolysis and oxidization reactions.

The model of Rein is based on the mechanism of Table 3-3, to which two more equations were added. The new reactions allowed production and destruction of a new solid species called β-foam. This species is an intermediary stage between virgin foam and char: β-foam is formed by virgin foam pyrolysis, and converted into char by pyrolysis and oxidization.

Under air atmosphere, Rein associated the first MLR peak to MLR of virgin foam, the second to MLR of β-foam and the third to MLR of char. Under nitrogen, the first peak of MLR is associated to the decomposition of virgin foam, and the second to char. The five-equations mechanism allowed Rein e*t al.* [108][109] to model the displacement of the smoulder front in both opposed and forward smouldering condition. The decomposition mechanism used by Rein is presented in Table 3-4.

Table 3-4. Kinetic mechanism for pyrolysis and oxidization of PU foam during smouldering combustion. Proposed by Rein in 2005 (Source [107]).

No	Reaction	Transformation
1	$foam \rightarrow v_{\beta,p}\beta - foam + v_{gp,p}gas$	Foam pyrolysis
2	$\beta - foam \rightarrow v_{c,p\beta}char + v_{gp,p\beta}gas$	Polyol pyrolysis
3	$foam + v_{O_2,o}O_2 \rightarrow v_{c,o}char + v_{gp,o}gas$	Virgin foam oxidization
4	$\beta - foam + v_{O_2,o\beta}O_2 \rightarrow v_{c,o\beta}char + v_{gp,o\beta}\beta gas$	β-foam oxidization
5	$char + v_{O_2,c}O_2 \rightarrow v_{r,c}residue + v_{gp,c}gas$	Char oxidization

Each reaction of the mechanism presented in Table 3-4 follows an Arrhenius law expressed in Eq. (3-27).

$$\dot{\omega}_i = A_i \exp\left(-\frac{E_i}{RT}\right)m_i^{n_i} y_{O_2}^{\delta}$$

(3-27)

Where, m_i is the normalized mass of solid species decomposed by the reaction i. y_{O_2} is the oxygen mass fraction. δ is the reaction order for oxygen mass fraction, which is set to 1 for oxidization reactions and 0 for pyrolysis reactions.

The kinetic parameters of the reactions are calculated by an optimization technique. The optimization is based on the comparison between experimental and calculated plots. In his work, Rein used Genetic Algorithms (GA). The principle of the GA is to define a randomly generated set of values (population). The population undergoes a process of selection such that only those giving the best description (fitting) of the experimental results (thermogravimetry) of every generation are selected to survive. Stochastic mutations are included for the parameters avoiding the trapping in a local extremum. The process is repeated until the convergence is achieved [110].

In order to calculate the kinetic parameters by mathematical fitting methods, other authors used various optimization techniques such as fuzzy logic, genetic algorithms, iterative approaches, etc.

3.2.7 The problem of thermal decomposition under vitiated atmospheres

In the last subsections were presented the methods most commonly used in literature to determine the decomposition mechanism of materials and calculate the respective kinetic parameters. In all cases, the models were stated to air and nitrogen atmospheres.

The problem of thermal decomposition under vitiated atmospheres has been poorly discussed in the past but is of great interest in FSE. Fires under vitiated atmospheres describe fire situations in which the oxygen mass fraction of the environment gas is found between zero and the one of air ($0 < y_{O_2} < 0.23$). This type of fire often occurs in closed rooms [111][112]. The oxygen initially present in the atmosphere is consumed by the flame during the phases of fire ignition and propagation (heterogeneous reactions are often neglected). Fire in closed rooms has two main consequences that highly affect the kinetics of thermal decomposition: the increase in the mean temperature and the depletion of oxygen into the room [113][114].

Figure 2-9 represents an example of the strong influence of temperature and oxygen mass fraction in the kinetic of decomposition of solids. The increase in temperature tends to increase the rate of solid decomposition and gas release. The effect of the oxygen depletion is the reverse of the one of temperature: A reduction of the quantity of oxygen in the surrounding atmosphere tends to reduce the decomposition rate. Nevertheless, a change in the kinetics of decomposition produces a change in the amount and the composition of the gas products. As discussed, the composition of the gas products controls the potential of chemical energy available to be converted into heat during a subsequent combustion.

Thus, a general model of thermal decomposition should accurately predict the rate of mass-loss as a function of temperature and oxygen mass fraction. Nevertheless, the determination of these two variables in real fire situations remains a tricky task because they are affected by a huge number of phenomena such as: turbulence, thermal balance, heat losses, diffusion velocity, ventilation, etc.

In this subsection are presented the few models and experimental finding referenced in literature which include a term of oxygen mass fraction. The quotes are not specific to PU but to wood, biomass and plastics. They could however be applied to PPUF.

Fang *et al.* [115] studied the relation between the kinetic parameters calculated during pyrolysis and combustion of wood under various oxygen concentrations. The samples were: merbau, cotton straw, birch, red sandal and their semi coke. They observe that the MLR curves have the same behaviour until 250 °C independently of the oxygen concentration. Above that temperature, the increase in oxygen concentration increases the MLR intensity.

The increase in the oxygen concentration, attempt the combustion process to vary from a single stage to double stage. If oxygen concentration continues increasing, a single-stage combustion is produced again. However, further researches are needed to characterise the critical concentrations of oxygen that allows many decomposition stages.

Caballero *et al.* [116] studied the decomposition of kraft lignin material using non-isothermal TGA. They characterise the biomass as being composed of various polymers which decompose at different temperatures. Their model assumes that a given fraction begins to decompose only if the temperature of the biomass is greater or equal to a characteristic temperature T_R. Thus, each component of the biomass has characteristic temperatures corresponding to the ones of the beginning and the end of the decomposition reaction. A function C is used to estimate the distribution of mass fractions that can react in each temperature range. So, CdT_R designate the mass fraction of the sample that can decompose at a given temperature range $T_R \leq T \leq T_R + dT_R$. The mass conservation is mathematically expressed in Eq. (3-28).

$$\int_0^\infty CdT_R = 1$$

(3-28)

The curve C cannot be measured directly, but can be deduced from the variation of the residue yield obtained at time infinity *vs* operating temperature T_R.

Senneca *et al.* [117] studied the kinetics of decomposition of four materials: bituminous coal, PET, PE and lignocellulosic material. The model called a power law kinetic model

is of the type presented in Eq. (3-29). This is one of the few models presented in literature that takes into account the presence of oxygen.

$$\frac{d\alpha}{dt} = -A\exp\left(-\frac{E}{RT}\right)\alpha^D P_{O_2}^n \tag{3-29}$$

Where, D is the strength of the dependency of the pyrolysis rate on the mass of unpyrolized carbon. P_{O_2} is the partial pressure of the oxygen. n is the reaction order with respect to oxygen partial pressure.

The parameters A, E and n were calculated by a non linear regression analysis of the peak temperatures at different heating rates and oxygen concentrations. Authors used the Kissinger and Friedman methods.

The general behaviour that Senneca *et al.* [117] found for all the materials tested (bituminous coal, PET, PE and lignocellulosic material) was:

- For all the materials, increasing the oxygen concentration shifts the weight loss towards lower temperatures especially at high heating rates, which is in accordance to observations of Caballero *et al.* [116]: A maximum pyrolysable fraction is observed for each final temperature (as observed in isothermal tests). The amount of residue was found not to be dependent on the heating rate, but on the final temperature and the nature of the biomass. This is also in accordance with the theory that different fractions decompose at different ranges of temperatures. Thus, the activation energy changes during the heating process.

- Materials can be classified into low, medium and high volatile content. In solid fuels with low volatile content, the diphasic combustion prevails over the release of volatiles. For materials with medium to high volatiles content, the release of volatiles and heterogeneous char combustion are both relevant and may occur in sequence. For materials with very high volatile content, the presence of oxygen results into conversion patterns that are not easy to predict.

The kinetics of thermal decomposition of materials that can suffer smoldering combustion need to be studied because it occurs in environments with reduced oxygen. They present a potential hazard because of the flameless combustion and high release of toxic gaseous products, particularly CO. The materials that can sustain

smoldering are powders, grains, particulates, aggregates, fibers, porous or alveolar matrix, such as: Coal, cotton, tobacco, paper, duff, wood, foams, etc. They facilitate the surface reaction with oxygen by providing a large (internal) surface for the heat and mass exchange [15].

Dosanjh *et al.* [50], in 1997, modelled the polyurethane foam smoldering as a single reaction process (Eq.(3-30)).

$$1g(Unburned\_solid) + \upsilon_o O_2 \rightarrow \upsilon_a (Ash) + \upsilon_{gp} (Gas\_products) + \upsilon_o (Q) \qquad (3\text{-}30)$$
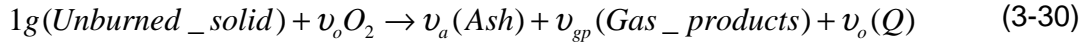
Where, υ are the stoichiometric coefficients in [g·g$_{Sample}^{-1}$]. Q is the energy released per unit of mass of O_2 consumed.

The calculation of the reaction rate is expressed in function of the oxygen mass fraction (y_{O_2}), the gas density (ρ_g), the fraction of unburnt solid polyurethane foam (y_{us}) and the density of the solid polyurethane foam (ρ_{us}). This is mathematically presented in Eq. (3-31).

$$\frac{d\omega}{dt} = A\exp\left(-\frac{E}{RT}\right)(y_{O_2}\rho_g)(y_{us}\rho_{us}) \qquad (3\text{-}31)$$

Because all of the incoming oxygen is consumed in the reaction zone, the total heat released is proportional to the initial oxygen mass flow. Both the smoldering velocity and the final temperature are highly dependent on the oxygen mass flow.

3.2.8 Some comments about the reaction rate equations

The last subsections presented many methods usually found in literature to determine the decomposition mechanism and the kinetic parameters of PPUF and various materials. The problem of the influence of oxygen in the kinetic of decomposition was also discussed. The methods presented were classified into groups: the model-fitting method, the isoconversional method (model-free), a combination of both and a multi-reaction multi-step model in which kinetic parameters are calculated using optimization techniques. Some less famous methods were also presented, such as the IKP method, etc.

The methods for the calculation of kinetic parameters use non-isothermal (various heating rates) or isothermal results. One method that uses TGA together with DSC results was also presented.

All works cited, as well as our own work, are based on the same principles of the science of solids decomposition. Some historical facts about Arrhenius equation and the models of solids decomposition need to be highlighted. Finding a physical meaning to the kinetic parameters has proved to be theoretically very difficult. However, this lack of knowledge has not prevented a progress in research, but has forced the physicists and researchers to deal with very complex problems even without accounting for a total comprehension of the problem.

van't Hoff, in 1884, was the first to suggest performing kinetic analysis for mechanistic interpretations. Thus, experimental measurements allowed writing empirical equations for which the meaning of the parameters was not very clear. The meanings were supposed to be found later. Using the principle of mechanistic interpretations, van't Hoff associated the concept of reaction order to the number of molecules participating in solid state reaction steps [82]. Nevertheless, Hinshelwood showed in 1926 that this is not necessarily the case in heterogeneous gas-phase reactions.

Arrhenius [118], in 1889, empirically established various forms of exponential and temperature dependences of the rate constant (see Eq. (3-2)) [95]. The most famous form is the first order equation in the integral form presented in Eq. (3-32) [118]. This equation was deduced during research works about the transformation of cane sugar (inactive) into "active cane sugar" by the removal of OH^- radicals.

$$k = A \exp\left(-\frac{E}{RT} \right)$$

(3-32)

Within the group of equations proposed at the end of the 19th century, Eq. (3-32) is the one for which integration at constant heating rates leads to intractable solutions [95]. According to Arrhenius, E is the heat absorbed in the process of transformation of inactive molecule into active molecules or, in other words, the heat (or energy) of activation. According to the original thermodynamic meaning, E was expected to be a constant, independent from the path taken by the system from initial to final states (Hess law). However, the concept of variable activation energy has shown to be more adequate to the multiple-step nature of solid-state reactions. A variable activation

energy should be used to describe the temperature dependence of the overall reaction rates.

The demonstration that E actually represents an energy of molecular reaction activation has shown not to be a simple task. Various rationales and theories for an exponential relation between the reaction rate and temperature have been developed. They are based on collision probabilities, energetic, thermodynamics, and/or statistical mechanics [95]. In 1935, Eyring, Evans and Polanyi developed the Transition-state theory (TST). TST is a statistical-mechanical treatments theory [119] based on the mechanistic interpretation method of van't Hoff. TST theory made possible to obtain quick estimates for reaction rates for a wide variety of processes even during the days when sophisticated computers were not available. "In 1978, Chandler [J. Chem. Phys. 68, 2959 (1978)] finally showed that especially when considering condensed phases, the activation energy is a free energy, it is the barrier height in the potential of mean force felt by the reacting system" [120].

To this day, a definite quantum TST has not been formulated, although some very useful approximate quantum rate theories have been invented. An open problem which is being intensively investigated is rate theory away from equilibrium. TST is no longer valid and cannot even serve as a conceptual guide for understanding the critical factors which determine rates away from equilibrium. The non-equilibrium quantum theory is even less well developed than the classical theory, and suffers from the fact that even today, we do not know how to solve the real-time quantum dynamics for systems with many degrees of freedom [120].

Cukrowski in 2006 [121], calculated the Arrhenius activation energy as a function of appropriate threshold energies for a simple reaction $A + A \leftrightarrow B + B$ in a dilute gas. E is calculated from a temperature dependence of the rate constant. It is obtained from the perturbation solution of the Boltzmann equation. The complexity of the equations threaded is greater while they take into account together the solid and gaseous phases transformations.

The temperature-independent pre-exponential factor has no theoretical justification yet. In some theoretical approaches, authors used temperature-dependent pre-exponential factors. However, in all cases, redefining the Arrhenius equation with temperature-dependent pre-exponential factor makes the new calculated parameters, E and A, strictly not comparable with parameters already published [95].

126

As shown, the validity of applying the Arrhenius equation to heterogeneous reactions has been largely questioned. The kinetic parameters (activation energy, pre-exponential factor and reaction order) do have practical value [41]. However, their theoretical interpretation is not very clear even in the higher spheres of research in physics.

As shown, the interpretation of parameters has not been clarified. Thus, it cannot be known reliably if kinetic parameters are constant or variable throughout the decomposition reaction [116]. It is neither clear if the approach used in this research is acceptable or not. In our method, a single group of kinetic parameters is valid for various experimental conditions (oxygen concentrations and heating rates). We assume (as many authors do) that the kinetic parameters are constant for each independent reaction and that this approach would be accepted.

3.3 Improvement of the model of PPUF thermal decomposition

In the last subsection, were presented the methods found in literature to study the thermal decomposition of materials. This section presents the improvements carried out to the model. The model allows calculation of the kinetic parameters of the decomposition reaction, which constitutes primordial input data for the pyrolysis-calculated CFD fire simulations presented in the next chapter.

A realistic model of thermal decomposition must be able to predict the bulk mass change as a function of the variation of temperature and oxygen mass fraction. It must also reproduce the release of gas species, which are responsible for the toxicity in real fire situations. As explained, the gas effluents also transport combustible species from the decomposed solid to the flame. It constitutes the term source of the energy balance.

Thus, a realistic model must simultaneously allow the calculation of kinetic and stoichiometric parameters from the reactions of solid and gas phases. The improvements of the model of thermal decomposition carried out in this research aims

at the coupling of the transformations suffered in the solid and gas phases. This allows stating a kinetic mechanism in accordance to the chemistry of the process: The mechanism can be considered as "chemically correct". However, because of the complexity of the problem of interaction between solid and gas phases, a pseudo mechanistic (simplified) approach [8][82] with as few reactions as possible is used to predict PPUF transformations.

The method used in this research to lay down the mathematical model is based on the works of Rein *et al.* [109]. The model has two main input data: The kinetic mechanism and the possible range of existence of each kinetic parameter from the Arrhenius equation. Up to date, the decomposition mechanisms have been defined based on the solid behavior observed in TGA. In this work, measurements of gas compounds release provide essential information to describe the decomposition mechanism. The experiments that allowed the chemical results used in the following analyses are presented in the section 2.4.

The method and results presented in the next subsections have to do with PPUF only. However, this method has also been used with other materials such as polyester resin, laminated glass reinforced polymer [122] and PMMA [123] with very satisfactory results.

3.3.1 Verification of the influence of the kinetic mechanism in MLR calculations

The decomposition mechanism is a primordial input data for the model because it allows stating the mass balance of solid and gaseous products release. The analysis of the experimental results of mass change as a function of temperature at various heating rates showed that various kinetic mechanisms permit to reproduce in a satisfying manner the curves of MLR obtained in TGA.

The three kinetic mechanisms that best allows the MLR prediction are compared here after: One is issued from literature (Figure 3-2) and two are proposed in this research (Figure 3-3 and Figure 3-4). However, only one of the three decomposition mechanism has a meaning according to the reactions actually taking place in the solid phase. One part of the improvements of the method proposed is a procedure to choose the

"correct" decomposition mechanism. This subsection studies the influence of the kinetic mechanism in the MLR calculations and constitutes one part of the method of identification of the actual decomposition patterns.

The kinetic mechanism issued from literature, is the one used by Rein *et al.* [109] schematized in Figure 3-2. Their mechanism was originally written using generic solid species: The virgin matter was called "foam" and the first decomposition product was called "β-foam" the nature of the solids was not determined. The analytical characterisation presented in Chapter 2 allows rewriting this mechanism using the specific condensed species identified.
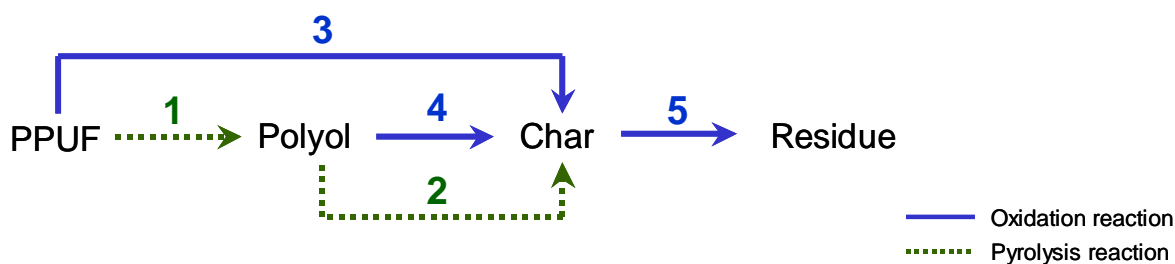
Figure 3-2 Kinetic mechanism used in the works of Rein *et al.* [109]. Written with the condensed species identified in this research.
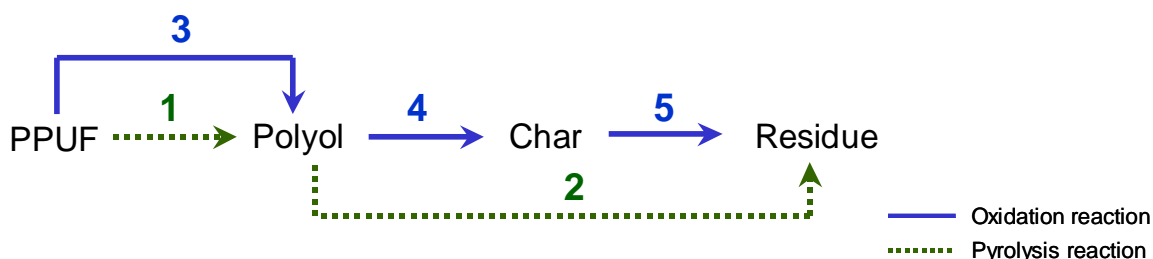
Figure 3-3 Kinetic mechanism 1 proposed in this research.
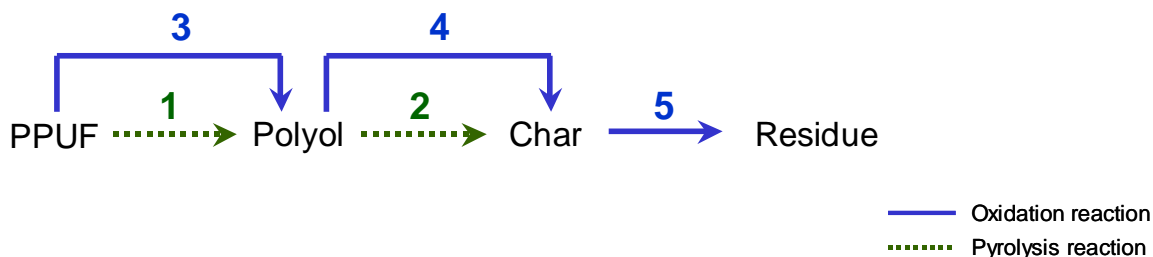
Figure 3-4 Kinetic mechanism 2 proposed in this research.

The two mechanisms proposed in this research are the ones presented in Figure 3-3 and Figure 3-4. Both mechanisms are allowed to explain the TGA results presented in Figure 2-9. They are as well in accordance with the visual observations of SEM and binocular images presented by Bustamante Valencia *et al.* [124] (see Figure 2-15 and Figure 2-16). Nevertheless, they are hypothetical. The deal of the following work is finding evidence that one of these mechanism is correct.

The three mechanisms considered have been written based on the hypothesis that each peak of the MLR curves of TGA is generated by a reaction at the solid phase, it is remainded that similar assumptions has been done by the authors that deduced the multi-reaction, multi-step model presented in section 3.2.6.

In order to be able to choose one mechanism, an unambiguous method to discriminate the "correct" pattern is required. The first option investigated, is to compare the kinetic parameters found with each kinetic mechanism. Here after is presented the method to carry out the modelling of the decomposition process. As example, the procedure is developed using the kinetic mechanism 1 (Figure 3-3) but the same steps has been followed using the mechanism from the literature (Figure 3-2) and kinetic mechanism 2 (Figure 3-4)

Each row of Figure 3-3 represents a reaction of pyrolysis or oxidization. Each reaction has an Arrhenius reaction rate, $\dot{\omega}_i$, defined in Eq. (3-27) and reminded in the following equation.

$$\dot{\omega}_i = A_i \exp\left(-\frac{E_i}{RT}\right) m_i^{n_i} y_{O_2}^{\delta}$$

Reminder of

Eq (3-27)

The reaction rates cannot be measured experimentally. However, they constitute the basis for the prediction of MLR. The MLR of each solid species, b, can be expressed as the balance of the reactions that create and destroy this species. The MLR produced by each one of these reactions is expressed as the product of the reaction rate, $\dot{\omega}_i$ and stoichiometric coefficient, υ_i, as presented in Eq. (3-33). υ_i represents the proportion of the initial mass that is converted into a product by a particular reaction.

$$MLR_i = \frac{dm_i}{dt} = \upsilon_i \cdot \omega_i$$

(3-33)

In order to help the comprehension of this problem, an analogy is done. The following analogy has only as purpose to help the understanding of the procedure to establish the bulk mass balance of the sample. It is called mass balance of "tanks connected with porous pipelines".

The mass of each solid species in Figure 3-3, is represented by a tank b. Each tank is connected with other tanks with porous pipelines i. Because of the pores in pipelines, only a portion of the mass that goes out from the $tank_b$ is able to arrive to $tank_{b+1}$. In this analogy, the stoichiometric coefficient represent the portion of mass that goes out from $tank_b$ and arrives to the $tank_{b+1}$ ($\upsilon_i < 1$) through the pipeline i. The mass lost through

the pipelines produce the gaseous products $(1-v_i)$. This is schematically presented for kinetic mechanism 1 in Figure 3-5, as well as the mass balance for each solid species as a function of time (differential equations).

$$\frac{dm_{PPUF}}{dt} =$$
$$-\dot{\omega}_1 - \dot{\omega}_3$$

$$\frac{dm_{Polyol}}{dt} =$$
$$+v_1 \cdot \dot{\omega}_1$$
$$v_3 \cdot \dot{\omega}_3$$
$$-\dot{\omega}_2 - \dot{\omega}_4$$

$$\frac{dm_{Char}}{dt} =$$
$$v_4 \cdot \dot{\omega}_4$$
$$-\dot{\omega}_5$$

$$\frac{dm_{Residue}}{dt} =$$
$$v_2 \cdot \dot{\omega}_2$$
$$+v_5 \cdot \dot{\omega}_5$$
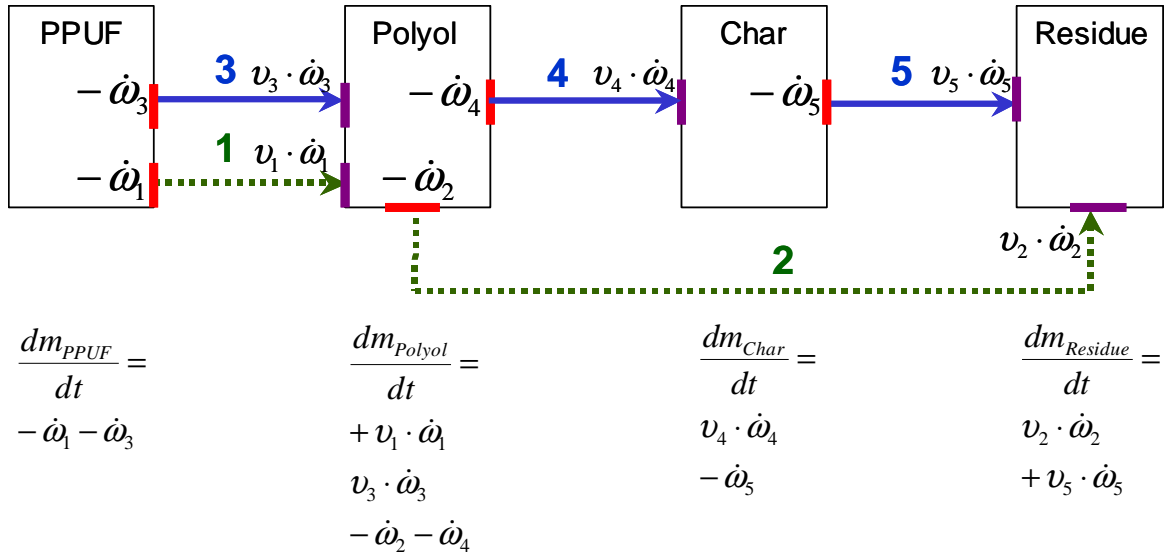
Figure 3-5 Schematic representation of the problem of mass transformation during the thermal decomposition of PPUF for the decomposition mechanism 1 see (Figure 3-3). The mass balance for each solid species is also presented.

Total mass remaining in TGA sample holder at a time t, can be obtained by addition of the mass of the individual solid or liquid products b. In the analogy, the total mass at time t, is determined by measuring the mass in all the tanks. It is written mathematically in Eq. (3-34).

$$\frac{dm}{dt} = \sum_{b=1}^{4} MLR_b = \frac{dm_{PPUF}}{dt} + \frac{dm_{Polyol}}{dt} + \frac{dm_{Char}}{dt} + \frac{dm_{Residue}}{dt} \tag{3-34}$$

The bulk mass balance of the system may be written in terms of reaction rates and stoichiometric coefficients by replacing Eq (3-33) in Eq. (3-34), resulting in Eq. (3-35). In this research, it was verified that the form of Eq. (3-35) remains unchanged for the three kinetic mechanisms (Figure 3-2 to Figure 3-4), although in each mechanism, the interpretation of kinetic coefficients is different due to the reactants and products involved in each reaction.

$$\frac{dm}{dt} = (v_1 - 1)\dot{\omega}_1 + (v_2 - 1)\dot{\omega}_2 + (v_3 - 1)\dot{\omega}_3 + (v_4 - 1)\dot{\omega}_4 + (v_5 - 1)\dot{\omega}_5 \tag{3-35}$$

In the mass balance presented in Eq. (3-35), the total number of unknowns (kinetic parameters) of the problem is 20. Each equation (row) from Figure 3-5 comprises four parameters that need to be adjusted: Pre-exponential factor, activation energy, reaction order and stoichiometric coefficient.

The kinetic parameters and stoichiometric coefficients of the decomposition process are those that best fit calculated and experimental curves (mass and MLR of TGA). In this research, the calculation of kinetic parameters is carried out by iteration using a Genetic Algorithms (GA) toolbox. The GA toolbox was developed by Houck *et al.* [110] and was used for the first time in thermal decomposition for fire applications by Lautenberger *et al.* [15] and Rein *et al.* [109].

The GA method has lots of advantages such as the ability to treat highly non-linear problems and search spaces having high dimensionality [110]. GA uses an evaluation function that compares experimental and calculated curves. The accuracy between curves is called fitness, ϕ. The improvement of fitness, means a best fitting between experiments and calculations. Optimum parameters are found with the maximisation of ϕ. Thus, based on the comparison of experimental and calculated curves, the evaluation function has a main role in the modelling while it indicates to the code if the result is adequate or not.

The evaluation function presented in Eq. (3-36) is the one used by Rein *et al.* [109]. Due to several lack of this function, two new evaluation functions have been developed and tested in this research see Eq. (3-37) and (3-38).

$$\phi = \sum_{\beta=1}^{c} \left[\left(\int \left| \frac{dm}{dt}^{Calc} - \frac{dm}{dt}^{Exp} \right| dT \right)^{-1} + \psi \left(\int \left| m^{Calc} - m^{Exp} \right| dT \right)^{-1} \right]_{\beta} \tag{3-36}$$

Where, c, is the number of heating rates that are compared (four in this research). The function presented in Eq. (3-36), is formed by the addition of two terms: The first term of the right hand side accounts for the absolute value of the difference between the experimental and calculated curves of MLR. The second term of the right hand side is the absolute value of the difference of the experimental and calculated curves of mass change in function of temperature. It is highlighted that:

- The terms of Eq. (3-36) are inversed because the GA toolbox is allowed only to maximise the evaluation function.

- A scale factor, ψ, is included in the second term of the right hand side in order to give to both terms the same order of magnitude. The authors did not specify a method to set this factor.

During the analysis of the model, this evaluation function showed not to be sensible enough to the different shapes of MLR and mass that can be obtained with different groups of kinetic parameters. This lack of sensitivity is caused by the fact that calculating the difference of absolute values is equivalent to quantifying the area found between the two curves. Nevertheless, the position of the area is not taken into account.

It was also found that if ψ is constant, an important error is induced in the fitness factor calculated when the fitting of the curves is low. Thus, the fitness appears to be higher than it actually is.

The fitness of Eq. (3-37) is based on the classical method to calculate errors: The square of the difference between two curves. It is in agreement with the evaluation function of Esperanza *et al.* [42] presented in Eq. (3-14).

$$\phi = \sum_{\beta=1}^{c} \sum_{j=1}^{k} \left(\frac{dm_j}{dt}^{Calc} - \frac{dm_j}{dt}^{Exp} \right)_{\beta}^{-2} \tag{3-37}$$

Where, k is the dimension of the vectors that are compared (only comparison of vectors of the same size are allowed). Evaluation function of Eq. (3-37), does not compare the curves of mass in function of temperature as done in Eq. (3-36), because it is assumed that a good fitting of the curves of MLR allows to predicting in an acceptable manner the mass remaining in the sample holder.

Eq. (3-37), is more restrictive than Eq. (3-36) because of the second power of the error. However, a poor performance in the code was observed. The low performance was verified by a longer calculation time and a low fitting between the calculation and experiments from the "optimum" solution found.

The best results in terms of calculation time and ability to fit the experiments and the calculation curves were obtained with the evaluation function of Eq. (3-38), being the function used in the present work.

$$\phi = \sum_{\beta=1}^{c} \left[\cos[\angle(\vec{x}, \vec{y})] \cdot \left[\frac{\|\vec{x} - \vec{y}\|}{\|\vec{x}\|} \right]^{-1} \right]_{\beta} \qquad (3\text{-}38)$$

$$\vec{x} = \frac{dm^{Exp}}{dT} \; ; \; \vec{y} = \frac{dm^{Calc}}{dT}$$

In Eq. (3-38), $\vec{x}$ and $\vec{y}$ are respectively, arrays of experimental and calculated mass-loss rates in function of temperature. These vectors are of the same dimension, *i.e.* the data points are taken at the same temperature. The evaluation function, presented in Eq. (3-38) has been obtained by the combination of the two indexes calculated in the standard ISO 16730:2007 [125] for the comparison of curves. These indexes have been defined based on the groups' theory of Hilbert *et al.* in 1928 [126].

The first index calculated in the standard corresponds to the first term of the right hand side of Eq. (3-38) which refers to the phase difference between the curves. The range of variation of this index is between -1 and 1.

The second index calculated by the standard, is found in the second term of the right hand side of Eq. (3-38). This term refers to the distance between the curves in the vertical direction (ordinate axis). The range of variation of this index is between 0 and 1. It is highlighted that in the case where the experimental and calculated curves are equal (same shape and location) the distance between them is null and the evaluation would not be defined, *i.e.* division by zero. However, this case has not been referenced yet in literature.

The definition of ϕ takes into account the scalar product $\langle \vec{x}, \vec{y} \rangle$ and the Euclidean norm of vectors $\|\vec{x}\|$. These functions are reminded in Eq. (3-39). The analysis carried out here was limited to Euclidean spaces, however, other non-Euclidean spaces can be used, *e.g.* Hellinger, secant, and a hybrid of Euclidean and secant.

$$\|\vec{x}\| = \sqrt{\sum_{i=1}^{m} x_i^2} \quad \text{with } m \text{ being the length of } \vec{x}$$ (3-39)

$$\cos[\angle(\vec{x}, \vec{y})] = \frac{\langle \vec{x}, \vec{y} \rangle}{\|\vec{x}\| \|\vec{y}\|}$$

$$\langle \vec{x}, \vec{y} \rangle = \sum_{i=1}^{m} x_i \, y_i$$

As explained, the aim is to verify the influence of the decomposition mechanism in the prediction of MLR. Three decomposition mechanisms are evaluated, but the optimum parameters can change while using a different evaluation function to compare experimental and calculated results. The vectorial evaluation function of Eq. (3-38) was selected because of his best capacity to predict TGA experimental results in a reasonably calculation time.

The initial conditions used for the MLR calculations are:

$$\begin{cases} m_{PPUF}(0) = 1; \ m_{polyol}(0) = 0; \ m_{char}(0) = 0; \ m_{residue}(0) = 0 \\ T(0) = 393K \\ \dfrac{dT}{dt} = \beta = \text{Constant} \end{cases}$$

The analysis of the influence of the kinetic mechanism on the optimum parameters was carried out using an inverse method. The inverse method means that we studied the change of the calculated MLR (output) with the three mechanisms presented in Figure 3-2 to Figure 3-4 using a single group of kinetic parameters. The comparison of the experimental and calculated MLR curves for $\beta = 10$ °C·min^{-1} is presented in Figure 3-6. The curve of kinetic mechanism 2 (Figure 3-4) is omitted because the shape is exactly the same as that of kinetic mechanism 1.
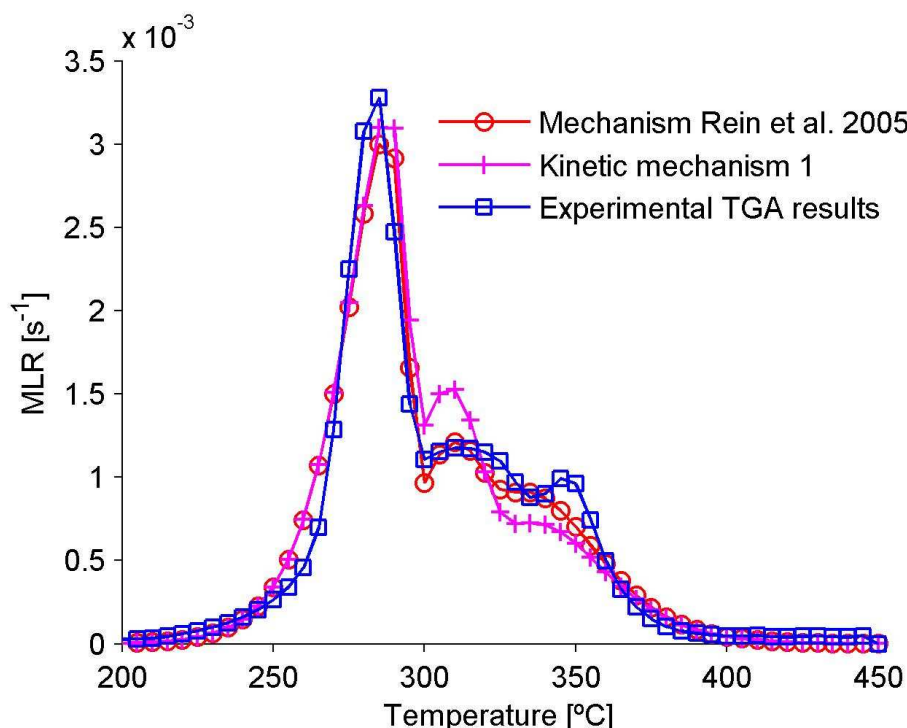
Figure 3-6 Comparison of MLR calculated with the three kinetic mechanisms from Figure 3-2 to Figure 3-4. $\beta = 10$ °C·min^{-1}. Kinetic mechanism 1 and kinetic mechanism 2 presented exactly the same shape.

The aim of the comparison of experimental and calculated MLR shapes, is to determine the best model, and to be allowed to select one kinetic mechanism of PPUF decomposition. The plots of Figure 3-6, are obtained using the group of kinetic parameters that best fit the model proposed by Rein *et al.* [109] and the experimental MLR. As showed, the first peak of MLR is well predicted by the three models (T = 370 °C). The second peak of MLR is found at a temperature near 310 °C. Kinetic mechanism 1 overestimates the second peak of MLR by 20% compared to the experimental curve. The third peak of MLR is found at 350 °C. The overestimation of kinetic mechanism 1 in the second peak is compensated by an underestimation of the third peak of MLR by 20%.

As shown in Figure 3-6, there is little difference in the results found with the three models. The comparison of MLR curves is performed to analyse the sensitivity to the decomposition mechanism. The inverse method that is used to analyse the sensitivity is based on the following principle: If each model requires a specific group of Arrhenius parameters to reproduce experimental MLR curves in a satisfying manner, then the

comparison of the groups of parameters would provide a mean to determine which model is the best. Nevertheless, it was found that a single group of kinetic parameters allows all the models to reproduce the MLR experiments in a satisfying manner. Thus, the actual kinetic mechanism of PPUF cannot be determined by the comparison of the respective kinetic parameters calculated with each model.

The comparison of the experimental and calculated curves of mass as a function of temperature has been also performed. However, the curves are not presented here because they do not provide additional useful information. As a conclusion, the comparison of the kinetic parameters calculated using various models does not constitute an unambiguous form that could be used to determine the actual decomposition mechanism of PPUF. As shown, various models are allowed to predict the behaviour of mass and MLR. The gas release with the change of temperature represents a means to gain information on the chemistry of the process allowing definition of the current decomposition mechanism and the model to be used.

3.3.2 Analysis of the kinetic mechanisms based on effluents measurements

The data presented in the last subsections corresponds to the identification of the kinetic mechanism based on the results from the solid phase. As shown, the analysis of the single data from the solid phase does not provide enough information to state accurately a realistic kinetic mechanism of PPUF decomposition. In this subsection, the observations of the solid phase are analysed together with data from the evolved effluents. The possibility of occurrence of a given kinetic mechanism is analysed from the point of view of gas release evidence.

The kinetics of the release of gases provide complementary information about the decomposition mechanism of PPUF. The effluents released during PPUF pyrolysis in dynamic temperature in TF under nitrogen atmosphere are presented in Figure 3-7. The effluents released under air atmosphere are plotted in Figure 3-8. The respective MLR shapes have been included for comparison of the behaviour of solid and gas phases.

138
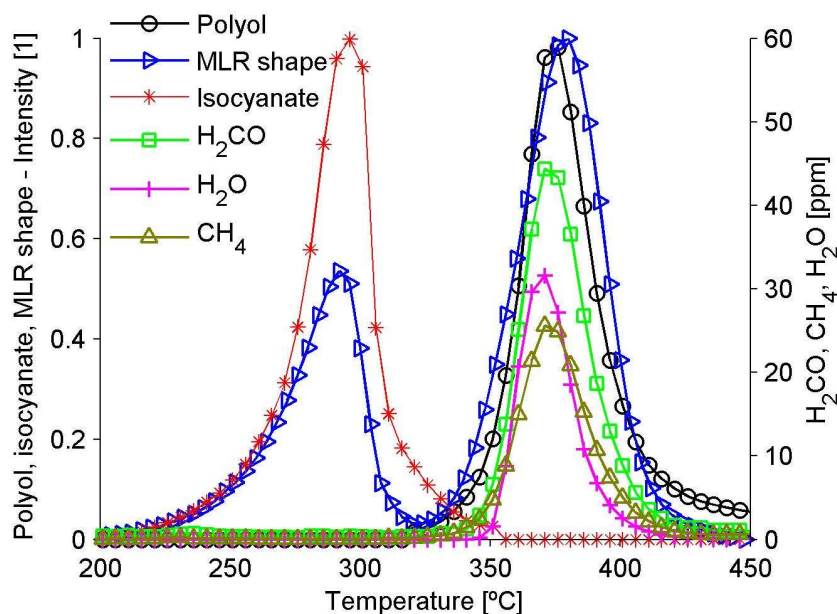
Figure 3-7 Effluents release in function of temperature under nitrogen atmosphere. Measurements carried out in TF + FTIR$_{qnt}$ and TF + FTIR$_{qlt}$ for $\beta = 10$ °C·min^{-1}. The MLR shape is included for comparison of the behaviour of solid and gas phases.

It is remebered that in Figure 3-7 and Figure 3-8, the compound labelled as 'polyol' is a gas product of the decomposition of semi-liquid polyol. The gas labelled 'Isocyanate' is the effluent released during the breakdown of the isocyanate contained in the polyurethane molecules.

The functions created by the thermal decomposition of polyol and isocyanate, are commonly destroyed in the flame region. Thus, such compounds are much more difficult to identify in large-scale tests (or real fires) because of factors such as the ventilation conditions and a high dilution rate of effluents. The functions from isocyanate are transformed into CO_2, CO, H_2O, NO_x and HCN, while the functions from polyol are transformed into CO_2, CO, H_2O [5][23][30][32][38][39].
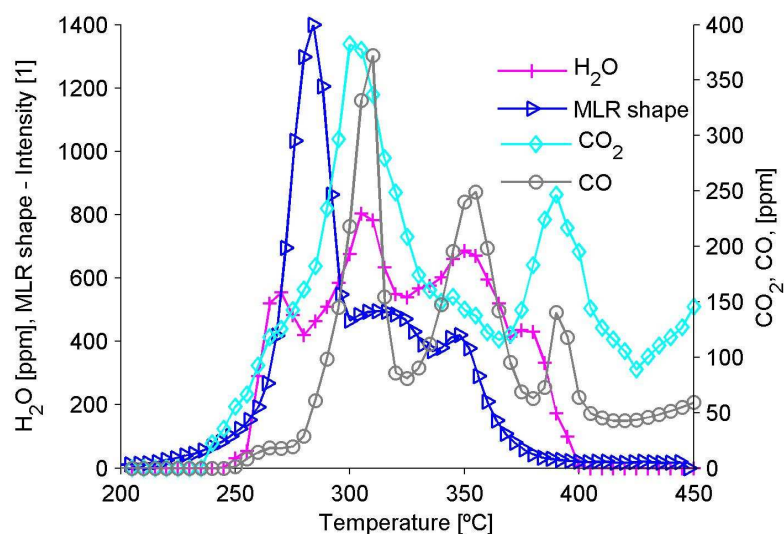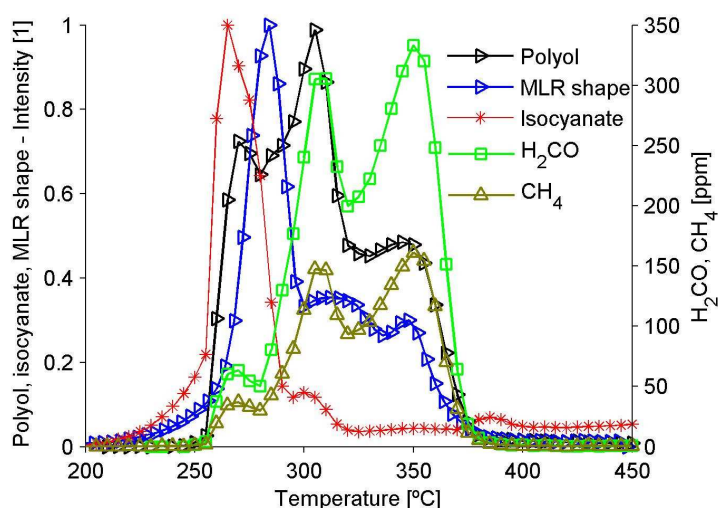
Figure 3-8 Release of gases in function of temperature under air. a) plots of H_2O, CO and CO_2; b) plots of polyol, isocyanate, H_2CO and CH_4. Measurements carried out in TF + $FTIR_{qnt}$ and TF + $FTIR_{qlt}$ for $\beta = 10$ °C·min^{-1}. The same MLR shape is included in both plots for comparison of the behaviour of solid and gas phases.

The close correspondence between the emission of effluents and MLR shown in Figure 3-7 and Figure 3-8, allows the analysis of both solid and gas phases in order to identify the actual kinetic mechanism of PPUF decomposition.

Table 3-5 summarizes the decomposition mechanisms analysed in this research. The following analysis requires taking into account the results of solid and gas phase behaviour, as well as the kinetic mechanisms.

140

Table 3-5 Kinetic mechanisms analysed

Decomposition mechanism	Source/figure
	Rein *et al.* [109]. See Figure 3-2.
	This research. Kinetic mechanism 1. See Figure 3-3.
	This research. Kinetic mechanism 2. See Figure 3-4.

The following analysis study one by one the reactions (arrows) in order to verify their existence according to the evidence of the solid and gas phase measurements.

The results of the solid and gas phases of PPUF decomposition under nitrogen atmosphere present two well-identified stages. The first stage releases isocyanate. As explained (see section 2.5.4), isocyanate is released during the collapse of the solid structure of PPUF. The condensed-phase product of this reaction is polyol, which remains in the sample holder as a semi-liquid. This reaction is presented by arrow No 1 in the three mechanisms. In Figure 3-7 is observed that the first reaction of pyrolysis release only isocyanate while in the second the polyol is pyrolysed as well as other gases.

The second stage of the pyrolysis evolves polyol, H_2CO, H_2O and CH_4. No CO and CO_2 are observed because no oxygen is present in the inlet gas stream, and the proportion of oxygen in the solid matrix of PPUF is weak. Discrepancies appear in the three mechanisms according to the transformations caused in the solid phase by the

second reaction, see arrow No 2. Experimental evidence shows that during pyrolysis no char is formed but do a residue. In other words:

- Char is a product of the reaction of solids with the oxygen (heterogeneous oxidization). Char can suffer further decomposition reaction in which oxidized molecules are broken down, releasing CO_2 and CO [127]. Oxidization of char is a process observed in polymeric fuels [128] as well as in biomass [129].

- The mass of the residue that remains in the holder at the end of the tests is higher under air (8%) than under nitrogen (3%). Thus, at the temperature of the end of the test (450 ℃), no further reaction occurs. The sample mass has been completely consumed.

- Comparison of MLR and gas release curves under air and nitrogen shows that char is decomposed to form a residue. During PPUF decomposition, char exists at a lower temperature than the one of residue formation. At a temperature of 450 ℃, the solid species remaining in the sample holder is a residue, not char. In tests not presented here, it was shown that the residue of PPUF found under nitrogen atmosphere (3%Wt) decomposes at nearly 600 ℃.

These observations show that the reaction represented by arrow No 2 actually transforms polyol into a residue. This kinetic step during PPUF pyrolysis is well predicted by the kinetic mechanism 1 presented in Figure 3-3. Thus, the mechanism of Figure 3-3 is the one that best explains the thermal behaviour of PPUF under nitrogen decomposition condition.

The same analysis is carried out to verify if the mechanism of decomposition under nitrogen is the best for the oxidization reactions.

The beginning of PPUF decomposition under air is shifted through the lower temperatures compared to tests under nitrogen as observed in the plots of MLR and gases evolution. This is in agreement with the observations made by Caballero *et al.* [116] and Senneca *et al.* [117]. The earlier reaction of PPUF under oxidizing atmosphere shows a strong influence of oxygen on the virgin foam decomposition reaction. This suggests that the oxidization reaction that transforms PPUF into polyol (arrow No. 3 in Figure 3-3) does exist and plays a very important role

in the kinetic mechanism. According to the oxidization reaction of PPUF, the kinetic mechanism proposed by Rein *et al*. [109] in Figure 3-2 does not seem very realistic.

Very important results supporting the existence of an oxidization reaction of PPUF to form polyol (arrow No 3) under oxidizing atmosphere can be found by analysing the plots of evolved gases (Figure 3-8). The first reaction of PPUF decomposition under air produces mainly H_2O, CO_2, polyol and isocyanate. Formation of these compounds can only occur in the presence of oxygen from the gas stream. This is a sign of heterogeneous reaction. It is shown in Figure 3-7 that under inert atmosphere, the release of polyol starts at a temperature neat to 320 ℃, while under oxidizing atmosphere it starts at 250 ℃. So, polyol is produced by pyrolysis but also by the reaction of oxidization, in other words arrow 3 transforms PPUF by oxidization into polyol: The kinetic mechanism 1 is allowed to reproduce this behaviour while the mechanism from the literature do not.

Isocyanate is released early compared to the other gases. The temperature of the first peak of MLR is 284 ℃ for a $\beta = 10$ ℃·min^{-1}. At the same temperature, the rate of production of effluents is increasing, except for isocyanate that is decreasing. The products released during oxidization reactions in the first stage of decomposition lets us affirm once again that the reaction of virgin PPUF oxidization to form semi-liquid polyol exists and has a strong influence on the decomposition kinetics.

The second peak of MLR observed in TGA occurs at a temperature of 312 ℃ (Figure 3-8). At the same temperature, CO_2, CO, H_2O, polyol, H_2CO and CH_4 are released. These compounds are representative of oxidization reactions under lean atmosphere. The reactions taking place between the gas and condensed phases, are oxidization of the semi-liquid residue remained in sample holder. As stated, the semi-liquid is mainly composed by polyol and oxidized products. This analysis allows concluding that, the reaction of polyol oxidization exists. It is included in the kinetic mechanisms 1: arrow No. 4 (Figure 3-3). This reaction produces char.

The beginning of the oxidization of char occurs at nearly 340 ℃ (arrow No 5 in Figure 3-3). The maximum reaction rate of char oxidization is found at 347 ℃. In this range of temperature CO_2, CO, H_2O, H_2CO, CH_4 and a small quantity of polyol are released. The reaction of oxidization of char produced the residue found at the end of the experiment. The species released during this stage (except CO_2 and CO) are similar to those produced during the decomposition in inert atmosphere.

In conclusion, the kinetic mechanism presented in Figure 3-3 is the one which seems to best corresponds to the observations of the chemical process. The analyses considered decomposition under air and nitrogen atmospheres. The following study is performed with the results obtained with this model.

The knowledge of the kinetic mechanism allows calculating the mass-loss rate and mass change in function of temperature in an accurate manner. Figure 3-9 presents the comparison of experimental and calculated results under two atmospheres (air and nitrogen) and four heating rates (5, 8, 10 and 15 °C·min^{-1}). The plots of mass change with temperature are not presented here, because they provide less useful information than MLR shapes.
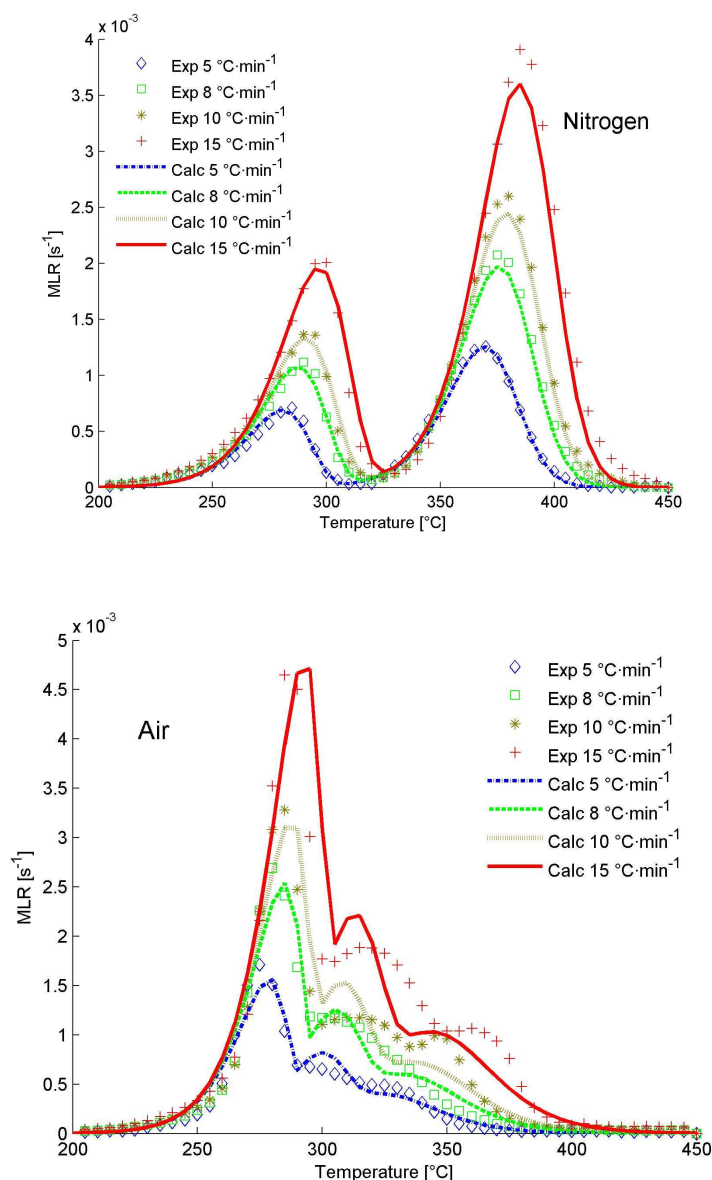
Figure 3-9 Comparison of MLR experimental and calculated at four heating rates: 5, 8, 10 and 15 °C·min $^{-1}$. Up: nitrogen. Bottom: air.

As shown in Figure 3-9, under nitrogen atmosphere, the two stages of decomposition are very well predicted by the model. . Under air atmosphere, the prediction of the intensity of the first peak is accurate. The predictions of the second and third peaks are less accurate. In general, the intensities of the peaks are well predicted but their positions are not. This is clearly caused by a lack of accuracy in the evaluation function (see Eq. (3-39)). As explained, one part of the evaluation function checks the intensity, the other the position (abscissa) of MLR curves. The component of the evaluation function that evaluates the position must be "proportionally stronger" than it is currently.

This, would help the GA tool to assign better fitness to candidates with accurate position.

3.3.3 Coupling of the model of solid phase to the model of gas effluents release rate

The last subsection analysed the kinetic mechanisms from the point of view of chemistry. The three possible kinetic mechanisms that can reproduce the mass change with temperature were analysed. It was concluded that the mechanism that is in best agreement with the chemistry of the process was kinetic mechanism 1, presented in Figure 3-3.

In this subsection the coupling of the model of solid phase to the model of effluents release rate is performed. A deductive method is used to couple the models of both phases. The first step consists in determining which gases are specifically produced by each reaction. The second step is the calculation of yields. The modelling of gas release provide further evidence to the discussion of the decomposition mechanism.

3.3.3.1 Determination of the gases released by each reaction

The determination of the gases that are released by each reaction is a main task of the coupling of the models of solid and gas phases. It is based on the following hypothesis: the curve of release of one particular gas can be obtained by the addition of the kinetics of release of this gas by various successive reactions. Thus, if the gases released by each reaction are carefully identified, the global gas release can be predicted.

The method to determine which gases are produced by each reaction consists in plotting the reaction rates calculated with Eq. (3-27) together with the curves of gases evolution. It is considered that one reaction releases one gas when common peaks are found between them. As example, the plots of CO_2 and polyol together with reaction rates are presented in Figure 3-10. The number of the reactions are the same as the

146

arrows of kinetic mechanism 1, which is reminded hereafter. Similar plots for the other gases are presented in Appendix B. The following analysis is developed only using the results obtained with kinetic mechanism 1.
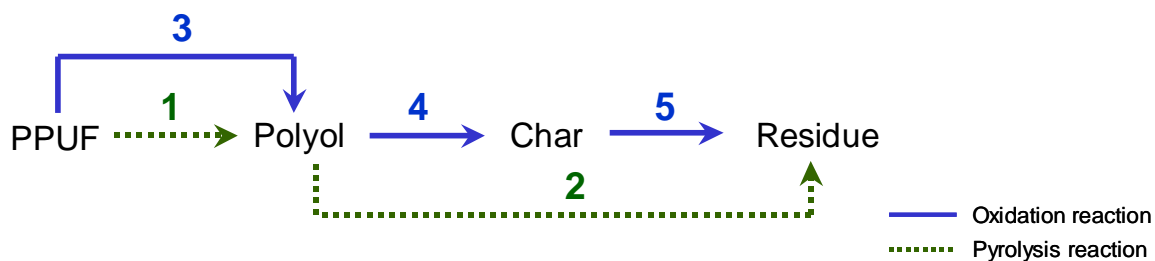
Reminder of Figure 3-3 Kinetic mechanism 1 proposed in this research.
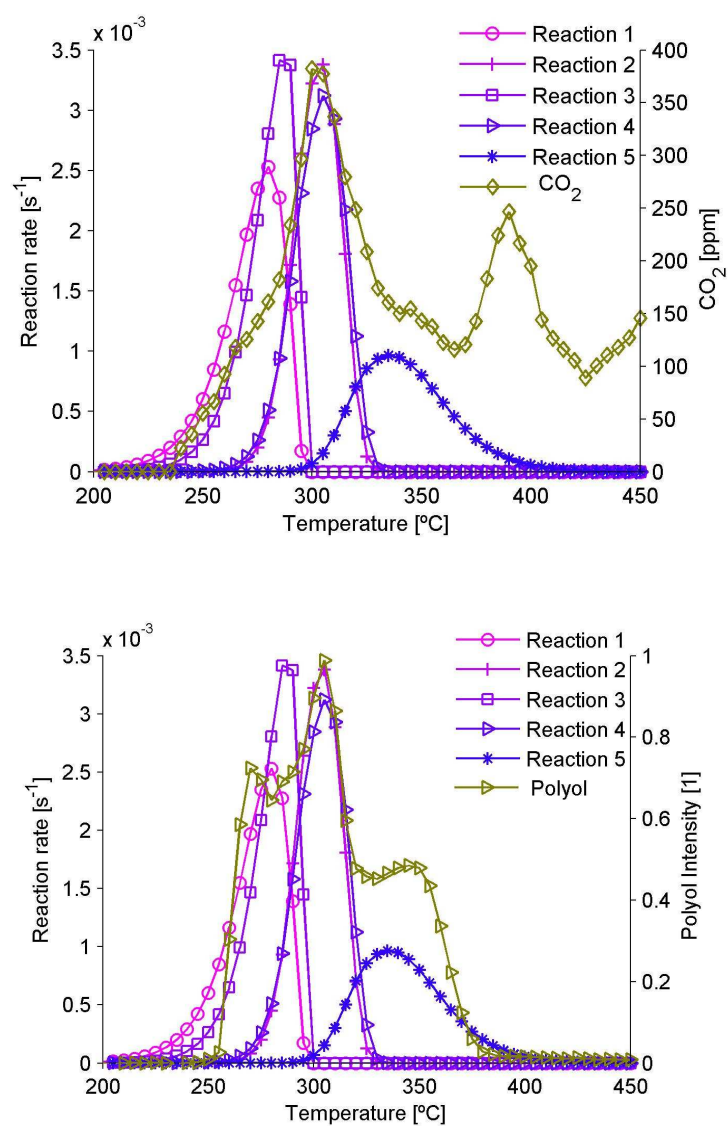
Figure 3-10 Coupling of plots of reaction rates and gases evolution: Up CO_2. Bottom polyol. Reaction 2 is scaled by a factor of 500 for easy of view.

All the information on the kinetic mechanism 1, including the transformations suffered by the solid and gas phases are summarized in Table 3-6.

Table 3-6 Kinetic mechanism of PPUF decomposition taking into account the behaviour of the solid and the gas phases

No	Type of reaction	Temp. [ºC]	Reactives	Products solid or liquid		Products gas
1	Pyrolysis	200 – 340	PPUF	$\rightarrow$ $\upsilon_1 \cdot$Polyol	+	$\tau_1 \cdot$[Isocyanate]
2	Pyrolysis	340 – 450	Polyol	$\rightarrow$ $\upsilon_2 \cdot$Residue	+	$\tau_2 \cdot$[Polyol + H_2CO + H_2O + CH_4]
3	Oxidation	200 – 275	PPUF + O_2	$\rightarrow$ $\upsilon_3 \cdot$Polyol	+	$\tau_3 \cdot$[Polyol + CO_2 + H_2O]
4	Oxidation	220 – 300	Polyol + O_2	$\rightarrow$ $\upsilon_4 \cdot$Char	+	$\tau_4 \cdot$[Polyol + H_2CO + CH_4+ CO + CO_2 + H_2O]
5	Oxidation	300 – 450	Char + O_2	$\rightarrow$ $\upsilon_5 \cdot$Residue	+	$\tau_5 \cdot$[Polyol + H_2CO + CH_4+ CO + CO_2 + H_2O]

In Table 3-6, the first column is the number of the reaction that corresponds to the number shown in Figure 3-3. The column "Reactives" is the substance that is transformed during the reaction i. The column "Products solid or liquid" corresponds to the condensed phase that remains in the sample holder at the end of the reaction. The gas effluents are listed in the column "Product gas".

In this subsection, the released gases were associated to each reaction. The next step is the prediction of the leak of each gas as a function of temperature.

3.3.3.2 Prediction of the kinetics of gas release

The cornerstone of the improvements carried out to the model of thermal decomposition of PPUF is to couple a model to predict the release of gas species. Thus, the prediction of the change of the mass as a function of temperature as well as the kinetics of the release of gases is allowed.

The coupling of models permits the calculation of υ_i and τ_i, which are the respective stoichiometric coefficients of the solid and gas phases (see Table 3-6). They are the quantification of the proportion of reactives that are transformed into solid or gas products, and are required for establishing the mass balances. The calculation of υ_i is presented in subsection 3.2.6.

The coupling of the models of solid and gas phases is conducted by means of the calculation of τ_i as a function of the stoichiometric coefficient of the solid phase υ_i. The optimization of υ_i allows predicting accurately the MLR with time (temperature)

and carry out the optmisation of τ_i, which allows the prediction of effluents release. The function between the stoichiometric coefficients υ_i and τ_i is presented in Eq. (3-40).

$$\tau_i = \gamma_i \cdot (1 - \upsilon_i) \tag{3-40}$$

The second term of the right hand side of Eq. (3-40) is the fraction of the solid transformed into gas during a reaction (see Table 3-6). γ_i, is a coefficient calculated in Eq. (3-41).

$$\gamma_i = \kappa_i \cdot \frac{Y_i^{Exp}}{\sum_{b=1}^{h} Y_b^{Exp}} \tag{3-41}$$

Where, Y_i^{Exp} is the experimental yield of gas released by the reaction i. h is the number of species released by the reaction i. $\sum_{b=1}^{h} Y_b^{Exp}$ is the total mass of gases released during the decomposition process.

In Eq. (3-41), the term κ_i is a dimension-less coefficient calculated using genetic algorithms. The optimum value of κ_i is the one that allows the best fitting between the experimental and calculated mass flow rate of gases. A single value of κ_i is calculated for each reaction of Table 3-6. The physical meaning of κ_i has not been determined yet, but it has been observed to be function of the particular gases that are produced during a reaction and their mass flow rate. The second term of Eq. (3-41) is the experimental yields that can be read directly from Table 3-7 (column Experimental yields – Air).

Eq. (3-33) presented the calculation of the mass-loss rate of a given solid species. A similar calculation is presented in Eq. (3-42) but referenced to the mass of gas produced by a reaction: The yield of gases produced by a given reaction i is calculated as the product of the stoichiometric coefficient, τ_i and the reaction rate $\dot{\omega}_i$.

$$\dot{Y}_i = \tau_i \cdot \dot{\omega}_i \tag{3-42}$$

The yield of a particular gas species b, is also calculated. This yield takes into account the fraction of the species b produced by each reaction. It is calculated in Eq. (3-43).

$$Y_b^{Calc} = \sum_{i=1}^{5} Y_{b,i}^{Calc} \tag{3-43}$$

Where, $Y_{b,i}^{Calc}$ is the yield of a gas b produced by the reaction i. The results of calculated yields Y_b^{Calc} are presented in Table 3-7.

Table 3-7 Comparison of experimental and calculated yields

| | Experimental yields | | | | | | Calculated yields | |
| | Air | | 10.5% O_2 | | Nitrogen | | Air | |
Gas	[mg·g^{-1}]	%	[mg·g^{-1}]	%	[mg·g^{-1}]	%	[mg·g^{-1}]	%
CO_2	42.3	35.6%	-	-	-	-	20.1	30.1%
CO	13.6	11.5%	6.8	23.1%	0.6	13.7%	13.1	19.6%
H_2O	47.7	40.1%	13.4	45.1%	0.7	15.8%	18.9	28.3%
H_2CO	10.1	8.5%	6.8	22.8%	2.3	53.8%	12.8	19.2%
CH_4	2.6	2.2%	1.8	6.1%	0.7	16.7%	1.8	2.7%
HCN	2.5	2.1%	0.8	2.8%	-	-	-	-
Total	118.9	100.0%	29.6	100.0%	4.2	100.0%	66.7	100.0%

Figure 3-11, presents the experimental and calculated kinetics of release of CO_2 and H_2CO under air atmosphere. The plots show the concentration of the gases and not their respective yield because the gas measurement has been obtained with tubular furnace, where the change of mass with the increase in temperature is not measured. The curve of MLR obtained in TGA is included as reference. The plots for the CO, H_2O and CH_4 are presented in Appendix C. The curves of polyol and isocyanate are not presented because no quantitative data are available.
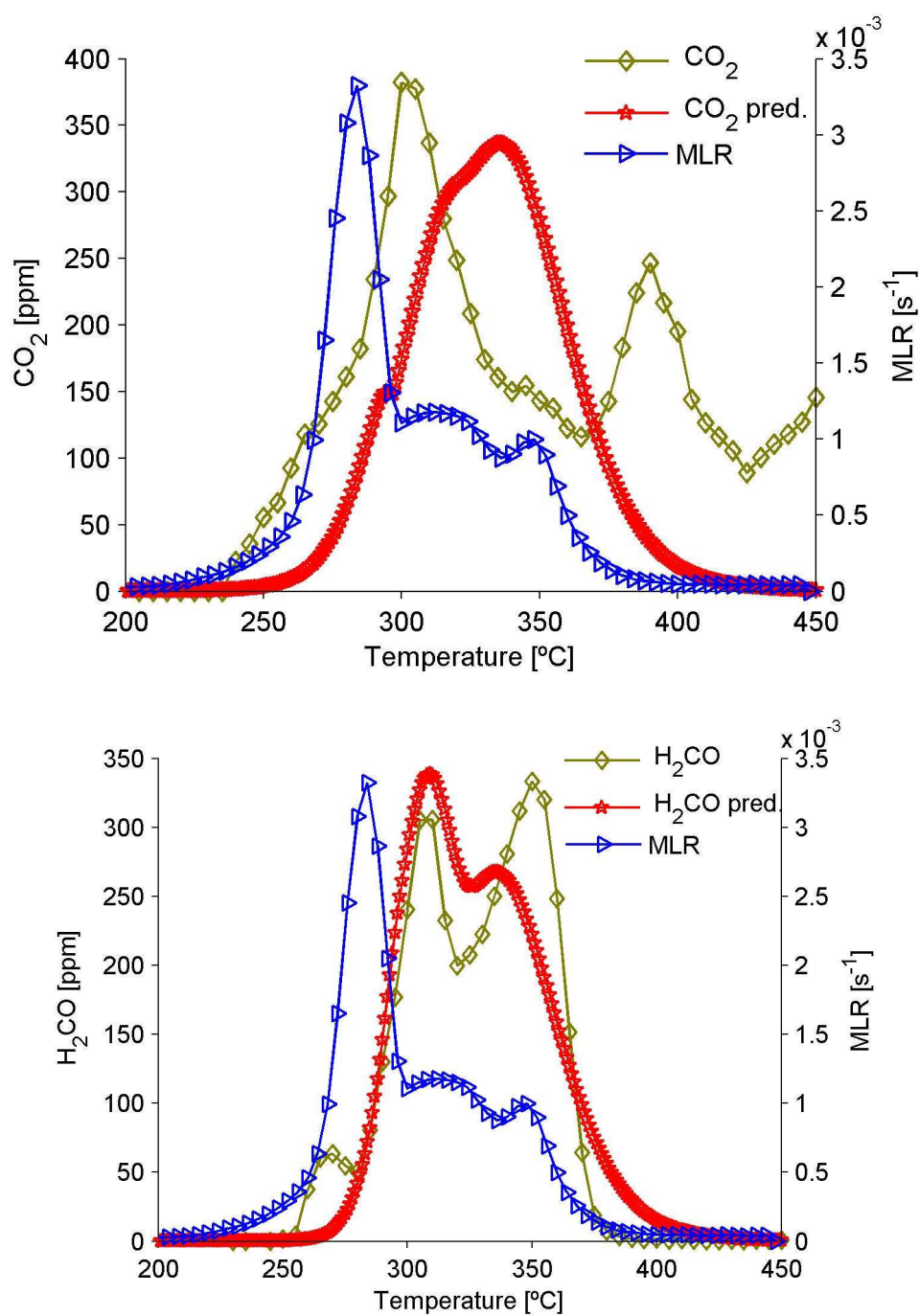
Figure 3-11 Comparison of experimental and calculated kinetics of release of gases. Up: CO_2. Bottom H_2CO. Experimental curves of gas release have been obtained in $TF+FTIR_{qnt}$ (see subsection 2.5.4). The MLR curbe obtained in TGA has been included as reference. $\beta = 10\ °C·min^{-1}$.

As shown in Figure 3-11, the prediction of CO_2 is quite satisfying. The fitting of the experimental and calculated curves is not perfect but the results are promising. To our

knowledge, this work is the first to offer an approach of the prediction of the kinetics of the main toxic gases release as a function of temperature.

The model as well as the experiments presents three peaks of gas release. The peaks are not located at the correct temperatures, but they reproduce the respective concentration of CO_2 production.

The position of the peak of CO_2 production found at a temperature of 400 ℃ is not well predicted. However, this peak also represents a discrepancy between the experimental results found in TF+FTIR$_{qnt}$ and TGA+FTIR$_{qlt}$ (see Figure 2-14-b in subsection 2.5.4). This discrepancy is also responsible for the difference found in the total yields (experimental and calculated) observed in Table 3-7. As stated, this difference can be due to the post-combustion of residues laid inside the TF quartz tube.

The prediction of H_2CO is more accurate than the one of CO_2. The entire shape of the curve is quite well reproduced, except that the third peak of the experimental one is higher, while in the model, the first one is the most intense. The model does not allow the prediction of the peak found at a temperature of 270 ℃.

In conclusion, the model that allows the calculation of the kinetics of gas release requires, as input data for the calibration, the experimental yield of the gases leaked by every reaction of the decomposition mechanism. The method for determining which gases are released by each reaction is the one presented in Figure 3-10, which is based on the hypothesis that a curve of gas release can be calculated as the sum of the gases released by each individual reaction. This allows setting one single parameter per reaction. The output of the model of gas phase is the prediction of the kinetics of gas release and their respective total yield.

Table 3-8, presents the kinetic parameters of the coupled model that allows predicting the behaviour of solid and gas phases. Each reaction has five parameters: three are specific to the solid phase (Arrhenius parameters) and two stoichiometric parameters, one for the solid phase and one for the gas phase. The five parameters of each reaction are optimized simultaneously using Genetic Algorithms.

Table 3-8 Output of the coupled model of solid and the gas phases. Each reaction of the kinetic mechanism has five kinetic parameters.

Reaction	Parameter	Value	Range		Units
			High	Low	
PPUF pyrolysis	E_1	169.9	190	150	kJ·mol^{-1}
	A_1	6.09 x 10^{13}	1 x 10^{22}	1 x 10^7	s^{-1}
	n_1	0.91	1	0.1	–
	υ_1	0.69	0.9	0.1	kg·kg^{-1}
	τ_1	–	9 x 10^9	1.5 x 10^9	–
Polyol pyrolysis	E_2	243.9	260	100	kJ·mol^{-1}
	A_2	4.42 x 10^{17}	1 x 10^{19}	1 x 10^7	s^{-1}
	n_2	1.26	1.5	0.1	–
	υ_2	0.10	0.81	0.1	kg·kg^{-1}
	τ_2	4.9 x 10^9	9 x 10^9	1.5 x 10^9	–
PPUF oxidization	E_3	214.1	240	161	kJ·mol^{-1}
	A_3	3.07 x 10^{18}	1 x 10^{20}	1 x 10^7	s^{-1}
	n_3	0.48	3	0.2	–
	υ_3	0.44	0.7	0.1	kg·kg^{-1}
	τ_3	8.9 x 10^4	1.5 x 10^5	3 x 10^4	–
Polyol oxidization	E_4	213.6	240	161	kJ·mol^{-1}
	A_4	1.26 x 10^{18}	1 x 10^{22}	1 x 10^7	s^{-1}
	n_4	0.95	3	0.3	–
	υ_4	0.56	0.7	0.1	kg·kg^{-1}
	τ_4	8 x 10^5	2.2 x 10^6	2 x 10^4	–
Char oxidization	E_5	160.8	240	160	kJ·mol^{-1}
	A_5	4.30 x 10^{12}	3 x 10^{15}	1 x 10^{11}	s^{-1}
	n_5	1.64	3	0.5	–
	υ_5	0.25	0.8	0.1	kg·kg^{-1}
	τ_5	3.4 x 10^6	9 x 10^6	1.7 x 10^5	–

In this section, the improvements carried out to the model of PPUF thermal decomposition are presented. A discussion is performed on the sensitivity to the decomposition mechanism and to the evaluation function. The need of analysing the chemistry in order to figure out the actual decomposition patterns is clearly identified. The method for the coupling of the models of solid and gas phases is also presented. Finally, the comparison of the experimental and calculated yields of gases is presented as well as the prediction of the kinetics of gas release. It is found that the coupled

models predict in a satisfying manner the behaviour of the solid phase and in a quite satisfying manner the behaviour of the gas phase.

The following sections discuss particular technical aspects of the code, such as the stability and the sensitivity to input parameters.

3.4 Analysis of code stability

In the last section the model used to predict the MLR of a sample being heated up was presented, to which a model that allows the prediction of the kinetic of toxic gases release is coupled. It is shown that the results are satisfying in both the solid and gas phases. This section deals with particular technical aspects of the code used to resolve the mathematical equations: Problems with the code stability have been found that made the computational process difficult. This section is devoted to the analysis of the code stability.

The stability of the code used for the model is a main requirement in order to allow a sensitivity analysis, *i.e.* the space of solutions must be continuous in order to enable the understanding of the influence of the input parameters on the output of the model (presented in the next section). The analysis of stability is aimed at verifying the ability of the solver of Ordinary Differential Equations (ODE) to converge to a solution. It is considered that the solver has successfully found a candidate solution (output) when it is able to calculate a MLR curve and a fitness factor between calculations and experiments. Successfully finding a candidate solution does not necessarily mean that the fitting between the experiments and calculations is good. It only means that the comparison is possible. During the process of ODE solutions, it was found that in some cases, the solver was unable to converge to a solution: the calculation time becomes unacceptably long or the code becomes trapped in infinite loops. The solver used in this research was 'ode15s' from MatLab®.

It is remembered that the input data for the model are the kinetic mechanism (discussed in chapter 3) and a range of values for each kinetic parameter (see Table 3-8). The output of the model is a group of 25 kinetic parameters that fits in a satisfying manner with the experimental results of mass and gas release. These parameters are

calculated by optimization using genetic algorithms. The analysis of code stability was performed giving to each kinetic parameter an input range as large as possible in order to explore the largest field of candidate solutions. The higher and lower limits of the ranges were established according to data found in literature or to the physical meaning of each kinetic parameter (see subsection 3.2.8).

As stated, one candidate group of kinetic parameters is formed by the combination of 25 random kinetic parameters. In total, 2 000 groups were produced and tested within the model. A specific application was developed in order to detect the lack of convergence of the ODE solver with some of the groups. Two limits were imposed to the solver: a critical calculation time and a critical number of iterations. Once the current calculation time or the number of iterations exceeds the critical limits, the ODE solver is forced to stop and classifies the group of kinetic parameters as "unsolvable".

Critical time was set to 5 s and critical number of iterations to 8 000. These limits were set beyond the calculation time and number of iterations required for a typical solved case. A typical solved case was achieved in a calculation time near to 0.25 s and required around 400 iterations. When these two limits were imposed to the solver, it was found that around 13.7% of the candidate groups were classified as unsolvable.

In order to find possible explanations to the problem, various studies were carried out with the groups of kinetic parameters that offered solved and unsolved cases. To discard one possible cause of problems, a verification of the random values generator was conducted. It was found that the values produced for each kinetic parameter followed a uniform distribution and behaved as independent variables, which is a characteristic of good performance for the random values generator. Thus, the ODE output is considered free of possible noise effects caused by dependency relations between the input variables[1].

Two different statistical studies were performed in order to characterise the instability of the code produced by some of the groups of kinetic parameters. The first is a classification of the unsolvable groups with respect to the input ranges given to each

---

[1] To avoid confusions, the possible dependency relations between input parameters is a different problem to compensation effects found by various authors. The compensation effect refers to groups of kinetic parameters that constitute accurate solutions of the model.

kinetic parameter. The second is a descriptive study that statistically compares the groups of parameters that produced unsolvable cases with the totality of the analysed groups. These studies are detailed here-after.

3.4.1 Study of the input ranges of the ODE unsolvable cases.

This study was limited to the groups of kinetic parameters classified as unsolvable. The groups were statistically analysed using the following method: The range of possible values of each variable (input range) was divided into ten subgroups. The number of unsolved ODE in each subgroup was counted. Histograms of the frequency of occurrence of unsolved ODE per subgroup were plotted. As an example of the results obtained, Figure 3-12 presents the frequency of unsolved ODE over the whole input range of pre-factor of decomposition reaction No 1, A_1 (see Table 3-6). Figure 3-13 shows the histograms of activation energy and reaction order of the decomposition reaction No 2, E_2 and n_2 respectively. These statistical analyses aim at highlighting possible common characteristics between the input parameters that produced unsolvable ODE.
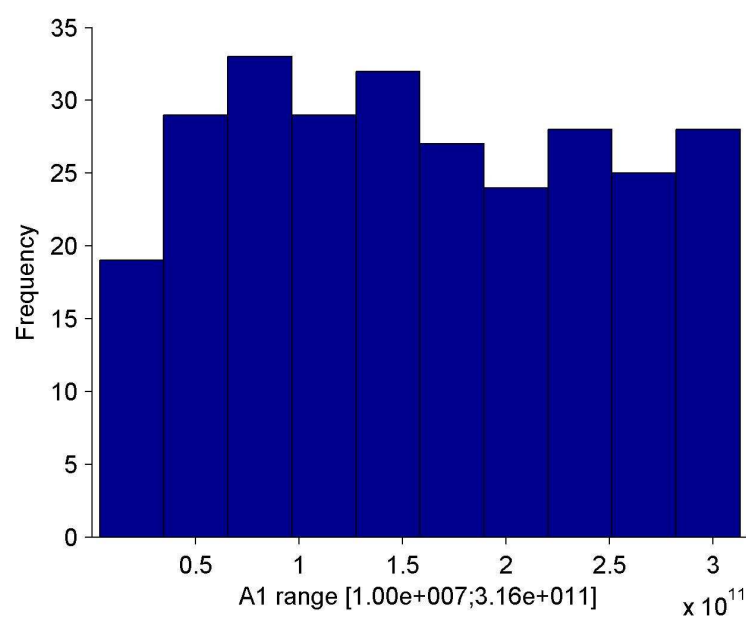
Figure 3-12 Frequency of unsolved ODE in function of the range of pre-factor of decomposition reaction No 1.

The histogram of Figure 3-12 shows that the unsolved cases are almost homogeneously distributed over the whole range of the pre-factor of the decomposition reaction No 1. This allows concluding that solvable and unsolved groups of kinetic parameters can be found independently of the value that this kinetic parameter takes. Thus, the pre-factor of decomposition reaction No 1 can be considered to do not affect the stability of the code.
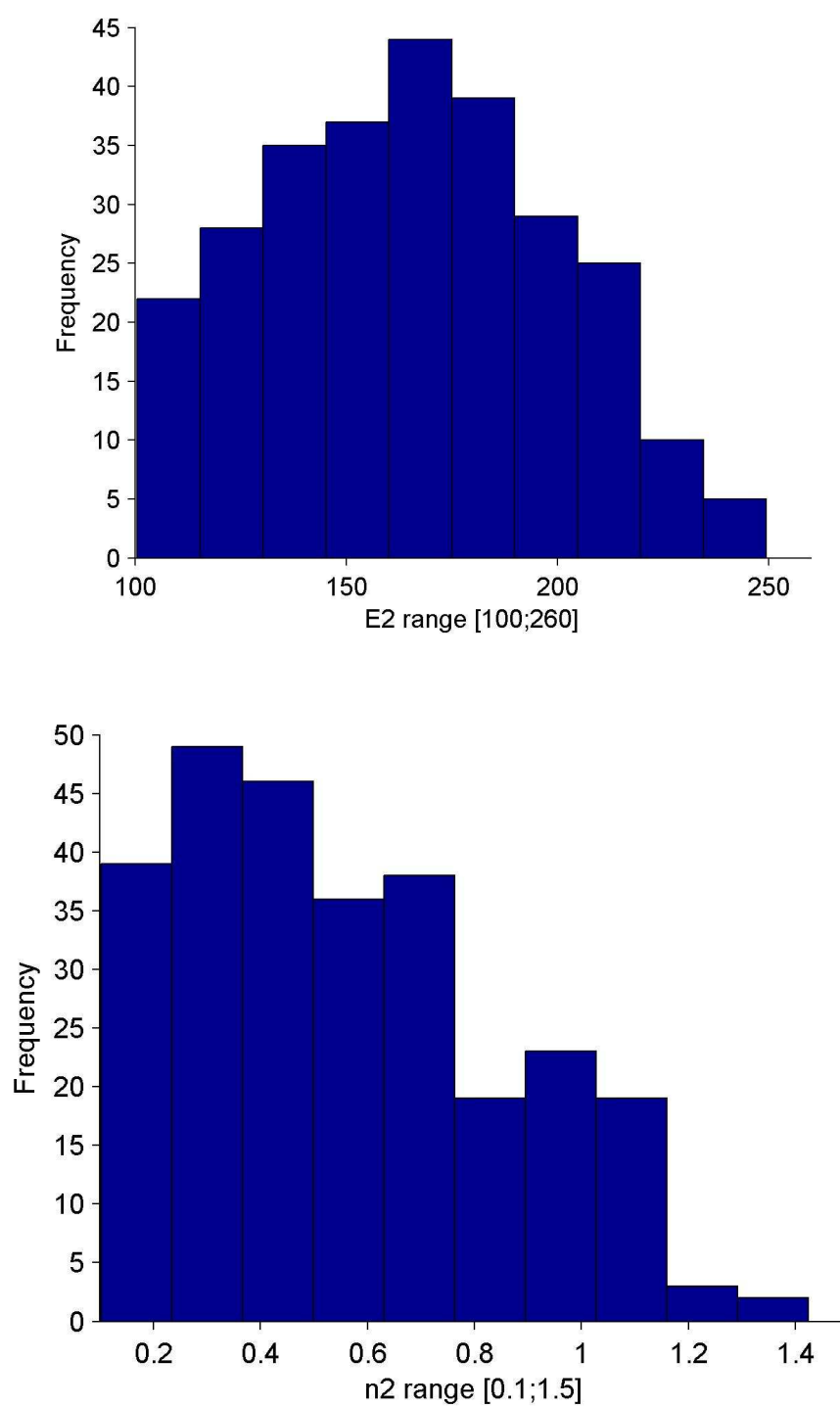
Figure 3-13 Frequency of unsolved ODE in function of variables range. Up, histogram of the activation energy of decomposition reaction No 2. Down, histogram of the reaction order of decomposition reaction No 2.

Contrary to what was observed for A_1 in Figure 3-12, the histograms of E_2 and n_2 present clear trends in the ODE insolvability. The upper histogram of Figure 3-13,

shows that at the center of the input range, the activation energy of decomposition reaction No 2 presents a higher probability of producing an unsolved ODE. However, the probability of finding an unsolved ODE is lower near to the extremes of the range.

A different behaviour is observed in the histogram of the reaction order of decomposition reaction No 2. Values of n_2 near to the lower limit of the input range tend to produce a great number of unsolved cases, while values near the upper limit tend to produce less unsolved ODE.

Under both atmospheres (air and nitrogen), it was found that the kinetic parameters of decomposition of reaction No 2 have a high influence on the stability of the code. The kinetic parameters of the other reactions showed not to be so critical in the production of unsolvable cases. A more detailed study is performed in order to understand why the stability of the code is controlled by the kinetic parameters of the reaction No 2.

3.4.2 Descriptive study

The descriptive study of the groups of kinetic parameters has two aims: The verification of the reproducibility of the appearance of unsolvable cases in the given input ranges of values, and the identification of the ranges of kinetic parameters that produce discontinuities in the field of outputs.

In total, the model was run four times. Twice under nitrogen atmosphere and twice under air atmosphere. Each run evaluated 2 000 groups of kinetic parameters and classified each candidate group as solvable or unsolvable. In all cases, the input ranges remained unchanged.

Table 3-9, presents the summary of the tests run and their respective number of unsolved cases.

Table 3-9 Analysis of reproducibility. Number of unsolved cases per model run. The ranges of input parameters have remained constant.

No	Atmosphere	Total cases	Unsolved cases	Ratio of unsolved
1	Nitrogen	2000	300	15.0%
2	Nitrogen	2000	283	14.2%
3	Air	2000	238	11.9%
4	Air	2000	237	11.9%
Mean			264.5	13.2%
St. Deviation			31.9	1.6%

As shown in Table 3-9, the problem of insolvability of some cases is reproducible. The results of Table 3-9, also confirm that the problem of stability is caused directly by the input data furnished to the model and not by the output produced by the ODE solver. It is remembered that the change of atmosphere modifies the mass balance because the solid species entering into account in the process are not the same, and the calculated reaction rates are different as well.

In Table 3-10 the descriptive study of E_2 and n_2 is presented, which is allowed by the reproducibility condition presented in Table 3-9. The study is focused on these two variables, because of their stronger influence in the stability of the code rather than any other kinetic parameters.

Table 3-10 Descriptive study of E_2 and n_2.

Kinetic parameter	Atm.-test No.	Solution status	Population	Mean	Standard deviation	Variation coefficient	Minimum	Maximum	Range extent
E_2	Nitrogen 1	Total	2000	181.25	46.24	25.51%	100.05	259.99	159.94
	Nitrogen 1	Unsolved	300	121.57	18.38	15.12%	100.05	258.04	158.00
	Nitrogen 1	Solved	1700	191.78	41.42	21.60%	100.10	259.99	159.89
	Nitrogen 2	Total	2000	180.66	45.99	25.45%	100.05	259.90	159.85
	Nitrogen 2	Unsolved	283	121.62	15.08	12.40%	100.05	222.02	121.97
	Nitrogen 2	Solved	1717	190.39	41.91	22.01%	100.10	259.90	159.80
	Air 1	Unsolved	238	119.55	15.34	12.83%	100.02	192.33	92.31
	Air 1	Solved	1762	187.62	42.70	22.76%	100.19	260.00	159.81
	Air 2	Unsolved	237	117.51	11.62	9.89%	100.17	167.89	67.72
	Air 2	Solved	1763	186.78	42.40	22.70%	100.50	259.95	159.44
n_2	Nitrogen 1	Total	2000	0.78	0.40	51.95%	0.10	1.50	1.40
	Nitrogen 1	Unsolved	300	0.54	0.34	63.69%	0.10	1.48	1.38
	Nitrogen 1	Solved	1700	0.82	0.40	48.72%	0.10	1.50	1.40
	Nitrogen 2	Total	2000	0.81	0.40	50.16%	0.10	1.50	1.40
	Nitrogen 2	Unsolved	283	0.58	0.38	64.86%	0.10	1.48	1.38
	Nitrogen 2	Solved	1717	0.84	0.40	47.07%	0.10	1.50	1.40
	Air 1	Unsolved	238	0.55	0.38	68.58%	0.10	1.47	1.36
	Air 1	Solved	1762	0.82	0.40	49.06%	0.10	1.50	1.40
	Air 2	Unsolved	237	0.58	0.38	66.19%	0.11	1.50	1.39
	Air 2	Solved	1763	0.84	0.40	48.29%	0.10	1.50	1.40

In Table 3-10, the column "Solution status" is linked to the "population": they represent the size of the sample. The "Variation coefficient" is calculated as the ratio between the

columns "Mean" and "Standard deviation". The column "Range extent" is calculated as the difference between "Maximum" and "Minimum".

As can be seen in Table 3-10, the mean of the parameter E_2 for the unsolved cases is considerably lower than the mean of total and resolved cases. Also, the unsolved cases have a lower standard deviation than the resolved and total cases. This suggests that lower values of E_2 contained in a small range cause the ODE solver to become unstable. Nevertheless, this conclusion is contradicted by the range extents of the unsolved cases that attain 158, which is very near to the one of the resolved and total cases (close to 159.9).

According to the kinetic parameter n_2, conclusions are much more difficult to obtain. The mean of the unsolved cases is lower than the one of the solved and total cases. However, the standard deviations and the variation coefficient are of the same order of magnitude, independently of the solution status. This suggests that the lower values of n_2 promote the instability of the code. Nevertheless, this is contradicted by the fact that the extent of the range is as large as that of the total cases. No further information can be obtained analysing the maximum and minimum limits and the range of extent.

Information of better quality than that obtained by the statistic study of Table 3-10, can be obtained from the combination of both parameters in a single plot. These results are presented in Figure 3-14, in which the reaction orders are plotted in function of the activation energies for all of parameter groups studied (2 000 groups of parameters). The solved cases are labelled "Ok" and the unsolved cases are labelled "Crash".
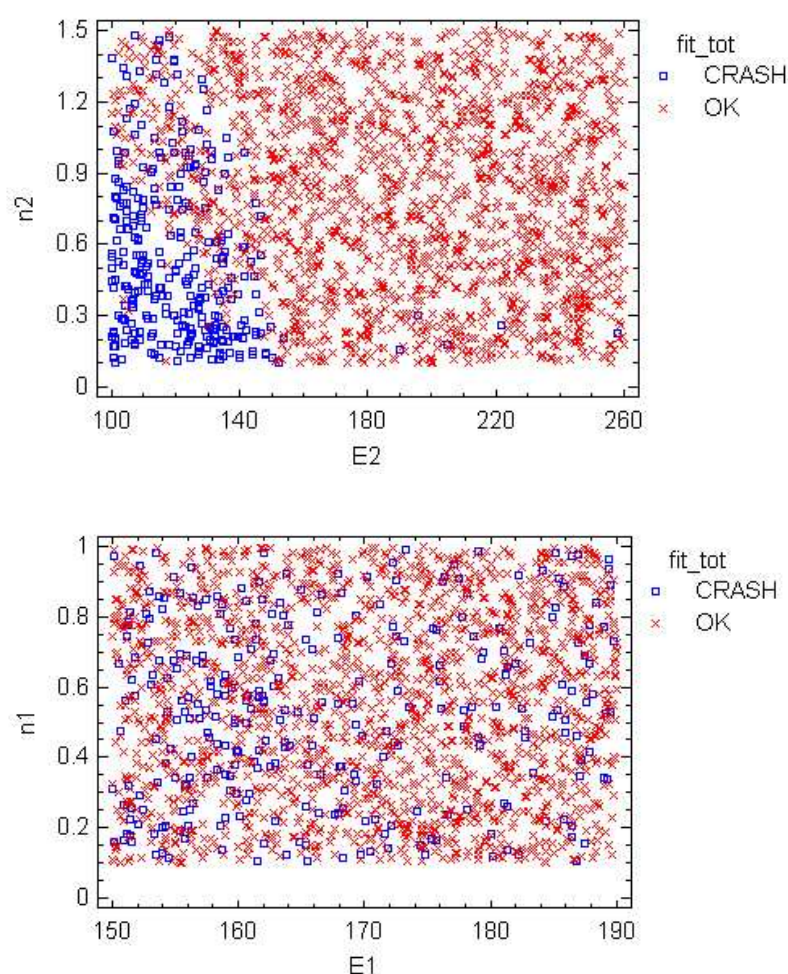
Figure 3-14 Plot of reaction orders in function of activation energies. Up, kinetic reaction No 2. Down, kinetic reaction No 1. The solved cases are labelled "Ok" represented as red x and the unsolved cases are labelled "Crash" represented in blue squares.

At the bottom of Figure 3-14 the typical distribution of variables that do not influence the stability of the code is presented. The squares and crosses are homogeneously distributed all over the area, which means that independently of the values given to these variables, the code can or cannot find a solution.

At the top of Figure 3-14, the results for the kinetic parameters of the decomposition reaction No 2 are presented. The unsolved cases are concentrated in the low values of E_2 and along all the values of the input range of n_2. Nevertheless, a few number of blue squares can be observed in a zone where the range of n_2 is [0.15;0.3] and the one of E_2 is [190;260]. These few unsolved cases are found in regions were the solver

was normally able to find ODE solutions. These visual results confirm the interpretation done according to the data of Table 3-10.

A reliable stability of the code is a primary requirement for further developments of the model. The improvement of the code stability can only be conducted understanding how the ODE solver works and why a given range of parameters produces instabilities. The high nonlinearity of the problem treated, makes it difficult to identify the wrong steps of the solver. However, finding the causes of the insolvability as well as implementing solutions are out of the scope of this research. In all the analyses performed in this research, the unsolved cases have not been taken into account.

3.5 Analysis of sensitivity

In section 3.4, the problem of the insolvability of a non-negligible portion of candidate groups of parameters was presented. The continuity of the space of solutions is a primary requirement of the analysis of sensitivity, thus it cannot be performed for the full range initially assigned to each variable (see Table 3-8).

The space of solutions of the model calculated using kinetic parameters set within a restricted interval is found to be continuous (Outputs: fitness factor and MLR curves). Because of the small size of the interval used, the analysis of sensitivity is called: "Fine parameters analysis of sensitivity".

The fine parameters analysis of sensitivity, is performed with parameters values comprised in an interval limited by $\pm 5\%$ of the optimum values presented in Table 3-8. This range has been selected as a compromise between the largest ranges of kinetic parameters in which the space of solutions remains continuous. The fine parameters analysis allows studying the change of MLR curve and fitness factor with the deviation of input parameters.

A total of 10 000 groups of parameters were tested in the range of $\pm 5\%$ of the optimum. The fitness factors under nitrogen atmosphere are between 0 and 52 and those under air are between 0 and 22. These intervals were divided into 10 subgroups.

The histograms of frequency of occurrence of a fitness factor in each subgroup are plotted in Figure 3-15.
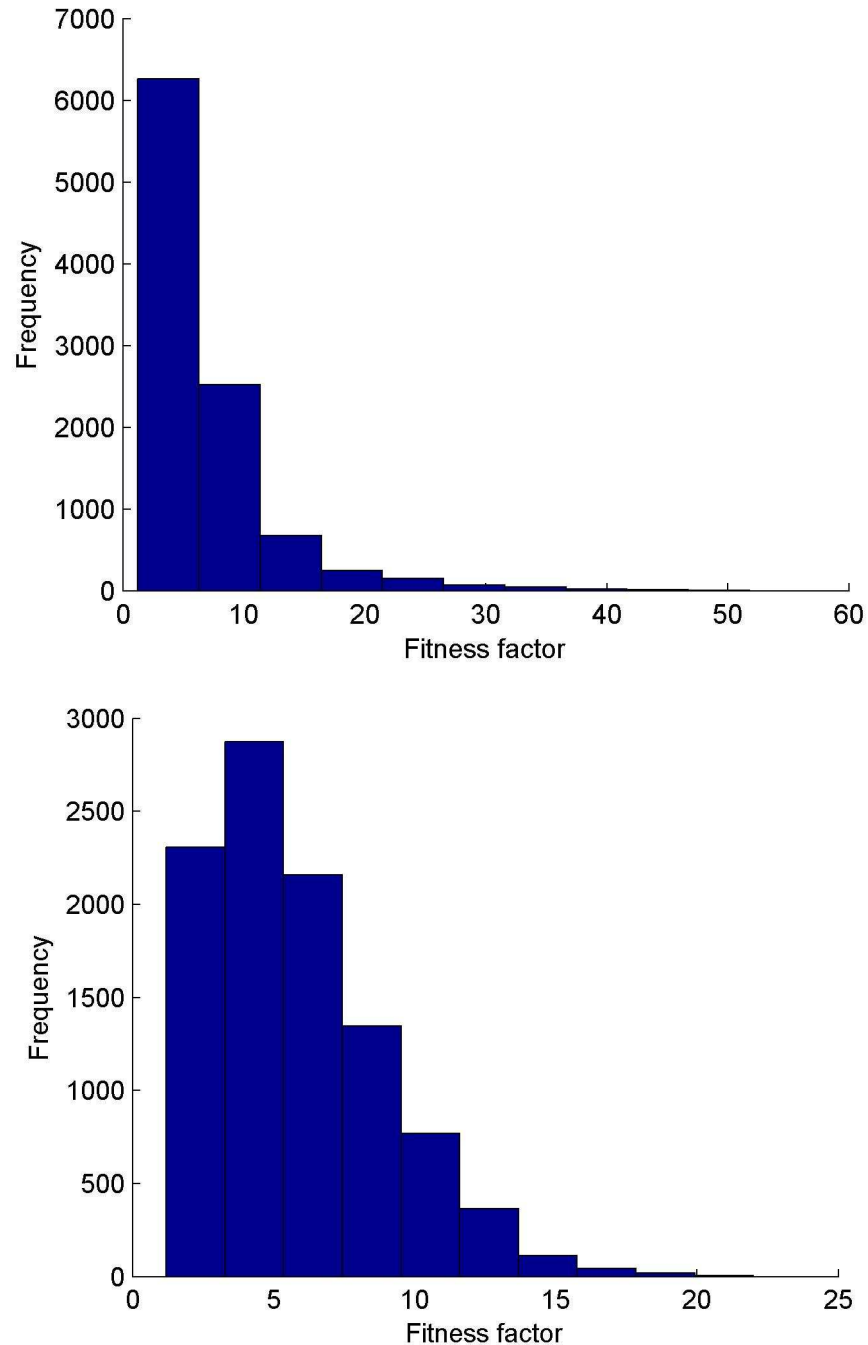
Figure 3-15 Histograms of fitness factors found in the fine parameters analysis of sensitivity. The range of kinetic parameters is limited by ± 5% of the optimum values. Up, Nitrogen atmosphere. Bottom, air atmosphere.

As can be seen in Figure 3-15, the precision of the kinetic parameters is crucial in order to obtain an accurate fitness between experimental and calculated curves. A tolerance of $\pm 5\%$ in the input parameters range shows to be unacceptable. For the 10 000 groups of kinetic parameters verified in this research, more than 95% presented a fitness factor lower than half of the optimum fitness factor. This acceptable uncertainty ($< \pm 5\%$) of the input data of the model is extremely low compared with the experimental uncertainties which are typically over 20%. Thus, the validity of the optimum group of kinetic parameters needs to be interpreted with much care.

An analysis of the influence of kinetic parameters on the fitness factor is carried out. The 500 groups of parameters (5%) that produced the best fitness factors were filtered and analysed independently. The ranges of the best kinetic parameters were divided into ten subgroups. Histograms of the frequency of occurrence of best fitness factors in each subgroup were plotted. It was found that the energies of activation remain the more influent parameters. As an example of the results obtained, the histogram of the activation energies of reaction No 4 is shown in Figure 3-16.
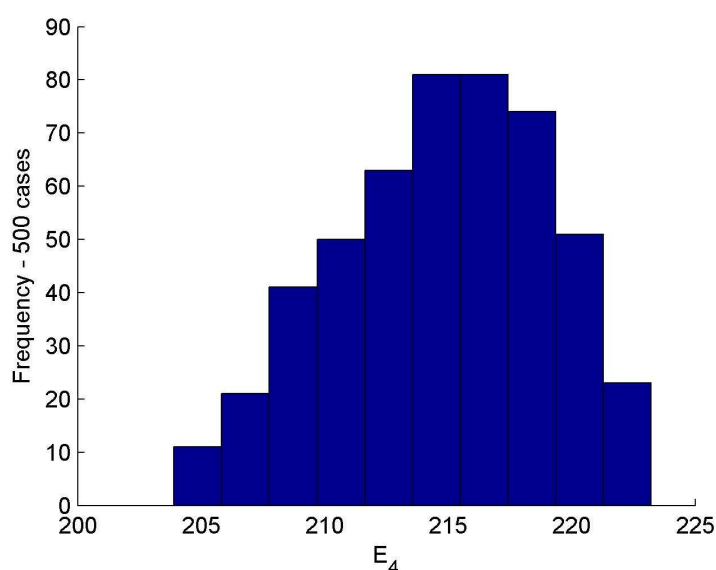
Figure 3-16 Histogram of influence of the activation energy of reaction No. 4 in the fitness factor. The 500 groups of parameters that best fit the calculations with experimental results are analysed. Atmosphere: Air.

The results presented in Figure 3-16 mean that the optimum fitness factor is found almost at the centre of the input range of activation energy of reaction No 4. However, the histogram is not symmetric. The asymmetry is caused by the high nonlinearity of

the mathematical equations used in the model. Asymmetry also means a high sensitivity to input parameters.

The high sensitivity to input parameters and the high nonlinearity of the model present a major drawback to this technique: The optimum group of kinetic parameters presented in Table 3-8 is from a statistical point of view a probable maximum, but not the absolute one. Further researches must analyse the possible existence of other combinations of kinetic parameters within different ranges to the ones used in this research that allow as well predicting the thermal behaviour of PPUF under air and nitrogen. If this is the case, the problem would be multi-solution.

3.6 Conclusion

The improvement of accuracy in prediction of PPUF decomposition is a prime task for thermal analysis and FSE, since it allows calculating the source term of fire, thus enabling the determination of the power of fire and the potential damages that can be cause to structures.

Many methods have been proposed in literature in order to model the thermal decomposition of PU. The great majority are based on TGA experimental results, which allow determining the decomposition mechanism and calculate the kinetic parameters of the Arrhenius reactions. Nevertheless, the group of parameters calculated depends on the method and the model defined. The kinetic parameters do not represent intensive properties of the matter. Moreover, it was found that TGA experimental results must be accurately reproduced by many decomposition mechanisms.

A reliable knowledge of the decomposition mechanism is required because it allows determining the mass balance and controls the number of parameters required for the calculation. The method used to find the decomposition mechanism was improved taking into account the effluents released, which enabled us to select the one that is in accordance to the chemistry of the process.

The model of thermal decomposition was improved as well. The new model can not only predict the MLR as a function of temperature, but also the kinetic of release of

exhaust gases. A single parameter calculated using genetic algorithms is necessary to enable the calculation of the yield of toxic gases. This is a promising result for the purpose of estimating toxic hazard in fire scenarios.

The main hypotheses and input data of the method used are:

- The mechanism of thermal decomposition must be determined prior to modelling. Experimental observations must enable the understanding of the decomposition patterns.

- Each reaction of decomposition follows an Arrhenius law. The Arrhenius equations are function of the remaining mass and the oxygen mass fraction.

- The kinetic parameters are calculated using genetic algorithms (optimization tool) by comparison of experimental and calculated curves of MLR and gases release in function of temperature. GA showed to be adequate for highly nonlinear mathematical problems such as those found in this model.

- Each variable (kinetic parameter) is optimized within a range defined by the user. The best solution is not a unique solution, but the one that statistically best fits the experimental and calculated results. In order to perform a general analysis, the ranges given were as wide as possible.

Three decomposition mechanisms, one from the literature (Rein *et al.* [107]) and two proposed in this research (kinetic mechanism 1 and 2) were analysed. The kinetic mechanism 1 was found to be the one that best explains the behaviour of the solid and the gas phases. The best kinetic mechanism was used to calculate the kinetic constants of the process. It was found as well, that the results of the modelling are dependent on the evaluation function used to compare the experimental and calculated curves. Three evaluation functions were analysed, the one that presented the best performance in terms of calculation time and ability to fitting nearly both curves is the one based on the Hilbert vectorial analysis.

A study of code stability was conducted in order to determine the possible causes of the insolvability of the ODE solver, which has been observed for some of the groups of kinetic parameters used. It was shown that the activation energy and reaction order are the most sensible parameters, particularly those of the second reaction of pyrolysis.

An analysis of sensitivity of the model to the input parameters was conducted. It was found that a deviation in input data of 5% is unacceptable. Nevertheless, in FSE applications, a tolerance lower than 5% in the input data of the model is not in the same order of magnitude as the experimental uncertainties, which are typically close to 20%. Thus, the validity of the optimum group of kinetic parameters needs to be interpreted with much care.

The output data of the model represent primary input data to the pyrolysis model of CFD simulations presented in the following chapter.

4 Small scale experiments and simulations

4.1 Introduction

In chapter 2 were presented the experimental results obtained at the matter scale, which allowed stating the decomposition mechanism of PPUF. Chapter 3 presented the model of decomposition kinetics of the foam. The model was improved in order to be able to consider the changes of the solid and gas phases with the increase in temperature. In both chapters, the masses concerned were under 250 mg. The samples are then considered as particles and no gradient effects are taken into account.

The decomposition mechanisms found at the matter scale is verified at a larger scales in order to analyse the influence of phenomena that play a main role in large scale such as thermal gradients, the effect of turbulence, the formation of a decomposition front, gradients of concentration of species, etc. So, the kinetic parameters obtained with the modelling performed at the matter scale are used in numerical simulations and a validation with experimental results is carried out. This chapter presents the experimental results and fire simulation at small scale, which is often called bench-scale in literature. It is greater than the one dealt with in the previous chapters, but is intermediary between the matter scale and the real scales concerned by FSE. The tests are performed using the Cone Calorimeter (CC) apparatus, so the masses considered are 11 ± 1 g.

The main difference between the samples used at the small scale compared to matter scale is that the samples cannot be considered as particles; the temperature of the

sample is therefore not homogeneous. Gradients of temperature are allowed between the boundaries and the centre of the sample. So, the sample is considered thermally thick (some comments about the Biot number are presented in section 5.1). Differential concentrations of gases, particularly oxygen, have also been found in-depth of porous samples, *e.g.* in smouldering combustion [130]. The gradient of gaseous species are formed by the diffusion of oxygen from the boundaries towards the centre of the sample and the subsequent transport of gas products from the decomposition zone towards the environment. Both gradients (temperature and species) strongly influence the PPUF decomposition kinetics.

At the matter scale, it is considered that the particles are homogeneously irradiated at all the exposed surface (sides) and the sample mass is at uniform temperature equal to the one of the furnace. The concentration of oxygen and gas species is homogeneous as well because there is not resistance to species transport. In the tests presented in this chapter, samples are heated by an external irradiation source concentred towards a single surface. It causes an increase in surface temperature that consequently initiates the decomposition process. Combustible gases are released during the breakdown of solid molecules, and are ignited by contact with a spark igniter.

In CC tests (small scale), gas effluents are analysed in order to acquire information on the chemistry of the processes taking place in the solid phase. The sampling of gases is conducted downstream of the CC fan, where no further reactions in the gas phase are supposed to occur.

The experimental results obtained in CC are compared to numerical simulations carried out using the widest spread CFD code used for fire simulation: FDS V 5.3.0. The process of thermal decomposition of the solid fuel is predicted, so the calculations are called "pyrolysis calculated fire simulation". The required input data can be classified into two groups: a) the thermal properties of the solids, and b) the decomposition mechanisms and their kinetic parameters. These input data are presented in sections 2.4 and 3.3 respectively. The main differencies between the pyrolysis calculated fire simulations and the set heat release rate simulations is explained later in the chapter.

The main objectives of the study at the small scale are:

- To determine the fire behaviour of PPUF by measurement of Heat Release Rate (HRR), MLR and Effective Heat of Combustion (EHC).

- To analyse the decomposition mechanism of the foam at the small scale in order to allow a comparison with the one observed at the matter scale.

- To analyse 16 gases in real time in order to understand the chemical process taking place.

- To measure the yield of release of the main toxic gases: CO_2, CO, H_2O, NO and total hydrocarbons.

- To establish a ratio between HRR and the release of gases.

- To conduct a numerical simulation of the fire behaviour of PPUF in order to predict the HRR and MLR, and to compare them with experimental results.

This chapter is divided into six sections. Section one is the introduction. Section two is the experimental setup used to analyse the PPUF reaction-to-fire. Section three presents the experimental results and the analysis. Section four presents the numerical simulation. Section five presents the comparison between experimental and calculated results. Section six presents the validation of the decomposition mechanism of PPUF in a simplified seat (product scale). Section seven is the conclusions of the chapter.

4.2 Reaction-to-fire experimental setup

This section presents the experimental setup used to determine the reaction-to-fire of the non-flame-retarded PPUF studied in this research. The experiments provide important understanding of its thermo-oxidative decomposition and evolved gases. The PPUF data required in this research include phenomena taking place in the gaseous and solid phases. The gaseous phase is characterized by measuring the mass flow of evolved gases as a function of time and CC irradiance level, while the MLR was used to study the solid phase. Analysing information from both phases provided very useful information about the chemistry of reactions taking place in the solid foam slab. The experimental devices used are cone calorimeter, Fourier Transform Infrared

spectroscopy analysis, Flame Ionisation Detection (FID) and Non-Dispersive Infrared analyser (ND-IR).

Figure 4-1 presents two pictures of the cone calorimeter (ISO 5 660-1 [131]) and a detail of the PPUF sample when exposed to irradiance level from the electric heater. The ignition spark is positioned above the sample so all the tests were performed in flaming condition.
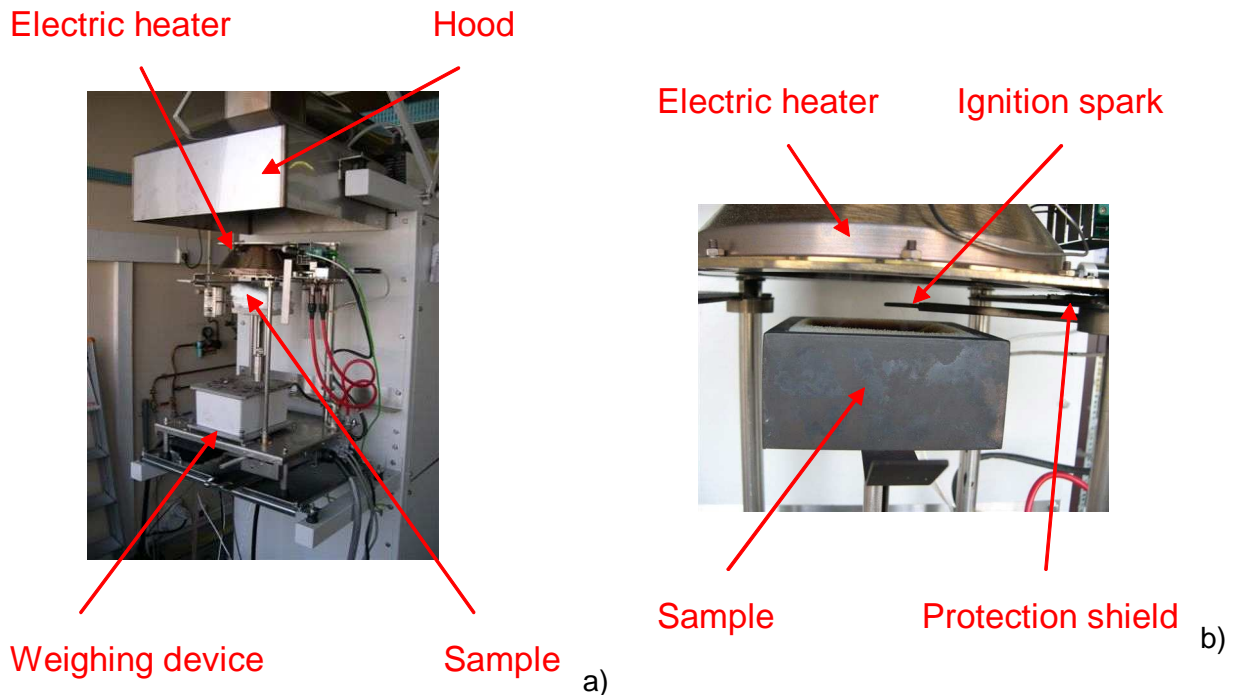
Figure 4-1 Pictures of the cone calorimeter used in this research. a) Cone calorimeter; b) Detail of the sample exposed to the radiative heat flux produced by the electric heater, the ignition spark is also shown.

As stated in section 2.3, the elementary analysis showed that no inert load, flame retardants or fillers were used during the manufacturing of PPUF; neither chlorine nor sulphur-based additives were found. The detection of such compounds is priority because they can change the reaction-to-fire of the sample by modifying the decomposition mechanism. The formula of the virgin foam istudies is $CH_{1.53}O_{0.27}N_{0.08}$.

This chemical composition is in agreement with other Polyether Polyurethane Foams found in the LNE Materials Database[2] and from the literature in Table 2-4.

The reaction-to-fire characterisation was carried out in a CC. PPUF specimens were conditioned at 23 ± 2 °C and at a relative humidity of $50 \pm 5\%$ for more than 88 h in accordance with the specifications of the ISO 291:2005 standard [132]. The sample dimensions were 100 ± 2 mm long, 100 ± 2 mm wide and 50 ± 2 mm high with a mass of 11 ± 1 g.

The evolved gases from the CC were passed through a desiccator and a cold trap to remove water vapour, thus improving the accuracy of the analyses (dry gas analysis). The paramagnetic analyser used to measure the instantaneous oxygen concentration was a Servomex 4000 that includes an ND-IR for CO and CO_2. Two additional gas analysers were coupled to the exhaust duct of the CC: FID and FTIR (see subsection 2.5.1). The FID is a Series AIX 2000 probe that was connected at a gas sampling port upstream of the CC fan. The FID flow rate was 1.7×10^{-5} $m^3 \cdot s^{-1}$, low enough to avoid affecting the main CC exhaust flow rate of 2.4×10^{-2} $m^3 \cdot s^{-1}$. For simplicity, the FTIR (flow rate of 1.0×10^{-4} $m^3 \cdot s^{-1}$) was plugged to the exit of the CC exhaust. Much care was taken in order to avoid cold points in the apparatuses connections. An Eurotherm Chessell 4100G temperature logger was used to measure the gas temperature in order to correct the molar flow rate of gas captured by FTIR. Figure 4-2 presents the layout of the coupling of CC and the gas analysers.

---

[2] The LNE Materials Database is a proprietary tool created in 2006 and containing composition information of more than 5000 registers of industrial materials. The family of polyurethane foam contains 57 registres.
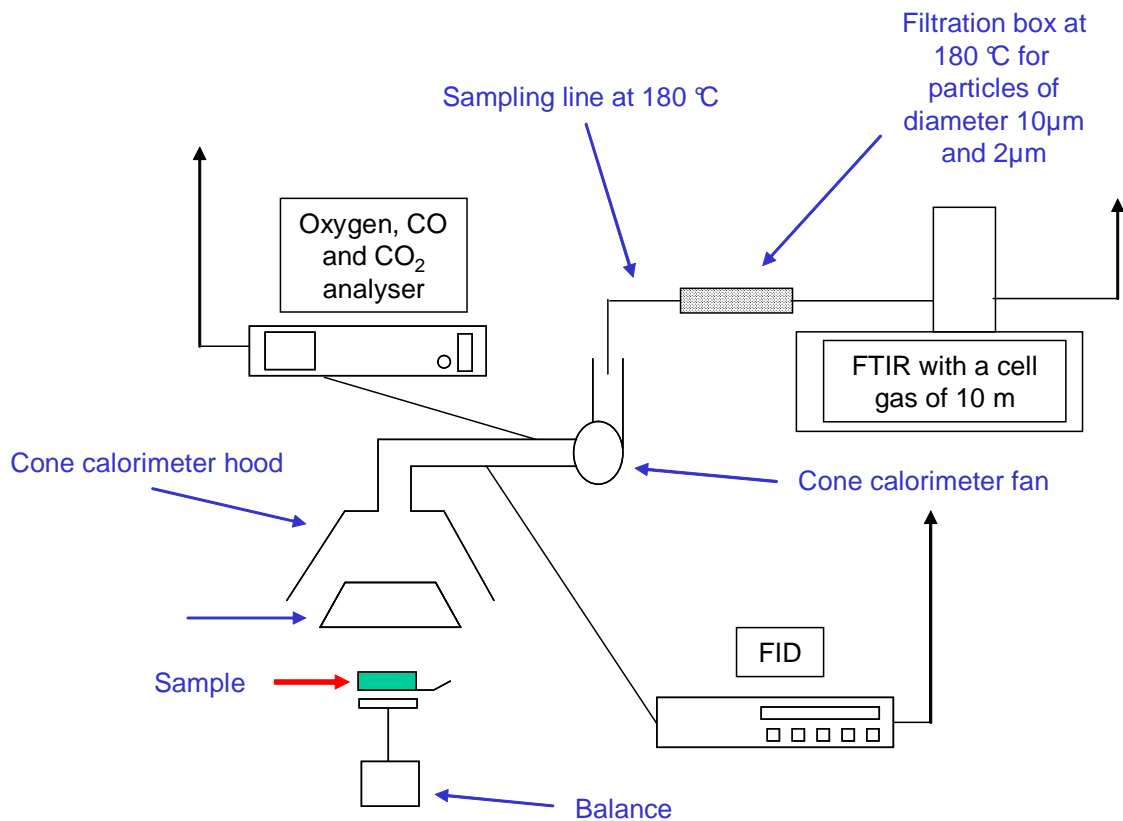
Figure 4-2 Schematic layout of the coupling of cone calorimeter and gas analysers: FTIR and FID. The temperature register is not shown in the scheme.

Five irradiance levels were used: 10, 20, 30, 40 and 50 $kW \cdot m^{-2}$. Tests at 10, 20 and 30 $kW \cdot m^{-2}$ were repeated four times, while those at 40 and 50 $kW \cdot m^{-2}$ were repeated twice. All the experiments were carried out under air atmosphere. The measurements were performed without an insulator on the bottom side of the sample. In order to analyse the influence of the insulator layer, tests were repeated using a 13-mm-thick silica wool insulation layer with a density of 64 $kg \cdot m^{-3}$ as described in the ISO 5 660-1 standard [131].

4.3 Cone calorimeter experimental results

HRR is an important variable for evaluating material fire hazards [133][134]. It was measured using the oxygen consumption calorimetry technique [20]. This technique is the basis of the ISO 5 660-1 standard [131] and uses Eq. (4-1) to calculate the HRR

in [kW·m^{-2}]. It is a function of E_{O_2}, the heat of combustion per unit mass of oxygen consumed (also known as the Thornton factor and assumed to be 13.1 MJ·kgO$_2$$^{-1}$ ± 5% [131]), Φ, the oxygen consumption factor defined in Eq. (4-2), and $\dot{m}_e$, the mass-flow rate in the CC exhaust duct defined in Eq. (4-3) and determined from the pressure drop across and temperature at an orifice plate:

$$HRR = 1.10 \cdot E_{O_2} \cdot x_{O_2}^o \cdot \left[\frac{\Phi}{(1-\Phi)+1.105 \cdot \Phi} \right] \cdot \dot{m}_e \qquad (4\text{-}1)$$

$$\Phi = \frac{x_{O_2}^0 \left(1 - x_{CO_2}\right) - x_{O_2} \left(1 - x_{CO_2}^0\right)}{x_{O_2}^0 \left(1 - x_{CO_2} - x_{O_2}\right)} \qquad (4\text{-}2)$$

$$\dot{m}_e = C \sqrt{\frac{\Delta p}{T_e}} \qquad (4\text{-}3)$$

In order to use these equations, some simplifications and experimental facts are required. The environmental H$_2$O concentration was neglected because the exhaust gas passes through a calcium chloride filter and a cold trap in order to eliminate all moisture. CO concentration was also neglected because of its typically low concentration during well ventilated flaming combustion (Notably in proportion to the CO$_2$ concentrations). Calculations were carried out to verify the influence of neglecting the release of CO, and the error in HRR was found to be less than 1%. Nevertheless, this error is low compared with the relative uncertainty of the cone calorimeter, which is 10% for HRR greather than 1 kW following to calculations carried out in LNE.

The baseline calibration of the CO$_2$ and O$_2$ analysers was conducted with pure nitrogen allowing an accurate determination of the environmental concentrations prior to test. The measurement of the oxygen concentration is the basis of the HRR calculation. It is assumed here that the mass of oxygen contained in the PPUF molecule (22.5Wt%) is low compared to the mass of air that is transported into the exhaust line (well-ventilated fire), thus the calculation of HRR is not affected by the oxygen present in the virgin PPUF.

At the beginning of each test, the CC calorimeter thermal shield was opened and the sample was suddenly exposed to the set irradiance level. A decomposition front was formed and advanced rapidly from the top to the bottom of the sample. The results

shown here correspond to flaming conditions initiated with a spark ignition source. In experiments not discussed in this dissertation, it was found that the critical irradiance level (CHF) for ignition of the foam is 9 kW·m^{-2} and the irradiance level for auto-ignition is 35 kW·m^{-2}.

Figure 4-1 shows the transient evolution of MLR and HRR at the five different irradiance levels. Since a good repetability of the experimental results has been observed, one experimental result has been chosen for the plots.

Figure 4-3 Results in cone calorimeter at five irradiance levels. a) Mass-Loss Rate; b) Heat Release Rate.

In Figure 4-3 time $t = 0$ marks the beginning of the exposure to the desired irradiance level rather than the moment of ignition. As shown, the shapes of HRR and MLR curves changed with the irradiance level. In the HRR plots are evidenced two stages of decomposition (combustion regimes) at all the irradiance levels. At 10 kW·m⁻², the two stages are very close making difficult the idenfication. The intensity of the secondary

179

HRR peak increases with the irradiance level and at an irradiance level of 50 kW·m^{-2}, the second peak has a similar intensity as the first peak.

In the MLR curves, two decomposition stages are identified as well, nevertheless the secondary peaks never reach the intensity of the first peak meaning that the ratio between the MLR and HRR is not constant. This observations are discussed later in the chapter.

Table 4-1 Experimental results of PPUF in CC measured at five irradiance levels (mean): time to ignition, time to extinction, total combustion time and ratio between burnt and initial sample mass

Irradiance level of CC	Time to ignition	Time to extinction	Combustion time	Ratio of burnt to initial mass
[kW·m^{-2}]	[s]	[s]	[s]	[%]
10	87	176	89	41
20	10	220	210	68
30	5	273	268	97
40	3	240	237	100
50	2	173	171	98

Table 4-1 presents the time to ignition, the time to extinction, the total combustion time of PPUF and the ratio between the burnt and initial masses. As expected, time to ignition decreased when the irradiance level increased. Total combustion time is the difference between time to extinction and time to ignition. Total combustion times were shorter at low and high irradiance levels, with a maximum at 30 kW·m^{-2}. This can be explained because for the low irradiance levels of 10 and 20 kW·m^{-2}, the initial mass of the sample was not totally consumed during combustion and the combustion rate is low. A significant amount of char remained in the sample holder after fire extinction. Thus, low irradiance levels provided shorter combustion times compared to the test at 30 kW·m^{-2}, in which the sample is completely burnt. At 50 kW·m^{-2}, the decomposition reaction rate was faster than at 30 kW·m^{-2} due to the strong irradiance received by the sample from the radiant cone. It provided a shorter combustion time.

Comparison tests were performed using a silica wool insulating layer instead of non-insulating backing at the PPUF sample to investigate the effect of this boundary condition. The results show that the decomposition kinetics, gas release and HRR do not change significantly with the insulating layer. This suggests that under the current

test conditions, the decomposition rate is not controlled by sample heat losses. The thermal balance of the experiments in CC is written in Eq. (4-4) [135].

$$Q_e'' + Q_{f(r+c)} - Q_{rr} - SMLR \cdot \Delta H = 0 \qquad (4\text{-}4)$$

Where, Q_e'' is the incident irradiance level from the electric heater. $Q_{f(r+c)}$ is the incident heat flux from the flame towards the sample which has radiative and convective fractions. Q_{rr} is the reradiation heat lose caused by the radiation of the hot sample surface towards the environment. $SMLR \cdot \Delta H$ is the heat of reaction, which accounts for the power consumed during the breakdown of the molecules from the condensed phase. The thermal balance allows to explain the change of HRR peak with the increase of the irradiance level. If it is considered that the heat of reaction and the reradiation heat losses are constant (acceptable hypotheses), the combustion process is controlled by the incident irradiance from the flame and the electric heater [135].

In addition to the heat release rate, the toxicity of the burning products must be taken into account when analysing the fire hazard of a material [113]. PPUF is manufactured from the condensation of polyisocyanates and polyether polyols in the presence of catalysts and/or additives [8][136]. Rogers *et al.* [23], Saunders *et al.* [37] and Woolley [35] studied the thermal decomposition of urethane-based plastics. They stated that, when PPUF is heated, urethane bonds break into polyol and isocyanate. In the first stage, isocyanate pyrolyses and oxidizes. It is released as yellow smoke. Liquid polyol remains in the sample holder as a semi-product of the decomposition process. Pyrolysis and oxidization of liquid polyol occur in a second decomposition stage. The gases released during a PPUF fire (burnt and unburnt) are considered highly hazardous to life, safety and the environment [9][45][137].
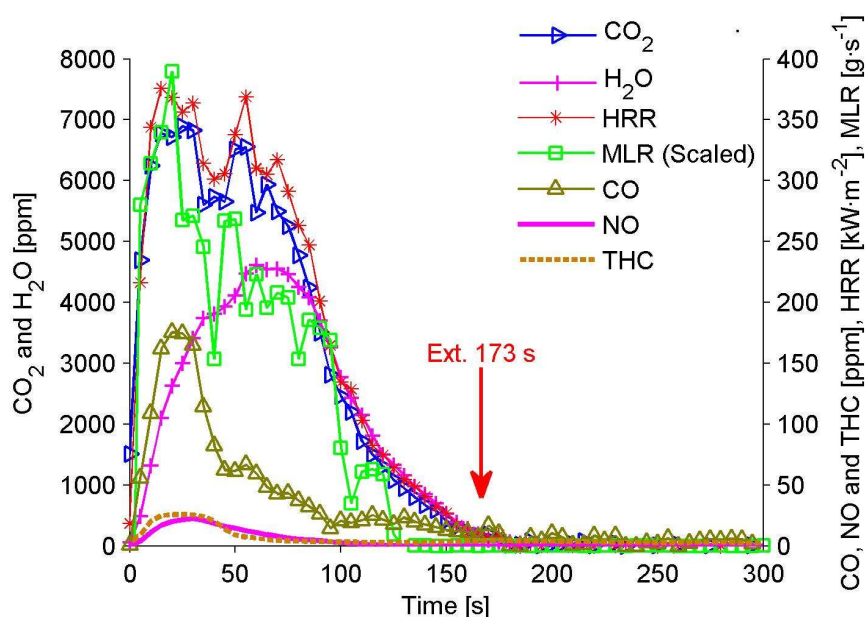
Figure 4-4 Change over time of HRR, MLR and gas species concentration during combustion of PPUF at an irradiance level of 50 kW·m^{-2} in CC. CO_2 and H_2O are quantified at the left-hand side y-axis. CO, NO, THC, HRR and MLR are quantified at the right-hand side y-axis. The MLR curve is scaled by a factor of 2000 (Source [138]).

Figure 4-4 presents the transient evolution of different gas species concentration, HRR and MLR at an irradiance level of 50 kW·m^{-2}. The x-axis is common for all curves. The concentrations of CO_2 and H_2O were quantified at the left-hand side y-axis. The concentrations of CO, NO and total hydrocarbons (THC) as well as the plots of HRR and MLR were quantified at the right-hand side y-axis. The plot of MLR has been scaled by a factor of 200 for ease of viewing. Gas concentrations are expressed in [ppm], with THC units as the ppm equivalent of methane because of the FID calibration method. The results have been corrected for the transport delay and the response time of the instruments.

Figure 4-4 shows that the general change with time of the HRR, MLR and the curves of gases release are similar, thus suggesting the underlying kinetics throughout the burning process. This provided important information about solid decomposition reactions and production of gas species. The release curves for the different gas species did not have the same shapes, but did share common maxima and minima at various points in time. These common points represent the basis for the analysis of the PPUF decomposition kinetics and allowed identifying the PPUF decomposition stages.

182

As shown in Figure 4-4, at an irradiance level of 50 kW·m^{-2}, the maximum in the HRR curve occurred approximately 17 s after the beginning of the exposure. Using the HRR peak as a reference, we can see that the first peaks of MLR, CO_2, THC, CO and NO occurred at exactly the same time. H_2O was not considered as a hazardous gas, but it served as a marker for the occurrence of one particular reaction. This reaction involved the combustion of polyol and occurred during the second stage of decomposition (hydroxyl groups [22]). The curve corresponding to H_2O concentration showed an important inflection point when the HRR reached a maximum. However, with increasing time, the amount of H_2O released continued to grow. Hydrogen was consumed by the production of H_2O. The late release of H_2O in comparison to CO_2 suggested that the reaction of most hydrogenated compounds of foam was delayed.

The maximum release of H_2O appeared 55 s after exposure to the CC irradiance. At about the same time, the second peak in the HRR and CO_2 appeared, along with a local minimum of MLR, a local maximum of CO and an important decrease in the amount of THC production. At 50 kW·m^{-2}, a third peak in the HRR curve appeared approximately 70 s after exposure to CC irradiance. This time corresponded to a maximum of CO_2 release, a local maximum of MLR, the beginning of the decrease of H_2O production and an important change in the slope of THC.

At 50 kW·m^{-2}, before the second peak of HRR at approximately 50 s, the solid has been completely consumed, leaving a semi-liquid residue in the holder. This dark brown viscous product consisted primarily of polyol with traces of isocyanate and oxidized residues. This semi-liquid product continued to oxidize as a pool fire until the extinction of flames, approximately 173 s after exposure to CC irradiance.

The evolution of gas species can be used to determine the decomposition stages in the solid phase. In the 50 kW·m^{-2} test (Figure 4-4), from the beginning of exposure at $t = 0$ to approximately 50 s (about 48 s after flaming ignition), high concentrations of CO, CO_2 and THC were measured coming from the sample, suggesting the presence of a rich combustible mixture. After 65 s, productions of CO and THC were low, but the release of CO_2 remained high (less rich combustible mixture).

The hydrocarbons, CO and CO_2 are released by the pyrolysis of PPUF process (see the molecular decomposition mechanism presented in subsection 2.2.2 and Eq (2-2)). As shown in Figure 4-4, the concentration of THC strongly decreases after 50 s attaining very low concentrations. Nevertheless, high amounts of CO and CO_2 are

produced. These results were explained by Dryer *et al.* [139][140], Glassman [141] and Yetter *et al.* [142][143]. They stated that in similar combustion conditions to the ones found in this experiments, the thermal decomposition of one combustible may forms CO by two ways: heterogeneous reaction with the solid, and the oxidization of hydrocarbons. Lately, the CO produced is oxydizated into CO_2. This mechanism allows explaining the decrease of CO release observed after 50 s while the release of CO_2 is still very high.

Nitrogen is a minor chemical element in the foam, but present only in the isocyanate chain. The FTIR analyser was calibrated to measure nitrogenated compounds (see Table 2-5) such as hydrogen cyanide (HCN), ammonia (NH_3), nitrous oxide (N_2O) and nitric dioxide (NO_2). In these experiments, except NO, all other nitrogen gas species were absent or present in quantities under their detection limits (HCN, 1.4 ppm; NH_3, 1.7 ppm; N_2O, 0.5 ppm; NO_2, 1.9 ppm). This can be due to:

- The low concentration of HCN and NH_3 formed during the thermal degradation process of PPUF.

- The fact that HCN and NH_3 react rapidly to form NO [144][145]. They are intermediary compounds formed and decomposition front that are reduced before their arrival to the FTIR measurement cell.

As shown in Figure 4-4, NO release increased during the first 25 s of combustion. At 25 s, the decomposition rate of foam was at its maximum and the mixture of gas products was fuel rich. This was a characteristic of the combustion of isocyanate and its higher volatility compared to polyol. After 25 s, the NO production steadily decreased and at 75 s, it was almost negligible. This suggested that all of the nitrogen contained in the isocyanate was released during the first stage. NO is formed during the first stage of combusion (peak of HRR), later it decreases. This result is in accordance with the mechanism presented: NO is released by the decomposition of PPUF to release isocyanate and its succesive pyrolysis. NO is oxydizated in the flame front and is reduced mainly into diatomic nitrogen [145][146][147].

Near 28 s, the release of CO was at its maximum. At the same time, H_2O release was increasing. With increasing time, the former decreased and the later increased. This suggests that polyol began to react before the end of the isocyanate release. Thus, the combustions of polyol and isocyanate are not completely separated in time. The

chemical analyses showed that the PPUF mass fractions of isocyanate and polyol were approximately 32% and 68%, respectively. Therefore, in the first 28 s, the majority of the mass loss would correspond to the decomposition of the isocyanate (32%), with most of the remaining mass corresponding to the polyol (68%) that decomposes later.

From Figure 4-5 until Figure 4-8 are presented the coupling of the thermal behaviour (HRR and MLR) of PPUF in CC with the kinetic of release of toxic gases at 10, 20, 30 and 40 $kW \cdot m^{-2}$.
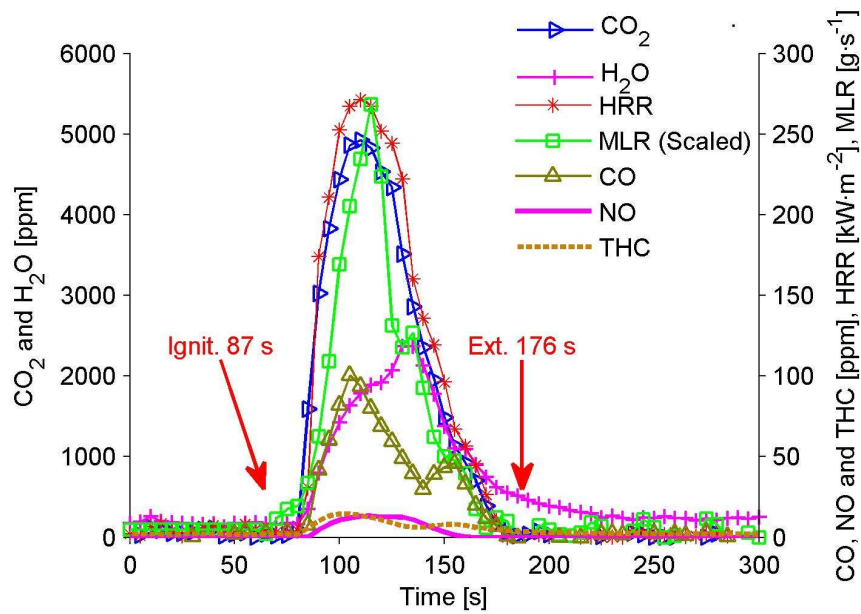
Figure 4-5 Change over time of HRR, MLR and gas species concentration during combustion of PPUF at an irradiance level of 10 kW·m^{-2} in CC. CO_2 and H_2O are quantified at the left-hand side y-axis. CO, NO, THC, HRR and MLR are quantified at the right-hand side y-axis. The MLR curve is scaled by a factor of 2000 (Source [138]).
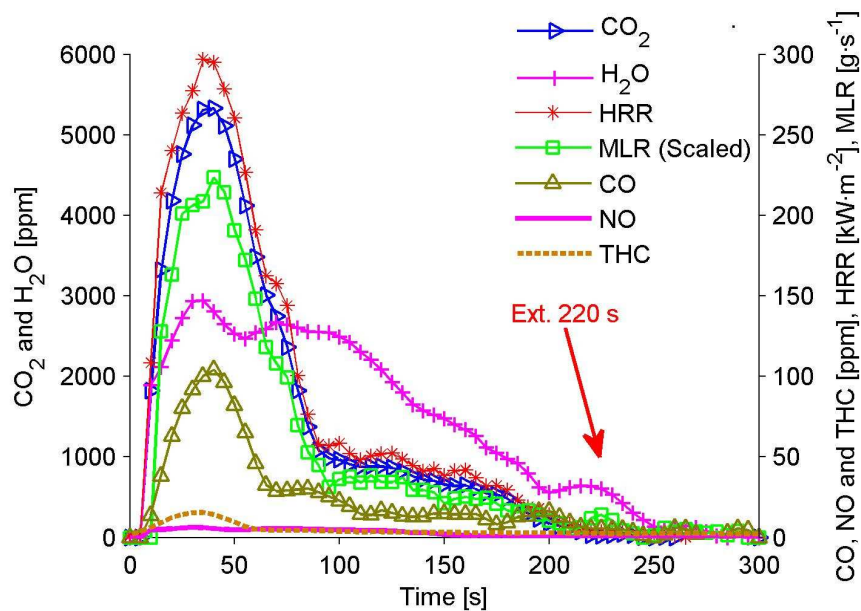
Figure 4-6 Change over time of HRR, MLR and gas species concentration during combustion of PPUF at an irradiance level of 20 kW·m^{-2} in CC. CO_2 and H_2O are quantified at the left-hand side y-axis. CO, NO, THC, HRR and MLR are quantified at the right-hand side y-axis. The MLR curve is scaled by a factor of 2000
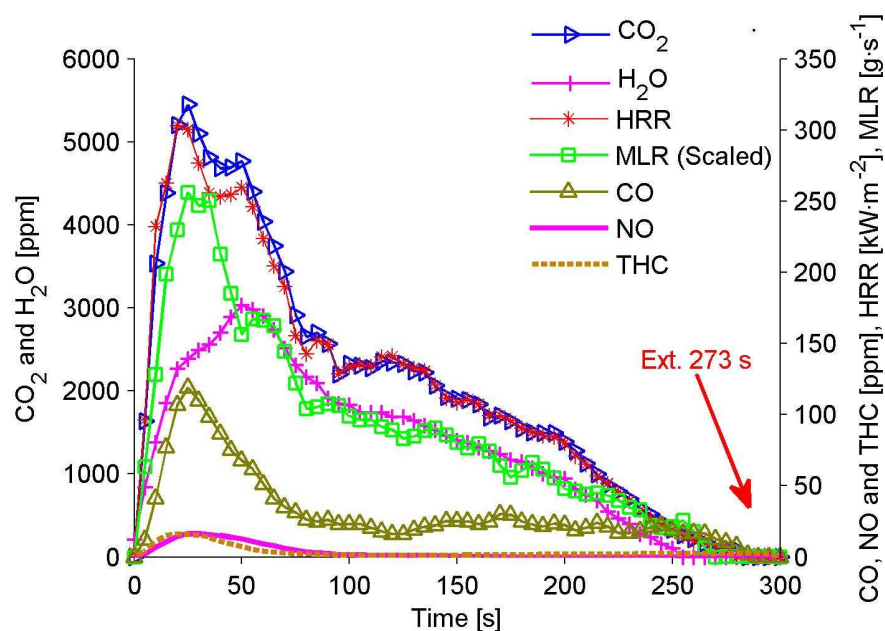
Figure 4-7 Change over time of HRR, MLR and gas species concentration during combustion of PPUF at an irradiance level of 30 kW·m^{-2} in CC. CO_2 and H_2O are quantified at the left-hand side y-axis. CO, NO, THC, HRR and MLR are quantified at the right-hand side y-axis. The MLR curve is scaled by a factor of 2000
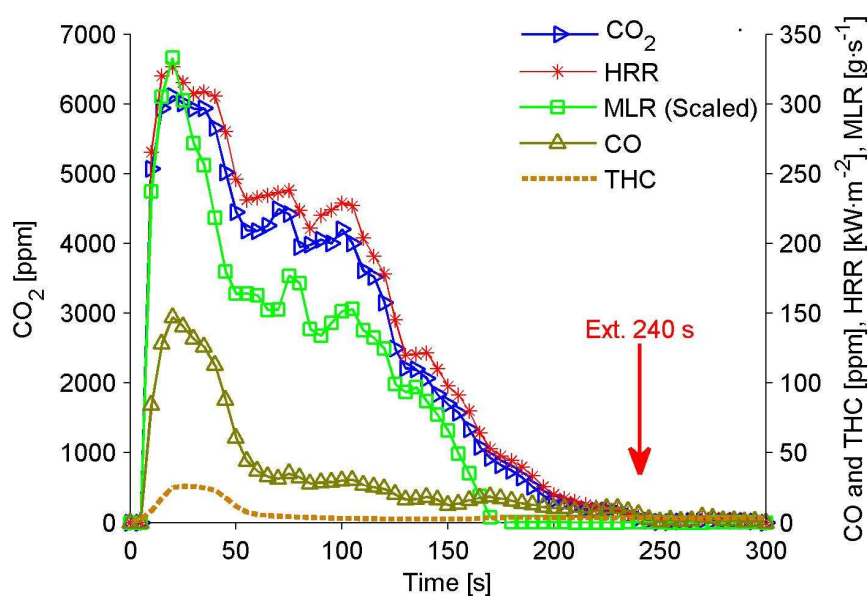
Figure 4-8 Change over time of HRR, MLR and gas species concentration during combustion of PPUF at an irradiance level of 40 kW·m^{-2} in CC. CO_2 is quantified at the left-hand side y-axis. CO, THC, HRR and MLR are quantified at the right-hand side y-axis. The MLR curve is scaled by a factor of 2000. At this irradiance level the plots of H_2O and NO are not available.

Figure 4-5 presents HRR, MLR and the concentration of the main gases released on CC at an irradiance level of 10 kW·m^{-2}. As in Figure 4-3, the initial time corresponds to initial exposure at the desired irradiance level. The difference in curve shapes between 10 and 50 kW·m^{-2} allowed us to extract a divergence in gas release: the maximum concentration of H_2O release for an irradiance of 10 kW·m^{-2} occurred at 140 s. This corresponded to an inflection point of HRR (in addition to the single peak in the HRR curve), the second peak of MLR, a local minimum of CO and the beginning of the decrease in NO release. Any further decomposition stages could be clearly identified at this irradiance level.

The thermal mechanism for PPUF decomposition analysed in this work was validated for the five irradiance levels studied (see Figure 4-4 until Figure 4-8). The validation was allowed by the coupling of the information from the gas phase to the one of the solid phase. The decomposition mechanism in CC under well-ventilated condition can be schematized as follows (see Figure 4-9).
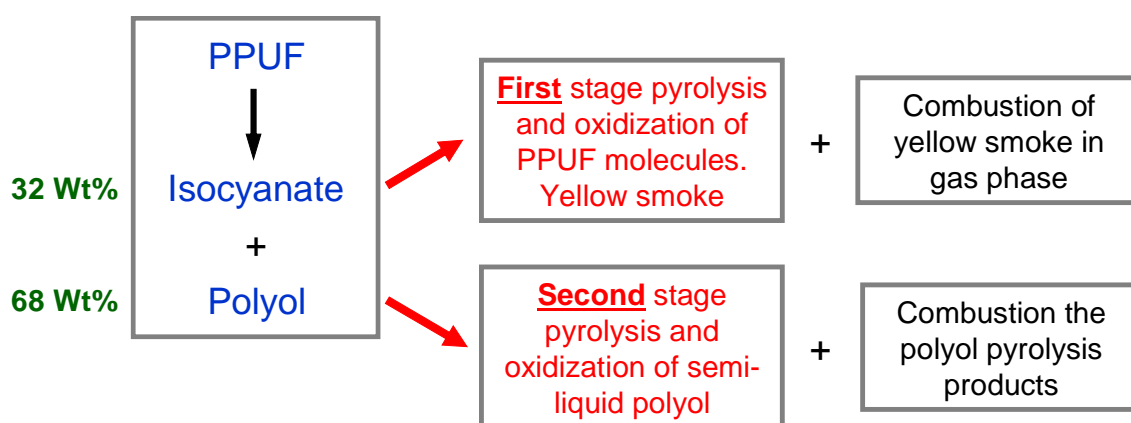
Figure 4-9 Schematic view of the PPUF decomposition mechanism observed in cone calorimeter at five irradiance levels 10, 20, 30, 40 and 50 kW·m^{-2} (Source [148]).

As a matter of fact, during the first decomposition stage, so the first peak of MLR the analysis of gaseous compounds released show the formation of hydrocarbon compounds, CO, CO_2 and NO that are produced during the molecules break-down process and the pyrolysis of isocyante.

Lately, during the second peak of MLR only the compounds containing carbon (particularly CO and CO_2) and water are formed, which is characteristic of the decomposition and combustion of polyol.

For comparison purposes, the kinetic mechanism determined at the matter scale is remembered here bellow.
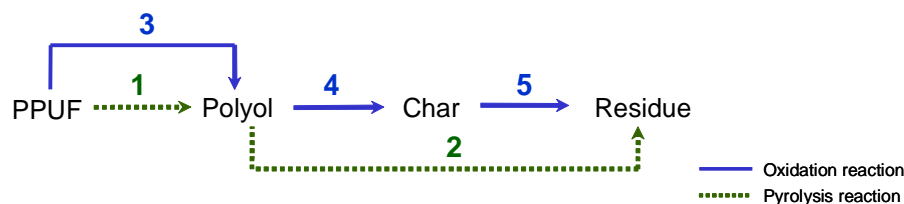
Reminder of Figure 3-3 Kinetic mechanism 1 proposed in this research.

The results of CC coupled to gas analysis (Figure 4-9) are in agreement with the decomposition patterns identified at the matter scale using $TF + FTIR_{qnt}$ and $TGA + FTIR_{qlt}$: when the material is heated up, the urethane bounds breakdown by pyrolysis and oxidization reactions, arrows 1 and 3 respectively. It releases as gas product the isocyanate and remains as condensed residue the polyol. It is reminded that the molecules breakdown occurs into the decomposition front which is thin and displaces from the top towards the bottom of the sample holder. The polyol is more thermally stable than isocyanate and than polyurethane molecules, so the irradiance level produced by the electric heater and the flame preferentially decomposes the urethane bounds and with the polyol remaining as a semi-liquid product. This explains for example, why the nitrogenated compounds are released in the first decomposition stage (see Figure 4-4).

The reactions represented by the arrows 2, 4 and 5 occurs mainly when the polyol is condensed at the bottom of the sample holder. Nevertheless as explained, due to the high incident irradiance level to which the sample is submitted in the CC, these reactions cannot be completely separated in time. So, the reactions represented by the five arrows take place at the same time.

At all studied CC irradiance levels, the curves for HRR and CO_2 release have similar shapes. However, the correlation between these two values may be more complicated than the shapes suggest, since HRR was measured as a function of oxygen depletion under air. This proportion is highly influenced by characteristics of the material being burnt, such as high oxygen content in the molecular structure [149].

The volume of each mole of species, the mass-flow rate and the yield of species were calculated using Eq. (2-7) to Eq. (2-9). Figure 4-10 shows the results of mass flow of

the main gases released during PPUF combustion (CO_2, CO, NO and THC), for easy of view only the results of three irradiance levels are presented.
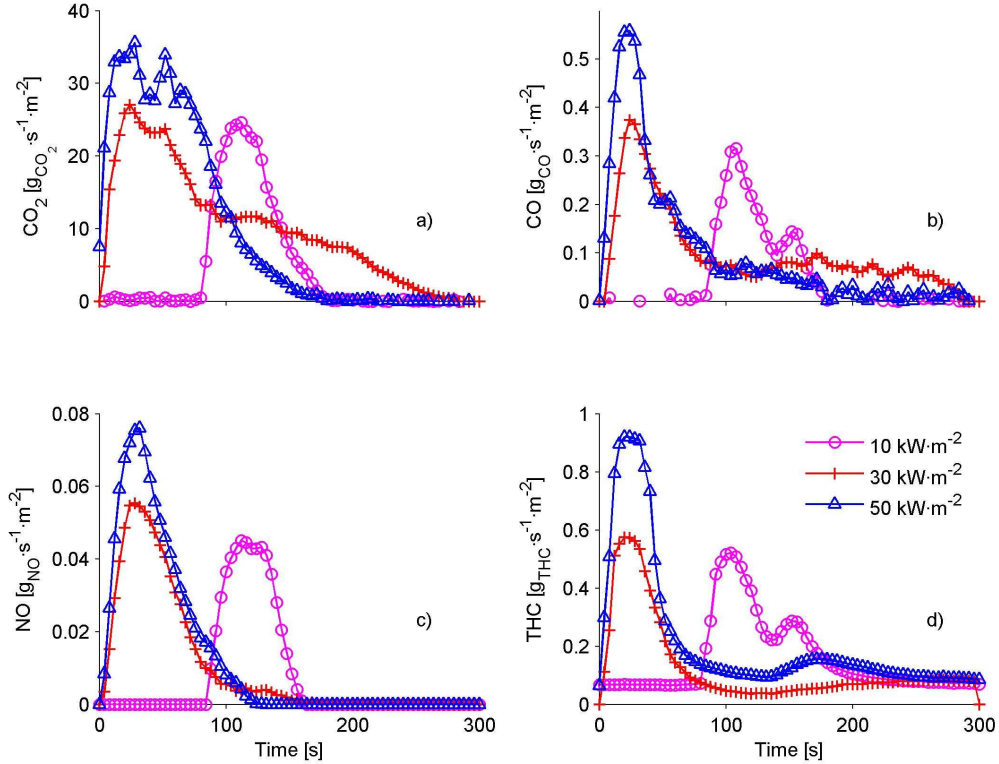
Figure 4-10 Evolution of mass flow of four gas species: a) CO_2, b) CO, c) NO and d) THC at three irradiance levels 10, 30 and 50 kW·m^{-2}.

The mass flux of a gas species is calculated as the mass-flow rate divided by the area of the solid sample ($\dot{m}_b'' = \dot{m}_b / A_r$). The area of the sample exposed to the irradiance level in CC is equal to 0.0088 m^2. Figure 4-10 shows the mass flux for four principal gas species CO_2, CO, NO and THC, at three irradiance levels 10, 30 and 50 kW·m^{-2}. The mass flux at 20 and 40 kW·m^{-2} are not shown for easy of view of the plots. These curves confirmed that the toxicity of the gases released during PPUF combustion changed with time. The maximum toxicity of the gas release stream occurred in the first 150 s of the fire. However, the single composition of the gas stream does not constitute enough information to stablish the toxicity hazard of the effluents because it depends of the properties of the material in fire, ventilation, dilution, exposition time, environment, etc [150].

The mass flux of total hydrocarbons (Figure 4-10-d) allowed us to conclude that at all irradiance levels, THC release rose steeply between 2 and 4 s prior to ignition. This would explain the presence of a volatile combustible mixture at the surface of the sample prior to ignition. The results in Figure 4-10 also allowed for the calculation of total gas compounds released, given in Table 4-2. The results presented in Table 4-2 are normalized by unit of burning surface allowing the comparison with experiments of different burning surface.

Table 4-2 Experimental results of PPUF in CC measured at five irradiance levels: total heat, CO_2 and CO released during a test. The results are normalized by unit of area.

Irradiance level of CC	Total heat released	Total CO_2 released	Total CO released
[kW·m^{-2}]	[GJ·m^{-2}]	[g$_{CO2}$·m^{-2}]	[g$_{CO}$·m^{-2}]
10	15.0	1310	13.8
20	21.3	1855	21.6
30	34.6	3028	29.5
40	35.7	3230	28.6
50	32.9	3029	29.9

Table 4-2 presents total heat, CO_2 and CO released during the full time of sample exposure at five different CC irradiance levels in well-ventilated condition. The maximum of total heat and CO_2 release occurred at an irradiance level of 40 kW·m^{-2}, while the maximum CO release occurred under an irradiance of 50 kW·m^{-2}. The different occurrences of these maxima may be explained by analysing the MLR and HRR (see Figure 4-3). The irradiance level in the CC exerted a strong influence on the decomposition rate of the semi-liquid polyol. With increasing irradiance level, the decomposition rate of the semi-liquid increased significantly (second stage). However, with increasing irradiance level, the rate of the breakdown of PPUF molecules and combustion of isocyanate does not vary in the same proportion (first stage). The speed of movement of the decomposition front from top to bottom of the foam slab was not highly different between the different irradiance levels. This explains the fact that the second peak (or inflection) in the HRR curves changed more significantly than the intensity of the first peak with increasing irradiance. The polyol pool fire released a non-negligible amount of energy, which was controlled by thermal balance and heat of gasification of the semi-liquid product.

The higher decomposition rate induced with the increase of the irradiance level is also responsible for the increase of total CO release (maximum at 50 kW·m^{-2}): The rate of

production of pyrolysed products is higher than that rate of transport of oxygen towards the flame. Thus, a fuel rich combustion regime is stablished promoting the formation of CO rather than CO_2. It is pointed out that the ventilation condition is remained constant for all the experiments, the difference in the combustion regimes is created by the pyrolysis rate established in function of the total irradiance level generated by the external source and the flame (see Eq. (4-4)).

Table 4-3 Yield of the main gas species released during PPUF combustion in well-ventilated condition. The column "mean" is the release of species in the semi-steady state period. "St Dev." is the standard deviation of the species releasing in the semi-steady state zone.

Irradiance level of CC [kW·m^{-2}]	Yield of chemical compounds [$g_{especies} \cdot g_{sample}^{-1}$]										CO/CO$_2$
	CO$_2$		H$_2$O		CO		NO		THC		
	Mean	St. Dev.	Mean	St. Dev.	Mean	St. Dev.	Mean	St. Dev.	Mean	St. Dev.	[%]
10	2.69	1.06	0.92	0.95	0.036	0.023	0.003	0.002	0.104	0.117	1.34%
20	2.17	0.24	1.54	0.74	0.029	0.012	0.004	0.003	0.062	0.028	1.32%
30	2.15	0.21	0.61	0.11	0.018	0.005	0.002	0.002	0.018	0.011	0.85%
40	2.32	0.39	-	-	0.016	0.007	-	-	0.028	0.018	0.68%
50	2.31	0.69	0.78	0.46	0.019	0.009	0.003	0.002	0.032	0.019	0.82%
Mean	2.33	0.52	0.96	0.57	0.024	0.011	0.003	0.002	0.049	0.039	1.01%

Table 4-3 gives yields of the main gas species released during PPUF combustion. Yields measured in experiments can be the basis for extrapolating results of gas species production from bench-scale to full-scale scenarios [20]. Yields have been calculated for the steady-state regime. The transient periods at the beginning and end of tests were not considered for calculations. Yields of CO_2, H_2O and THC were at their lowest at an irradiance level of 30 kW·m^{-2}, with the lowest yield of CO at 40 kW·m^{-2}. There was no clear dependence of NO yield on irradiance level. However, accounting for the calculated standard deviations, only CO_2 yield measurements are of high consistency. The very limited amount of data found in the literature on the gas product yields of polyurethane foam is listed in Table 4-4. Note that the polyurethane formulations significantly differ from one type of foam to another.

Table 4-4 Data in the literature [151][152][153] on yields of gas species released from polyurethane formulations in CC at various irradiances levels.

| Irradiance level of CC [kW·m^{-2}] | Yield [g$_{especies}$·g$_{sample}^{-1}$] | | |
	CO_2 Mean	CO Mean	NO Mean
10	0.37[b,c]	0.001[b,c]	-
20	3.05[b]	0.065[b,c]	-
30	2.59[b]	0.055[b,d]	-
35	2.43[a]	0.014[a]	0.011[a]
	1.26[e]	0.037[e]	-
40	2.62[b]	0.058[b]	-
50	2.72[b]	0.059[b]	-

[a] Source Hertzberg *et al.* [151] A yield of 0.0015 g$_{HCN}$·g$_{sample}^{-1}$ is also reported

[b] Source Kotresh *et al.* [152]

[c] Authors reported non-ignition at 10 kW·m^{-2}

[d] This value replaces the data of table 2 that must contains a typographical mistake

[e] Source Fabian *et al*. [153] Mean of results of two tests with matress polyurethane foam

As seen in Table 4-4, yields of CO_2 and CO measured in this work are in the same order of magnitude as those found by other authors [151][152][153]. A significant difference is found in the CO_2 yield for an irradiance level of 10 kW·m^{-2}, as Kotresh *et al.* [152] reported non-ignition of the polyurethane sample. Only one data point was found for NO yield [151], which is 5.5 times larger than the value found in current tests. Also, Hertzberg *et al.* [151] reported an HCN yield of 0.0015 g$_{HCN}$·g$_{sample}^{-1}$. We did not detect HCN in our research, which suggests a possible difference between the two test conditions in either the ventilation conditions or composition of the virgin foam; it has been observed that the length of the main chains of the urethane molecules can produce a huge difference in the fire behaviour. Hertzberg *et al.* [151] measured soot production with a low-pressure impactor, reporting a yield close to 2.5 mg·g$_{sample}^{-1}$ at an irradiance level of 35 kW·m^{-2}. This soot yield is small compared to the CO_2 yield of 2.43 g·g$_{sample}^{-1}$ measured by the same study [151]. Kotresh *et al.* [152] calculated a ratio between CO and CO_2 mass flows near 2%, while our experiments give a ratio of 1% for all the irradiance levels (see column CO/CO_2 of Table 4-3).

In Table 4-5 is established the carbon balance of the combustion process, so the carbon content in the burnt fraction of virgin sample is compared with the carbon content of the gas effluents, the difference is soot.

Table 4-5 Carbon balance between the burnt fraction of virgin PPUF (determined by elementary analysis) and the gas emissions (measured by gas analysis) for five irradiance levels. The mass of soot is calculated as the difference between the mass of carbon in the burnt PPUF and the mass of carbon contained in the gas products.

Irradiance level of CC [kW·m^{-2}]	Carbon balance [g]				
	Burned	Gaseous products			Difference
	PPUF	CO_2	CO	THC	Soot
10	3.58	3.16	0.033	0.016	0.371
20	4.87	4.47	0.052	0.016	0.332
30	7.71	7.30	0.071	0.013	0.326
40	7.99	7.79	0.069	0.021	0.110
50	7.43	7.31	0.072	0.022	0.026

During the burning process, the carbon initially present in the PPUF is converted into gas carbon oxides, THC and soot. Table 4-5 shows the carbon balance between the burnt fraction of solid PPUF (from elementary analysis presented in Table 2-4) and carbon contained in the evolved gases. The total carbon content in a gas species is the molar fraction of carbon in the total mass released of one gas. The total mass released of each gas has been obtained integrating the mass flux calculated with Eq. (2-8). Soot production was not measured; thus the carbon in soot was taken as the difference of carbon in the burnt foam and carbon in the gas products. Without soot, the resulting carbon balance in gas products accounted for 90-99% of the total carbon contained in solid PPUF. This is a satisfactory result because solid and gas phases can be analysed together. Enlarged uncertainty of FTIR gas analysis was estimated at the LNE laboratory as being 3.6% in the range of the gas concentrations found.

Using the same methodology to the one used to establish the balance of carbon, calculations have also been conducted in order determine the balance of hydrogen and nitrogen present in the solid foam and into the gas products. It was found that H_2O accounts for the largest proportion of hydrogen present in the virgin PPUF. A very small proportion was found in THC. Unfortunately, The balance of nitrogen is less accurate than the one of carbon. NO is the only detectable compound containing nitrogen in the product gases. The nitrogen contained in the mass of NO released during the combustion process accounted for only between 2% and 3% of the total

nitrogen contained in the virgin sample. Two different hypotheses can explain this difference: a) nitrogen may be reduced into N_2, which is impossible to detect by the FTIR because it is a symmetric molecule (This is the most accepted hypothesis in PU combustion) and b) nitrogen did not only form NO, but reacted to form other nitrogenated compounds in very low concentrations that could not be measured in the conditions of dilution generated by cone calorimeter ventilation.
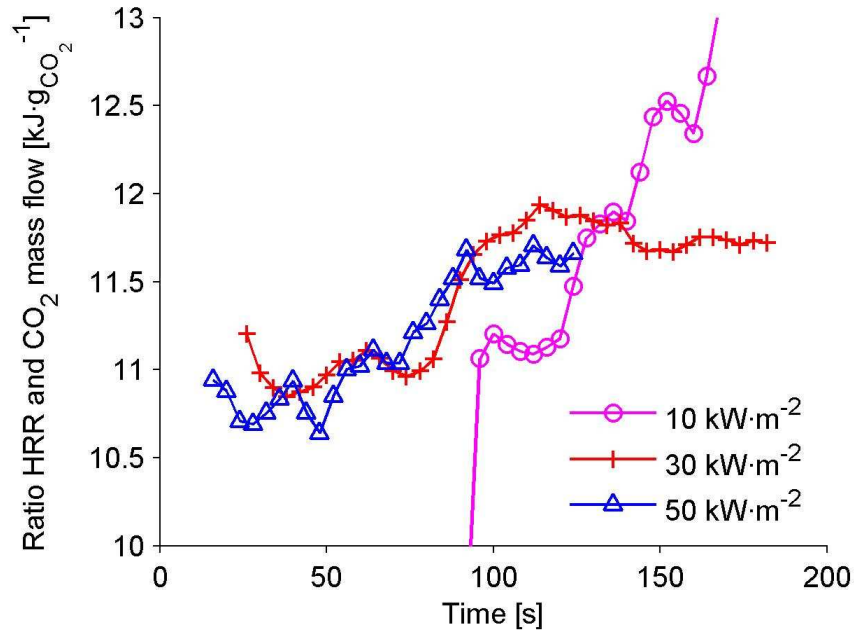
Figure 4-11 Ratio of HRR to CO_2 mass flow at three CC irradiance levels 10, 30 and 50 kW·m^{-2}.

Figure 4-11 shows curves representing the ratio between HRR and CO_2 mass flow at three cone calorimeter irradiance levels of 10, 30 and 50 kW·m^{-2}. This ratio expresses the equivalent quantity of released heat when 1 g of CO_2 was produced. For materials with single-stage decomposition kinetics (*e.g.* PMMA), the gas fuel molecules produced over the entire decomposition process are of the same nature and this ratio is therefore constant. During PPUF combustion, at least two different products were burning and each one released a different amount of heat and CO_2. The slopes, a_i, y-intercepts, b_i, and the least-squares fit factors, R_i^2, of straight lines that best fit the three curves in Figure 4-11 are, respectively, $a_{10} = 0.038$, $b_{10} = 6.6$, $R_{10}^2 = 0.87$; $a_{30} = 0.0068$, $b_{30} = 10.7$, $R_{30}^2 = 0.68$; $a_{50} = 0.011$, $b_{50} = 10.4$, $R_{50}^2 = 0.88$.
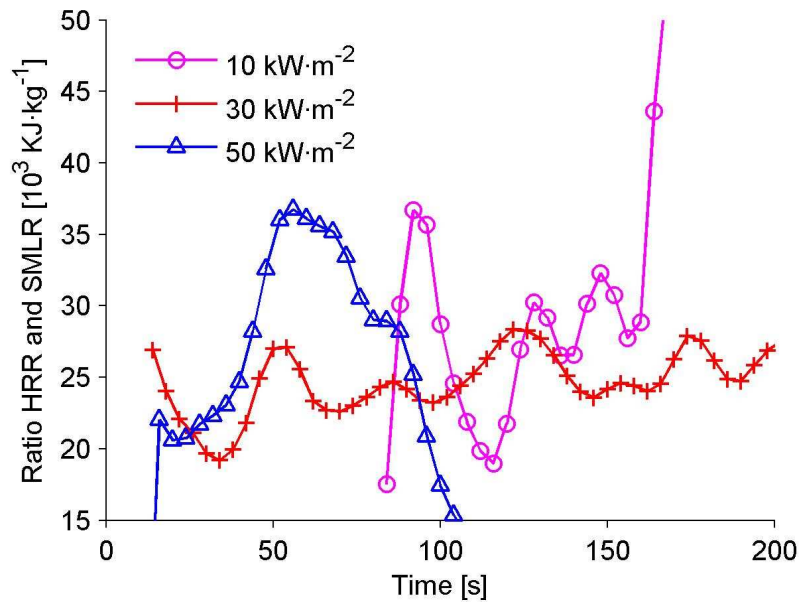
Figure 4-12 Ratio of HRR to SMLR (*i.e.* the EHC) for three irradiance levels 10, 30 and 50 kW·m^{-2}.

Figure 4-12 shows for three irradiance levels the ratio between HRR and Specific Mass-Loss Rate (SMLR), which is defined as the mass-loss rate by sample unit area. This ratio is equivalent to the Effective Heat of Combustion (EHC). In general, the EHC is seen to vary in time and also depends on the irradiance level with values ranging from 20 000 to 40 000 kJ·kg^{-1} with the average at 26 134 kJ·kg^{-1}. The mean and standard deviations for each irradiance level are calculated and presented in Table 4-6.

Table 4-6 Mean and standard deviation of the effective heat of combustion (EHC) measured at five irradiance levels.

Irradiance level of CC	EHC = HRR / SMLR	
	Mean	St. Dev.
[kW·m-2]	[kJ·kg^{-1}]	
10	26379	5443
20	25665	2743
30	24502	2577
40	25658	1698
50	28467	6061
Mean	26134	3704

As shown in Table 4-6, the highest EHC values are found at the extreme irradiance levels 10 and 50 kW·m^{-2}, but have standard deviations of up to 20.6% and 21.3% with respect to the mean value. For irradiance levels between 20 and 40 kW·m^{-2}, the standard deviations are between 6% and 10%.

Babrauskas and Grayson [20] reported an EHC value of 23 900 kJ·kg^{-1} for a polyurethane with the chemical formula $CH_{1.53}O_{0.27}N_{0.08}$ and with a molecular weight 20.63 g·mol^{-1} (for reference, the molecular weight of the foam used in our study is 19.10 g·mol^{-1}). Babrauskas and Grayson [20] also report a general range of EHC values between 26 100 and 31 600 kJ·kg^{-1} for a wide variety of flexible polyurethane foam formulations in the market. The EHC value for the material in this work is closer to the lower limit of the range reported by Babrauskas. Hirschler in Ref. [20], which presented HRR curves of non-fire retarded polyurethane foam at three cone calorimeter irradiance levels of 20, 40 and 70 kW·m^{-2}. Their respective maxima of heat release rates were near 290, 710 and 1 220 kW·m^{-2}, while in our research, irradiance levels of 20 and 40 kW·m^{-2} resulted in HRR maxima at 300 and 330 kW·m^{-2}. The shapes of the HRR curves found by Babrauskas and Grayson [20] were not the same as those found in this research. The author reported two peaks, with the intensity of the first lower than the second, while in our research, the first peak is always higher than the second. This means that even if the two foams had a similar density, the kinetics of solid decomposition differed probably because of the PU composition.

In conclusion, the analysis of gas release in cone calorimeter represents a main tool to identify the decomposition mechanism of polyurethane foam in any irradiance level. It also represents a new approach to the identification of the transient toxicity of the gaseous effluents with the advance of the combustion process. In the case of PPUF used, the first 50 s after ignition are critical because of the release of the most toxic compounds. It was also verified that fire behaviour of PPUF is extremely sensitive to the raw materials used during manufacture.

4.4 Numerical simulation of cone calorimeter results

The work performed at the matter and small scales aimed at acquiring experimental information on the decomposition mechanism of PPUF. This information represents the main input data to the codes that allow predicting the fire behaviour by calculated

pyrolysis. As we have already mentioned, an accurate prediction of the fire behaviour is crucial in FSE in order to enable performance-based design of buildings and structures.

The numerical simulations of fire are pyrolysis calculated and imposed HRR. The main difference between them is that in the former the HRR is predicted and in the later it is set as input data. The pyrolysis calculated simulations require as input data the kinetic parameters of the solid decomposition process. A discussion on the advantages and disadvantages of the pyrolysis calculated simulations in comparison to imposed HRR fire simulations is performed in section 5.4.

In this research, the CFD code used to simulate the fire behaviour is Fire Dynamics Simulator (FDS) V 5.3. FDS is an open-source software for computational fluid dynamics simulation of fire-driven fluid flows. FDS numerically solves a form of the Navier-Stokes equations appropriate for low-speed, thermally-driven flows with an emphasis on smoke and heat transport from fires [154]. The formulation of the equations and the numerical algorithm are contained in the FDS Technical Reference Guide [155].

The aim of this research is not to perform a huge description of how FDS V 5.3 operates. The reader can find this information in a number of thesis and papers such as [85][156][157][158][159][160]. In this chapter only the equations required to understand the problems treated are presented.

The cone calorimeter fire simulations have been performed using a virtual reconstitution of the real cone. All the geometrical characteristics have been reproduced as close as possible to those of the real cone. Three mesh sizes were defined: 1 800, 14 400 and 96 000 cells with respective calculation times near to 5 min, 3 days and one week. The three mesh sizes have been designed to study the sensitivity to the cell dimension; nevertheless, as shown above, the sensitivity to input parameters needs to be studied prior to taking into account the problem of grid size. Figure 4-13 presents a picture of the simulated cone with 1 800 mesh.
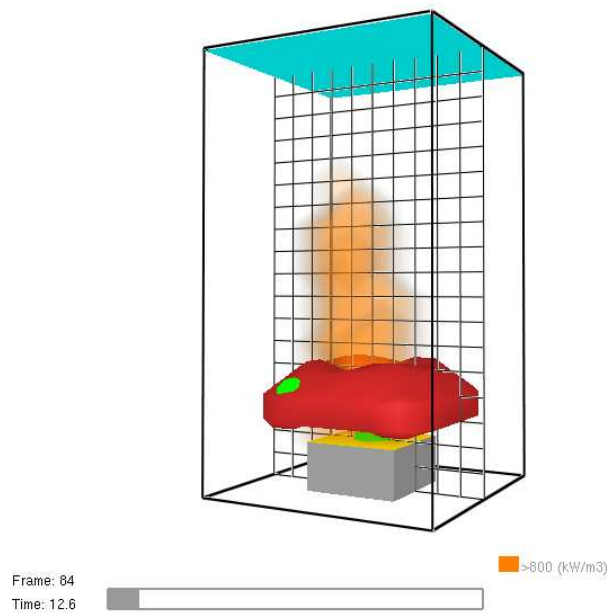
Figure 4-13 Virtual cone calorimeter, 1 800 mesh. The temperature imposed on the heater is 880 °C producing an irradiance level on t he surface of the material equal to 50 kW·m^{-2}

The centre of the following numerical study is to perform only calculated pyrolysis simulations (any set HRR simulation is carried out). The discussion concerns two objectives: a) to verify the ability to predict the CC results when the pyrolysis model is used (the kinetic parameters are specified), and b) to analyse the results when the thermal properties set are the ones find experimentally. These aspects need to be studied because very few fire simulations can be found in the literature in which pyrolysis models are used and some others use thermal properties that are extremely different to the experimental ones; a wide discussion about this is performed in section 5.4.

Providing correct input data to the fire simulation codes represent a main strategy to guarantee the reliability of the calculations. Very often, data from the publications cannot be used reliably because the solid fuels are not well characterised, so the material simulated and the one found in literature are not exactly the same. In this research, we wanted to find experimentally the thermal and kinetic properties, the input data provided to numerical simulations has a very good traceability.

The input data for the following simulations have been obtained with the experiments and calculations conducted in chapters 2 and 3, however in particular cases, different

input data are used in order to analyse the fitness of the calculations. The results of HRR obtained in CC presented in section 4.3, are used here to verify the fitting between the experiments and the calculations.

Four numerical simulations are discussed; the aim is to compare the results obtained when particular changes in the input data are carried out. The interest of each one of the following simulations can be summarized as follows:

- Case 1 compares the experimental and numerical results of HRR and MLR when the decomposition mechanism and the thermal parameters are those found in this research.

- Case 2 compares the experimental and numerical results of MLR when the parameters are changed by trial-and-error in order to better fit the CC measurements.

- Case 3 compares the experimental and numerical MLR when the reaction of char is erased from the kinetic mechanism. The residue represents around 1% of the initial mass.

- Case 4 compares the experimental and numerical MLR when the conductivity and the specific heat are not set as scalars but as vectors in function of temperature.

The philosophy of each case is largely detailed later in the chapter. The FDS code presented in Appendix D is the one that produced the result of the case 1 (see Figure 4-14). The thermal and kinetic properties used are listed In Table 4-7.

Table 4-7 Thermal and kinetic properties set to the fire simulation labelled case 1. The code of the simulation is presented in Appendix D.

Simulation	Material	Thermal properties					Kinetic prop.		Comments
		Conductivity $W \cdot m^{-1} \cdot K^{-1}$	Specific heat $kJ \cdot kg^{-1} \cdot K^{-1}$	Density $kg \cdot m^{-3}$	Heat of reactions $kJ \cdot kg^{-1}$		Residue yield $kg \cdot kg^{-1}$		
Case 1	PPUF	0.04	1.3	22	-318	1400	0.69	0.44	Residue is formed by the
Fig. 4-14	Polyol	0.8	2	800	-236	2000	0.1	0.45	pyrolysis of polyol and the
	Char	0.12	2.50	300	400	-	0.25	-	oxydation of char
	Residue	0.08	1.34	300	-		-	-	

The input data used for the FDS simulation of case 1 are the ones found in this research: The five-reactions decomposition mechanism was discussed in section 3.3 (see Figure 3-3). The kinetic parameters are the ones listed in Table 3-8. The thermal properties were the ones found at room temperature, in other words they are

considered as scalars and do not change with temperature. The heat of reaction was deduced using Figure 2-1 and the thermal capacity was set using the data from Figure 2-2 (see section 2.4). The results of the case 1 calculated pyrolysis FDS simulation is presented in Figure 4-14.
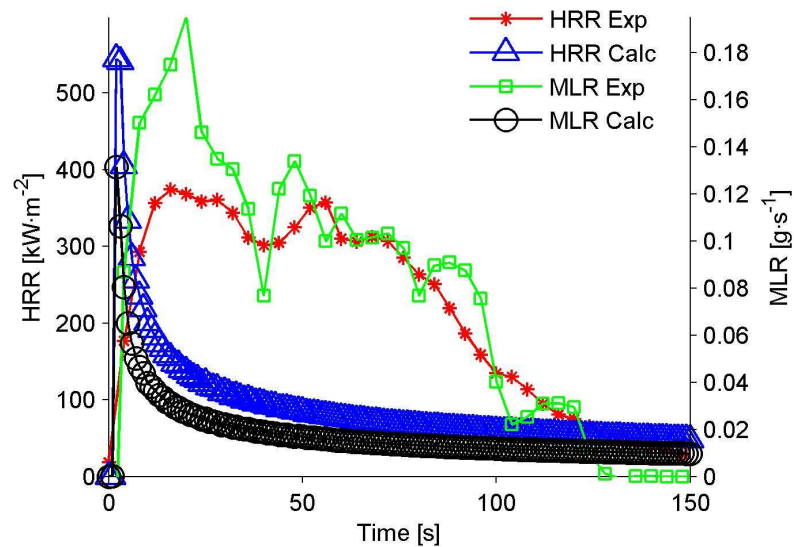
Figure 4-14 Case 1. Comparison of experimental and calculated results of HRR and MLR. Experiments: cone calorimeter at an irradiance level of 50 kW·m^{-2}. Calculations: FDS V.5.3, five-stages decomposition mechanism set to the pyrolysis model.

As shown in Figure 4-14, the intensity of the first peak of MLR is underestimated by 30% in comparison to the experiments. Moreover, the shape of the curve is not the same. The model is unable to predict the multiple peaks observed in the MLR and HRR curves: The decomposition stages do not seem to be succesive one after the other. The experimental peak of MLR found at $t \sim 20\,\mathrm{s}$ is produced by the process of virgin PPUF molecules break-down which is responsible as well of the displacement of the decomposition front. The pyrolysis model of FDS cannot simulate the displacement of the decomposition front, so the zone of MLR growing until $t \sim 20\,\mathrm{s}$ cannot be predicted accurately.

For the following comparison of results, only the experimental and calculated curves of MLR are presented. The HRR curves have the same shapes as the MLR ones because HRR is calculated as the product of the mass of combustible fuel released and the set heat of combustion. The heat of combustion is the energy released per unit

mass of fuel gas that mixes with oxygen and combusts; it was similar for all the solid species.

In order to obtain the results of case 2 presented in Figure 4-15, a few input data were changed with respect to case 1. For example, the thermal conductivity of PPUF in case 2 was set to 0.005 $W \cdot m^{-1} \cdot K^{-1}$ while in case 1 was 0.04 $W \cdot m^{-1} \cdot K^{-1}$. The specific heat in case 2 was 1.885 $kJ \cdot kg^{-1} \cdot K^{-1}$ while in case 1 was 1.3 $kJ \cdot kg^{-1} \cdot K^{-1}$. The same procedure was followed for the rest of the thermal and kinetic properties labelled "case 2" in Table 4-8. Appart to the properties listed in Table 4-8 the code was remained unchanged.

Table 4-8 Thermal and kinetic properties that were modified with respect to case 1 to obtain the simulations of case 2, 3 and 4. The code used during the simulations is presented in Appendix D in which the listed thermal properties were changed.

Simulation	Material	Thermal properties					Kinetic prop.		Comments
		Conductivity	Specific heat	Density	Heat of reactions		Residue yield		
		$W \cdot m^{-1} \cdot K^{-1}$	$kJ \cdot kg^{-1} \cdot K^{-1}$	$kg \cdot m^{-3}$	$kJ \cdot kg^{-1}$		$kg \cdot kg^{-1}$		
Case 2	PPUF	0.005	1.885	22	550	-850	0.69	0.44	Residue is formed by the
Fig. 4-15	Polyol	0.8	1.885	820	236	-1297	0.1	0.45	pyrolysis of polyol and the
	Char	0.8	1.34	820	-1297	-	0.25	-	oxydation of char
	Residue	0.08	1.34	820	-	-	-	-	
Case 3	PPUF	0.04	1.3	22	-318	1400	0.69	0.44	The pyrolysis of polyol (Reac. 2)
Fig. 4-16	Polyol	0.8	2	800	-236	2000	0	0.45	and the oxydation of char (Reac.
	Char	0.12	2.50	300	400	-	0	-	3) does not produce solid
	Residue	0.08	1.34	300	-	-	-	-	residue
Case 4	PPUF	0.045…0.084	1.885…2.469	22	-318	1400	0.69	0.44	The pyrolysis of polyol and
Fig. 4-17	Polyol	0.045…0.084	2	800	-236	2000	0	0.45	oxydation of char do not produce
	Char	0.12	1.337…1.784	300	400	-	0	-	solid residue. Thermal prop. In
	Residue	0.08	1.34	300	-	-	-	-	function of Temp.

The thermal properties used for the simulation (case 2) presented in Figure 4-15 are not the ones found in this research. They were set by trial-and-error in order to improve the fitness of the calculations with respect to the experiments. Around 300 simulations were developed in which the input parameters were changed as "potentiometers". So, the input data allowed a better fitness of the curves but they do not have physical meaning according to the material studied.

Figure 4-15 Case 2.Comparison of cone calorimeter experimental and calculated results. Five reactions decomposition mechanism. Thermal and kinetic parameters set in order to improve the fitness between the experimental and calculated curves.

It is highlighted that Figure 4-15, is obtained by increasing the yields of polyol residue by 10 times: it is 0.01 kg·kg^{-1} in case 1 and it is 0.1 kg·kg^{-1} in case 2. The char residue has been changed as well, from 0 kg·kg^{-1}. in case 1 to 0.25 kg·kg^{-1} in case 2. The negative heat of reactions means that the reactions are endothermic, which is the case for pyrolysis reactions[3].

As can be seen in Figure 4-15 (case 2), the change of thermal and kinetic properties of the solid species with respect to case 1 produced a MLR peak three times greater than the experimental one. Moreover, the numerical peak is located 20 s earlier. This simulation allowed reproducing the phase of MLR decay observed at time $t > 20\,s$. However, the shape of the calculation is very noisy, making it difficult to get the bulk behaviour of the curve. In general terms, the calculations do not follow the experimental shape.

At an irradiance level as high as 50 kW·m^{-2}, the mass of the residue remaining in the sample holder was lower than 2%. In FDS simulations, it was observed that properties

---

[3] In FDS simulations an endothermic reaction has a negative heat of reaction, while in the enthalpy measurements presented in subsection 2.4.1 (page 57) an endothermic reaction has a positive sign. This is due to the units of the enthalpy measurement.

of the residue in the sample holder have a very strong influence on the bulk MLR output. In other words, any change in the yield and properties of the very last residue strongly modify the shape of MLR, even if the mass is low. This is shown in the simulation labeled case 3 presented in Figure 4-16.
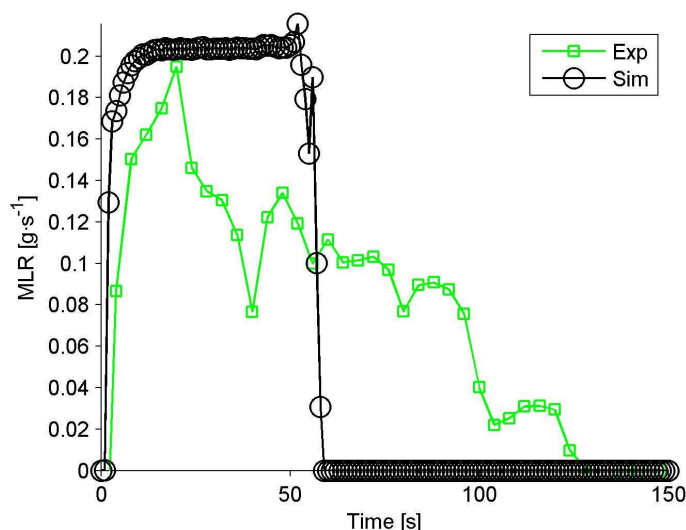
Figure 4-16 Case 3. Comparison of cone calorimeter experimental results. Five-reactions decomposition mechanism, three solid species entering into reaction. The yield of residue of pyrolysis (reaction 2) and the oxidation of char (reaction 5) have been set to 0 kg·kg⁻¹

The input data of the simulation presented in Figure 4-16 are listed in Table 4-8 in the row labeled case 3 where the yields of the residues remained by polyol and char have been set to 0 kg·kg⁻¹. It is highlighted that the only differences between the codes used for case 1 and case 3 are the yields.
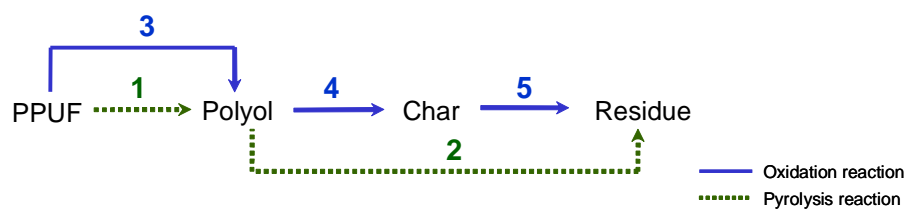
Reminder of Figure 3-3 Kinetic mechanism 1 proposed in this research.

According to the decomposition mechanism 1 presented in Figure 3-3, the solid species "residue" is formed by the pyrolysis of polyol (reaction 2) and the oxidation of char (reaction 5). The physical meaning of the simulation presented in case 3 is that reaction 2 and 3 produce gases but any solid residue. In other words, instead of four

species, only three enter into reaction. Eq. (3-35), which allows the calculation of total MLR at the matter scale modelling is transformed into Eq. (4-5).

$$\frac{dm}{dt} = (v_1 - 1)\dot{\omega}_1 - \dot{\omega}_2 + (v_3 - 1)\dot{\omega}_3 + (v_4 - 1)\dot{\omega}_4 - \dot{\omega}_5 \qquad (4\text{-}5)$$

The verification that this modifications do not change strongly the decomposition mechanism and the ability to predict the MLR at the matter scale is carried out: the modelling was run setting to zero the stoichiometric coefficients of the reactions 2 and 5, v_2 and v_5 respectively. The comparison of MLR experimental and calculated using the decomposition mechanism presented in Figure 3-3 with four and three solid species are presented in Figure 4-17.
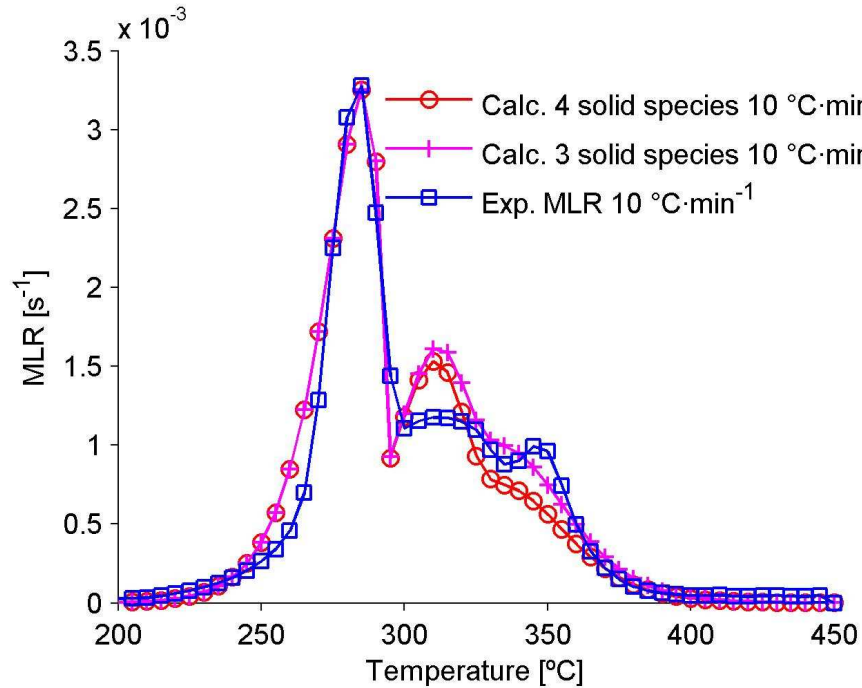
Figure 4-17 Comparison of MLR experimental and calculated with the decomposition mechanism stated in Figure 3-3 and with the modifications presented in case 3. Comparison at $\beta = 10$ °C·min^{-1}.

As presented in Figure 4-17, setting the stoichiometric coefficients v_2 and v_5 to zero, do not change strongly the prediction of MLR at the matter scale. Nevertheless, the shape of the FDS (small scale) simulations changes strongly. This is the sign of a great uncertainty about how the fire code interprets the input data of the pyrolysis model.

The comparison between Figure 4-15 and Figure 4-16 evidences a huge difference in the MLR shapes. The MLR shape of Figure 4-16 attains a level that is at the same observed experimentally and remains as a plateau for about 55s. After the "steady state" zone where the combustible matter is completely consumed at a constant rate, the MLR drops to zero and remains at this level until the end of the calculation time. The change of the decomposition mechanism seems to induce uncontrolled changes in the output of MLR while the mass of residue was negligible (*i.e.* in case 1 yield of polyol residue = 0.1 kg·kg^{-1}).

In this research, the thermal properties were measured in function of the temperature. The influence of setting variable thermal properties in function of temperature was also verified: To the case 3 presented in Figure 4-16 were included the variable thermal properties (see Table 4-8) releasing case 4. The MLR release is presented in Figure 4-18.
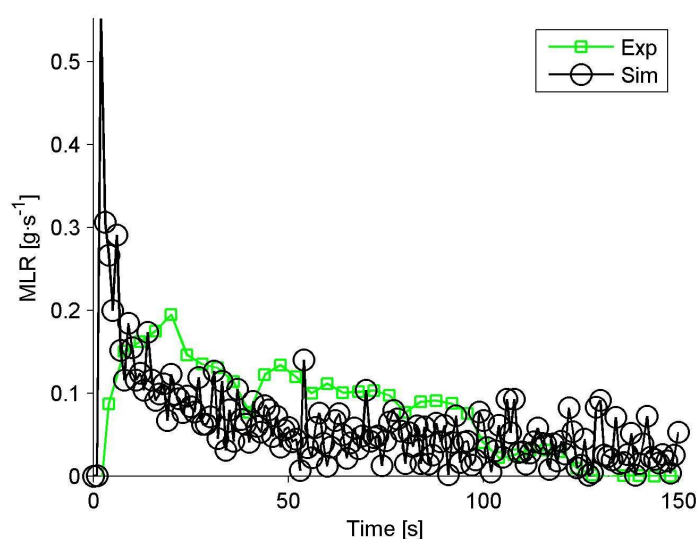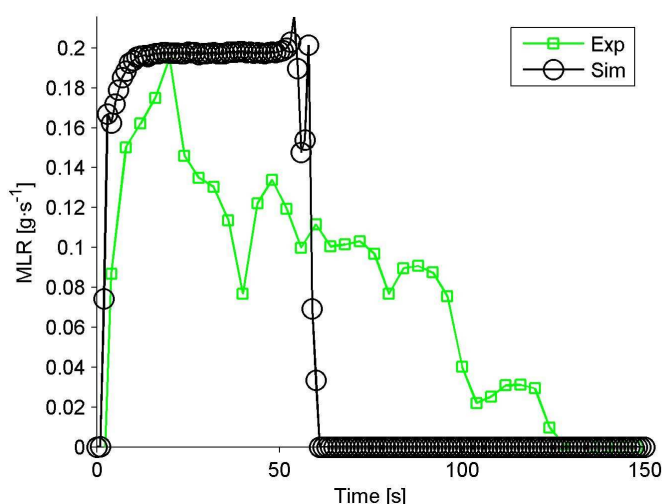

Figure 4-18 Case 4. Comparison of cone calorimeter experimental and calculated results. Five-reactions decomposition mechanism, three solid species entering into reaction. The thermal properties are expressed as a function of temperature.

Figure 4-16 and Figure 4-18 present exactly the same shape, the MLR level at which both plateaux are found is 0.2 g·s^{-1}. The influence of the thermal properties in this case is difficult to understand and does not seems to follow the trend observed in the comparison between cases 1 and 2.

Because of the lack of accuracy of the simulations in comparison to the experimental results, it is concluded that further researches are required in order to understand how

to use the pyrolysis model of FDS in the case of PPUF where the decomposition is multi-reaction. A huge discussion about the possible causes of the lack of accuracy is presented in section 5.4.

4.5 Fire behaviour of a simplified seat (product-scale)

Fire experiments were performed on a simplified seat. The aim of these experiments is to compare the decomposition mechanism at large scale with the one found at matter-scale. In this section, no simulations are presented because of the lack of accuracy found between the experiments and the calculations at the small-scale. Numerical prediction of the small-scale results constitutes the preliminary stage before the prediction of the product-scale tests. A huge understanding of the pyrolysis model is a prime requirement before considering simulations at a larger scale in which further phenomena need to be taken into account.

The layout of the seat is presented in Figure 4-19. The structure that supports the sample is the one used for assessing the ignitability of upholstered furniture as described in the standard NF D 60-013 [51]. In the seat and the back of the structure were placed a thermal insulating layer of calcium silicate 20 mm thick, an aluminum foil to avoid dripping and the polyurethane foam slabs. The two PPUF slabs were of the same dimensions 300x450x150 mm^3 and were of the same foam used throughout this research. The structure and the sample were located in a weighing device in order to determine the MLR.
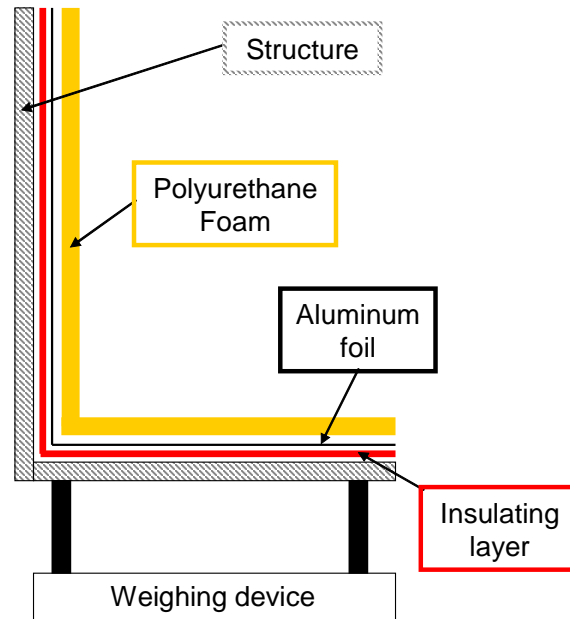
Figure 4-19 Layout of the simplified seat used to analyse the fire behaviour of PPUF in a real configuration (source [161]).

The ignition source to PPUF was a propane burner of 7 kW equivalent to a 100 g paper cushion burning. The burner is also described in the standards NF D 60-013 [51] and prCEN/TS 45545-1 [162], it was applied to the surface of the sample for 120 s and removed when that time was reached. The burner was located at the centre of the seat; gaps of 10 mm were left with the back (vertical surface) and the seat (horizontal surface) in order not to affect the mass measurement, see Figure 4-20. The curves of MLR and HRR as well as the visual characteristics of the burning solid are presented in Figure 4-20.
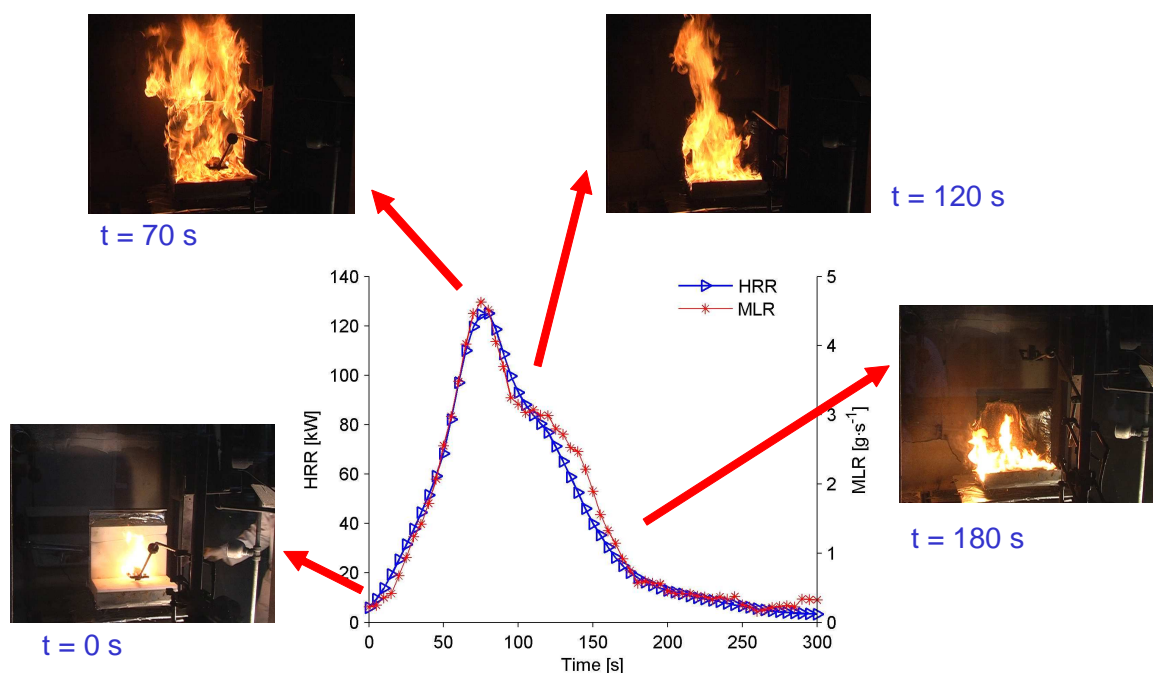
Figure 4-20 MLR and HRR measurements of a simplified seat (source [161]).

As can be seen in Figure 4-20, the visual characterisation of the fire and the solid behaviour (MLR) allows identifying two different combustion stages. The first one is comprised between ignition at $t = 0\,\text{s}$, until around $t = 120\,\text{s}$ with the maximum present at $t = 70\,\text{s}$. During this period, the fire propagates from the seat (where the ignition is induced) to the back. The HRR and MLR are increasing.

At $t = 70\,\text{s}$, the HRR and MLR are maximum; the entire sample is on fire. The PPUF is burning as a solid; nevertheless, a semi-liquid residue is formed. This semi-liquid drops by gravity onto the seat. The second stage of combustion is observed at $t = 120\,\text{s}$ and is produced by the burning of a different product than the one burning in the first stage. It is caused by the pyrolysis and oxidation of polyol that burns near a pool fire.

The evidence of the two stages of decomposition that were found while analysing the MLR and HRR is also supported by the yield of gases released during the combustion of the simplified seat presented in Figure 4-21. The gas measurements were carried out using the FTIR presented in section 2.5. The sampling was performed at the effluents evacuation duct before the fan see Ref. [51].
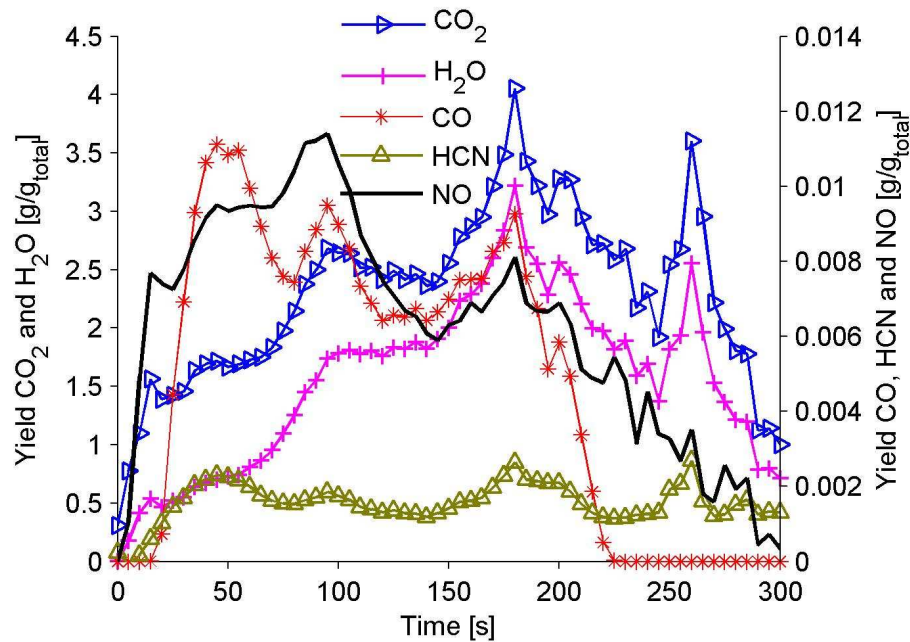
Figure 4-21 Yield of toxic gases during the combustion of a simplified seat
(Souce [161]).

As presented in Figure 4-21, the rate of gas release changes at $t = 120\,\mathrm{s}$, meaning a change in the combustion regime: The first stage is characterized by a higher production of NO and CO as well as the peak of HRR. The second stage is characterized by the higher yield of H_2O and a lower HRR. This behaviour of both, the solid and gas phases is similar to the one presented at the matter scale (see Figure 3-8) and at the small scale (see Figure 4-4).

The higher release of very toxic gases in the first 120 s of the combustion process, causes the first stage to be of higher hazard than the second one. Nevertheless, the second stage of decomposition also needs to be analysed because of the risk of fire spread by the dripping of combustible liquid in fire.

The results presented, allows accomplishing the first aim of the analysis at larger scale (simplified seat). Unfortunately, no fire simulations can be carried out in order to predict the fire behaviour of the product on fire. Our inability to reproduce the results found at the cone calorimeter scale in a satisfying manner prevents us from simulating fire experiments at a larger scale.

4.6 Conclusions

This chapter presented the study of the release of the main gas species produced during the combustion of a non-flame-retarded Polyether Polyurethane Foam (PPUF) of density of 20.9 kg·m^{-3} in the cone calorimeter apparatus. Five irradiance levels are studied: 10, 20, 30, 40 and 50 kW·m^{-2}. HRR, MLR, bulk gas mass flow and yields of gas species are measured. The numerical simulation of the CC experiments is also presented for an irradiance level of 50 kW·m^{-2}.

The analysis of the gas products was performed using FTIR, FID and ND-IR. It allowed studying the different stages in the kinetics and quantification of the gas composition. Of the seventeen different gas species that are monitored simultaneously, the main species found are CO_2, CO, H_2O, NO and THC. According to the species released, two decomposition stages are clearly identified. In the first stage, the solid structure breaks down triggering the decomposition of isocyanate, which is characterized by the detection of CO, NO and THC gases. The second stage involves the decomposition and combustion of polyol, which is characterized by the formation of H_2O.

The thermal mechanism for PPUF decomposition proposed in this work is valid for the five irradiance levels studied. The two stages observed are in agreement with the decomposition mechanism proposed in the literature [23][35][37] but the data presented here constitute, to the best knowledge of the authors, the first experimental study of the behaviour of burning PPUF taking also into account the release of gas species.

The yields of the major gases released during steady-state combustion are calculated. Results are compared with data available in the literature, showing very good correlation.

Foam characterisation is carried out by an elementary analysis of the matrix, with the raw chemical formula being $CH_{1.53}O_{0.27}N_{0.08}$. The chemical formula allows carbon, hydrogen and nitrogen to be balanced between burnt mass and gas products. Carbon and hydrogen balances are accurate, but the nitrogen balance is not, with only 3% of total nitrogen content in the solid foam accounted for in the gases.

The ratio between HRR and CO_2 releases was calculated. The EHC was not constant and depended on the irradiance level with an average value of 26 134 kJ·kg^{-1}. The EHC results correspond to the polyurethane the EHC values found in the literature. The ratio between HRR and CO_2 mass flow are calculated for each irradiance level in order to verify the mass of gas release per unit of power released.

Fire simulations were performed to predict the behaviour of the foam in cone calorimeter. The input data for the fire simulations were obtained by the experiments at the matter scale and the modelling of the thermal decomposition. The use of the decomposition mechanism found at the small scale (TGA experiments and modelling) as well as the thermal properties measured do not guarantee the adequate fitting between the experimental and the numerical results; the simulation results are not satisfactory. A great uncertainty exists on what input parameters must be provided to the FDS pyrolysis model and their corresponding physical meaning. Further works are required to improve the predictions.

Fire experiments were also performed at a larger scale. A simplified seat was burnt and the MLR, HRR and gas release was measured. It was verified that the decomposition mechanism remains unchanged with respect to the one observed in cone calorimeter. The verification of the decomposition mechanism was performed analysing the MLR and the kinetics of release of toxic gases. Nevertheless, our inability to numerically reproduce the experiments restrains our ability to predict the fire behaviour of a simplified product (seat).

5 Discussions

5.1 Discussions about the matter scale (TGA and TF) experiments

In chapter 2 the experimental results obtained at the matter scale are presented. They are based on the hypothesis that diffusion effects are avoided when analysing a small sample, and that the measurements reflect solely the thermal behaviour of the solid in thermal decomposition.

The information found in literature is generally related to the solid phase or to the gas phase. Very few information has been found combining both of them. One of the contributions of this work is a method to couple the information from the solid and the gas phases. To our knowledge, this is the first time that such analysis is carried out.

Data found in literature showed that the decomposition mechanism is usually determined by the model itself by means of the plot of energy of activation in function of the degree of conversion (E vs α). In this research, it was shown that the model did not allow determining unambiguously the decomposition mechanism, which must rather be determined analytically by studying the chemistry of the thermal processes.

However, the method to determine the decomposition mechanism based on the chemistry is not standard, huge analysis of the chemical reactions taking place need to be carried out. Also, the coupling of instruments using TGA + FTIR is relatively recent and has not been widely used in fire applications to find input data for the models. The coupling of these instruments represents a great opportunity to gain knowledge about the influence of temperature and oxygen mass fraction from atmosphere in the kinetics

of decomposition. Very few authors have discussed the influence of oxygen in the decomposition process and the ones who did were limited to two atmospheres: air (so oxygen mass fraction of 0.23) and nitrogen, but not vitiated condition (oxygen mass fraction between 0 and 0.23).

The quantitative analysis of gases was made possible by the comparison of the results obtained in TF + FTIR$_{qnt}$ and TGA + FTIR$_{qlt}$. The basis for the coupling of these experiments was the similar shapes of gas release obtained in both cases. It was shown that save for a few exceptions, the release was similar. The matter scale analyses have many advantages such as the homogeneity of the temperature, gas species and a precise determination of the decomposition mechanism. So, no boundary conditions and transfer problems need to be considered. Nevertheless, it provides limited information about the real behaviour of materials on fire.

The Biot number is the ratio between resistance to heat transfer due to conduction inside the solid and the resistance to heat transfer due to convection in the fluid, which allows defining whether a material behaves as thermally thick or thin [163]. It is mathematically expressed as $Bi = dh_c/k_s$. Where, d is the thickness, h_c is the convective heat transfer coefficient (15 W·m^{-2}·K^{-1}), k_s is the thermal conductivity (0.04 W·m^{-1}·K^{-1}). For the TGA samples[4], $d = 0.001\,\mathrm{m}$, and for TF samples $d = 0.012\,\mathrm{m}$, thus the respective Biot numbers are $Bi = 4.5$ and $Bi = 0.38$ respectively. The Biot number cannot be accurately applied to polyurethane foam. This index is defined for solid materials and the results for alveolar ones are not adequate. As a conclusion, the Biot number is not a criterion that can be used to compare the experimental facilities used in this research [163].

5.2 Discussion about the matter scale (TGA and TF) modelling

---

[4] This data is given only to bear on mind an order of magnitude. The TGA samples are considered as particles, so, the thickness is negligible.

The modelling of the behaviour of PPUF with the increase of temperature at various experimental conditions was investigated. The modelling is used together with genetic algorithms in order to calculate the kinetic parameters that control the reactions of the solid and gas phases.

In subsection 3.2.8 the problem of the physical meaning of the Arrhenius parameters has been discussed. Nevertheless, these kinetic parameters are used to describe the kinetics of macroscopic reactions, not the molecular processes that probably follow non-Arrhenius reaction rates (semi-mechanistic approach).

The Arrhenius kinetic parameters have been used for engineering purposes with good success. Nevertheless, the ability to use these variables for prediction purposes is limited. The kinetic parameters calculated are dependent of the model. So, the results from two different models are rarely comparable between them (*e.g.* from the literature). Moreover, until now, no relation has been found between the activation energy and the temperature of ignition [9]. The temperature of ignition of a material is not a physical-chemical constant of the system. It depends on the chemical construction, thermal conductivity, pressure, geometric characteristics, testing equipment, the environmental conditions, etc.

The kinetic parameters calculated using genetic algorithms made the prediction of the MLR in air and nitrogen possible, and the numerical process helped to improve the mechanistic comprehension of the decomposition patterns. In other words, a chemically correct decomposition mechanism was possible. The main experimental data to determine the mechanism in accordance with the chemistry of the process is TF + FTIR$_{qnt}$ and TGA + FTIR$_{qlt}$.

However, it was observed that a more intelligent strategy to set the evaluation function must be implemented. This strategy can be established based on the improvement of acceptability criteria. In other words, a calculated curve of MLR must be classified as acceptable or unacceptable according to engineering concepts. The acceptability of a numerical MLR curve must be defined based on its ability to reproduce the more critical characteristics of the experimental MLR, such as: the peak intensities, the number of peaks, the general shape of the curve, the position of the peaks, the slope of the growing phase, the time of decay, etc. Following the criteria that are defined as the prime ones, the evaluation function can be improved *i.e.* to use the function that best

reproduces the desired characteristic. It is important to bear in mind that the calculated Arrhenius parameters are also function of the evaluation function.

The heterogeneous chemical reactions taking place during the gasification of solids in the experimental facilities are not well known. Moreover, the reaction occurs in transient state because of the increase of the sample temperature that changes continuously the potential of chemical reactions. The engineering method used in this research to predict the toxic gases release seems to be a promising method. Verification of the results with various atmospheres is required to establish a cartography of the yield of toxic gases with multiple experimental conditions (oxygen mass fractions).

5.3 Discussion about the small scale (cone calorimeter) experiments

The comparison of experimental results at different scales represents a major issue because the phenomena observed are not the same. Also, the limitations and/or the possible influence of each experimental technique in the result must be understood. As an example, the main TGA and TF parameter is the temperature, while in CC it is the irradiance level, and these two cannot be compared.

The cone calorimeter tests comprise gradient effects of temperature and oxygen mass fraction at the surface and into the solid matrix that are not considered at the matter scale. These are conditions found in real fires that need to be simulated adequately, because they influence the kinetics of decomposition. Extrapolating the results of models and tests at bench scale to tests carried out at real scale, presumes that the mechanisms are invariable for the range of temperatures, heating rates and ventilation found in both cases [82].

In chapter 3 the experimental results performed in cone calorimeter were presented. It was observed that the decomposition front moves from the top towards the bottom of the sample slab. The hypothesis is that the decomposition zone is of constant thickness and fresh polymer replaces the decomposed polymer by surface

regression [28]. However, the movement of the decomposition front is influenced by the external irradiance level, the temperature gradients and the diffusion effects of oxygen (rate of heterogeneous reactions). It was shown that the effects of the combination of oxygen mass fraction and temperature are not well known. Currently, no adapted models exist to predict their influence on the fire behaviour of solids.

The models require as input data the properties of all the solids that are present at the different stages of decomposition. Some thermal properties such as conductivity, specific heat or others can be specified as function of temperature. Nevertheless, some experimental obstacles need to be overcome:

- The thermal properties of polymers can only be defined for a very precise range of temperatures. When the solid is heated, the decomposition processes produce the change of the solid matrix, making the measurements highly uncertain or even impossible. On the other hand, the fire simulation codes require input data over a very wide range of temperature, which cannot be obtained experimentally.

- Within numerical simulation, the influence of the thermal parameters on the output of the simulation is difficult to determine. The influence of the parameters needs to be also studied in terms of the shape of the property as a function of temperature, not only in terms of initial or final values.

The physical and chemical transformations of the solid need to be more closely studied in order to understand how the properties of the solid remaining in the sample holder change with the progress of the reaction. The knowledge of the role of the transformation in the kinetics of mass-loss rate and the kinetics of gas release also need to be improved. The alveolar nature of PPUF needs also to be taken into account while the diffusion of species inside the matrix and the heat transfer are modified with the collapse of the solid structure. The lack of knowledge of the boundary conditions (oxygen diffusion and temperature) largely limits the capacity to simulate the behaviour of the foam in cone calorimeter and in larges scales.

Pitts [164] carried out experiments at the NIST using a polyurethane foam similar to the one used in this research. The cone calorimeter was ISO 5660 and was used in non-piloted ignition condition. The exposed surface of the fuel bed was facing upwards. The samples were of the same density to the ones used in this research 22 kg·m^{-3} so the mass of the samples were 11 g. No fire retardants were used for the manufacture of

the foam. The sample of polyurethane was surrounded by an aluminium foil used as a folder during the cone experiments. The experimental results obtained at an irradiance level of 50 kW·m^{-2} are shown on Figure 5-1.
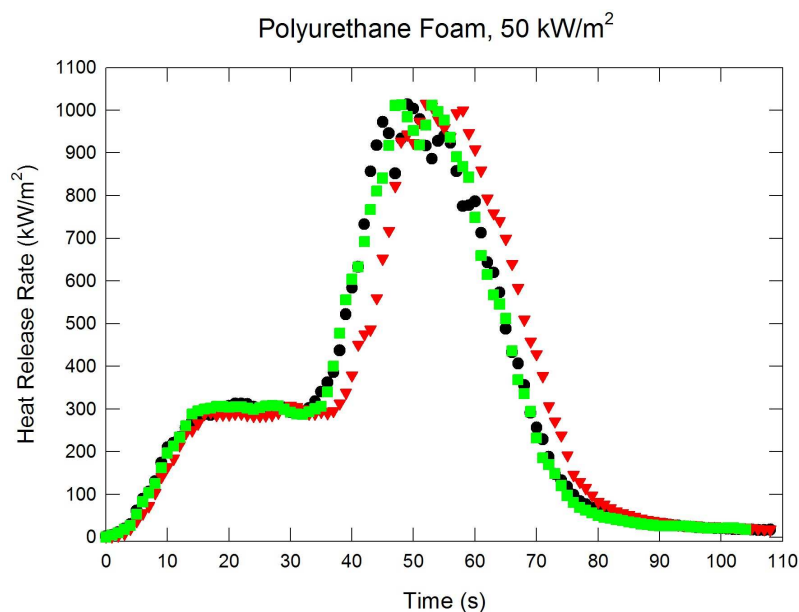
Figure 5-1 Experimental result of cone calorimeter experiments obtained with a foam of density 22 kg·m^{-3}. The irradiance level was 50 kW·m^{-2} imposed in horizontal configuration (Source [164]).

The shape of HRR obtained by Pitts [164] are very different to the one found in this research (see Figure 4-3). The two foams and experiments were similar, except that in the present research a cone calorimeter holder was used, while the NIST experiments were carried out using an aluminium foil as holder. The holder does not explain the great difference in the results.

As stated in chapter 2, the formulations of polyurethanes can be very different. Various raw polyols and isocyanates can be used to produce polyurethanes with similar physical properties [24]. Nevertheless, the fire behaviour of the product depends on the properties of the raw molecules during the first stage of decomposition (reported in literature and found in this research), which is the break-down the PPUF molecules to release isocyanate as a gas and polyol as a condensed phase residue. As a conclusion, chemical analysis of the structure of the material needs to be carried out in order to understand their behaviour to fire.

218

5.4 Discussions about the small scale (cone calorimeter) simulations

The experimental results obtained in CC are compared to numerical simulations in order to identify the ability to predict the fire behaviour of solids. The numerical study is carried out with the most widespread CFD code used for fire simulation: FDS V 5.3.0. This code can be used in two modes: The largest one is used by setting the HRR as a function of time. Thus, the power released constitutes an input data that must be determined experimentally. The great disadvantage of this method is that a new measurement of HRR must be carried out with every burning element and every possible configuration of the room or fire scenario. This approach requires the classification and rating of the fire scenarios according to the risks that they can produce. The rating can only be done by fire experts based on their knowledge in fluid mechanics, chemistry, propagation, heat transfer, etc.

The second mode of the CFD code is the "pyrolysis calculated fire simulations", meaning that the process of thermal decomposition of the solid fuel (MLR and HRR) is predicted using set kinetic parameters. This method has been included to FDS recently and has not been used by many authors, particularly in multi-reaction cases. The main advantage of the pyrolysis calculated simulations is a better knowledge of the requirements of the process of thermal decomposition and the possibility to predict the fire behaviour in multiple configurations. As a consequence, less large-scale tests are needed, which considerably reduces experimental costs.

The main input of the pyrolysis calculated fire simulations can be classified into two groups: a) thermal properties, and b) decomposition mechanism and the respective kinetic parameters. In this research, these input parameters were presented in section 2.4 and section 3.3 respectively.

As presented in section 4.4, the simulations results did not make it possible to reproduce the experiments in a satisfying manner. Instabilities and results not in agreement with the physics are often observed. The lack of accuracy can be due to many causes. Some of the possible causes are discussed here; nevertheless, the aim of this research is not to evaluate their relevance. Understanding the influence of the

inaccuracy of the results of calculations is the key to improve the models of fire behaviour.

Written in a simplified manner and using the notation of this dissertation, the FDS reaction rates are calculated with Eq. (5-1). The Eq (3-27) used for the modelling work carried out in this research is also reminded.

$$\dot{\omega}_i = \left(\frac{\rho_i}{\rho_0}\right)^{n_i} A_i \exp\left(-\frac{E_i}{RT}\right) \max\left[0, T_s - T_{thr,i}\right]$$

(5-1)

$$\dot{\omega}_i = A_i \exp\left(-\frac{E_i}{RT}\right) m_i^{n_i} y_{O_2}^{\delta}$$

Reminder of
Eq. (3-27)

Where, $T_{thr,i}$, is an optional "threshold" temperature that allows the definition of non-Arrhenius pyrolysis function and ignition criteria (by default $T_{thr,i} = 273.15°C$). In contrast to the equation used to express the reaction rates in this research, Eq. (3-27), the pyrolysis model from FDS V.5.3, Eq. (5-1), does not contain a term of oxygen mass fraction. The mixture fraction combustion model used for the calculation of the flame surface does not allow calculating the concentration of oxygen in the fuel side of the reaction zone. It means that in FDS, the heterogeneous oxidation reactions cannot be considered and all the decomposition reactions are of pyrolysis. Thus, corrections must be introduced to the kinetic parameters calculated at the matter scale or to the decomposition mechanism. These corrections must force FDS to calculate the correct MLR at a given temperature in order to produce the adequate quantity of gas fuel.

However, some authors argued that, experimentally speaking, it could be considered that the decomposition of the sample in CC occurs purely in absence of oxygen (pyrolysis), yet no demonstration of this phenomenon has been performed on solid combustibles with multi-reaction decomposition.

There is a serious lack of knowledge regarding the sensitivity of the Arrhenius parameters (input data of pyrolysis model) in the MLR output. Moreover, the combination of the lack of knowledge of the sensitivity of thermal and Arrhenius parameters makes the task of accurately fitting the experimental MLR curve very complicated. In the preliminary tests performed (not detailed here), it was found that the influence of the Arrhenius parameters and the decomposition mechanism are very

220

strong. Thus, the experimental effort (and cost) needed to determine the thermal properties in function of temperature for simulation purposes is perhaps not justified until an improvement of the models is carried out.

The shape of MLR released by FDS depends on the temperature provided to the Arrhenius equation. The temperature is calculated by the solution of the energy balance of the solid. The energy balance must take into account:

- The heat contribution of the flame (convection and radiation) and of an external heat source

- The heat losses by radiation and convection

- The heat conduction into the material

- The heat of reaction, that is to say the power consumed for the gasification of the solid fuel.

The energy balance of the solid is affected by many phenomena produced at the same time by the interaction between the solid and gas phases (*e.g.* combustion) and the intrinsic characteristics of the solid. If the energy balance is not established in an adequate manner, the bulk decomposition reaction can appear to go faster, slower or follow a shape that is different from the actual one. Some of the terms of the heat exchange are very difficult to determine experimentally. They are estimated using correlations or constant values set by experience.

The conduction model of FDS is presented in Eq. (5-2), which plays a main role in the energy balance.

$$\rho_s c_s \frac{\partial T_s}{\partial t} = \frac{\partial}{\partial x} k_s T \frac{\partial T_s}{\partial x} + \dot{q}_s''' \tag{5-2}$$

Where, $\dot{q}_s'''$, is the source term consisting of chemical reactions and radiative absorption. Eq. (5-2) is a one-dimensional heat conduction equation for the solid phase temperature $T_s(x,t)$ is applied in the direction x pointing into the solid (the point $x = 0$ represents the surface) [155]. This equation does not allow calculating the heat losses in the transversal direction to the incident heat flux. It neither takes into account the

effects caused by the alveolar nature of the foam, nor the change of the solid characteristics (*i.e.* solid to semi-liquid).

The in-depth distribution of the temperature of the PPUF foam slab was not reliably measured in this research. Some preliminary tests carried out using thermocouples into the solid showed a great uncertainty because of the formation of a char layer in the welding during the displacement of the decomposition front. A comparison of the experimental and calculated temperature profiles would allow the validation of the conduction model of FDS. The knowledge of the temperature profile can also help the comprehension of the formation, thickness and displacement velocity of the decomposition front.

The CC irradiance level imposed to the solid may be increased by around 40% by the contribution of the flame radiation towards the solid surface [74]. This increase of total heat income modifies the kinetics of decomposition (gas fuel production). The curve of HRR in FDS is calculated as the linear combination of the reaction rate and the heat of combustion of each solid in decomposition. But, up to date, the heat of combustion for every product reacting cannot be determined experimentally. As shown in Figure 4-12, the experimental EHC is not constant and changes greatly with the irradiance level and the combustion advancement. In other words, the model cannot be used to predict the actual heat release rate by solids with multiple decomposition stages in which the potential chemical energy varies with the reaction progress.

The CC numerical simulations have shown to be extremely sensible to the heat of reaction. It is highlighted that in the simulations presented from Figure 4-14 to Figure 4-15, the heat of reactions used are in the order of magnitude of the experimental enthalpic results. Nevertheless, these parameters represent a non negligible drawback, both numerically and experimentally. Numerically, because: a) a very reliable input value is required in order to reproduce the cone calorimeter results; b) the values that would allow an acceptable fit between calculations and experiments do not necessarily correspond to the ones measured experimentally. Experimentally, it is not possible to measure the enthalpy of every species present in the decomposition mechanism. As showed in Figure 2-1, under nitrogen, two distinct stages of decomposition were observed, for which it is possible to measure the enthalpy. However, under air a single datum of enthalpy was measured. We can therefore only hypothesize which one reflects the power released or consumed by every single reaction of the mechanism.

To avoid confusions, it is important to clarify that PPUF is a non-charring thermoset polymer in flaming condition[5]. In the decomposition mechanism found during the matter scale analysis, one of the solid species has been called "char". Nevertheless, this species represents a small mass fraction and does not have characteristics similar to those of the char yielded by wood or other charring materials.

Experimentally, the rate of decomposition of charring materials is highly influenced by the mass of char while this layer produces a thermal barrier that prevents heat from penetrating into the material. An accurate description of the char layer is required in order to model the heat transfer inside the solid, which is responsible for the in-depth decomposition of the solid sample. The case of PPUF decomposition during flaming combustion is very different: no char is produced, thus no thermal barrier exists. The residue remaining at the bottom of the holder does not influence the decomposition kinetics during the combustion process; is the residue remaining at the very end of the process. In the FDS pyrolysis model, there is no particular setting indication for charring or non-charring material. Perhaps the "interpretation of the role" of the residue in the model is responsible for the strong differences observed in Figure 4-15 and Figure 4-16.

Lautenberger *et al.* [15] developed a methodology that uses GA to estimate the material properties (model parameters) needed for CFD-based fire growth modelling of bench-scale fire test data. The inputs of the method are the MLR and surface temperature histories. This method was used for charring materials (redwood and red oak) and a thermoplastic material (polypropylene), considering an infinitely thin pyrolysis front and volatiles that were instantaneously transported towards the surface. The approach of the decomposition process was single-stage, where the virgin foam is transformed only into char. This tool was integrated to FDS V 4.0. The reaction properties calculated were the Arrhenius parameters and the heat of reaction. The material properties calculated were the thermal conductivity, specific heat and density of char and virgin material.

---

[5] Experiments in cone calorimeter showed that in non flaming condition a char layer is formed mainly at the bottom of the sample holder which contains a non negligible residual mass.

The same methodology was generalised to multi-step reactions. The TGA behaviour of a fire-retarded (brominated) polyester is predicted. This information was used subsequently to reproduce the MLR of a fiber reinforced polymer slab in Fire Propagation Apparatus [165]. This methodology has been generalised to the multi-stage, multi-reaction combustion of solids from various natures [166] and released as an independent code called "Gpyro" that can be coupled to FDS V.5.3 [167][168]. Some preliminary tests of this code have shown that it is very expensive in calculation time and generates results that are difficult to interpret.

Researchers from other teams estimated the thermal properties of pyrolysis solids using GA. The input data were TGA and CC experimental results. The optimum kinetic parameters and thermal properties were those that best fitted the results from both experimental techniques. In their work, virtual TGA and cone calorimeter were "built" using FDS [169]. This method was used for up to two decomposition stages of materials such wood and non-fire retarded polymers [170]. The authors defined thumb rules about which property to change in order to attain a desired movement from the MLR curve. Some of the kinetic parameters calculated do not seem in accordance with the ones normally found in literature, for example reaction orders as high as seven [169]. The same method was also used to estimate the parameters of electrical cables for nuclear power plants [171][172].

In order to clarify the sensitivity to kinetic, stoichiometric and thermal input parameters of the numerical simulations, a parametric study was launched. In total 7 000 FDS simulations were carried out with random input parameters in each simulation. The simulations tried to reproduce the CC experiments presented in section 4.4. Unfortunately, the results have not been treated and the results are not available yet.

An interesting discussion should take place among the scientific community of fire in order to answer to the following questions: Is it useful to keep on devoting time and effort to fit numerically fit curves by using parameters that do not have a physical meaning and that have a very uncertain application domain? How could the models be improved in order be able to use the experimental results?

If the scientific community answers the former question and finds that it is necessary to mathematically fit the curves, the best progress would be obtained by determining numerically which parameters actually have a strong influence on the simulation output. The experimental efforts must focus on the measurement of the very high

sensible parameters rather than the low sensible ones. The analysis of sensitivity must also clarify what parameters need to be determined in function of temperature and which ones can be set as scalars. Ho in 2007 [156] performed an interesting analysis of sensitivity, centred on the ignition criteria and fire propagation in wood. His study was performed using FDS V.4.0, which did not allow multi-reaction pyrolysis processes.

Concerning the latter question, a huge work must be carried out in order to improve the reliability of the experimental measurements in order to be able to provide accurate description of the interaction between the solid and the gas phases and providing as well data in all the stages of the decomposition as a function of temperature. Using this experimental data, improvements to the models can be performed.

As a conclusion, the greatest disadvantage of the pyrolysis calculated fire simulation is that the method is still very recent and very intensive research is being carried out to improve the models. There is no input data for the model, and in some cases it is not very clear how to perform the experimental measurements. As a matter of fact, NIST, WPI, SwRI and SFPE are currently working on a project, the main goal of which is to develop a standard guide with procedures for obtaining material parameters for fire models input such as algebraic, zone and field/CFD. These parameters include, but are not limited to, thermal parameters, ignition parameters, pyrolysis parameters and kinetic parameters [173].

5.5 Discussions about the oxygen mass fraction

The oxygen mass fraction plays a major role in the decomposition mechanism and kinetics. In this research, the decomposition pattern was determined in apparatuses where the sample masses were small. It is hypothesised that no transport effects exists from the centre of the particle toward the boundaries. The oxygen mass fraction contained in the air stream is supposed to be enough to create a condition of well-ventilated oxidation reaction. Unfortunately, no tests were performed to verify the

shape of MLR under vitiated or oxygen-rich atmosphere conditions, *i.e.* oxygen mass fractions of 0.11 and 0.3 kg·kg^{-1}.

Nevertheless, tests with various vector gas mass flows must be conducted in order to verify if it influences the decomposition kinetics. Thus, the data to be considered as the current patterns are the ones of the lower mass flow that do not cause a change in the shape of MLR. This validation would be performed considering the change of the solid phase as well as the gas phase. It can constitute a basis for the study of the differentiation of the heterogeneous reactions and the homogeneous reactions. It is perhaps a more precise method than the one used in this research to determine which gases are released by each decomposition stage.

In general terms, the increase of the oxygen in the atmosphere shift the reaction rate towards the lower temperatures in TGA and TF facilities and causes the ignition and maximum of HRR to occur faster in cone calorimeter [115]. The influence of oxygen in CC decomposition kinetic needs to be studied from three points of view:

- The oxygen mass fraction can change over the surface of the CC sample because of the oxygen consumption in the flame. In other words, a gradient of concentration may exist from the boundary to the centre of the CC sample, which can have a non-negligible influence on the decomposition kinetics.

- The oxygen mass fraction can change in-depth in a porous material. This produces a gradient of oxygen present from the surface to the core of the matrix, which causes the kinetics of decomposition in the decomposition front to change with the thickness.

- The oxygen mass fraction of the atmosphere changes in a closed room on fire. The oxygen available for the combustion in gas phase and heterogeneous reactions between gas and solid changes with time. The depletion of oxygen has a main influence in the kinetics of decomposition and the nature of the toxic gases released.

In conclusion, the influence of oxygen needs to be analysed in all the scales considered in this research. The availability of oxygen in the atmosphere influences the amount of power release by the fire as well as the toxicity potential in the environment.

6 General conclusions and future works

6.1 Conclusions

The improvement of fire safety in dwellings can be attained by the combination of a huge number of strategies focused on reducing the hazards caused by fire. The improvement of our knowledge of the physics and chemistry of fire and our ability to predict fire behaviour is the major issue in order to reduce these hazards. The reliable prediction of fire behaviour allows performance-based fire safety design of buildings, which has become the trend nowadays.

In this research the decomposition mechanism of PPUF was studied using techniques of thermal analysis and gas release measurements. Analysing together the solid and gas phases required the coupling of multiple measurement facilities. It allowed for the first time to state a "chemically correct" decomposition mechanism that takes into account the chemistry of the process. A part of the complexity of the problem is that, at any scale, the decomposition process occurs in a transient state: since the decomposition of PPUF presents many stages, the steady state is never reached. The scales considered in the present study are: matter scale analysed using TF and TGA apparatus; small scale studied using CC; and product scale tested with SBI calorimeter. The FTIR for examining the gas composition was used in all the scales.

The most common methods of thermal analysis found in literature allow hypothesising a decomposition mechanism and calculating the decomposition parameters. Nevertheless, it was found that these methods are not necessarily in accordance with the chemical reactions taking place in the solid phase.

Improvements to a multi-stage, multi-decomposition mechanism were carried out in order to use the new decomposition mechanism but also to predict the toxic gas release. A single supplementary kinetic parameter is required to enable the prediction of toxic gases. To the best of our knowledge, this is the first time that a method is proposed to predict the toxic gases released by the decomposition of polyurethane. The hypothesis used for this improvement was to consider that the curve of release of one gas could be calculated as the sum of the mass of this gas released by the successive reactions. From the results at the matter scale under air and nitrogen, two new decomposition mechanisms have been proposed. One mechanism from the literature has also been considered. A discussion was developed in order to determine which mechanism is correct and constitutes main input data for the modelling of thermal decomposition. The kinetic parameters of each reaction were calculated using genetic algorithms. The comparison of the numerical results with the experimental ones, particularly concerning the MLR and pollutants emission have permitted to validate the mechanism of PPUF decomposition.

The results of gas release prediction are very promising. Some differences between the experimental and calculated shapes were found. Nevertheless, the lack of fitness between the experimental and calculated curves can be explained by the differences found between the experimental facilities that were coupled in this research.

A single group of kinetic and stoichiometric parameters allowing the prediction of the mass and gas phase behaviour at various heating rates under two atmospheres (air and nitrogen) was found.

Experimental measurements were also performed in cone calorimeter. The MLR and HRR in function of time were determined by the oxygen consumption calorimetry. The results are in agreement with the results found in literature. The cone calorimeter was coupled to gas analysers (FTIR and FID). The coupled experiments allowed the verification of the decomposition mechanism at this scale. A two-stages decomposition was found, which remains unchanged independently of the irradiance level set to the electric heater: The first stage is the breakdown of PPUF molecules that carry the pyrolysis and oxidation of isocyanate remaining polyol as a semi-liquid residue. The second stage is the pyrolysis and oxidation of polyol that burns near a pool fire. The two stages of decomposition cannot be isolated in time. This decomposition

mechanism is valid at bench-scale (CC measurements) as well as at larger scales (simplified product burning).

The kinetic and thermal parameters found at the matter scale were used as input data in the pyrolysis-based fire simulation of CC experiments. Inaccurate results were found, caused by the combination of effects such as: the pyrolysis mechanism set in FDS cannot take into account heterogeneous oxidation reactions, the experimental thermal parameters are not allowed to fit adequately the experiments and calculations, strong uncertainties exist in the experimental measurement in function of temperature, the model of heat conduction is not allowed to take into account the heat losses by the lateral boundaries as well as the change of properties with the change of physical and chemical structure, etc.

At all the scales considered in this research, the decomposition mechanism was the same. A strong influence of the oxygen was verified but unfortunately, the models currently found in literature do not make it possible to predict the effects of the oxygen diffusion and the temperature distribution in-dept of the foam slab.

6.2 Future works

The analysis of the gases released during pyrolysis and combustion showed to be crucial information in order to understand the transformation taking place in the solid phase. The techniques such as FTIR that allows measuring multiple gases in real time have a very high potential in fire analysis. Nevertheless, these techniques in fire applications are still recent and their implementation is not easy. The TGA + FTIR or TGA + GC/MS for example are very promising techniques that need to be extensively used by the teams working on thermal decomposition.

In this research, the yield of soot was not measured at any scale. Considering soot is a primary need in further researches in order to determine the carbon balance. The carbon balance constitutes a good means of verifying the reliability of the gas phase measurements. It also allows writing a semi-steady state combustion equation that can be used as an engineering approach for the toxic gases production estimation.

Further works must also be conducted to understand the transport of the tar produced during the pyrolysis of PPUF. Some authors also reported tar transport in gas effluents of experiments carried out under oxidizing atmosphere. The PU tar has shown to solidify even with a lean decrease of temperature causing problems in the connexion lines of experimental facilities.

Efforts must focus on the improvement of the understanding of the transformations suffered by the nitrogen contained in the solid phase. A low portion of the nitrogen contained in the solid phase was found in the gas phase. It was hypothesised that the vast majority was reduced into N_2. However, experimental evidence should support this claim. The need for an analysis of the transformation of nitrogen is prompted by the potential to form very toxic compound (*i.e.* NOx, HCN, etc).

Interesting experimental techniques such as Laser Pyrolysis-FTIR [174] need to be considered in order to analyse the decomposition mechanism of polymers. This technique offers the advantage of very rapid testing on small samples. Moreover, the control of the power of the laser allows setting well-controlled irradiance levels at the surface of the sample. This may constitute a complement to cone calorimeter results, because the experiments can be performed on small samples where the conduction problems can be simplified.

The models also need to be improved based on the knowledge of the decomposition kinetics. The influence of oxygen in the atmosphere needs to be taken into account as well as the problem of the oxygen diffusivity inside the solid structure. Better methods to set the parameters of the simulation need to be stated, making the results of various calculations comparable between them.

The methods to determine and set the input data in the fire codes need to be improved for other materials than thermoplastics. A great deal is the charring materials: Their decomposition mechanism can be determined using TGA and TF as presented in this research. Nevertheless the fire behaviour in CC is difficult to predict because of the great number of reactions taking place in depth of the solid structure. So, for charring materials the hypothesis of infinitely thin decomposition front is not valid. The study of the mechanisms of decomposition must be kept out with other materials used in dwellings.

7 References

[1]   CHIVAS C, GUILLAUME E, SAINRAT A, BARBOSA V. Assessment of risk and benefits in the use of flame retardants in upholstered furniture in continental Europe. Fire Safety Journal **44** (2009): 801-807.

[2]   Unknown author. Standardisation mandate to CEN relative to the safety requirement for cigarettes. Commission of the European Communities, Directorate General Health and Consummers, 2008. M/425 EN.

[3]   Unknown author. Fire statistics – United Kingdom, Department of communities and Local Government, 2008. ISBN: 978 1 4098 0046 0 <www.communities.gov.uk>.

[4]   BEYLER C, HIRSCHLER M. Thermal decomposition of polymers. In: SFPE Handbook of Fire Protection Engineering (second edition), 1995, Section 1, Chapter 7: 99-199. ISBN 0-87765-354-2.

[5]   HILEMAN F, VOORHEES K, WOJCIK L, BIRKY M, RYAN P, EINHORN I. Pyrolysis of a flexible urethane foam. Journal of Polymer Science **13** (1975): 571-584.

[6]   TROITZSCH J. *Plastics Flammability Handbook. Principles, regulations, testing and approval* (Third edition). Carl Hansel Verlag, Munich, 2004. ISBN 3-446-21308-2.

[7]   Unknown author. IAL CONSULTANTS. PU chemicals and products in Europe, Middle East & Africa (EMEA), 2007. <http://www.ialconsultants.com/>.

[8]   MAROTEL Y. Polyuréthannes. Techniques de l'ingénieur, traité de plastiques et composites. AM3 **425** (2000): 1-18.

[9]   PAL G, MACSKASY H. *Plastics: Their Behaviour in Fires*. Elsevier Sciences Publishers, Amsterdam, Netherlands, 1991, 431 pp. ISBN 0-44-98766-5.

[10]   BRANCA C, DI BLASI C, CASU A, MORONE V, COSTA C. Reaction kinetics and morphological changes of a rigid polyurethane foam during combustion. Thermochimica Acta **399** (2003): 127-137.

[11]   BILBAO R, MASTRAL J, CEAMANOS J, ALDEA M. Kinetics of the thermal decomposition of polyurethane foams under nitrogen and air atmospheres. Journal of Analytical and Applied Pyrolysis **37** (1996): 69-82.

[12] SAINRAT A. Regulatory trends and standardization towards the reaction to fire of the upholstery furniture in France and in Europe. In: Flame Retardants 2006 Proceedings.

[13] CEAMANOS J, MASTRAL J, MILLERA A, ALDEA M. Kinetics of pyrolysis of high density polyethylene. Comparison of isothermal and dynamic experiments. Journal of Analytical and Applied Pyrolysis **65** (2002): 93-110.

[14] DUQUESNE S, LE BRAS M, BOURBIGOT S, DELOBEL R, POUTCH F, CAMINO G, ELING B, LINDSAY C, ROELS T. Analysis of fire gases released from polyurethane and fire-retarded polyurethane coatings. Journal of Fire Sciences **18** (2000): 456-482.

[15] LAUTENBERGER C, REIN G, FERNANDEZ-PELLO C. The application of a genetic algorithm to estimate material properties for fire modeling from bench-scale fire test data. Fire Safety Journal **41** (2006): 204-214.

[16] MAMLEEV V, BOURBIGOT S, LE BRAS M, DUQUESNE S, SESTAK J. Modelling of nonisothermal kinetics in thermogravimetry. Physical Chemistry Chemical Physics **2** (2000): 4708-4716.

[17] CHANG T, SHEN W, CHIU Y, HO S. Thermo oxidative degradation of phosphorus-containing polyurethane. Polymer Degradation and Stability **49** (1995): 353-360.

[18] KETATA N, SANGLAR C, WATON H, ALAMERCERY S, DELOLME F, RAFFIN G, GRENIER-LOUSTALOT ME. Thermal degradation of polyurethane bicomponent systems in controlled atmospheres. Polymer and Polymer Composites **13**, 1 (2005): 1-26.

[19] FRIEDMAN H. Kinetics of thermal degradation of char forming plastics from thermogravimetry. application to a phenolic plastic. Journal of Polymer Science, Part C, **6** (1963): 183-195.

[20] BABRAUSKAS V, GRAYSON S. *Heat release in fires.* Elsevier Science Publishers Ltd, Essex, England, 1992. ISBN 1-85166-794-6.

[21] YANG W, MACOSKO C, WELLINGHOFF S. Thermal degradation of urethanes based on6 4,4'-diphenylmethane diisocyanate and 1,4-butanediol (MDI/BDO). Polymer **27** (1986): 1235-1240.

[22] OHTANI H, KIMURA T, OKAMOTO K, TSUGE S. Characterization of polyurethanes by high-resolution pyrolysis-capillary gas chromatography. Journal of Analytical and Applied Pyrolysis 12 (1987): 115-133.

[23] ROGERS F, OHLEMILLER T. Pyrolysis kinetics of a polyurethane foam by thermogravimetry; a general kinetic method. Journal of Macromolecular Science A **15**, 1 (1981): 169-185.

[24] SHARMA V, KUNDU P. Condensation polymers from natural oils. Progress in Polymer Science **33** (2008): 1199-1215.

[25] WANG T, HSIEH T. Effect of polyol structure and molecular weight on the thermal stability of segmented poly(urethaneureas). Polymer degradation and stability **55** (1997): 95-102.

[26] FONT R, FULLANA A, CABALLERO J, CANDELA J,GARCÍA A. Pyrolysis study of polyurethane. Journal of Analytical and Applied Pyrolysis **58-59** (2001): 63-77.

[27] PRAGER F, ROSTECK H. *Polyurethane and fire: fire performance testing under real conditions*. Wiley-Vch Verlag Gmbh & Co, KGaA, Weinheim, 2006. ISBN 3-527-30805-9.

[28] ALLEN N, EDGE M, *Fundamentals of polymer degradation and stabilisation*. Elsevier Science Publishers Ltd, England,1992. ISBN 1-85166-773-3.

[29] ELOMA M, SARVARANTA L, MIKKOLA E, KALLONEN R, ZITTING A, ZEVENHOVEN C, HUPA M. Combustion of polymeric materials. Critical Reviews in Biochemistry and Molecular Biology **27**, 3 (1997):137-197.

[30] VOORHEES K, HILEMAN F, EINHORN I, FUTRELL J. An investigation of the thermolysis mechanism of model urethanes. Journal of Polymer Science **16** (1978): 213-228.

[31] ZHANG Y, XIA Z, HUANG H, CHEN H. Thermal degradation of polyurethane based on IPDI. Journal of Analytical and Applied Pyrolysis **84** (2009): 89-94.

[32] LATTIMER R, POLCE M, WESDEMIOTIS C. MALDI-MS analysis of pyrolysis products from segmented polyurethane. Journal of Analytical and Applied Pyrolysis **48** (1998): 1-15.

[33] EZEKOYE O, BRUNS M. Radical based thermal decomposition of polyethylene. NIST Annual Fire Conference, USA, 2008.

[34] FABRIS H. Thermal and oxidative stability of urethanes. Advances in Urethane Science and Technology **4** (1976): 89-111.

[35] WOOLLEY W. Nitrogen-containing products from the thermal decomposition of flexible polyurethane foams. British Polymer Journal **4** (1972): 27-43.

[36] MOLERO C, DE LUCAS A, RODRIGUEZ J. Recovery of polyols from flexible polyurethane foam by "split-phase" glycolysis: Study on the influence of reaction parameters. Polymer Degradation and Stability **93** (2008): 353-361.

[37] SAUNDERS J, BACKUS J. Thermal degradation and flammability of urethane polymers. Rubber Chemistry and Technology **39** (1961): 461-480.

[38] RAVEY M, PEARCE E. Flexible polyurethane foam. I. Thermal decomposition of a polyether-based, water-blown commercial type of flexible polyurethane foam. Journal of Applied Polymer Science **63** (1997): 47-74.

[39] ROTIVAL C, RENACCO C, ARFI C, PAULI A, PASTOR J. Gases emitted during thermal decomposition of a polypropylene film and a polyurethane adhesive. Journal of Thermal Analysis **41** (1994): 1519-1527.

[40] GABORIAUD F, VANTELON J. Thermal degradation of polyurethane based on MDI and propoxylated trimethylol propane. Journal of Polymer Science **19** (1981): 139-150.

[41] BROWN M. *Introduction to thermal analysis: Techniques and applications*. Chapman and Hall Ltd. Cambridge, 1988. ISBN 0 412 30230 6.

[42] ESPERANZA M, GARCIA A, FONT R, CONESA J. Pyrolysis of varnish based on a polyurethane. Journal of Analytical and Applied Pyrolysis **52** (1997): 151-166.

[43] STEC A, HULL T, LEBEK K, PURSER J, PURSER D. The effect of temperature and ventilation condition on the toxic product yields from burning polymers. Fire and Materials **32** (2008): 49-60.

[44] BLOMQVIST P, HERTZBERG T, TUOVINEN H, ARRHENIUS K, ROSELL L. Detailed determination of smoke gas contents using a small-scale controlled equivalence ratio tube furnace method. Fire and materials **31** (2007): 495-521.

[45] GUILLAUME E. *Effets du feu sur les personnes*. Synthèse bibliographique. Laboratoire national de métrologie et d'essais (LNE), 2006.

[46] BOCKHORN H, HORNUNG A, HORNUNG U, JAKOBSTRÖER P. Modelling of isothermal and dynamic pyrolysis of plastics considering non-homogeneous temperature distribution and detailed degradation mechanism. Journal of Analytical and Applied Pyrolysis **49** (1999): 53-74.

[47] SAHA B, GHOSHAL A. Thermal degradation kinetics of poly(ethylene terephthalate) from waste soft drink bottles. Chemical Engineering Journal **111** (2005): 39-43.

[48] FENG J, LI W.Y, XIE K. Relation between coal pyrolysis and corresponding coal char gasification in CO_2. Energy Sources **26** (2004): 841-848.

[49] GAYTON-ELY M, SHAKLEYA D, BELL S. Application of a pyroprobe to simulate smoking and metabolic degradation of abused drugs through analytical pyrolysis. Journal of Forensic Sciences **52** (2007): 473-478.

[50] DOSANJH S, PAGNI P, FERNANDEZ-PELLO C. Forced Cocurrent Smoldering Combustion. Combustion and Flame **68** (1987): 131-142.

[51] NF D 60-013. Protocol for assessment of the ignitability of upholstered furniture – Ignition source equivalent to a burning 20 g paper cushion – Coverings and upholstered materials. ICS 13.220.40, 97.140.

[52] BS 3379:1991. Flexible polyurethane cellular materials for loadbearing applications. UDC 678.664 405.8:006.3/8. ISBN 0 580 18176 6.

[53] NF EN ISO 11357-1 (1997). Plastics - Differential scanning calorimetry (DSC) – Part 1: General principles. ICS: 83.080.01.

[54] BUSTAMANTE VALENCIA L, ROGAUME T, GUILLAUME E, REIN G, TORERO J. Improving the Modelling of Thermal Decomposition of Polyether

Polyurethane Foam. Poster presented in the 9th Symposium on Fire Safety Science 2008, Germany.

[55] ISO 11357-4:2005. Plastics - Differential scanning calorimetry (DSC) – Part 4: Determination of specific heat capacity.

[56] SCOARNEC V., HAMEURY J., HAY B., FILTZ J. A new reference guarded hot plate designed for thermal conductivity measurements at high temperature. Poster presented in the 14th International Congress of Metrology 2009, France.

[57] NF EN ISO 1716:2002 Reaction to fire tests for building products – Determination of the heat of combustion. ICS: 13.220.50.

[58] NF ISO 1928:2004. Solid mineral fuels - Determination of gross calorific value by the bomb calorimetric method, and calculation of net calorific value. ICS: 75.160.10.

[59] SARAJI-BOZORGZAD M, GEISSLER R, STREIBEL T, MUHLBERGER F, SKLORZ M, KAISERSBERGER E, DENNER T, ZIMMERMANN R. Thermogravimetry coupled to single photon ionization quadrupole mass spectrometry: A tool to investigate the chemical signature of thermal decomposition of polymeric materials. Analytical Chemistry **80** (2008): 3393-3403.

[60] SOUDAIS Y, MOGA L, BLAZEK J, LEMORT F. Coupled DTA-TGA-FT-IR investigation of pyrolytic decomposition of EVA, PVC and cellulose. Journal of Analytical and Applied Pyrolysis **78** (2007): 46-57.

[61] DEL CAMPO S. *Identification des paramètres d'autenthicité du lait et produits laitiers* (thèse de doctorat). Institut national agronomique Paris-Grignon, France, 2006.

[62] PIELICHOWSKI K, LESZCZYNSKA A. TG-FTIR Study of the thermal degradation of polyoxymethylene (POM)/Thermoplastic Polyurethane (TPU) Blends. Journal of Thermal Analysis and Calorimetry **78** (2004): 631-637.

[63] RAHKAMAA-TOLONEN K. *Investigation of catalytic NOx reduction with transient techniques, isotopic exchange and FTIR spectroscopy* (PhD. Thesis). Åbo Akademi University, Turku, Finland, 2001.

[64] PEPIN MARIEY L. *Etude par spectroscopie IR-TF de l'adsorption et de la réactivité de l'ozone sur oxydes métalliques* (thèse de doctorat). Université de Caen, France, 1997.

[65] MASMOUDI H. *Vieillissement d'émulsions cosmétiques : apports comparés de la spectroscopie IRTF et de la rhéologie* (thèse de doctorat). Université Paul Cézanne, Aix-Marseille, France, 2005.

[66] MALINGREY B. Spectrométrie d'absorption dans l'infrarouge : Appareils. Techniques de l'Ingénieur, P2855 parution 01/1981.

[67] MARSCHALLEK-WATROBA K. *Analyse de flammes prémélangées méthane, monoxyde d'azote, air: expérience, modélisation, application à la réduction des*

oxydes d'azote (thèse de doctorat). Université des sciences et technologies de Lille, France, 2006.

[68] POTTEL H. Quantitative models for prediction of toxic component concentrations in smoke gases from FTIR spectra. Fire and Materials **20** (1996): 273-291.

[69] SARAGOZA L, YARDIN C, GUILLAUME E. Dosage des gaz dans les effluents de combustion par spectroscopie infrarouge à transformée de Fourier (selon la norme ISO 19702) : incertitude des spectres étalons. Proceedings of the 14th International Congress of Metrology, France, 2009.

[70] ISO 19702:2006. Toxicity testing of fire effluents – Guidance for analysis of gases and vapours in fire effluents using FTIR gas analysis. ISC 13.220.01.

[71] HAKKARAINEN T. *et al.* Smoke gas analysis by Fourier Transform Infrared Spectroscopy – Summary of the SAFIR project results. Fire and Materials **24** (2000): 101-112.

[72] Unknown author. Thermogravimétrie – Thermal analysis excellence. Mettler Toledo, Schwerzenbach, Suize 2007.

[73] CONESA J, MARCILLA A, CABALLERO J, FONT R. Comments on the validity and utility of the different methods for kinetic analysis of thermogravimetric data. Journal of Analytical and Applied Pyrolysis **58-59** (2001): 617-633.

[74] RHODES B, QUINTIERE J. Burning rate and flame heat flux for PMMA in cone calorimeter. Fire Safety Journal **26** (1996): 221-240.

[75] SAINRAT A. Personal communication. Laboratoire national de métrologie et d'éssais. 2009.

[76] Unknown author. Final Report. Fire standardisation research in railways - Firestarr Project. Contract SMT4 – CT 97 – 2164 Commission of the European Communities, 2001.

[77] NATO AC/301 SG/B. NATO Reaction-to-fire tests for materials – Toxicity of fire effluents. Edition 2: Draft I, Dec 2005.

[78] NF X 70-100-2 Fire tests - Analysis of gaseous effluents - Part 2: Tubular furnace thermal degradation method. ICS : 13.220.40 AFNOR 2006.

[79] ISO 16312-2:2006 Guidance for assessing the validity of physical fire models for obtaining fire effluents toxicity data for fire hazard and risk assessment – Part 2: Evaluation of individual physical fire models. Afnor 2006. ICS 13.220.99.

[80] REIN G. From pyrolysis kinetics to models of condensed-phase burning. In: Recent Advances in Flame Retardancy of Polymeric Material **19** (2008): 1-10 <www.era.lib.ac.uk/handle/1842/1152>.

[81] Unknown author. Benefits of fire safety engineering in the EU – BENEFEU project. The potential benefits of fire safety engineering in the European Union. Final report to DG Enterprise, 2002. (EC contract EDT/01/503480).

[82] VYAZOVKIN S. Kinetic concepts of thermally stimulated reactions in solids: a view from a historical perspective. International Reviews in Physical Chemistry **19** (2000); 45-60.

[83] KISSINGER H. Reaction Kinetics in Differential Thermal Analysis. Analytical Chemistry **29**, 11 (1957): 1702-1706.

[84] BABRAUSKAS V. Fire Modeling Tools for Fse: Are They Good Enough? Journal of Fire Protection Engineering **8**, 2 (1996): 87-93.

[85] JIANG Y. *Decomposition, ignition and flame spread on furnishing material* (PhD. Thesis). Victoria University, Australia, 2006.

[86] MOGHTADERI B. Pyrolysis of char forming solid fuels: a critical review of the mathematical modelling techniques. 5th AOSFST, Newcastle, Australia, 2001. <www.newcastle.edu.au>

[87] ANDZI BARHE T, ROGAUME T, RICHARD F, TORERO J. Numerical characterization of the mechanism of NOx formation during MSW incineration. Proceedings of the 6th Mediterranean Combustion Symposium 2009. France.

[88] KANNAN P, BIERNACKI J, VISCO D. A review of physical and kinetic models of thermal degradation of expanded polystyrene foam and their application to the lost foam casting process. Journal of Analytical and Applied Pyrolysis **78** (2007): 162-171.

[89] ANDERSON M, SLEIGHT R, TORERO J. Downward smolder of polyurethane foam: ignition signatures. Fire Safety Journal **35** (2000): 131-147.

[90] FONT R, MANCILLA A, GARCIA A, CABALLERO J, CONESA J. Comparison between the pyrolysis products obtained from different organic waste at high temperatures. Journal of Analytical and Applied Pyrolysis **32** (1995): 41-49.

[91] MANCILLA A, CONESA J. Reciclado terciario de plásticos vía pirólisis. Revista de plásticos modernos **79**, 527 (2000): 559-566.

[92] CHAO C, WANG J. Comparison of the thermal decomposition behaviour of a non-fire retarded and a fire retarded flexible polyurethane foam with phosphorus and brominated additives. Journal of Fire Sciences **19**, 2 (2001): 137-156.

[93] CONESA J, CABALLERO J, MANCILLA A, FONT R. Analysis of different kinetic models in the dynamic pyrolysis of cellulose. Thermochemica Acta **254** (1995): 175-192.

[94] MÜLLER-HAGEDORN M, BOCKHORN H, KREBS L, MÜLLER U. A comparative kinetic study on the pyrolysis of three different wood species. Journal of Analytical and Applied Pyrolysis **68-69** (2003): 231-249.

[95] FLYNN J. The 'Temperature Integral' – Its use and abuse. Thermochimica Acta **300** (1997): 83-92.

[96] VYAZOVKIN S. Thermal analysis. Analytical Chemistry **80**,12 (2008): 4301-4316.

[97] VYAZOVKIN S. A unified approach to kinetic processing of nonisothermal data. International Journal of Chemical Kinetics **28** (1996): 95-101.

[98] CRIADO J, GONZALEZ M, ORTEGA A, REAL C. Some considerations regarding the determination of the activation energy of solid-state reactions from a series of isothermal data. Journal of Thermal Analysis **29** (1984): 243-250.

[99] VYAZOVKIN S, DOLLIMORE S. Linear and nonlinear procedures in isoconversional computations of the activation energy of nonisothermal reactions in solids. Journal of Chemical Information and Computer Science **36** (1996): 42-45.

[100] LEFEBVRE J, DUQUESNE S, MAMLEEV V, LE BRAS M, DELOBEL R. Study of the kinetics of pyrolysis of a rigid polyurethane foam: use of the invariant kinetics parameters method. Polymers for Advanced Technologies **14** (2003): 796-801.

[101] JANKOVIC B. Kinetic analysis of the nonisothermal decomposition of potassium metabisulfite using the model fitting and isoconversional (model free) methods. Chemical Engineering Journal **139** (2008): 128-135.

[102] MAMLEEV V, BOURBIGOT S. Calculation of activation energies using the sinusoidally modulated temperatures. Journal of Thermal Analysis and Calorimetry **70** (2002): 565-579.

[103] MAMLEEV V, BOURBIGOT S, LE BRAS M, DUQUESNE S, SESTAK J. Modelling of nonisothermal kinetics in thermogravimetry. Physical Chemistry Chemical Physics **2** (2000): 4708-4716.

[104] CANCELLIERI D, LEONI E, ROSSI J. Kinetics of the thermal degradation of Erica arborea by DSC: Hybrid kinetic method. Thermochemica Acta **438** (2005): 41-50.

[105] BENBOW A, CULLIS F. The combustion of flexible polyurethane foams: mechanisms and evaluation of flame retardance. Combustion and Flame **24** (1975): 217-230.

[106] OHLEMILLER T. Modeling of smoldering combustion propagation. Progress in Energy and Combustion Science **11** (1985): 277-310.

[107] REIN G. *Computational Model of Forward and Opposed Smoldering Combustion with Improved Chemical Kinetics* (PhD. Thesis). University of California, Berkeley, San Francisco, US, 2005.

[108] REIN G, FERNANDEZ-PELLO C, URBAN D. Computational model of forward and opposed smoldering combustion in microgravity. Proceedings of THE Combustion Institute **31**, 2 (2007): 2677-2684. <http://www.era.lib.ed.ac.uk/bitstream/1842/897/1/Rein_Heidelberg.pdf>.

[109] REIN G, LAUTENBERGER C, FERNANDEZ-PELLO C, TORERO J, URBAN D. Application of genetic algorithms and thermogravimetry to determine the kinetics of polyurethane foam in smoldering combustion. Combustion and Flame **146** (2006): 95-108.

[110] HOUCK C, JOINES J. A genetic algorithm for function optimization: a matlab implementation. Report NCSU IE TR 95-09. <http:// www.ise.ncsu.edu>.

[111] MOWRER F. Enclosure smoke filling revisited. Fire Safety Journal **33** (1999): 93-114.

[112] ABECASSIS-EMPIS C, RESZKA P, STEINHAUS T, COWLARD A, BITEAU H, WELCH S, REIN G, TORERO J. Characterisation of Dalmarnock fire test one. Experimental Thermal and Fluid Science **32** (2008): 1334-1343.

[113] WICHMAN I. Material flammability, combustion, toxicity and fire hazard in transportation. Progress in Energy and Combustion Science **29** (2003): 247-299.

[114] DELICHATSIOS M. Piloted ignition times, critical heat fluxes and mass loss rates at reduced oxygen atmospheres. Fire Safety Journal **40** (2005): 197-212.

[115] FANG M, SHEN D, LI Y, YU C, LUO Z, CEN K. Kinetic study on pyrolysis and combustion of wood under different oxygen concentrations by using TG-FTIR analysis. Journal of Analytical and Applied Pyrolysis **77** (2006): 22-27.

[116] CABALLERO J, FONT R, MANCILLA A, CONESA J. New kinetic model for thermal decomposition of heterogeneous materials. Industrial and Engineering Chemistry Research **34** (1995): 806-812.

[117] SENNECA O, CHIRONE R, SALATINO P. Oxidative pyrolysis of solid fuels. Analytical and Applied Pyrolysis **71** (2004): 959-970.

[118] ARRHENIUS S. On the reaction velocity of the inversion of cane sugar by acids. Zeitschrift für Physikalische Chemie **4**, 226 (1889).

[119] LAIDLER K, KING M. The Development of Transition-State Theory. Journal of Physical Chemistry **87** (1983): 2657-2664.

[120] POLLAK E., TALKNER P. Reaction rate theory: What it was, where is it today, and where is it going? Chaos **15** (2005): 026116-026116-11; DOI:10.1063/1.1858782.

[121] CUKROWSKI A. Relations between the arrhenius activation energy and threshold energy for simple models of the reactive cross sections in a dilute gas. Acta Physica Polonica B. **37** (2006): 1715-1726.

[122] MARQUIS D, BUSTAMANTE VALENCIA L, GUILLAUME E, PAVAGEAU M, CHIVAS C. Modélisation du comportement au feu d'un composite par calcul de pyrolyse : approche combinée expérience-simulation à petite échelle. Mécanique & Industries **10** (2009) : 245-253.

[123] COMUCE M. Comportement au feu des matières plastiques – Application à la sécurité incendie. Meeting GDR Incendies in CORIA UMR 6614, 2009, France.

[124] BUSTAMANTE VALENCIA L, ROGAUME T, GUILLAUME E, REIN G, TORERO J. Characterization of the kinetic of decomposition of polyether polyurethane foam (ppuf) – A way for finding input data for fire simulations. BFRL Annual Fire Conference 2008. USA.

[125] ISO 16730:2007 (E). Fire safety engineering-Assessment. Verification and validation of calculation methods.

[126] HILBERT D, NEUMANN J, NORDHEIM L. Über die Grundlagen der Quantenmechanik. Mathematische Annales **98**, 1 (1928): 1-30.

[127] DI BLASI C, Modeling chemical and physical processes of wood and biomass pyrolysis. Progress in Energy and Combustion Science **34** (2008): 47-90.

[128] DI BLASI C. The state of the art of transport models for charring solid degradation, Polymer International **49** (2000): 1-14.

[129] DI BLASI C. Modeling and simulation of combustion processes of charring and non-charring solid fuels. Progress in Energy and Combustion Science **19** (1993): 71-104.

[130] TORERO J, FERNANDEZ-PELLO A. Forward smolder of polyurethane foam in a forced air flow. Combustion and Flame **106** (1996): 89-109.

[131] ISO 5 660-1:2002 Reaction to fire tests – Heat release, smoke production and mass loss rate – Part 1 Heat release rate (cone calorimeter method). Second edition 2002.

[132] ISO 291:2005. Plastics – Standard atmospheres for conditioning and testing. ISC: 83.080.01.

[133] BABRAUSKAS V, PEACOCK R. Heat release rate: the single most important variable in fire hazard. Fire Safety Journal **18** (1992): 255-272.

[134] BABRAUSKAS V. *Ignition Handbook*. Fire Sciences Publishers, 2003. ISBN 0-9728111-3-3.

[135] TEWARSON A. Generation of heat and gaseous, liquid, and solid products in fire. The SFPE Handbook of Fire of Fire Protection Engineering, fourth edition, section 3, chapter 4, P 109-194. National Fire Protection Association, USA, 2008. ISBN-10: 0-87765-821-8.

[136] NORMANT H, NORMANT J. Chimie organique – Cours de chimie (deuxième édition), Masson et Cie Editeurs, 1968.

[137] RASBASH D, DRYSDALE D. Fundamentals of smoke production. Fire Safety Journal **5**, 1 (1982): 77-86.

[138] BUSTAMANTE VALENCIA L, ROGAUME T, GUILLAUME E, REIN G, TORERO J. Analysis of principal gas products during combustion of polyether polyurethane foam at different irradiance levels. Fire Safety Journal **44** (2009): 933–940.

[139] DRYER F, NAEGELI D, GLASSMAN I. Temperature dependence of the reaction $CO+OH \longrightarrow CO_2+H$. Combustion and Flame **17** (1971): 270-272.

[140] DRYER F, GLASSMAN I. High temperature oxidation of CO and CH4. Proceeding of the 14th International Symposium on Combustion, The Combustion Institute (1972): 987-1003.

[141] GLASSMAN I. *Combustion*, Third edition, Academic Press, 1996.

[142] YETTER R, DRYER F, RABITZ H. A comprehensive reaction mechanism for carbon monoxide/hydrogen/oxygen kinetics. Combustion Science and Technology **79** (1991): 97-128.

[143] YETTER R, DRYER F, RABITZ H. Flow reactor studies of carbon monoxide/hydrogen/oxygen kinetics. Combustion Science and Technology **79** (1991): 129-140.

[144] GLARBORG P, ALZUETA M, DAM-JOHANSEN K, MILLER J. Kinetic modeling of hydrocarbons/nitric oxide interactions in a flow reactor. Combustion and Flame **115** (1998) 1-27.

[145] ROGAUME T, JABOUILLE F, TORERO J. Computational model to investigate the mechanisms of formation of NO_x during waste incineration. Combustion Science and Technology **176** (2004): 925-943.

[146] GLARBORG P, MILLER J, KEE R. Kinetic modeling and sensitivity analysis of nitrogen oxide formation in well stirred reactors. Combustion and Flame **65** (1986): 177-202.

[147] DE SOETE G. Mécanismes de formation et de destruction des oxydes d'azote dans la combustion. Revue Générale de Thermique **330-331** (1989): 353-373.

[148] BUSTAMANTE VALENCIA L, ROGAUME T, GUILLAUME E, REIN G, TORERO J. Yield of toxic species in cone calorimeter tests during polyether polyurethane foam fire. Proceeding of the 6th Mediterranean Combustion Symposium, France, 2009.

[149] BITEAU H, STEINHAUS T, SCHEMEL C, SIMEONI A, MARLAIR G, BAL N, TORERO J. Calculation methods for the heat release rate of materials of unknown composition. Proceedings of the 9th International Symposium of Fire Safety Science IAFSS, 2008.

[150] GUILLAUME E., CHIVAS C. Fire models used in toxicity testing. In: Hazard of combustion products. Proceedings of the hazard of combustion products: toxicity, opacity, corrosivity and heat release conference, Interscience Communications Limited, UK, 2008. ISBN 978-0-9556548-2-4.

[151] HERTZBERG T, BLOMQVIST P, DALENE M, SKARPING G. Particles and isocyanates from fires, SP Swedish National Testing and Research Institute, 2003:05, Boras, 2003.

[152] KOTRESH T *et al.* Effect of heat flux on the burning behaviour of foam and foam/Nomex III fabric combination in the cone calorimeter. Polymer Testing **25** (2006): 744-757.

[153] FABIAN T, GANDHI P. Smoke characterization project. Technical report. NFPA – Underwriters Laboratories Inc., 2007. <http://www.nfpa.org/>.

[154] MCGRATTAN K, KLEIN B, HOSTIKKA S, FLOYD J. Fire Dynamics Simulator (Version 5.3), User's Guide. NIST Special Publication 1019-5, National Institute of Standards and Technology, Gaithersburg, Maryland, February 2009.

[155] MCGRATTAN K, BAUM H, REHM R, HOSTIKKA S, FLOYD J. Fire Dynamics Simulator (Version 5.3), Technical Reference Guide. NIST Special Publication 1018-5, National Institute of Standards and Technology, Gaithersburg, Maryland, February 2009.

[156] HO K. *Flame spread modelling using FDS 4 CFD model* (PhD Thesis). University of Canterbury, Christchurch, New Zealand, 2007.

[157] DESANGHERE S. *Détermination des conditions d'échauffement de structure extérieure à un bâtiment en situation d'incendie* (PhD thesis), INSA de Rouen, France, 2006.

[158] FUENTES A. *Interaction entre la zone réactionnelle et le champ de concentration des suies : cas de la flamme de diffusion laminaire au sein d'une couche-limite* (PhD thesis). Université de Poitiers, France, 2006.

[159] KWON J. *Evaluation of FDS V4: Upward flame spread* (MSc thesis). Worcester Polytechnic Institute, Massachusetts, US, 2006.

[160] LIANG K, MA T, QUINTIERE J, ROUSON D. Application of CFD modeling to room fire growth on walls. NIST GCR 03-849, 2003.

[161] BUSTAMANTE VALENCIA L, ROGAUME T, GUILLAUME E. New method for simulating the kinetic of toxic gases production of upholstered furniture fire. Proceedings of the 12th Fire and Material Conference 2009, USA.

[162] prCEN/TS 45545-1 to prCEN/TS 45545-7. Railway applications – Fire protection of railway vehicles, final draft. CEN, CENELEC, 2008. ICS 45.060.01.

[163] QUINTIERE J. *Fundamentals of fire phenomena*. John Wiley & Sons Ltd, England, 2006. ISBN 13 978-0-470-09113-5.

[164] PITTS W. Ignition of cellulosic fuels by heated and radiative surfaces. NIST Technical note 1481, 2007. <www.fire.nist.gov/bfrlpubs/fire07/art014.html>.

[165] LAUTENBERGER C, KIM E, DEMBSEY N, FERNANDEZ-PELLO C. The role of decomposition kinetics in pyrolysis modeling – Application to a fire retardant polyester composite. Proceedings of the 9th Symposium on Fire Safety Science IAFSS, 2008.

[166] LAUTENBERGER C, FERNANDEZ-PELLO C. Generalized pyrolysis model for combustible solids. Fire Safety Journal **44** (2009): 819-839.

[167] LAUTENBERGER C. Gpyro– A generalized pyrolysis model for combustible solids. Users' Guide, 2009. <http://code.google.com/p/gpyro/>.

[168] LAUTENBERGER C. Gpyro– A generalized pyrolysis model for combustible solids. Technical reference, 2009. <http://code.google.com/p/gpyro/>.

[169] MATALA A. *Estimation of solid phase reaction parameters for fire simulation* (Master's thesis). Helsinki University of Technology, Finland, 2008.

[170] MATALA A, HOSTIKKA S, MANGS J. Estimation of pyrolysis model parameters for solid materials using thermogravimetric data. Proceedings of the 9th International Symposium of Fire Safety Science IAFSS, 2008.

[171] MATALA A. Application of genetic Algorithm in pyrolysis model parameter estimation. <http://www.sal.tkk.fi/Opinnot/Mat-2.108/pdf-files/emat07.pdf>.

[172] HOSTIKKA S, MATALA A. Modelling the fire behaviour of electrical cables. 20th International Conference on Structural Mechanics in Reactor Technology (SMiRT 20) – 11th International Post Conference Seminar on Fire Safety in Nuclear Power Plants and Installations, 2009.

[173] DEMBSEY N, JANSSENS M, HURLEY M. Fire Pyrolysis Parameters Guidance. <http://sites.google.com/a/fire-pyrolysis-parameter-guidance.org/>, 2009.

[174] BODZAY B, MAROSFOI B, IGRICZ T, BOCZ K, MAROSI G. Polymer degradation studies using laser pyrolysis-FTIR microanalysis. Journal of Analytical and Applied Pyrolysis **85** (2009): 313-320.
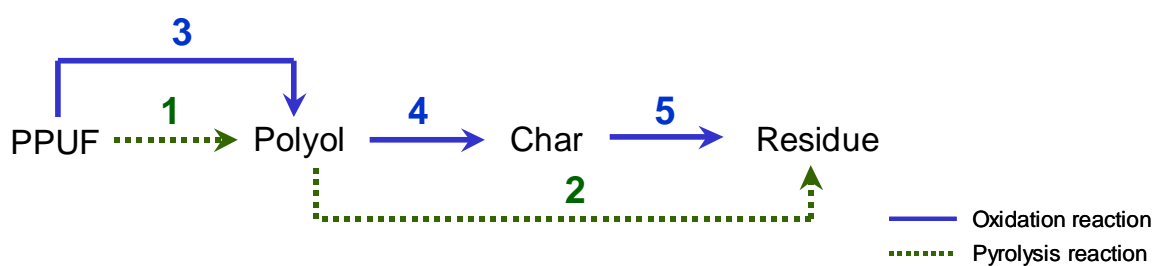
Appendix A

Here after are presented the SEM pictures obtained by Branca *et al.* [10]. The material studied is a rigid polyurethane foam of density 38 kg·m^{-3}. SEM pictures are about virgin (top) foam and foam submitted to an irradiance level of 50 kW·m^{-2} in cone calorimeter (bottom). These figures are to be compared with the SEM pictures presented in this research on subsection 2.6.1 (Pictures reproduced under authorisation).
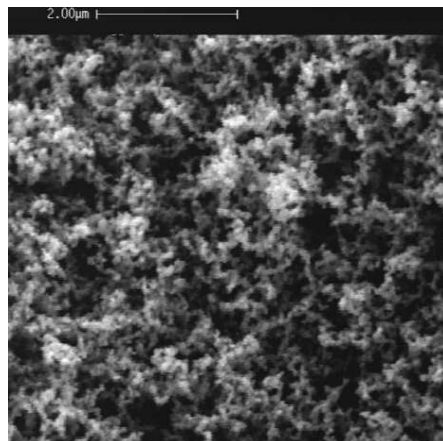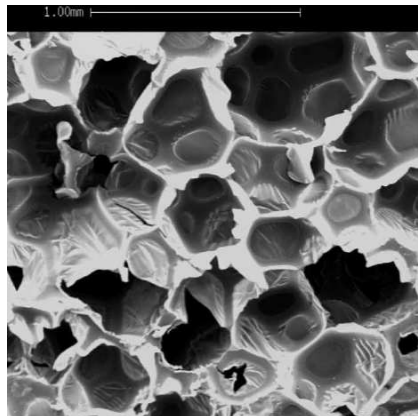
Appendix B

Appendix B present the plots of reaction rates together with the kinetic of gases release. This curves allow to define which gases release by each reaction of the decomposition mechanism 1 presented in Figure 3-3 and reminded here after.

Reminder of Figure 3-3 Kinetic mechanism 1 proposed in this research
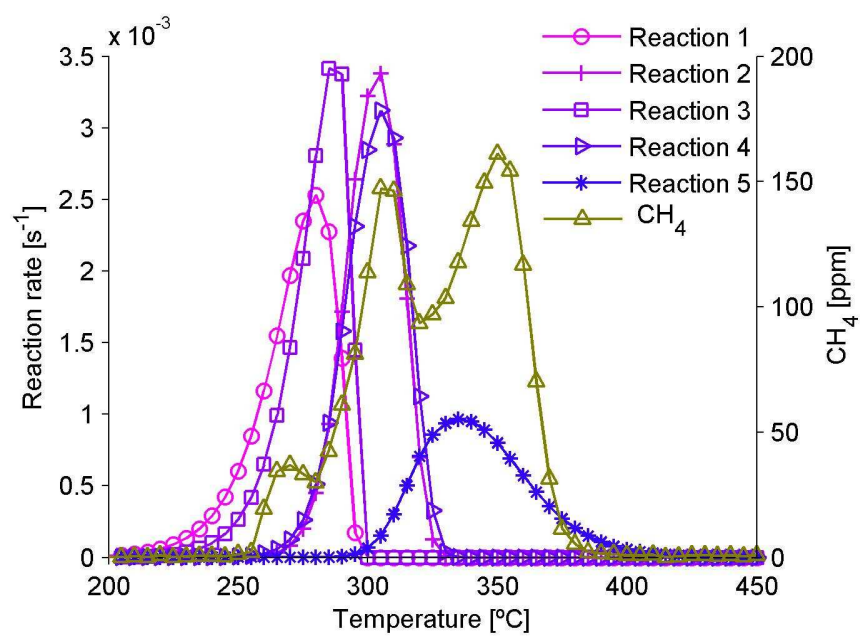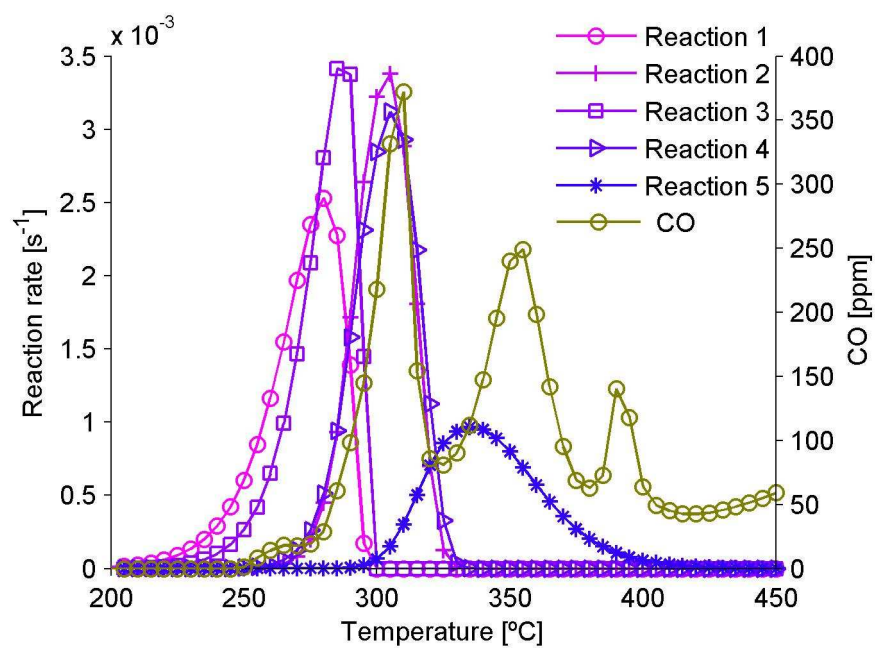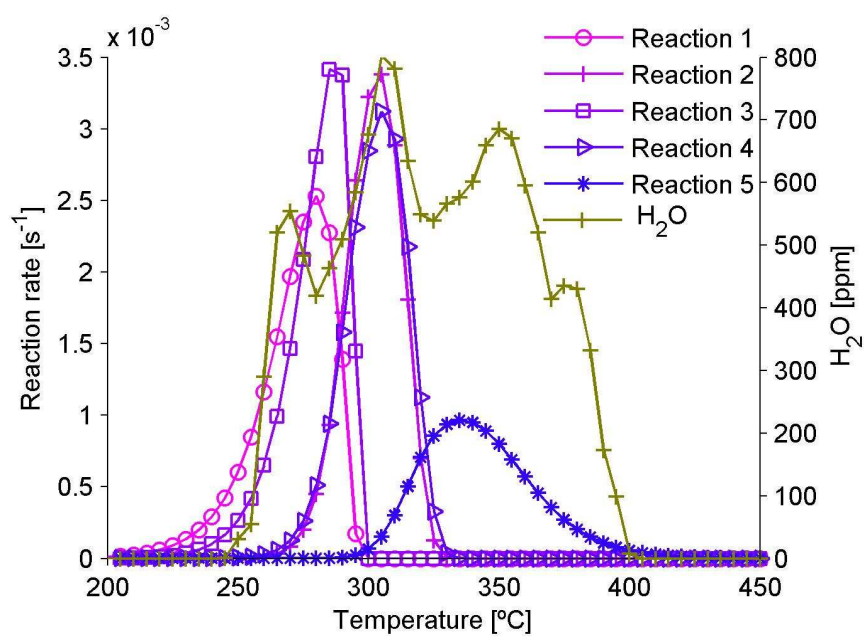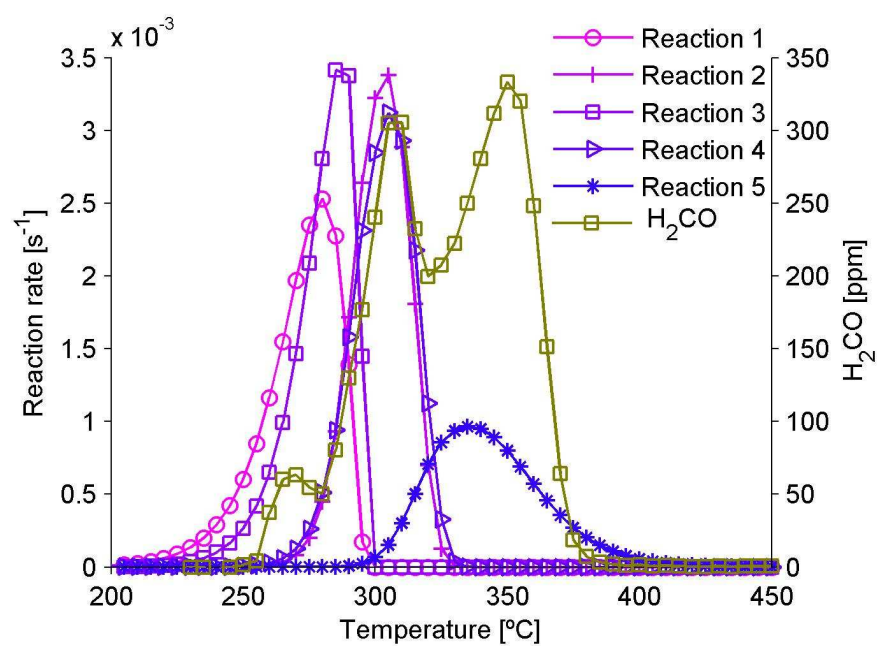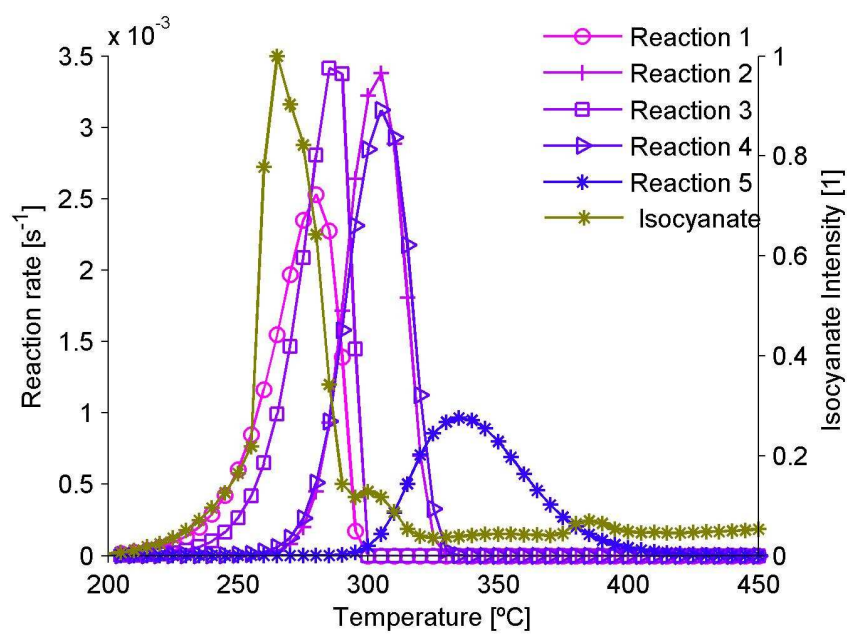
Appendix C

Appendix C presents the experimental and calculated kinetic of gas release of CO, H_2O and CH_4 (see subsection 3.3.3.2).
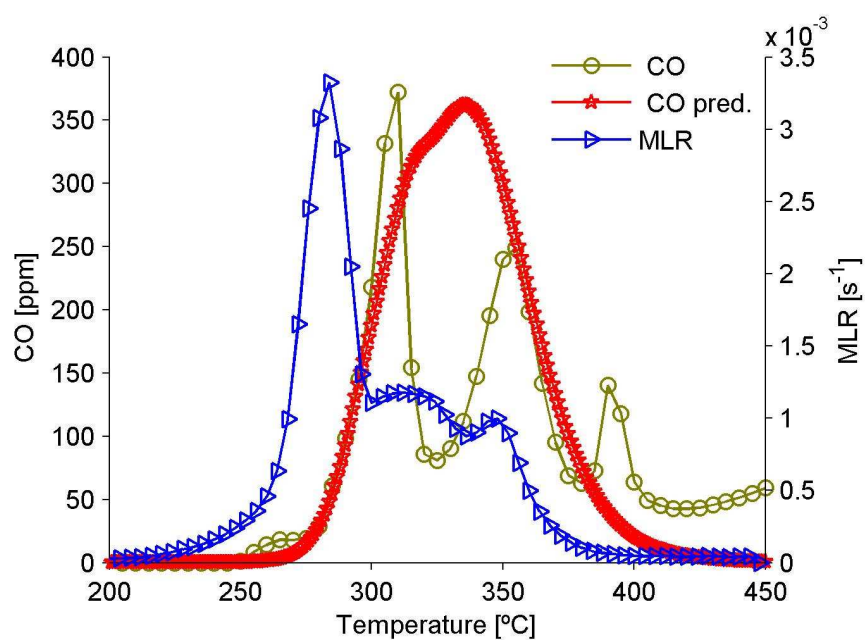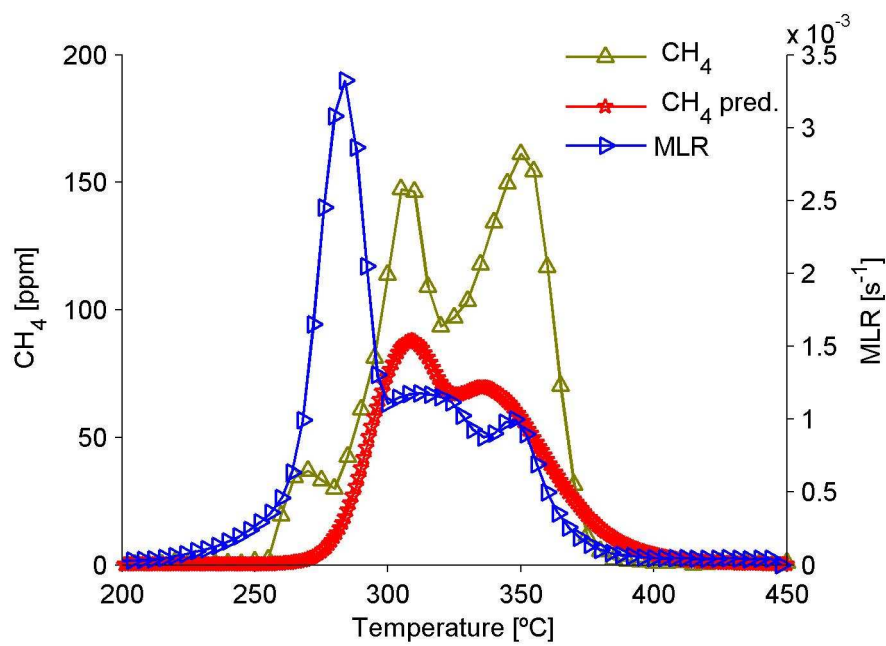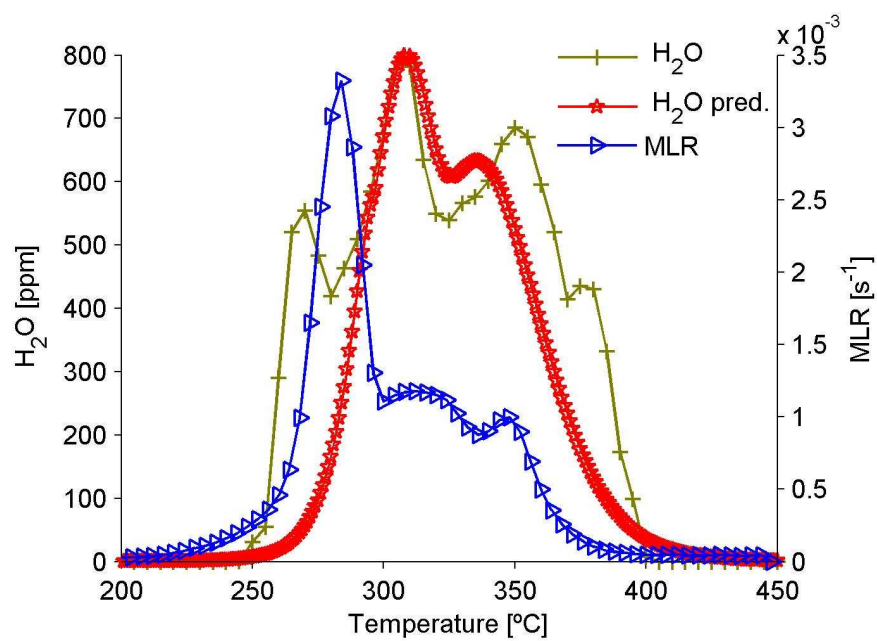
Appendix D

```
&HEAD CHID='PPUF_air_cone_grossier' ,TITLE='Virtual cone calorimetre - 50 kW_m-2,low
resolution'/

&TIME TWFIN = 100.0, WALL_INCREMENT = 1./
&MESH IJK = 10,10,18, XB = -0.125,0.125,-0.125,0.125,-0.075,0.375/
&DUMP DT_HRR=1., DT_DEVC=1., DT_PROF=30./

Recall of input data units:
---------------------------
/ THICKNESS                 = [ m ]
/ CONDUCTIVITY              = [ W m-1 K-1 ]
/ SPECIFIC_HEAT             = [ kJ kg-1 K-1 ]
/ DENSITY                   = [ kg m-3]
/ REFERENCE_TEMPERATURE     = [ °C ]
/ HEAT_OF_REACTION          = [ kJ kg-1 ]
/ HEAT_OF_COMBUSTION        = [ kJ kg-1 ]
/ HRRPUA                    = [ kW m-2 ]
/ A                         = [ s-1 ]
/ E                         = [ kJ_Kmol-1]
/ N_S                       = [ 1 ]

Recall of the decomposition mechanism:
--------------------------------------
/ PPUF -o-3-o-> Polyol -o-4-o-> Char -o-5-o-> Residue
/      ---1--->        ----------2--------->

Convention:                -----> pyrolysis reaction
                           --o--> oxydation reaction

Sample definition:
------------------
&SURF ID                   = 'PPUF SLAB'
   STRETCH_FACTOR          = 0.5
   CELL_SIZE_FACTOR        = 0.25
   COLOR                   = 'GOLD'
   MATL_ID                 = 'PPUF'
   THICKNESS(1:2)          = 0.05/

Matter properties:
//////////////////////////////////////////////////////////////////////
&MATL ID                   = 'PPUF'
   CONDUCTIVITY            = 0.04
   SPECIFIC_HEAT           = 1.3
   DENSITY                 = 22
   N_REACTIONS             = 2
   E(1:2)                  = 169938.9,      214144.2
   A(1:2)                  = 6.09E+13,      3.07E+18
   N_S(1:2)                = 0.91,          0.48
   NU_RESIDUE(1:2)         = 0.69,          0.44
   NU_FUEL(1:2)            = 0.31,          0.56
   HEAT_OF_REACTION(1:2)   = -318,          1400
   RESIDUE(1:2)            = 'POLYOL',      'POLYOL'
   HEAT_OF_COMBUSTION      = 26000/

&MATL ID                   = 'POLYOL'
   CONDUCTIVITY            = 0.8
   SPECIFIC_HEAT           = 2
   DENSITY                 = 800
   N_REACTIONS             = 2
   E(1:2)                  = 243927.3,      213625.3
   A(1:2)                  = 4.42E+17,      1.26E+18
   N_S(1:2)                = 1.26,          0.95
   NU_RESIDUE(1:2)         = 0.1,           0.45
   NU_FUEL(1:2)            = 0.9,           0.55
   HEAT_OF_REACTION(1:2)   = -236,          2000
   RESIDUE(1:2)            = 'RESIDUE',     'CHAR'
   HEAT_OF_COMBUSTION      = 26000/
```

```
&MATL ID                    = 'CHAR'
  CONDUCTIVITY              = 0.12
  SPECIFIC_HEAT             = 2.5
  DENSITY                   = 300
  N_REACTIONS               = 1
  E(1)                      = 160866.2
  A(1)                      = 4.30104E+12
  N_S(1)                    = 1.64
  NU_RESIDUE(1)             = 0.25
  NU_FUEL(1)                = 0.75
  HEAT_OF_REACTION(1)       = 400
  RESIDUE(1)                = 'RESIDUE'
  HEAT_OF_COMBUSTION        = 26000/

&MATL ID                    = 'RESIDUE'
  EMISSIVITY                = 0.9
  CONDUCTIVITY              = 0.08
  SPECIFIC_HEAT             = 1.337
  DENSITY                   = 300./
//////////////////////////////////////////////////////////////////////
```

Definition of properties as a function of temperature
//
Conductivity of virgin PPUF

```
                    [°C]  [ W·m-1·K-1 ]
&RAMP ID='k_ramp', T= 24.,  F=0.045 /
&RAMP ID='k_ramp', T= 99.,  F=0.062 /
&RAMP ID='k_ramp', T= 148., F=0.076 /
&RAMP ID='k_ramp', T= 178., F=0.084 /
```

Specific heat of virgin PPUF

```
                    [°C] [ kJ·kg-1·K-1 ]
&RAMP ID='c_ramp', T= 23.,  F=1.885 /
&RAMP ID='c_ramp', T= 50.,  F=1.988 /
&RAMP ID='c_ramp', T= 100., F=2.135 /
&RAMP ID='c_ramp', T= 150., F=2.246 /
&RAMP ID='c_ramp', T= 200., F=2.349 /
&RAMP ID='c_ramp', T= 250., F=2.469 /
```

Specific heat of Residue

```
                         [°C] [ kJ·kg-1·K-1 ]
&RAMP ID='c_ramp_residue', T= 23.,  F=1.337 /
&RAMP ID='c_ramp_residue', T= 50.,  F=1.340 /
&RAMP ID='c_ramp_residue', T= 100., F=1.370 /
&RAMP ID='c_ramp_residue', T= 150., F=1.425 /
&RAMP ID='c_ramp_residue', T= 200., F=1.495 /
&RAMP ID='c_ramp_residue', T= 250., F=1.573 /
&RAMP ID='c_ramp_residue', T= 300., F=1.650 /
&RAMP ID='c_ramp_residue', T= 350., F=1.718 /
&RAMP ID='c_ramp_residue', T= 400., F=1.769 /
&RAMP ID='c_ramp_residue', T= 450., F=1.793 /
&RAMP ID='c_ramp_residue', T= 500., F=1.784 /
//////////////////////////////////////////////////////////////////////
```

Definition of the sample and sample holder
//
Definition of the sample:

```
&OBST  XB = -0.05, 0.05, -0.05, 0.05, -0.075, -0.025,
SURF_ID6 ='Porte_eprouvette', 'Porte_eprouvette',  'Porte_eprouvette',
'Porte_eprouvette', 'Porte_eprouvette', 'PPUF SLAB'/
```

Definition of the sample holder:

```
&SURF ID                    = 'Porte_eprouvette'
  MATL_ID                   = 'porte_ep'
  THICKNESS                 = 0.005
  COLOR                     = GRAY /

&MATL ID                    = 'porte_ep'
  DENSITY                   = 7850.
  SPECIFIC_HEAT             = 0.460
  CONDUCTIVITY              = 50./
//////////////////////////////////////////////////////////////////////
```

Definition of the cone calorimeter facility
//

```
Definition of the heater:
-------------------------
&SURF ID                   = 'Four'
  TMP_FRONT                = 880,
  COLOR                    = FIREBRICK/

Calibration of the CC irradiance level:
---------------------------------------
Modify 'TMP_FRONT' in order to change the irradiance level
/10kWm-² => TMP_FRONT = 502°C --> Verified May 23rd 2009
/20kWm-² => TMP_FRONT = 645°C --> Verified May 23rd 2009
/25kWm-² => TMP_FRONT = 698°C
/30kWm-² => TMP_FRONT = 742°C --> Verified May 23rd 2009
/35kWm-² => TMP_FRONT = 782°C
/40kWm-² => TMP_FRONT = 817°C --> Verified May 23rd 2009
/50kWm-² => TMP_FRONT = 880°C --> Verified May 23rd 2009
/75kWm-² => TMP_FRONT = 1002°C

Material for irradiance level calibration
-----------------------------------------
/&OBST  XB = -0.05 ,   0.05 ,  -0.05 ,   0.05 ,  -0.075,  -0.025, SURF_ID6
='Porte_eprouvette', 'Porte_eprouvette', 'Porte_eprouvette', 'Porte_eprouvette',
'Porte_eprouvette', 'INERT'/

Definition of the CC fan:
-------------------------
&SURF ID                   = 'Extracteur',
  VOLUME_FLUX              = 0.024,
  COLOR                    = CYAN/

Definition of the boundary conditions:
--------------------------------------
&VENT  SURF_ID='OPEN' , MB = 'XMIN'  /
&VENT  SURF_ID='OPEN' , MB = 'XMAX'  /
&VENT  SURF_ID='OPEN' , MB = 'YMIN'  /
&VENT  SURF_ID='OPEN' , MB = 'YMAX'  /
&VENT  SURF_ID='OPEN' , MB = 'ZMIN'  /
&VENT  SURF_ID='Extracteur' , MB = 'ZMAX'/

Definition of the heater:
-------------------------
&OBST XB=-0.09, -0.075, -0.075, 0.075, 0.0, 0.025, SAWTOOTH=.FALSE., SURF_ID= 'Four' /
&OBST XB= 0.075, 0.09, -0.075,  0.075, 0.0, 0.025, SAWTOOTH=.FALSE., SURF_ID= 'Four' /
&OBST XB=-0.075, 0.075, -0.09,-0.075,  0.0, 0.025, SAWTOOTH=.FALSE., SURF_ID= 'Four' /
&OBST XB=-0.075, 0.075, 0.075, 0.09,  0.0, 0.025, SAWTOOTH=.FALSE., SURF_ID= 'Four' /
&OBST XB=-0.075,-0.05, 0.05,  0.075,  0.0,  0.025, SAWTOOTH=.FALSE., SURF_ID= 'Four' /
&OBST XB=-0.075,-0.05,-0.075, -0.05,  0.0,  0.025, SAWTOOTH=.FALSE., SURF_ID= 'Four' /
&OBST XB=0.05, 0.075, 0.05,  0.075 ,  0.0,  0.025, SAWTOOTH=.FALSE., SURF_ID= 'Four' /
&OBST XB=0.05, 0.075, -0.075, -0.05,  0.0, 0.025, SAWTOOTH=.FALSE., SURF_ID= 'Four' /
&OBST XB=-0.075,-0.05,-0.05,  0.05 , 0.025, 0.05, SAWTOOTH=.FALSE., SURF_ID= 'Four' /
&OBST XB= 0.05, 0.075, -0.05,  0.05,  0.025, 0.05,SAWTOOTH=.FALSE., SURF_ID= 'Four' /
&OBST XB=-0.05, 0.05, -0.075, -0.05,  0.025, 0.05, SAWTOOTH=.FALSE., SURF_ID= 'Four' /
&OBST XB=-0.05, 0.05,  0.05, 0.075,  0.025, 0.05, SAWTOOTH=.FALSE., SURF_ID= 'Four' /
&OBST XB=-0.05,-0.025, 0.025, 0.05 ,  0.025, 0.05, SAWTOOTH=.FALSE., SURF_ID= 'Four' /
&OBST XB=-0.05,-0.025,-0.05, -0.025 ,  0.025, 0.05, SAWTOOTH=.FALSE., SURF_ID= 'Four' /
&OBST XB=0.025, 0.05, 0.025,  0.05 ,  0.025,0.05, SAWTOOTH=.FALSE., SURF_ID= 'Four' /
&OBST XB= 0.025, 0.05,-0.05,  -0.025 ,  0.025,0.05, SAWTOOTH=.FALSE., SURF_ID= 'Four' /
/////////////////////////////////////////////////////////////////////

Measurements
/////////////////////////////////////////////////////////////////////
Irradiance level:
-----------------
&DEVC ID                   = 'Flux' ,
  QUANTITY                 = 'HEAT_FLUX' ,
  XYZ                      = 0.,  0., -0.025,
  IOR                      = 3 /

Heater wall temperature:
------------------------
&DEVC ID                   = 'Temperature_wall_cone' ,
  QUANTITY                 = 'WALL_TEMPERATURE' ,
  XYZ                      = -0.05,  -0.075,  0.025,
  IOR                      = -3 /

Sample burning rate:
--------------------
&DEVC ID                   = 'BURNING_RATE' ,
  QUANTITY                 = 'BURNING_RATE' ,
  XYZ                      = 0.,  0.,  -0.025,
  IOR                      =3./
/////////////////////////////////////////////////////////////////////
&TAIL /
```